UNIVERSITY OF SOUTHAMPTON

DEPARTMENT OF ELECTRONICS & COMPUTER SCIENCE

FUSED TAPER SINGLE MODE FIBRE COUPLERS

by

Masamichi S. Yataki

A Thesis Submitted for the Degree of

Doctor of Philosophy

August 1988

University of Southampton

ABSTRACT

Faculty of Engineering and Applied Science

Electronics and Computer Science

Doctor of Philosophy

FUSED TAPER SINGLE MODE FIBRE COUPLERS

by Masamichi S. Yataki

This thesis contains a complete study of the symmetric fused taper single mode fibre coupler.

A new fabrication technique for the coupler is developed and a stable and reliable coupler package is designed and implemented.

Fundamental aspects of tapers and taper couplers are examined experimentally and the cladding mode nature of these structures is discovered. The cladding mode picture gives an elegant simplification of the description of fused taper couplers in terms of the interference of the two lowest order cladding modes of the composite waveguide formed through the lateral fusion and tapering of the two fibres.

Through this picture the relationship of the coupler's performance to the extent of tapering, the rate of tapering, the cross-sectional geometry and length of the coupling region, the refractive index of the external medium and the wavelength and polarisation state of the incoming light can be explicitly revealed.

Acknowledgements

I would like to thank Professor W.A. Gambling and Dr. D.N. Payne for giving me the opportunity to work in the Optical Fibre Group at Southampton.

I am grateful to my supervisor Dr. C.D. Hussey for his help and useful discussions on all aspects of this thesis and particularly for his helpful comments on the preparation of the manuscript.

All members of the Optical Fibre Group both past and present have contributed in some way to this work. Dr. F.P. Payne (now at Cambridge University), Dr. K. Morishita (from OSAKA-Electro Communications University, Japan) and Dr. J.D. Love (from ANU Australia) have provided useful discussions from time to time. Dr. R.D. Birch (now at ICI, Gloucester), Dr. E.J. Tarbox (now at Pirelli, Eastleigh), Dr. S.P. Poole, Mr. R.D. McGowan (now with BR) and Miss J.E. Townsend supplied most of the fibres used in the experiments for which I am very grateful.

Many thanks are due to Mrs. T. Pateman for her patience and good humour in typing the manuscript.

Lastly I gratefully acknowledge York V.S.O.P. for providing a studentship.

LIST OF PUBLICATIONS

1. M.S. Yataki, M.P. Varnham, D.N. Payne:
"Fabrication and properties of very-long fused taper couplers",
Proc. 8th Optical Fibre Conference, San Diego, 1985.

2. M.S. Yataki, D.N. Payne, M.P. Varnham:
"All-fibre wavelength filters using concatenated fused-taper couplers",
Electron. Lett., 1985, 21, pp. 248-249.

3. M.S. Yataki, D.N. Payne, M.P. Varnham:
"All-fibre polarising beamsplitter",
Electron. Lett., 1985, 21, pp. 249-251.

4. M.S. Yataki, M.P. Varnham, D.N. Payne:
"An all-fibre polarising beam splitter and spectral filter",
Presented at IEE Colloquium "Advances in Coherent Optic Devices and Technologies", IEE, London, March 1985.

5. F.P. Payne, C.D. Hussey, M.S. Yataki:
"Modelling fused single-mode fibre couplers",
Electron. Lett., 1985, 21, pp. 461-462.

6. F.P. Payne, C.D. Hussey, M.S. Yataki:
"Polarisation analysis of strongly fused and weakly fused tapered couplers",
Electron. Lett., 1985, 21, pp. 461-563.

7. F.P. Payne, C.D. Hussey, M.S. Yataki:
"Polarisation in fused single-mode fibre couplers",
Proc. IOOC-ECOC, 1985, Venice, pp. 571-573.

8. F.P. Payne, T. Finnegan, M.S. Yataki, R.J. Mears, C.D. Hussey:
"Dependence of fused taper couplers on external refractive index",
Electron. Lett., 1986, 22, pp. 1207-1209.

9. K. Morishita, M.S. Yataki, W.A. Gambling:
"Wavelength-insensitive couplers using dispersive material",
Optics Letters, 1987, 12, pp. 534-535.

10. K. Morishita, M.S. Yataki, W.A. Gambling:
"In-line optical fibre filters using dispersive materials",
Electron. Lett., Vol. 23, pp. 319-321, 1987.

LIST OF CONTENTS

CHAPTER 1: INTRODUCTION AND BACKGROUND

Single-mode optical fibres have emerged recently to play a dominant role in the fields of optical communications and optical fibre sensors (1,2). Single-mode fibres have virtually infinite bandwidth because there is no intermodal dispersion (3,4). In addition, the fibre's unique ability to transmit faithfully intensity, phase and, in special cases, polarisation information, and the ease with which single-mode power can be modulated and switched in low crosstalk integrated optical modulators and switches, has led to its increasing importance for future systems whether they be coherent communication systems or interferometric sensor systems (5-9).

The economic viability of optical fibres is now without question (10). As a transmission medium the optical fibre and particularly the single-mode fibre offers very low attenuation (11,12) coupled with extremely large bandwith (12-15). Fibres are small, have little weight, are very flexible and are reasonably cheap to produce and cable (16-20). The fibre is a dielectric and therefore relatively immune to electromagnetic interference (EMI) from outside sources. Virtually no electromagnetic radiation leaks from the fibre cable, making the fibre more secure since the optical signals cannot be easily intercepted or tapped. Consequently fibres can also be densely packed without fear of crosstalk (21,22).

The freedom from electromagnetic interference and the

associated freedom from any electrical spark hazard makes the optical fibre also attractive for use in sensors for hazardous environments (23).

It is mentioned above that the single-mode fibre has only recently emerged to play the dominant role in communications and sensors, yet when research into fibres for transmission first began about twenty years ago (24) it was thought that the single-mode fibre would be the most likely candidate to exploit the huge bandwidth available due to the recently invented laser source (25,26).

To understand the delay in the emergence of the single-mode fibre and the dominance of the multimode fibre over the past two decades it is necessary to take a close look at fibres themselves and single-mode fibres in particular.

A conventional silica-based optical fibre consists of a core, which provides the guiding function; and a cladding having a refractive index slightly lower (normally by less than 1%) (4,11,27-30) than that of the core. Whether a fibre is single moded or multimoded depends on the core dimension, the refractive index difference between the core and the cladding and the operating wavelength. All of these factors are embodied in the fibre's normalised frequency parameter or V-value, which is a measure of the fibre's capacity for guidance, defined as (27-30):

$$V = \frac{2\pi a}{\lambda} (n_{co}^2 - n_{cl}^2)^{\frac{1}{2}} \quad (1.1a)$$

$$= \frac{2\pi a}{\lambda} NA \quad (1.1b)$$

where

a = core radius

λ = operating wavelength

n_{co} = maximum core refractive index

n_{cl} = uniform cladding refractive index

NA = numerical aperture

For the special case where the core refractive index is uniform, the fibre becomes single moded for V-values less than 2.405, which corresponds to the cutoff V-value for the second mode (27-30).

For operating wavelengths in the range 0.8 -1.6μm, core diameters are typically 5 - 10 μm and 50 - 100 μm for single-mode and multimode silica-based telecommunications fibres respectively (27-30). These are shown schematically in Figure 1.1.

Single-mode fibres are generally operated close to the second-mode cutoff wavelength thereby allowing for the largest core size for a given numerical aperture. At this wavelength approximately 80% of the fundamental mode power is contained in the core; the remaining power is contained in the evanescent cladding field (28). Very little power spreads beyond three core diameters, Figure 1.2.

A perfectly circularly symmetric single-mode fibre propagates the fundamental or HE_{11} mode (25,27-30). The HE_{11} mode is approximately a plane wave with two orthogonally polarised components, so that, in polarisation terms, the fibre is double moded (31), as shown schematically in Figure 1.3. In general the two polarisation states are degenerate, i.e. they have the same propagation constants. Distortions of the core from perfect circularity or anisotropic strain applied across the core causes the polarisation states to become non-degenerate and the fibre becomes birefringent (32,33). Highly-birefringent fibres are capable of maintaining a single state of polarisation along the length of the fibre (32,33).

There are single-mode fibres to suit virtually every application and design criterion. Fibres can be designed to minimise microbending loss (34), to be dispersion flattened (35,36) or to be disperesion shifted (37,38). Fibre cores can be singly clad, doubly clad (35,36) or multiply clad (37). Fibres can have linear (32,33,39), elliptical (40), circular (41,42) or even zero birefringence (43). There are Bow-Tie fibres (39), PANDA fibres (44), spun fibres (40,43) twisted fibres (41,42) even four-leaved-clover fibres (42). There are fibre lasers (45), fibre amplifiers (46), fibre filters (47), fibre modulators (48), fibre polarisers (49). The list is becoming endless.

The more important single-mode fibres are described in

Figure 1.4. For transmission, the most important fibre is still the simple singly-clad or "matched cladding" step index fibre, although the doubly-clad or W-fibre is gaining in prominence.

Two main factors pushed research in the direction of the multimode fibre in the early years, each related to the fact that both the fibre and laser technologies were completely new.

Firstly, there was the lack of a suitable long life semiconductor laser source to provide good launching efficiency into the single-mode fibre. Secondly, the large cored multimode fibre was necessary to provide convenient fibre handling such as fibre splicing and connecting, as well as being necessary to achieve sufficient launch power from the LED sources then available.

Under the constraints of operating with multimode fibres, the graded index fibre then emerged as the fibre which would provide ultimate bandwidth by equalising the delay times of the different modes (50-52). System components varying from simple connectors to optical processing elements such as the directional coupler and beamsplitter were developed (53-63). The directional coupler provides the signal distribution required for any network. The most popular directional coupler in multimode technology was (and is) the fused and tapered coupler (58,59,63). Other components such as filters (64),

multiplexers (65,66) and switches (67) were achieved by adapting bulk optics components.

Interest in single-mode fibres was regenerated with the achievement of long-life semiconductor laser sources operating in the wavelength range of 0.8 -1.6μm (1,68-72) together with the development of semiconductor detectors sensitive in this range (73-75). It was found that a lot of the technology developed for multimode fibres could be readily adapted for use with single-mode fibres. The net result is that single-mode fibres are being used not only in long haul trunk networks (1), but they are also competing with multimode fibres in local area networks (LAN's) (76). Additional bonuses of using single-mode fibres instead of multimode fibres are that the fibre is much easier to manufacture, and the refractive index distribution in the core is no way as critical as in the graded index case (77). The development of components compatible with single-mode fibre technology has been very slow, although such components are gradually emerging (44,49,78-88). Single-mode fibre splicing can be achieved in the field with losses below 0.1dB (89,90), while single-mode fibre connectors can have insertion losses of 0.2dB (91) which is less than the Fresnel loss.

The development of single-mode fibre circuits, whether they be for communications or sensor systems, and the adoption of such systems over competing systems will rely on

the ready availability of passive optical processing components such as directional couplers, connectors, filters, polarisers etc., as well as active devices such as laser diodes, detectors, switches, amplifiers and modulators. These components need to be fibre compatible so that no special techniques are required to incorporate them into the system other than conventional splicing, alignment and interconnection methods.

A key component in the single-mode fibre optical circuit is the passive directional coupler which plays the same role as the beamsplitter in bulk optics.

The most popular single-mode fibre coupler has been available for quite a number of years and is produced, in a manner identical with the multimode coupler, by fusing and tapering two (or more) single-mode fibres together (92-115). This coupler can be produced with negligible throughput loss and with any desired throughput power splitting characteristic at any specified wavelength (92-115). This coupler has become known, not surprisingly, as the fused taper coupler or the fused biconical taper coupler and is the topic of study in this thesis.

It may seem strange that it was decided to study a very well-established device in single-mode fibre technology but it should be understood that, at the commencement of this work over five years ago, the operation of the device was not understood even at the most rudimentary level.

In the intervening years a considerable effort has been expended worldwide in investigating the behaviour of the fused taper coupler (99-127). While the work reported in this thesis has contributed in no small way towards the fundamental understanding of the coupling mechanism and has influenced the direction of research in other laboratories, work undertaken elsewhere has in turn influenced the development of the present study.

Outline of the Thesis

This thesis attempts a complete study of the fused taper coupler. Topics covered will include coupler fabrication, coupler packaging, long term reliability and stability studies, coupler measurements, experimental results for various coupler parameters, theoretical modelling of the coupler and some novel applications.

Presentation will be such as to present the current understanding of fused taper couplers as conveniently as possible through detailed experimental studies but also by drawing on results obtained independently elsewhere. The new theory of the fused taper coupler as outlined in this thesis does not simply explain the existing experimental results but has led to the development of new devices based on both the single fibre taper and the taper coupler, some of which are included in the present work (103,106) while others are currently being developed by colleagues at Southampton University (87,128) and other workers elsewhere

(107,110,113,114).

In Chapter 2 the different types of single-mode fibre couplers are reviewed and the relative merits of the fused taper coupler are outlined. The basic parameters and properties of single mode directional couplers are presented. The general properties of polarisation effects in single mode couplers are examined for the first time.

Details of the development of a novel coupler fabrication method is presented in Chapter 3. The new method is based on a gravity pulling scheme which is very simple to implement both on an individual and mass production scale. The design of the coupler package with regard to reliability and stability is described and the results of long term stability, temperature stability, vibration and reliability tests are presented.

In Chapter 4 the simple taper is examined both experimentally and theoretically and it is shown conclusively that the taper is a cladding mode device. It is found that tapers can be optimised with regard to both loss and stability. The fact that the tapers are restricted in application to matched cladding fibres is explained. It is concluded that tapers are a useful and versatile component in their own right.

In Chapter 5 most of the experimental results on fused taper couplers are presented. Couplers are examined with regard to wavelength, length, degree of taper, degree of fusion, polarisation and external refractive index.

In Chapter 6 a cladding mode model for the taper coupler is presented and justified. This model allows for the coupling coefficients in the coupler to be described explicitly in terms of the taper dimensions, the wavelength, the length and the external index for certain coupler cross sections. The model is found to account in general terms for most of the experimental results found in Chapter 5. A new version of this cladding mode model is proposed where the coupler is described in terms the coupling between two parallel slab waveguides. This model is computationally tractable and allows for a bit more flexibility than the simpler model given earlier. Studies in terms of the variation of the cross section as well as wavelength, external refractive index and polarisation can, at least qualitatively, be described with this model. The observed behaviour of increase in loss and decrease in extinction ratio with increased degree of fusion of the coupler cross section can now be accounted for.

Using the unique properties of the fused tapered coupler two completely different applications areas are possible. The first is in fibre circuits and the second is in fibre sensors. In Chapter 7 a spectral band pass filter and a temperature sensor are described. Other applications

of taper components which depend explicitly on the cladding mode nature of such components are reviewed.

The Appendix contains a description of the measurement system used throughout the experimental work.

References to Chapter 1

1. T. Li:
"Advances in optical fiber communications: an historical perspective",
IEEE J. Selected Areas in Communications, 1983, SAC-1, pp. 356-372.

2. T.G. Giallorenzi, J.A. Bucaro, A. Dandridge, G.H. Sigel, J.H. Cole, S.C. Rashleigh and R. Priest:
"Optical fiber sensor technology",
IEEE J. Quant. Electron., 1982, QE-18, pp. 626-665.

3. K. Kapron and D.B. Keck:
"Pulse transmission through a dielectric optical waveguide",
Appl. Opt., 1971, 10, pp. 1519-1523.

4. D. Gloge:
"Dispersion in weakly guiding fibres",
Appl. Opt., 1971, 10, pp. 2442-2445.

5. O.E. Delange and A.F. Dietrich:
"Optical heterodyne experiments with enclosed transmission paths",
Bell Syst. Tech. J., 1968, 47, pp. 161-178.

6. Y. Yamamoto:
"Receiver performance evaluation of various

digital modulation-demodulation systems in the 0.5 - 19μm wavelength region",
IEEE J. Quant. Electron., 1980, QE-16, pp. 1251-1259.

7. T. Okoshi:
"Heterodyne and coherent optical fiber communications: recent progress",
IEEE Trans. Microwave Theory Tech., 1982, MTT-30, pp. 1138-1148.

8. V. Vali and R.W. Shorthill:
"Fiber ring interferometer",
Appl. Opt., 1976, 15, pp. 1099-1100.

9. J.A. Bucaro, H.D. Dardy and E. Carome:
"Fibre optic hydrophone",
J. Acoust. Soc. Amer., 1977, 62, pp. 1302-1304.

10. S. Simada and K. Masuno:
"Optical fibre transmission system field trial",
NTT (Japan), Kenkyu Jitsuyoka Hokoku (ECL Tech. J.), 1979, 28, pp. 1803-1822.

11. F.P. Kapron, D.B. Keck and R.D. Maurer:
"Radiation losses in glass optical waveguides",
Appl. Phys. Lett., 1970, 17, pp. 423-425.

12. T. Miya, Y. Terunuma, T. Hosaka and T. Miyashita:
"Ultimate low-loss single-mode fibre at 1.55μm",

Electron. Lett., 1979, 15, pp. 106-108.

13. E. Iwahashi:
"Trends in long-wavelengths single-mode transmission system and demonstrations in Japan", IEEE J. Quantum Electron., 1981, QE-17, pp. 890-896.

14. J. Yamada, S. Machida and T. Kimura:
"2 Gbit/s optical transmission experiments at 1.3μm with 44km single-mode fibre", Electron. Lett., 1981, 17, pp. 479-480.

15. K. Iwashita, K. Nakagawa, T. Matsuoka and T. Nakahara:
"400 Mbit/s transmission test using a 1.53μm DFB laser diode and 104km single-mode fibre", Electron. Lett., 1982, 18, pp. 937-938.

16. S. Mochizuki, K. Ishihara and N. Nakatani:
"Optical fibre cable structure design", NTT (Japan), Kenkyu Jitsuyoka Hokoku (ECL Tech. J), 1978, 27, pp. 2451-2466.

17. Edited by S.E. Miller and A.G. Chynoweth:
"Optical Fibre Telecommunications", Academic Press, 1979.
Chapter 13, "Optical cable design", by M.I. Schwartz, D. Gloge and R.A. Kempf.

18. M. Yataki and K. Abe:
"Large size fiber optic cables (design concept)",
Bell-Northern Research, 1980, TM31156.

19. M. Yataki:
"Optical Cables",
U.S. Patent 4474426, 1984.

20. M. Yataki:
"Optical Cables",
Canadian Patent 1185468, 1985.

21. Edited by S.E. Miller and A.G. Chynoweth:
"Optical Fibre Telecommunications",
Academic Press, 1979.
Chapter 1, "Evolution of optical communications",
by A.G. Chynoweth and S.E. Miller.

22. Y. Suematsu and K. Iga:
"Introduction to Optical Communications",
Translated by H. Matsumura and W.A. Gambling,
Prentice-Hall, 1982.

23. R.T. Murray:
"Fibre-optic sensors fit for the chemical
industry",
Tech. Digest OFS, San Diego, pp. 138, 1985.

24. K.C. Kao and G.A. Hockham:
"Dielectric-fibre surface waveguides for optical
frequencies",

Proc. IEE, 1966, 113, pp. 1151-1158.

25. T.H. Maiman:
"Stimulated optical radiation in ruby",
Nature (London), 1960, 6, pp. 106.

26. A.L. Schawlow and C.H. Townes:
"Infrared and optical lasers",
Phys. Rev., 1958, 112, pp. 1940.

27. E. Snitzer:
"Cylindrical dielectric waveguide modes",
J. Opt. Soc. Amer., 1961, 51, pp. 491-498.

28. A.W. Snyder:
"Approximate expressions for eigenfunctions and eigenvalues of a dielectric or optical waveguide",
IEEE, Trans. Microwave Theory Tech., 17, 1969, pp. 1130-1138.

29. D. Gloge:
"Weakly guiding fibres",
Appl. Opt. 1971, 10, pp. 2252-2258.

30. A.W. Snyder and J.D. Love:
"Optical Waveguide Theory",
Chapman and Hall (London and New York), 1983.

31. S.C. Rashleigh and R. Ulrich:
"Polarisation mode dispersion in single-mode fibres",

Opt. Lett., 1978, 3, pp. 60-62.

32. R.B. Dyott, J.R. Cozens and D.G. Morris:
"Preservation of polarisation in optical fibres with elliptical cores",
Electron. Lett., 1979, 15, pp. 380-382.

33. R.H. Stolen, V. Ramaswamy, P. Kaiser and W. Pleibel:
"Linear polarisation in birefringent single-mode fibres",
Appl. Phys. Lett., 1978, 6, pp. 699-701.

34. K. Peterman:
"Fundamental mode microbending loss in graded index and W-fibres",
Opt. & Quantum Electron., 1977, 9, pp. 167-175.

35. S. Kawakami and S. Nishida:
"Characteristics of a doubly clad optical fiber with a low index inner cladding",
IEEE J. Quant. Electron., 1974, QE-10,
pp. 879-887.

36. S. Kawakami and S. Nishida:
"Perturbation theory of a doubly clad optical fibre with a low index inner cladding",
IEEE J. Quantum Electron., 1975, QE-11,
pp. 130-138.

37. M.A. Saifi, S.J. Jang, L.G. Cohen and J. Stone:
"Triangular profile single mode fiber",
Opt. Lett., 1981, 7, pp. 43-45.

38. K.I. White:
"Design parameters for dispersion shifted
triangular-profile single-mode fibres",
Electron. Lett., 1982, 18, pp. 725-727.

39. R.D. Birch, D.N. Payne and M.P. Varnham:
"Fabrication of polarisation-maintaining fibres
using gas phase etching",
Electron. Lett., 1982, 18, pp. 1036-1038.

40. J.R. Qian and L. Li:
"Current sensors using highly birefringent spun
Bow-Tie fibres",
Tech. Digest, OFS, Tokyo, 1986, pp. 85-88.

41. M.P. Varnham, R.D. Birch and D.N. Payne:
"Helical core circularly birefringent fibres",
Tech. Digest, IOOC-ECOC, Venice, 1985,
pp. 135-138.

42. C.D. Hussey, Y. Fujii and R.D. Birch:
"Circularly birefringent single-mode optical
fibres",
Electron. Lett., 1981, 22, pp. 129-130.

43. D.N. Payne, A.J. Barlow and J.J. Ramskov Hansen:
"Development of low- and high-birefringence

optical fibres",
IEEE J. Quant. Electron., 1982, QE-18,
pp. 477-488.

44. T. Hosaka, K. Okamoto, T. Miya, Y. Sasaki
and T. Edahiro:
"Low-loss single-polarisation fibres with
asymmetrical strain birefringence",
Electron. Lett., 1981, 19, pp. 530-531.

45. R.J. Mears, D.N. Payne, S.B. Poole, L. Reekie,
I.P. Alcock, A.I. Ferguson, D.C. Hanna and
A.G. Tropper:
"Single-mode neodymium fibre lasers",
Presented at National Quantum Electronics
Conference, Cannes, September 1985.

46. R.J. Mears, L. Reekie, I.M. Jauncey and
D.N. Payne:
"High-gain rare-earth-doped fibre amplifier at
1.54μm",
Tech.Dig. IOOC/OFC, Reno, January 1987.

47. M.C. Farries, J.E. Townsend and S.B. Poole:
"Very high-rejection optical fibre filters",
Electron. Lett., 1986, 22, pp. 1126-1128.

48. L. Li, R.D. Birch and D.N. Payne:
"An all-fibre Kerr modulator",
Presented at IEE Colloquium: Advanced Fibre

Waveguide Devices, London, May 1986.

49. L. Li, R.D. Birch and D.N. Payne:
"High-performance composite metal/glass fibre polarisers",
Proc. ECOC, Barcelona, 1986.

50. W. Streifer and C.N. Kurtz:
"Scalar analysis of radially inhomogeneous guiding media",
J. Opt. Soc. Amer., 1967, 57, pp. 779-786.

51. S. Kawakami and J. Nisdhizawa:
"An optical waveguide with the optimum distribution of the refractive index with reference to waveform distortion",
IEEE Trans. Microwave Theory Tech., 1968, MTT-16, pp. 814-818.

52. D. Gloge and E.A.J. Marcatili:
"Multimode theory of graded core fibres",
Bell Syst. Tech. J., 1973, 52, pp. 1563-1578.

53. H. Kuwahara, J. Hamasaki and S. Saito:
"Power transfer of a parallel optical fiber directional coupler",
IEEE Trans. Microwave Theory Tech., 1975, MTT-23, pp. 178-179.

54. H. Kuwahara, J. Hamasaki and S. Saito:

"A semi-transparent mirror-type directional coupler for optical fiber applications", IEEE Trans. Microwave Theory Tech., 1975, MTT-23, 179-180.

55. T. Ozeki and B.S. Kawasaki: "Optical directional coupler using tapered sections in multimode fibers", Appl. Phys. Lett., 1976, 28, pp. 528-529.

56. H. Fujita, Y. Suzaki and A. Tachibana: "Optical fiber wave splitting coupler", Appl. Opt., 1976, 15, pp. 2031-2032.

57. Y. Suzuki and H. Kashiwagi: "Concentrated-type directional coupler for optical fibers", Appl. Opt., 1976, 15, pp. 2032-2033.

58. B.S. Kawasaki and K.O. Hill: "Low-loss access coupler for multimode optical fiber distribution networks", Appl. Opt., 1977, 16, pp. 1794-1795.

59. K.O. Hill, B.S. Kawasaki and D.C. Johnson: "Efficient power combiner for multiplexing multiple sources to single-fiber optical systems", Appl. Phys. Lett., 1977, 31, pp. 740-742.

60. Y. Tsujimoto, H. Serizawa, K. Hattori and M. Fukai:

"Fabrication of low-loss 3dB couplers with multimode optical fibres",
Electron. Lett., 1978, 14, pp. 157-158.

61. E. Weidel and D. Gruchmann:
"Tee-coupler for single-mode fibres",
Electron. Lett. 1979, 15, pp. 737-738.

62. D. Opielka and D. Rittich:
"Low-loss optical Y-branch",
Electron. Lett., 1979, 15, pp. 757-759.

63. D.C. Johnson, B.S. Kawasaki and K.O. Hill:
"Fused biconical tapered fiber-optic devices: application to data buses",
Fiber and Integrated Optics, 1980, 3, pp. 263-284.

64. H.F. Mathlein, H. Michel, W. Raucher, A. Reichett and G. Winzer:
"Interference filter all fibre directional coupler for W.D.M.",
Electron. Lett., 1980, 16, pp. 584-585.

65. W.J. Tomlinson and G.D. Aumiller:
"Optical multiplexer for multimode fiber transmission systems",
Appl. Phys. Lett., 1977, 31, pp. 169.

66. K. Nosu, H. Ishio and K. Hashimoto:

"Multireflection optical multi-demultiplexer using interference filters",
Electron. Lett., 1979, 15, pp. 414-415.

67. G.S. Duck, M. Yataki, J. Straus and W.J. Sinclair: "Optical Switch",
US Patent 4378144, 1983.

68. I. Hayashi, M.B. Panish, P.W. Foy and S. Sumski: "Junction lasers which operate continuously at room temperature",
Appl. Phys. Lett., 1976, 28, pp. 709-711.

69. J.J. Hsieh, J.A. Rossi and J.P. Donnelly: "Room-temperature CW operation of GaInAsP/InP double-heterostructure lasers emitting at 1.1μm",
Appl. Phys. Lett., 1976, 28, pp. 709-711.

70. A.Y. Cho, R.W. Dixon, H.C. Casay JR. and R.L. Hartman:
"Continuous room-temperature operation of GaAs-$Al_xGa_{1-x}As$ double-heterostructure lasers prepared by molecular-beam epitaxy",
Appl. Phys. Lett., 1976, 28, pp. 501-503.

71. A.A. Bergh, J.A. Copeland and R.W. Dixon: "Optical sources for fibre transmission systems",
Proc. IEEE, 1980, 68, pp. 1240-1247.

72. M. Yano, H. Imai, K.I. Hori and M. Takusagawa: "High temperature characteristics of stripe

geometry InGaAsP/InP double-heterostructure lasers",
IEEE J. Quant. Electron., 1981, QE-17, pp. 619-626.

73. R.P. Riesz:
"High speed semiconductor photodiodes",
Rev. Sci. Inst., 1962, 33, pp. 994-998.

74. C.E. Hurwitz and J.J. Hsieh:
"GalnAsP/InP avalanche photodiodes",
Appl. Phys. Lett., 1978, 32, pp. 487-489.

75. R. Chin, N. Holonyak Jr., G.E. Stillman, J.Y. Tang and K. Hess:
"Impact ionization in multilayered heterojunction structures",
Electron. Lett., 1980, 16, pp. 467-469.

76. K. Tomimori, T. Ogawa and M. Mori:
"High capacity transmission ('Dai youryoh densoh' in Japanese)",
O plus E, 1985, 62, pp. 76-83.

77. W.J. Stewart:
"Simplified parameter-based analysis of single-mode optical guides",
Electron. Lett., 1980, 16, pp. 380-382.

78. W. Eickhoff:

"In-line fibre-optic polariser",
Electron. Lett., 1980, 16, pp. 762-763.

79. R. Kishimoto:
"Optical coupler for laser redundancy system",
Electron. Lett., 1982, 18, pp. 140-141.

80. C.A. Villarruel, M. Abebe, W.K. Burns and
R.P. Mueller:
"In-line birefringent polariser",
Tech. Digest, OFC, New Orleans, 1984, pp. 14-15.

81. M. Kawachi and M. Kobayashi:
"Fibre-optic polarizing directional coupler",
Opt. Lett., 1984, 9, pp. 183-185.

82. F. De Fornel, M.P. Varnham and D.N. Payne:
"Finite cladding effects in highly birefringent
fibre taper-polarisers",
Electron. Lett., 1984, 20, pp. 398-399.

83. W.V. Sorin and H.J. Shaw:
"Single-mode fibre evanescent grating reflector",
Technical Digest of OFS, 1984, pp. 132.

84. I. Yokohama, K. Okamoto and J. Noda:
"Fibre-optic polarising beam splitter employing
birefringent-fibre coupler",
Electron. Lett., 1985, 21, pp. 415-416.

85. M.S. Whalen and K.L. Walker:

"In-line optical-fibre filter for wavelength multiplexing",
Electron. Lett., 1985, 21, pp. 724-725.

86. I. Yokohama, K. Okamoto and J. Noda:
"Optical circulator consisting of a YIG spherical lens, PANDA-fibre polarisers and a fibre-optic polarising beam splitter",
Electron. Lett., 1985, 21, pp. 746-748.

87. K.P. Jedrzejewski, F. Martinez, J.D. Minelly, C.D. Hussey and F.P. Payne:
"Tapered-beam expander for single-mode optical-fibre gap devices",
Electron. Lett., 1986, 22, pp. 105-106.

88. M.S. Whalen, M.D. Divino and R.C. Alferness:
"Demonstration of a narrowband Bragg-reflection filter in a single-mode fibre directional coupler",
Electron. Lett., 1986, 22, pp. 681-682.

89. T. Onodera, I. Suzuki, T. Yamada, Y. Osato and O. Watanabe:
"Splicing characteristics of single-mode fibres by the direct core detection splicer",
IECE (Japan) National Convention Record, 1985, pp. 2237.

90. Edited by S.E. Miller and A.G. Chynoweth:

"Optical Fibre Telecommunications",
Academic Press, 1979.

91. N. Suzuki, M. Saruwatari, M. Okuyama and K. Iwasa:
"Convex polished optical fibre connectors",
IECE (Japan) National Convention Record, 1985,
pp. 2606.

92. C.A. Villarruel and R.P. Moeller:
"Fused single-mode fibre access couplers",
Electron. Lett., 1981, 17, pp. 243-244.

93. B.S. Kawasaki, K.O. Hill and R.G. Lamont:
"Biconical-taper single-mode fiber coupler",
Opt. Lett., 1981, 6, pp. 327-328.

94. M. Kawachi, B.S. Kawasaki, K.O. Hill and
T. Edahiro:
"Fabrication of single-polarisation single-mode-
fibre couplers",
Electron. Lett., 1982, 18, pp. 962-964.

95. C.A. Villarruel, M. Abebe and W.K. Burns:
"Birefringence correction for single-mode fibre
couplers",
Opt. Lett., 1982, 7, pp. 626-628.

96. C.A. Villarruel, M. Abebe and W.K. Burns:
"Polarisation preserving single-mode-fibre
coupler",
Electron. Lett., 1983, 19, pp. 17-18.

97. B.S. Kawasaki, M. Kawachi, K.O. Hill and
D.C. Johnson:
"A single-mode-fiber coupler with a variable coupling ratio",
J. Lightwave Tech., 1983, LT-1, pp. 176-178.

98. C.M. Ragdale, D.N. Payne, F. De Fornel and
R.J. Mears:
"Single-mode fused biconical taper fibre couplers",
Proc. IEE Conference on Optical Fibre Sensors, 1983, pp. 75-78.

99. M. Kawachi:
"Fabrication of polarisation-maintaining (3x3) single-mode-fibre couplers",
Electron. Lett., 1983, 19, pp. 781-782.

100. T. Bricheno and A. Fielding:
"Stable low-loss single-mode couplers",
Electron. Lett., 1984, 20, pp. 230-232.

101. P.M. Kopera, H.H.A. Krueger, V.J. Tekippe and
D.L. Wuensch:
"Performance evaluation of single-mode couplers,
Proc. SPIE., 1984, 479, pp. 9-15.

102. R.G. Lamont, D.C. Johnson and K.O. Hill:
"Power transfer in fused biconical-taper single-mode fibre coupler dependence on external

refractive index",
Appl. Opt., 1985, 24, pp. 327-331.

103. M.S. Yataki, M.P. Varnham and D.N. Payne:
"Fabrication and properties of very-long fused taper couplers",
Tech. Digest OFC, San Diego, 1985, pp. 108-110.

104. M.S. Yataki, M.P. Varnham and D.N. Payne:
"All-fibre polarising beam splitter and spectral filter",
Presented at IEE Colloquium "Advances in Coherent Optic Devices and Technologies", London, 1985.

105. M.S. Yataki, D.N. Payne and M.P. Varnham:
"All-fibre wavelength filters using concatenated fused-taper couplers",
Electron. Lett., 1985, 21, pp. 248-249.

106. M.S. Yataki, D.N. Payne and M.P. Varnham:
"All-fibre polarising beamsplitter",
Electron. Lett., 1985, 21, pp. 249-250.

107. T. Bricheno and V. Baker:
"All-fibre polarisation splitter/combiner",
Electron. Lett., 1985, 21, pp. 251-252.

108. F.P. Payne, C.D. Hussey and M.S. Yataki:
"Modelling fused single-mode fibre couplers",
Electron. Lett., 1985, 21, pp. 461-462.

109. F.P. Payne, C.D. Hussey and M.S. Yataki:
"Polarisation analysis of strongly fused and weakly fused tapered couplers",
Electron. Lett., 1985, 21, pp. 561-563.

110. D.B. Mortimore:
"Wavelength-flattened fused couplers",
Electron. Lett., 1985, 21, pp. 742-743.

111. F.P. Payne, C.D. Hussey and M.S. Yataki:
"Polarisation in fused single-mode fibre couplers",
Tech. Digest IOOC-ECOC, Venice, 1985, pp. 571-573.

112. K.O. Hill, D.C. Johnson and R.G. Lamont:
"Wavelength dependence in fused biconical taper couplers: measurement and control",
Tech. Digest IOOC-ECOC, Venice, 1985, pp. 567-570.

113. Y. Namihira, S. Ryu, S. Yamamoto and K. Mochizuki:
"Fused-taper-twisted single-mode fibre couplers as a quarter-wave device",
Tech. Digest OFS, Tokyo, 1986, pp. 351-354.

114. S. Lacroix, F. Gonthier and J. Bures:
"All-fiber wavelength filter from successive biconical tapers",

Opt. Lett., 1986, 11, pp. 671-673.

115. F.P. Payne, T. Finnegan, M.S. Yataki, R.J. Mears and C.D. Hussey:
"Dependence of fused taper couplers on external refractive index",
Electron. Lett., 1986, 22, pp. 1207-1209.

116. J. Bures, S. Lacroix and J. Lapierre:
"Analyse d'un coupleur bidirectional a fibres optiques monomodes fusionees",
Appl. Opt., 1983, 22, pp. 1918-1922.

117. A.W. Snyder and F.F. Ruhl:
"Radiation losses from couplers",
J. Lightwave Tech., 1985, LT-3, pp. 31-36.

118. J.D. Love and A. Ankiewicz:
"Modal cutoffs in single- and few mode fibre couplers",
J. Lightwave Tech., 1985, LT-3, pp. 100-110.

119. J.D. Love and M. Hall:
"Polarisation modulation in long couplers",
Electron. Lett., 1985, 21, pp. 519-521.

120. A.W. Snyder:
"Polarising beam splitter from fused taper couplers",

Electron. Lett., 1985, 21, pp. 623-625.

121. J.V. Wright:
"Variational analysis of fused tapered couplers",
Electron. Lett., 1985, 21, pp. 1064-1065.

122. W.J. Stewart and J.D. Love:
"Design limitation on tapers and couplers in single mode fibres",
Tech. Digest IOOC/ECOC, Venice, 1985,
pp. 559-562.

123. D.T. Cassidy, D.C. Johnson and K.O. Hill:
"Wavelength-dependent transmission of monomode optical fiber tapers",
Appl. Opt., 1985, 24, pp. 945-950.

124. A.W. Snyder and X.H. Zheng:
"Fused couplers of arbitrary cross-section",
Electron. Lett., 1985, 21, pp. 1079-1080.

125. J.D. Love and W.M. Henry:
"Quantifying loss minimisation in single-mode fibre tapers",
Electron. Lett., 1986, 22, pp. 912-914.

126. A. Ankiewicz, A.W. Snyder and X.H. Zheng:
"Coupling between parallel optical fibre cores - critical examination",
J. Lightwave Tech., 1986, LT-4, pp. 1317-1323.

127. A.W. Snyder and X.H. Zheng:
"Optical fibres of arbitrary cross-sections",
J. Opt. Soc. Amer., 1986, A3, pp. 600-609.

128. J.D. Minelly and C.D. Hussey,
"Single-mode fibre Y-Junction beamsplitter",
Electron.Lett., 1987, 23, pp. 1087-1088.

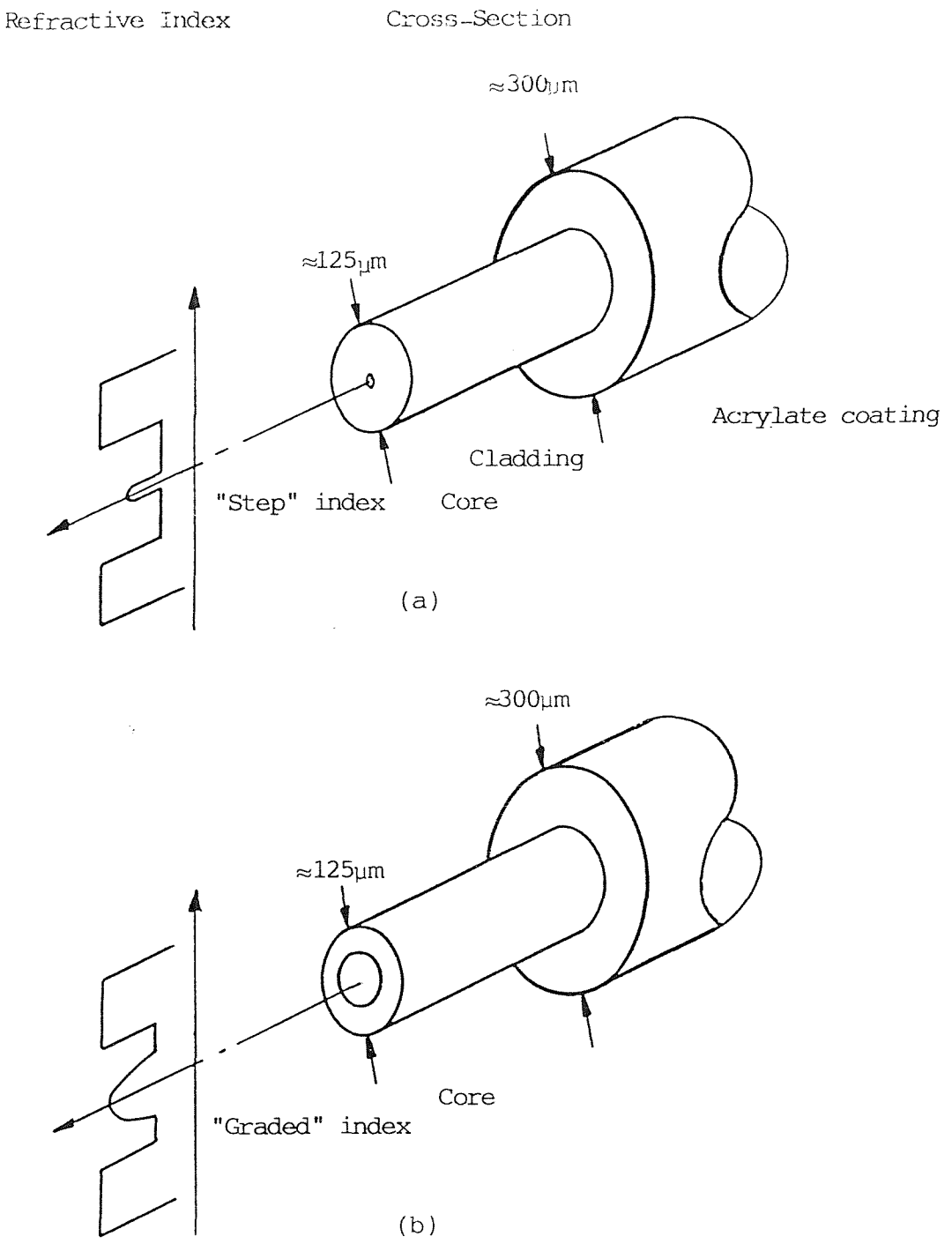

Figure 1.1. Cross-sections of (a) single-mode and (b) multimode fibres showing protective coating, typical dimensions and refractive index distributions.

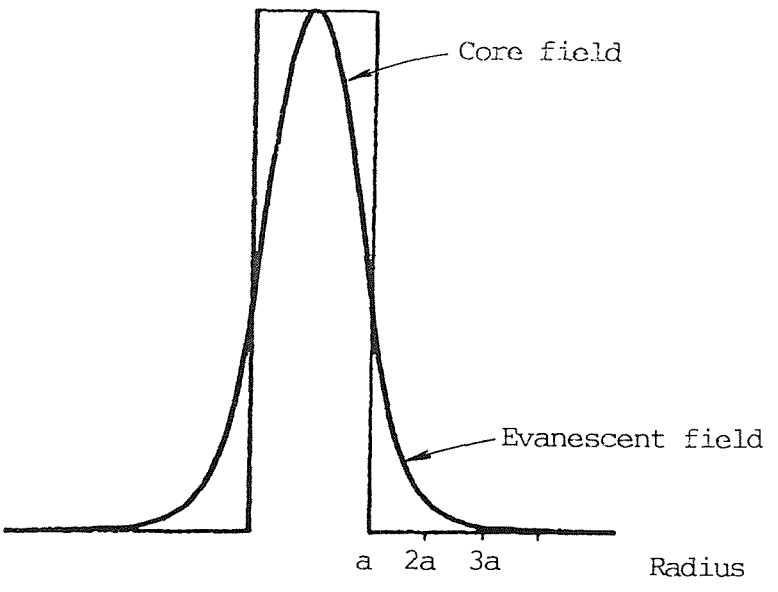

Figure 1.2. Fundamental (HE_{11}) mode field distribution in a step index fibre of V=2.405. 80% of the power is contained in the core field and 20% in the evanescent cladding field.

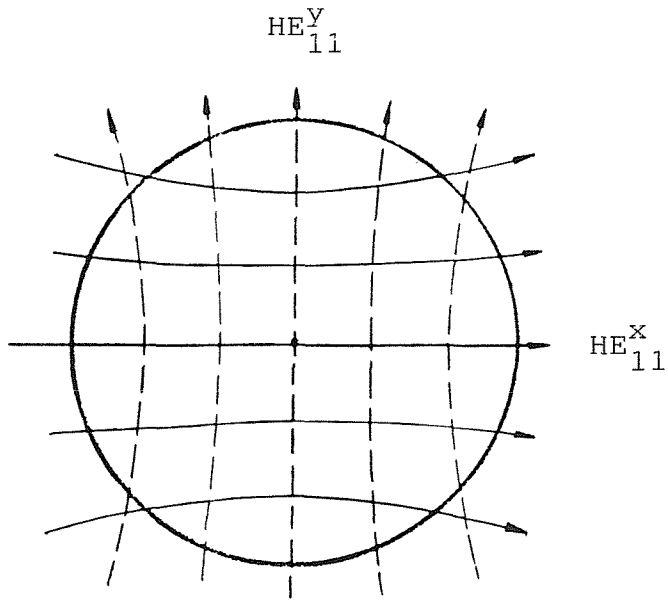

Figure 1.3. The two orthogonal polarisations of the fundamental (HE_{11}) mode in a single-mode fibre. The polarisations are approximately plane polarised.

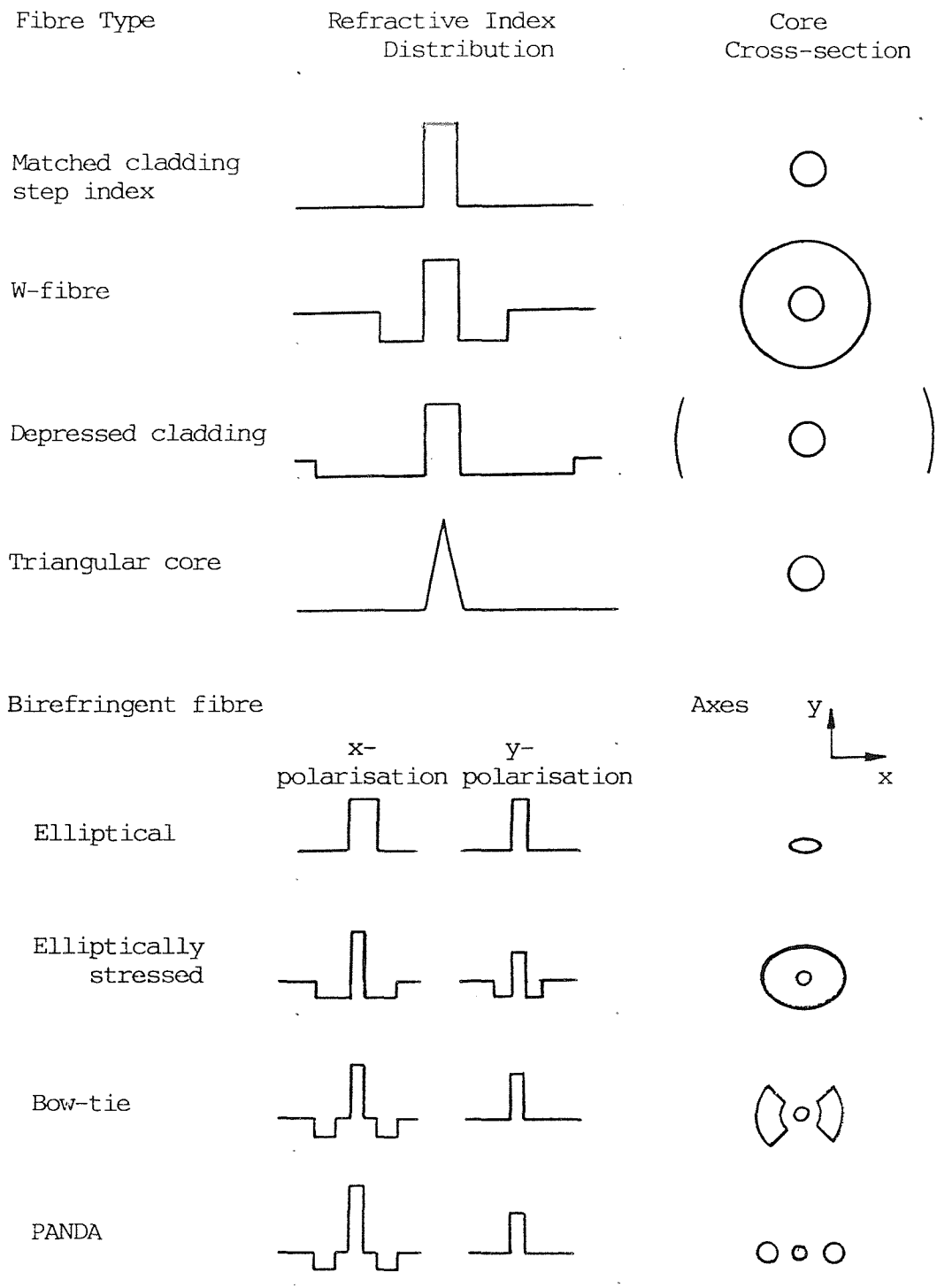

Figure 1.4. The more important single-mode fibres to date.

CHAPTER 2: SINGLE-MODE FIBRE DIRECTIONAL COUPLERS: TYPES AND GENERAL PROPERTIES

2.1 Introduction

In this chapter the functions and characteristics of single-mode fibre directional couplers are outlined. The various types of single-mode fibre directional coupler are reviewed and the reasons for the popularity of the fused tapered coupler are explained. Conventional theories describing the general behaviour of four-port couplers are outlined. A new, more general, theory is given which accounts in a straightforward way for polarisation effects in single mode couplers. Parameters which specify coupler performance are also defined.

2.2 Functions of the Directional Coupler

A directional coupler is a 2N port device where N has a value of 2 or more and is the number of input or output ports. Power in the input ports is mixed and monitored in the output ports or power in one of the input ports is divided between the output ports.

The most important directional coupler is the 4-port coupler indicated schematically in Figure 2.1. The present study is restricted to this device. For the rest of this thesis the term "coupler" will imply a 4-port single-mode fibre directional coupler.

2.3 Necessary Coupler Characteristics

In order to be good enough for serious systems applications, and to be suitable for mass production, couplers should satisfy the following criteria (1):

(i) beam splitting ratio as specified,

(ii) low insertion loss,

(iii) minimal temperature dependences of (i) and (ii),

(iv) optical stability,

(v) mechanical ruggedness,

(vi) semipermanent lifetime,

(vii) fibre preparation should be minimal or automatic,

(viii) fabrication should be reproducible and fast or automatic.

2.4 Types of Single-Mode Fibre Coupler

A fibre coupler must transfer power laterally from one fibre to another with minimal loss. Such coupling is achieved by causing optical field overlap between the two fibres (2,3). In the single-mode fibre the achievement of field overlap is no trivial task since, in a standard 125μm diameter fibre, the optical power is contained in a region of approximately 30μm diameter surrounding the core (3).

Two approaches have proved successful in achieving coupling between single-mode fibres. By removing the bulk of the intermediate cladding and bringing the fibre cores close together, the evanescent portion of the optical fields

of both fibres are caused to overlap giving rise to evanescent coupling (2-16). Coupling can also be achieved by bringing two tapered fibres into intimate contact. In the taper the optical field expands from the core into the cladding such that the cladding provides guidance at its boundary with the external medium. This form of coupling has become known as cladding mode coupling (17-28).

Loss is kept at a minimum in couplers by ensuring that any transitions undergone by the propagating optical field are slow, or adiabatic (21).

Some specific single-mode fibre couplers are now examined.

2.4.1 Evanescent couplers

Various ingenious approaches have been used to achieve evanescent coupling. The more popular are the grinding and careful polishing of the fibre, or the controlled chemical etching of the fibre, down to the desired proximity to the fibre core.

2.4.1.1 Polished couplers

The polished coupler is made of two substrate blocks each provided with a narrow groove in one surface into which the fibre, stripped of primary coating, is fixed (2,4-7). The bottom of the groove is given a specified curvature which fixes the axis of the fibre glued into the groove. The surface of each substrate is ground and then carefully

polished down to the desired distance from the fibre core as in Figure 2.2(a). The coupler is formed by bringing the two polished fibres face to face as in Figure 2.2(b). The coupling strength is determined by the radius of curvature of the base of the groove, the grinding depth and the contact conditions. In practice index matching material must be applied between the two elements which are firmly held together.

As with most single-mode fibre couplers the transfer characteristics in the polished coupler can be very wavelength dependent; however the characteristics can be tuned to any desired value at any desired wavelength by simply sliding one block laterally and thereby varying the core-to-core separation, which in turn controls the coupling strength, Figure 2.2(c) (2).

The wavelength dependence of the polished coupler has been used to advantage for achieving wavelength multiplexing (29) and wavelength filtering (2).

There is no restriction on the type of fibre which can be polished and thereby formed into a coupler. Couplers with very special properties can therefore be constructed. Of particular interest are couplers made from highly birefringent fibres which will maintain polarisation not only in the coupling section but also in the coupler leads. Polarisation-maintaining single-mode fibre couplers have been constructed from elliptically stressed fibres (6), Bow-

Tie fibres (30) and PANDA fibres (31).

Loss can be kept below 0.5dB (6) while the long term reliability and stability of the coupler can be assured by permanently bonding the two substrate blocks together. The tunable couplers tend to degrade with time since the index matching material between the substrate blocks is very temperature sensitive and is also prone to evaporation (32).

The substrate blocks are either of fused quartz, with the groove machined onto one surface, or silicon with the groove etched along crystal planes; the latter being more reproducible. Automatic manufacturing and mass production techniques have been attempted with both types of substrate material (7,33).

The half block, i.e. a single fibre on a single substrate, has proved to be very convenient for achieving field access. Devices constructed around the half coupler include laser amplifiers (34,35,36), polarisers (37), grating filters (38), variable attenuators and phase modulators (39).

2.4.1.2 Etched couplers

One of the earliest methods of achieving evanescent coupling was by the chemical etching of the fibre to remove most of the cladding (1,9,10). Power transfer occurs when two such fibres are brought into contact as shown schematically in Figure 2.3.

The first coupler made with this technique was the "bottle" coupler since the device was etched, cleaned and packaged in a specially designed bottle container (9). Tuning could be achieved by twisting the fibres about each other (1). This coupler proved very temperature sensitive with fluctuations in the output power splitting ratio of up to 10-20% / °C and the insertion loss increasing from less than 1dB to greater than 10dB over a period of a few months (9).

Attempts to stabilise the etched coupler with either a curable rubber compound or a silica glass gel potting technique had some measure of success (1). However, the process proved too cumbersome and was superceded by other approaches.

2.4.1.3 Semi-circular fibre or D-fibre couplers

Because of the critical tolerances in etching, machining and aligning the fibres in the above two techniques, an alternative approach based on the machining of the preform prior to fibre drawing and coupler construction was proposed (11).

The preform from which the fibre is drawn is ground parallel to the core. This means that the core is close to the flattened surface. Over a certain range of drawing temperatures the drawn fibre has a D-shaped cross-section like that of the preform.

The coupler is formed by aligning the flat faces of the

fibres over a short distance. The fibres are then fixed using a polysilicone coating (11), or a glass capilliary collapsed onto the aligned fibres (12) as in Figure 2.4 or even by permanently arc-fusing the two fibres together (11).

Generally the D-shaped fibre has some linear birefringence, with the birefringent axes lying parallel and perpendicular to the flat surface, so that the couplers can have polarisation maintaining ability with no axis alignment problems (12,13).

The losses have been less than 0.2dB. Long term stability has not been reported but should be excellent if the fibres are permanently arc fused together or if the fibres are permanently held in a collapsed glass capilliary.

One of the main problems with the D-fibre coupler is the difficulty of reliably splicing the D-fibre to conventional circular fibre for low loss. Special tools and handling procedures would also have to be developed for the special D-fibre.

2.4.1.4 Double core fibres

A fibre with two cores has been used to achieve distributed evanescent coupling along the length of the fibre (14,15,16). Again, machining and core alignment are carried out on the fibre preform so that tolerances for the core spacings are much less critical than in the other evanescent couplers described above.

Launching (and extraction) of light simultaneously into (from) both cores (spacing approximately 10μm) is very difficult. However, some applications require the launching (and extraction) of light into (from) only one core (15). In these cases, one of the cores is disposed in the centre of the fibre and the second off-centre so that splicing to standard fibres is easy and reliable (15). Spectral filters have been constructed from the concatenation of double core and single core fibres (15). Such fibres have also been proposed for sensor applications since the extent of coupling will depend on external fibre perturbations (14-16) such as bends and twists.

2.4.2 Cladding mode couplers

The mechanism of cladding mode coupling will be described in detail in Chapter 6. Cladding mode couplers rely on the tapering of the fibre and, for reasons outlined in Chapter 4, only a very restricted set of fibres can be conveniently tapered with low loss (21). Fortunately, the matched cladding fibres used for telecommunications are suitable for tapering and are therefore employed in cladding mode couplers.

Tapers are formed by heating the fibre and then pulling to the desired length.

On tapering a single-mode fibre, the core diameter as well as the cladding diameter decreases. The fundamental mode field expands out of the core and quickly becomes

guided at the contracting cladding boundary (17,18).

2.4.2.1 Biconical pretaper couplers

This coupler is formed by joining two tapered fibres together, with an adhesive having a refractive index lower than silica (40), as shown in Figure 2.5. These couplers have not proved very stable because of the difficulty in maintaining contact between the fibres, and the technique has become superceded for single-mode fibres by the fusing and tapering of two fibres together as described in the next section.

The pretapering of one fibre prior to its fusion to an untapered fibre and the subsequent tapering of both together has led to a fused taper coupler with wavelength insensitive characteristics (41). This coupler will be discussed in the same context as the fused taper couplers.

2.4.2.2 Fused tapered couplers

By far the most popular single-mode fibre coupler is the fused taper coupler. In this coupler the two fibres, stripped of primary coating, are twisted together, heated and then pulled into a biconic taper (42-62) as shown in Figure 2.6. During heating and pulling the fibres fuse together forming a very stable and secure contact. Details of coupler fabrication and packaging will be described in Chapter 3 of this thesis.

The fused taper coupler has proved to be very stable

over long periods of time and over a wide temperature range, and to have very little excess loss (42-62). The power splitting ratio is wavelength dependent but in production a desired splitting ratio can be achieved at any wavelength. As with the polished coupler, the wavelength dependence of taper couplers has also been used for spectral conditioning (57,58,62). Limited success of tuning the device by bending the coupling region has been reported (61).

The fused taper coupler has proved very attractive for the mass production of stable compact low loss devices. Fibre preparation prior to fabrication is minimal and coupler fabrication straightforward, with a high success rate. The investment in fabrication and measurement equipment can be very low.

The technique has so far been limited to matched cladding fibres, but by careful fibre design polarisation maintaining fused taper couplers can be made (63,64).

2.5 General Features of Single-Mode Directional Couplers

There exists a considerable body of literature on the topic of single-mode (fibre and integrated optic) directional couplers (23,65-70). A coupler is shown schematically in Figure 2.7(a) and consists of five distinct regions:

A = optically isolated input ports 1 and 2

B = input transition region

C = parallel waveguide coupling region

D = output transition region

E = optically isolated output ports 3 and 4.

Most treatments of couplers restrict themselves to analysing the parallel coupling region (Region C in Figure 2.7(a)) only. Coupling is described by the interaction between the modes of the two waveguides taken in isolation, or more simply by the interference between the two normal modes of the parallel composite two waveguide structure (3), as shown in Figure 2.7(b).

In order to effect power transfer between the two waveguides, both normal modes must be present. Since the two normal modes in general travel with different phase velocities, they can interfere with one another to set up a standing or "beat" wave pattern. Power transfer is thus effected by the interference of these two normal modes and for this reason such couplers are known as "mode interference directional couplers" (66). If for example a 100% coupler is desired, that is, complete power transfer from one waveguide to another, the coupler is ended after half a "beat" length (or this length plus an integral number of beat lengths). Similarly, if a 3dB coupler is desired, that is a 50-50 power division between the two waveguides, the coupler is ended after one-quarter of a beat length (or this length plus an integral number of half beat lengths). Since such couplers depend on interference of normal modes to effect power transfer they are inherently wavelength

dependent (66).

2.5.1 Coupling Coefficients

When two dielectric waveguides are placed alongside each other, the introduction of the second waveguide distorts the field distributions of the guided modes in the first waveguide. In the case of weak coupling the assumption is made that each waveguide mode distribution remains unperturbed. In any case the unperturbed fields of each waveguide can be expressed as a linear combination of the fields of the two-waveguide system (3).

Let ψ_1 and ψ_2 be the fundamental modes of the two decoupled (or optically isolated) identical waveguides, and ψ_e and ψ_o the exact lowest order even and odd normal modes in the coupling region. All the modes are normalised to unit power. For unit power into port 1 and assuming the simplest case of weak-coupling, the field at the coupler input can be written as follows:-

$$\psi_1 = \frac{1}{\sqrt{2}} (\psi_e + \psi_o) \qquad (2.1)$$

At a distance z along the coupling region the total field ψ_T is given by:-

$$\psi_T = \frac{1}{\sqrt{2}} \left\{ \psi_e e^{-i\beta_e z} + \psi_o e^{-i\beta_o z} \right\} \qquad (2.2)$$

The output field, after a coupling length of L, is

$$\psi_{out} = \frac{1}{\sqrt{2}} \left\{ \frac{1}{\sqrt{2}} (\psi_1 + \psi_2) \right\} e^{-i\beta_e L}$$

$$+ \frac{1}{\sqrt{2}} \left\{ \frac{1}{\sqrt{2}} (\psi_1 - \psi_2) \right\} e^{-i\beta_o L} \qquad (2.3)$$

$$= \frac{1}{2} \left\{ \psi_1 (1+e^{+i\Delta\beta L}) + \psi_2 (1-e^{+i\Delta\beta L}) \right\} e^{-i(\beta+\frac{\Delta\beta}{2})L} \qquad (2.4)$$

where $\Delta\beta = (\beta_e - \beta_o)$, and $\beta = (\beta_e + \beta_o)/2$

The power in the output ports, for unit input power, will be:-

$$p_3 = \frac{1}{2} (1+ \text{Cos}\Delta\beta L) = \text{Cos}^2 \frac{\Delta\beta}{2} L \qquad (2.5)$$

$$p_4 = \frac{1}{2} (1- \text{Cos}\Delta\beta L) = \text{Sin}^2 \frac{\Delta\beta}{2} L \qquad (2.6)$$

Equations 2.5 and 2.6 describe the periodic interchange of power between the two waveguides in the coupler as the length of the coupler is varied. The coupling coefficient C of the coupler is defined as (65-67)

$$C = \Delta\beta/2 = (\beta_e - \beta_o)/2 \qquad (2.7)$$

which is simply one half of the difference in the propagation constants of the even and odd normal modes.

In general C is wavelength dependent and equations 2.5 and 2.6 indicate that the output powers must vary periodically with wavelength as shown schematically in Figure 2.8. The period or wavelength channel spacing $\Delta\lambda$ will, in general, itself be wavelength dependent and will

be given by

$$\Delta\lambda = \pi / \left| \frac{\delta C}{\delta \lambda} \right| \qquad (2.8)$$

2.5.2 Polarisation Effects

In the above discussion we have not mentioned the polarisation properties of the light. The symmetry of the coupler indicates that the even and odd modes can each have two orthogonal polarisations which we shall call x and y. (8,19,20,22,24-26). We must specify coupling coefficients C_x and C_y corresponding to light input with either x or y polarisations. The output powers will then be

$$\begin{aligned} p_3^x &= \cos^2 C_x L & p_4^x &= \sin^2 C_x L \\ p_3^y &= \cos^2 C_y L & p_4^y &= \sin^2 C_y L \end{aligned} \qquad (2.9)$$

The coupling coefficients are still given by equation 2.7 but with the phase shifts referred to the appropriate polarisations. In general C_x and C_y will be different and this has some very interesting consequences. Let it be assumed that a coupler can be made so that C_x and C_y satisfy the following relations (8,9,20,24,53,57-60).

$$C_x = n\pi/L \qquad C_y = (m + \tfrac{1}{2})\pi/L \qquad (2.10)$$

where m and n are integers. Then, for unit power into port port 1, the output powers corresponding to the two possible polarisations are

$$\begin{aligned} p_3 &= 1 & p_3 &= 0 \\ p_4 &= 0 & p_4 &= 1 \end{aligned} \qquad (2.11)$$

This means that x- polarised light emerges completely from port 3 and y- polarised light emerges from port 4. This property will cause the coupler to act as a polarising beamsplitter, with unpolarised light in port 1 being split equally into x and y components at ports 3 and 4.

The power in port 3 is given by

$$p_3 = (\mathrm{Cos}^2 C_x L + \mathrm{Cos}^2 C_y L)/2 \qquad (2.12a)$$

which can be rewritten as

$$p_3 = [1 + \mathrm{Cos}\ (C_x + C_y)\ L\ \mathrm{Cos}(C_x - C_y)\ L]/2 \qquad (2.12b)$$

If C_x and C_y are wavelength dependent then p_3 must have a modulated periodic response as indicated in Figure 2.9, the modulation minima corresponding to the polarisation beamsplitting points. The two periods $\Delta\lambda$ (oscillation period) and $\delta\lambda$ (polarisation modulation period) as indicated in Figure 2.9 are given by

$$\Delta\lambda = 2\pi/|\delta(C_x + C_y)/\delta\lambda| \qquad (2.13)$$

$$\delta\lambda = \pi/|\delta(C_x - C_y)/\delta\lambda| \qquad (2.14)$$

Other polarisation control devices can also be achieved with couplers e.g. half-wave and quarter-wave devices (71). The conditions for achieving these devices are summarised in Table 2.1.

References to Chapter 2

1. D.C. Tran, K.P. Koo and S.K. Sheem:
"Single-mode fiber directional couplers fabricated by twist-etching techniques",
IEEE J. Quant. Electron., 1981, QE-17,
pp. 988-991.

2. M.J.F. Digonnet and H.J. Shaw:
"Analysis of a tunable single-mode optical fiber coupler",
IEEE J. Quantum Electron., 1982, QE-18,
pp. 746-754.

3. A.W. Snyder and J.D. Love:
"Optical Waveguide Theory".
Chapman and Hall (London, New York), 1983.

4. R.A. Bergh, G. Kotler and H.J. Shaw:
"Single-mode fibre optic directional coupler",
Electron. Lett., 1980, 16, pp. 260-261.

5. O. Parriaux, S. Gidon and S.S. Kuznetsov:
"Distributed coupling on polished single-mode optical fibers",
Appl. Opt., 1981, 20, pp. 2420-2423.

6. B.K. Nayar and D.R. Smith:
"Monomode-polarisation-maintaining fiber directional couplers",
Opt. Lett., 1983, 8, pp. 543-545.

7. P. Jaccard, B. Scheja, H. Berthou, F. Cochet, O. Parriaux and A. Brugger:
"A new technique for low cost all-fiber device fabrication",
SPIE., 1984, 479, pp. 16-19.

8. A.W. Snyder and A. Stevenson:
"Polarisation splitters and birefringent couplers",
Electron. Lett., 1985, 21, pp. 75-77.

9. S.K. Sheem and T.G. Giallorenzi:
"Single-mode fiber-optical power divider: encapsulated etching technique",
Opt. Lett., 1979, 4, pp. 29-31.

10. S.K. Sheem, H.F. Taylor, R.P. Moeller and W.K. Burns:
"Propagation characteristics of single-mode evanescent field couplers",
Appl. Opt., 1981, 20, pp. 1056-1059.

11. G. Schoner, E. Klement, G. Schiffner and N. Douklias:
"Novel method for making single-mode optical fibre directional couplers",
Electron. Lett., 1982, 18, pp. 566-568.

12. R.B. Dyott and J. Bello:
"Polarisation-holding directional coupler made from

elliptically cored fibre having a D section",
Electron. Lett., 1983, 19, pp.601.

13. R.B. Dyott, V.A. Handerek and J. Bello:
"Polarisation holding directional couplers using D fiber",
SPIE., 1984, 479, pp. 23-27.

14. G. Schiffner, H. Schneider and G. Schoner:
"Double-core single-mode optical fiber as directional coupler",
Appl. Phys., 1980, 23, pp. 41-45.

15. K. Okamoto and J. Noda:
"Fibre-optic spectral filters consisting of concatenated dual-core fibres",
Electron. Lett., 1986, 22, pp. 211-212.

16. C.M. Truesdale and D.A. Nolan:
"Core/clad mode coupling in a new multiple-index waveguide structure",
Tech. Digest ECOC, Barcelona, 1986.

17. J. Bures, S. Lacroix and J. Lapierre:
"Analyse d'un coupleur bidirectionnel a fibres optiques monomodes fusionees",
Appl. Opt., 1983, 22, pp. 1918-1922.

18. F.P. Payne, C.D. Hussey and M.S. Yataki:
"Modelling fused single-mode-fibre couplers",

Electron. Lett., 1985, 21, pp. 461-462.

19. F.P. Payne, C.D. Hussey and M.S. Yataki:
"Polarisation analysis of strongly fused and weakly fused tapers couplers",
Electron. Lett., 1985, 21, pp. 561-563.

20. F.P. Payne, C.D. Hussey and M.S. Yataki:
"Polarisation in fused single-mode fibre couplers",
Tech. Digest IOOC/ECOC, Venice, 1985, pp. 571-573.

21. W.J. Stewart and J.D. Love:
"Design limitation on tapers and couplers in single-mode fibres",
Tech. Digest IOOC/ECOC, Venice, 1985, pp. 559-562.

22. J.D. Love and M. Hall:
"Polarisation modulation in long couplers",
Electron. Lett., 1985, 21, pp. 519-521.

23. J.V. Wright:
"Variational analysis of fused tapered couplers",
Electron. Lett., 1985, 21, pp. 1064-1065.

24. A.W. Snyder:
"Polarising beamsplitter from fused taper couplers",
Electron. Lett., 1985, 21, pp. 623-625.

25. A.W. Snyder and X.H. Zheng:

"Optical fibres of arbitrary cross-sections",
Electron. Lett., 1985, 21, pp. 1079-1080.

26. A.W. Snyder and X.H. Zheng:
"Optical fibers of arbitrary cross-sections",
J.Opt. Soc. Amer., 1986, A3, pp. 600-609.

27. J.D. Love and W.M. Henry:
"Quantifying loss minimisation in single-mode fibre tapers",
Electron. Lett., 1986, 22, pp. 912-914.

28. F.P. Payne, T. Finnegan, M.S. Yataki, R.J. Mears and C.D. Hussey:
"Dependence of fused taper couplers on external refractive index",
Electron. Lett., 1986, 22, pp. 1207-1209.

29. O. Parriaux, S. Gidon and A.A. Kuznetsov:
"Distributed coupling on polished single-mode optical fibers",
Appl. Opt., 1981, 20, pp. 2420-2423.

30. York V.S.O.P. Catalogue:
"Single-mode polarisation-preserving coupler",
5/85.

31. S. Tai, K. Kyuma and K. Hamanaka:
"Polarisation maintaining optical fiber directional coupler",

IECEE. (Japan) National Convention Record, 1986, pp.854.

32. B.Y. Kim:
Private communication.

33. S.T. Nicholls:
"Automatic manufacture of polished single-mode fibre directional coupler",
Electron. Lett., 1985, 21, pp. 825-826.

34. B.F. Lamouroux, A.G. Orszag, B.S. Prade and J.Y. Vinet:
"Continuous laser amplification in a monomode fiber longitudinally pumped by evanescent field coupling",
Opt. Lett., 1983, 8, 504-505.

35. W.V. Sorin, K.P. Jackson and H.J. Shaw:
"Evanescent amplification in a single-mode optical fibre",
Electron. Lett., 1983, 19, pp. 820-822.

36. W.V. Sorin and M.H. Yu:
"Single-mode-fiber ring dye laser",
Opt. Lett., 1985, 10, pp. 550-552.

37. W. Eickhoff:
"In-line fibre-optic polariser",
Electron. Lett., 1980, 16, pp. 762-764.

38. W.V. Sorin and H.J. Shaw:
"Single-mode fibre evanescent grating reflector",
Tech. Digest OFS, 1984, pp. 132.

39. B.K. Nayar, R. Kashyap and K.I. White:
"Electro-optic monomode fibre devices with liquid crystal overlays",
Tech. Digest ECOC Barcelona, 1986.

40. T. Ozeki and B.S. Kawasaki:
"Optical directional coupler using tapered sections in multimode fibres",
Appl. Phys. Lett., 1976, 28, pp. 528-529.

41. D.B. Mortimore:
"Wavelength-flattened fused couplers",
Electron. Lett., 1985, 21, pp. 742-743.

42. C.A. Villarruel and R.P. Moeller:
"Fused single mode fibre access couplers",
Electron. Lett., 1981, 17, pp. 243-244.

43. B.S. Kawasaki, K.O. Hill and R.G. Lamont:
"Biconical-taper single-mode fiber coupler",
Opt. Lett., 1981, 6, pp. 327-328.

44. M. Kawachi, B.S. Kawasaki and K.O. Hill:
"Fabrication of single-polarisation single-mode-fibre couplers",
Electron. Lett., 1982, 18, pp. 962-964.

45. C.A. Villarruel, M. Abebe and W.K. Burns:
"Birefringence correction for single-mode fiber couplers",
Opt. Lett., 1982, 7, pp. 626-628.

46. C.A. Villarruel, M. Abebe and W.K. Burns:
"Polarisation preserving single-mode-fibre coupler",
Electron. Lett., 1983, 19, pp. 17-18.

47. B.S. Kawasaki, M. Kawachi, K.O. Hill and D.G. Johnson:
"A single-mode-fiber coupler with a variable coupling ratio",
J. Lightwave Tech., 1983, LT-1, pp. 176-178.

48. C.M. Ragdale, D.N. Payne, F. De Fornel and R.J. Mears:
"Single-mode fused biconical taper fibre couplers",
Presented at Optical Fibre Sensor Conference, IEE., London, 1983, pp. 75-78.

49. T. Bricheno and A. Fielding:
"Stable low-loss single-mode couplers",
Electron. Lett., 1984, 20, pp.230-232.

50. J. Bures, S. Lacroix and C. Veilleux:
"Some particular properties of monomode fused fiber couplers",

Appl. Opt., 1984, 23, pp. 968-969.

51. C.M. Ragdale, M.H. Slonecker and J.C. Williams:
"Review of fused single-mode coupler technology",
SPIE., 1984, 479, pp. 2-8.

52. P.M. Kopera, H.H.A. Krueger, V.J. Tekippe and
D.L. Wuensch:
"Performance evaluation of single-mode couplers",
SPIE., 1984, 479, pp. 9-15.

53. I. Yokohama, K. Okamoto, M. Kawachi and J. Noda:
"Polarising fibre coupler with high extinction
ratio",
Electron. Lett., 1984, 20, pp. 1004-1005.

54. R.G. Lamont, K.O. Hill and D.C. Johnson:
"Tuned-port twin biconical-taper fiber splitters:
fabrication from dissimilar low-mode-number
fibers",
Opt. Lett., 1985, 10, pp. 46-48.

55. M.S. Yataki, M.P. Varnham and D.N. Payne:
"Fabrication and properties of very-long fused
taper couplers",
Tech. Digest OFC, San Diego, 1985, pp. 108-110.

56. R.G. Lamont, D.C. Johnson and K.O. Hill:
"Power transfer in fused biconical taper single-
mode fiber coupler: dependence on external
refractive index",

Appl. Opt., 1985, 24, pp. 327-331.

57. M.S. Yataki, M.P. Varnham and D.N. Payne:
"All-fibre polarising beam splitter and spectral filter",
Presented at IEE Colloquium "Advances in Coherent Optic Devices and Technologies", IEE, London, 1985.

58. M.S. Yataki, D.N. Payne and M.P. Varnham:
"All-fibre wavelength filters using concatenated fused-taper couplers",
Electron. Lett., 1985, 21, pp. 248-249.

59. M.S. Yataki, D.N. Payne and M.P. Varnham:
"All-fibre polarising beamsplitter",
Electron. Lett., 1985, 21, pp. 249-250.

60. T. Bricheno and V. Baker:
"All-fibre polarisation splitter/combiner",
Electron. Lett., 1985, 21, pp. 251-252.

61. R.G. Lamont, K.O. Hill and D.C. Johnson:
"Tuned-port twin biconical-taper fiber splitters: fabrication from dissimilar low-mode-number fibers",
Opt. Lett., 1985, 10, pp. 46-48.

62. K.O. Hill, D.C. Johnson and R.G. Lamont:
"Wavelength dependence in fused biconical taper couplers: measurement and control",
Tech. Digest IOOC/ECOC, Venice, 1985,

pp. 567-570.

63. M. Kawachi, B.S. Kawasaki, K.O. Hill and T. Edahiro:
"Fabrication of single-polarisation single-mode-fibre couplers",
Electron. Lett., 1982, 18, pp. 962-964.

64. I. Yokohama, M. Kawachi, K. Okamoto and J. Noda:
"Polarisation-maintaining fibre couplers with low excess loss",
Electron. Lett., 1986, 22, pp. 929-930.

65. W.H. Louisell:
"Coupled mode and parametric electronics",
John Wiley & Sons, 1960.

66. W.H. Louisell:
"Analysis of the single tapered mode coupler",
Bell System Tech. J., 1955, 34, pp. 853-870.

67. A. Yariv:
"Introduction to optical electronics",
Holt, Rinehart and Winston Inc. (New York) 1971.

68. A.W. Snyder:
"Coupled-mode theory for optical fibers",
J. Opt. Soc. Am., 1972, 62, pp. 1267-1277.

69. P.D. McIntyre and A.W. Snyder:
"Power transfer between optical fibres",

J. Opt. Soc. Am., 1973, 63, pp. 1518-1527.

70. W. Wijngaard:
"Guided normal modes of two parallel circular dielectric rods",
J. Opt. Soc. Am., 1973, 63, pp. 944-950.

71. Y. Namihira, S. Ryn, S. Yamamoto and K. Mochizuki,
"Fused-taper-twisted single-mode fibre couplers as a quarter-wave device",
Tech. Digest 4th OFS, pp.351-354, 1986.

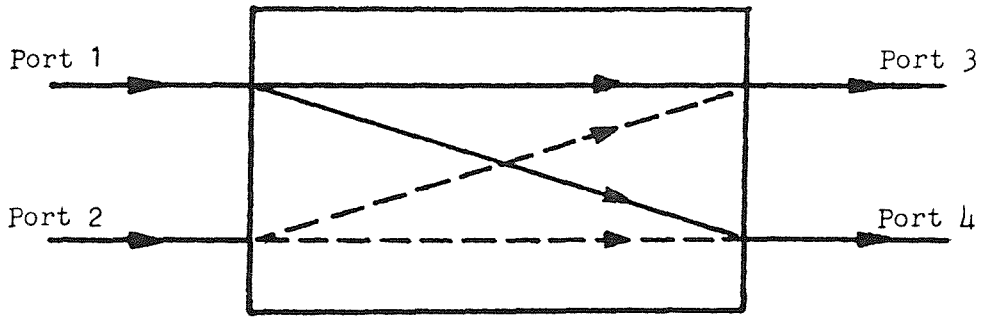

Figure 2.1. Schematic of a 4-port directional coupler showing the port number convention adopted in this thesis.

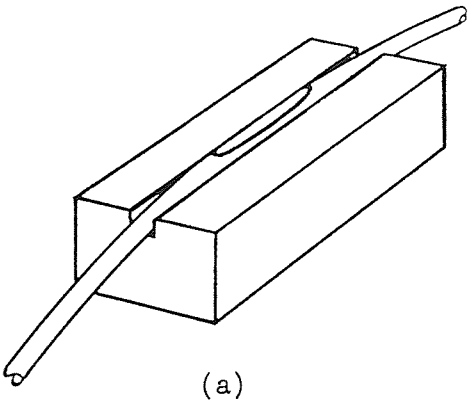

(a)

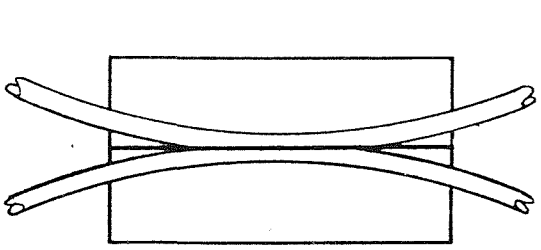

(b)

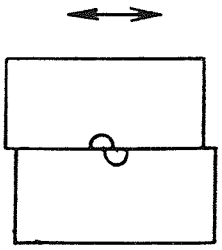

(c)

Figure 2.2. Polished coupler assembly.
(a) Single polished block.
(b) Two blocks aligned for coupling.
(c) Tunability achieved by sideways movement of one block.

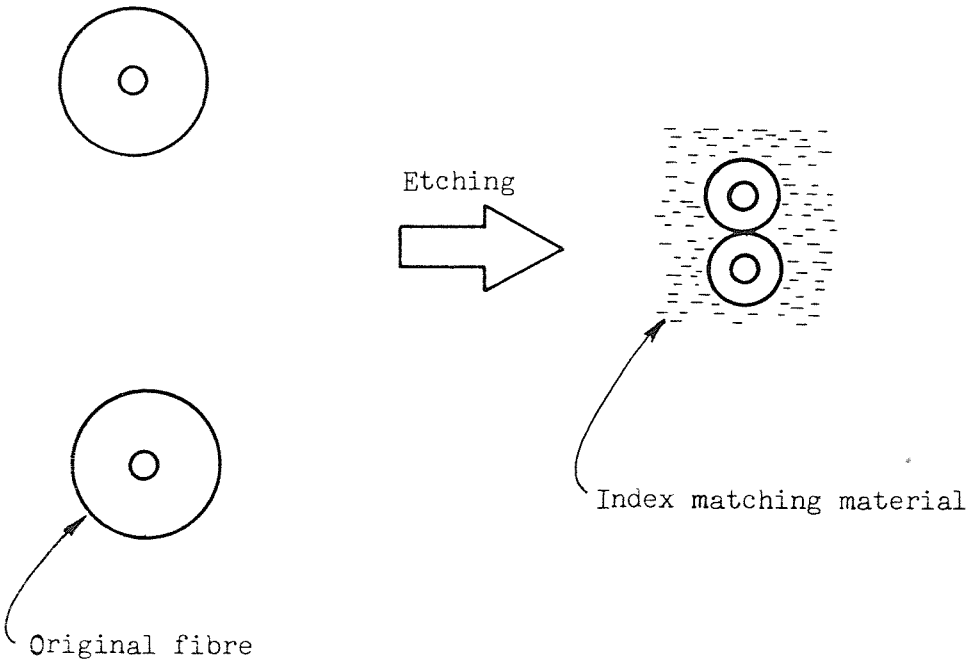

Figure 2.3. Etched fibre coupler fabrication process.

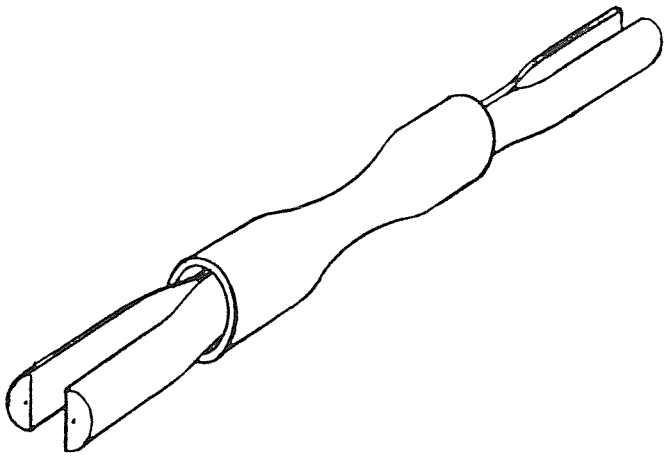

Figure 2.4. D-fibre coupler showing the configuration of the fibers in the collapsed glass capillary.

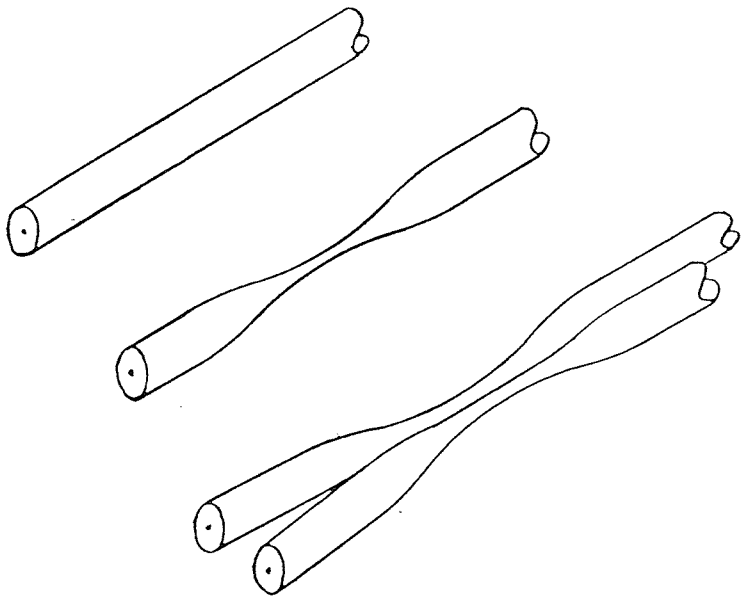

Figure 2.5. Construction of pretaper coupler.

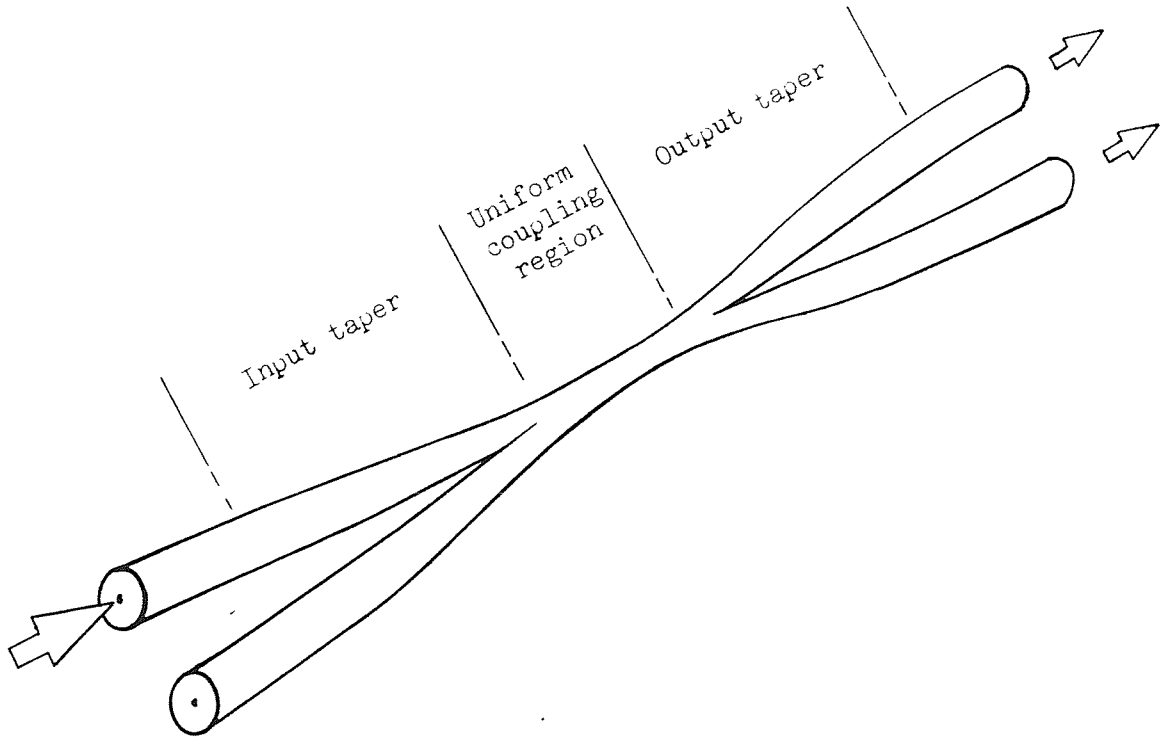

Figure 2.6. Structure of the fused taper coupler.

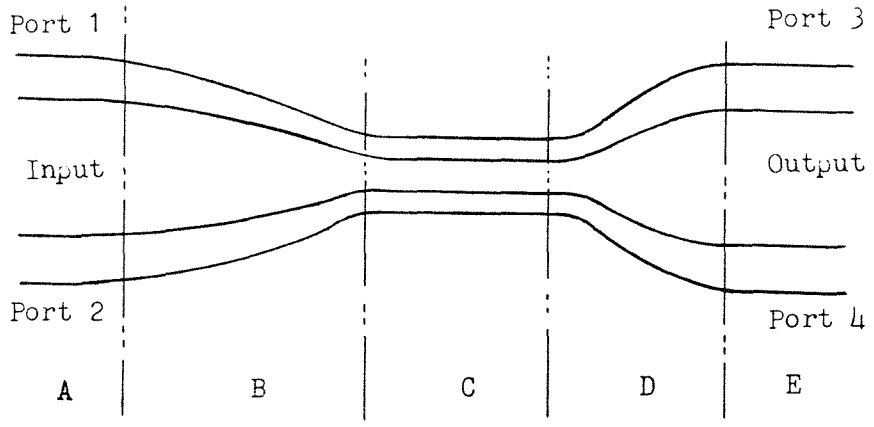

(a)

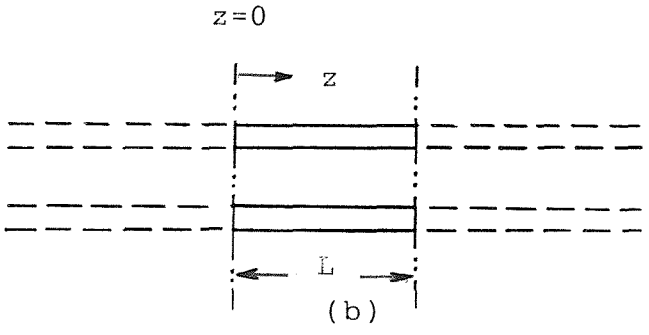

(b)

Figure 2.7. (a) Schematic of a complete coupler showing optically isolated input (A) and output (E) ports, input (B) and output transitions (D) and the uniform coupling region (C).

(b) Configuration used for analysis showing a section of an infinitely long parallel two waveguide structure.

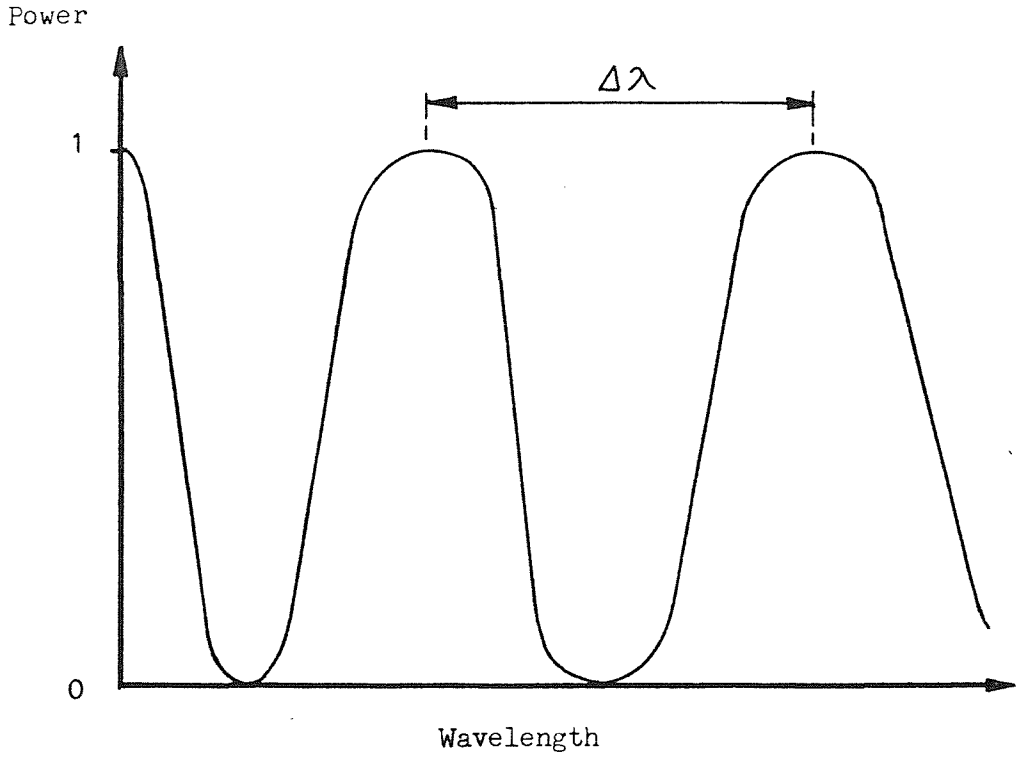

Figure 2.8. Schematic representation of the spectral dependence of a coupler.

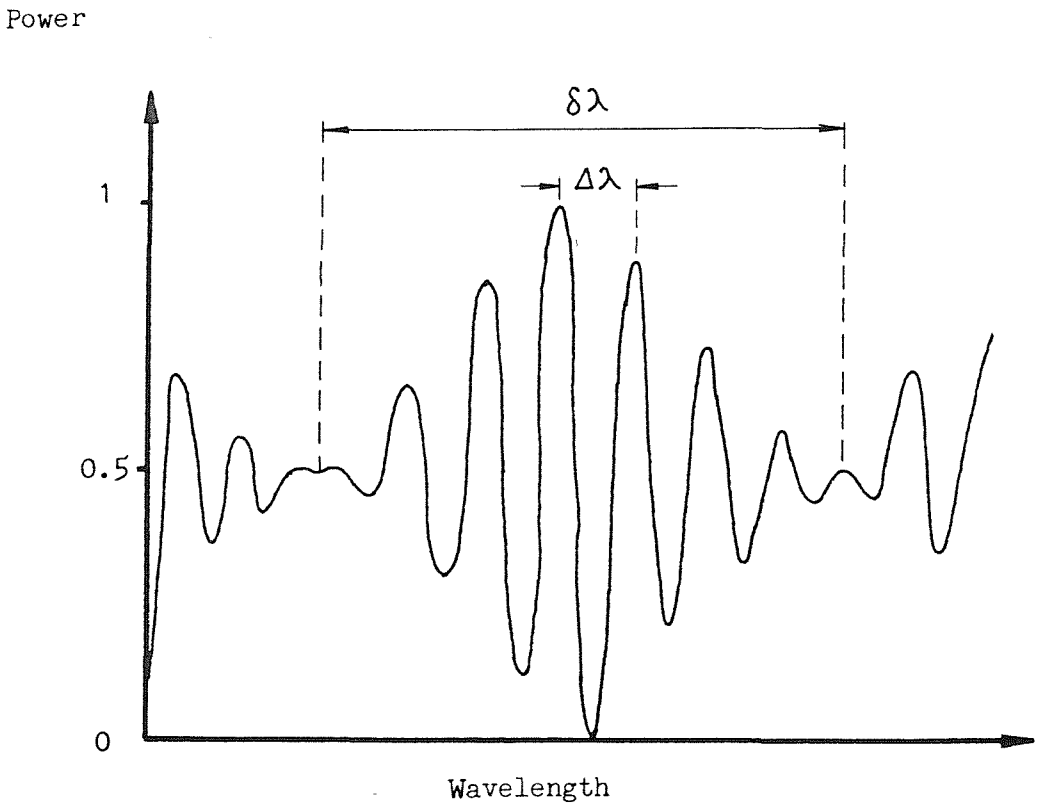

Figure 2.9. Schematic representation of the spectral dependence of a polarising beam splitter coupler.

Functions	Polarising beam splitter		Phase delay device	
Phase	Required conditions			
$\lvert \beta_e^x - \beta_o^x \rvert z$	$2m\pi$	$(2m-1)\pi$	$2m\pi$	$(2m-1)\pi$
$\lvert \beta_e^y - \beta_o^y \rvert z$	$(2n-1)\pi$	$2n\pi$	$2n\pi$	$(2n-1)\pi$
Input polarisation state	Output ports			
			Output ports depend on the phase delay	
X-polarisation	3 only	4 only	(3 only)	(4 only)
Y-polarisation	4 only	4 only	(3 only)	(4 only)
X & Y-polarisation	3 and 4	3 and 4	(3 only)	(4 only)
			Phase delay $\{(\beta_e^x + \beta_o^x)/2 - (\beta_e^y + \beta_o^y)/2\}z$ Special cases as above $=(2l+1)\pi/2$	

Table 2.1. Some ideal conditions to achieve polarisation control devices. m,n and l = 1,2,3,4,5....

CHAPTER 3: FABRICATION, PACKAGING AND RELIABILITY TESTING OF FUSED TAPER COUPLERS

3.0 Prologue:

This chapter discusses the fabrication and packaging of the fused taper coupler which results in a viable device suitable for both research and mass production by satisfying the criteria outlined in Chapter 2.

The design analysis of the coupler fabrication system is described, and a simple yet new fabrication technique is developed. The package design for a rugged and stable component is also presented together with test results for temperature and vibration stability and long term reliability of the coupler.

3.1 Introduction

The fused taper coupler requires the two fibres to be fused and tapered longitudinally as shown in Figure 3.1. Typically, the tapering reduces the fibre dimension by at least a factor of three, and causes the optical field to be guided at the external boundary of the fibre.

As shall be seen in later chapters (with reference to Figure 3.1), the input and output taper angles, the length of the coupling region, the taper ratio and the degree of fusion are all critical factors in determining the loss and overall performance of the coupler. The control of these factors puts a strict requirement on the fabrication technique.

In this chapter a design exercise is undertaken in order to develop a straightforward taper coupler fabrication technique. This exercise leads to a very simple gravity pulling method which is not only suitable for mass production but is also flexible and adaptable enough for the research purposes of this thesis.

The fused taper coupler is inherently stable with temperature, since the fibres are permanently fused together. However, the small dimensions of the tapered region and the maintenance of a clean and optically guiding external boundary puts a severe requirement on the package of the device for it to have complete environmental stability and long term reliability. The design and testing of a suitable package is undertaken in the latter half of this chapter.

3.2 Fabrication System Design

These are several essential operations required in the overall coupler fabrication system. These operations are listed as follows:

(i) fibre preparation
(ii) fibre holding
(iii) fibre heating
(iv) fibre fusing
(v) fibre tapering
(vi) optical monitoring
(vii) coupler packaging

These operations have been pin-pointed through the use of the FAST (Function Analysis System Technique) diagram method (1,2). The complete FAST diagram for fused taper coupler fabrication is drawn in Figure 3.2 with the essential operations indicated in the heavy lined boxes.

The above operations are elementary, but are fundamental to the process. The optical monitoring can take place throughout the whole process, even at the packaging stage. The fibre preparation and coupler packaging can be carried out separately from the other operations. Both tapering and fusing must take place while the fibres are held and heated. In the simplest case, the four operations of holding, heating, tapering and fusing are performed simultaneously as indicated Figure 3.3. Alternatively, the tapering and fusing can be performed separately as indicated in Figure 3.4. In the latter case the overall process becomes more complex because the tapering and fusing operations must have their own independent holding and heating operations, so that the holding and heating would need to be duplicated in consecutive stages of the fabrication process. Such duplication may be required for special purposes; for example, in the fabrication of wavelength insensitive couplers (3) by pretapering one fibre prior to the normal fusing and tapering operations. For the purposes of the research work in this thesis it was decided that the holding, heating, fusing and tapering operations

would, however, be carried out simultaneously as in Figure 3.3.

3.2.1 Fabrication Control Parameters

Since the four control operations are to be carried out simultaneously it is necessary to coordinate the entire operation carefully. Table 3.1(a) is a list of the important variables involved in the holding, heating, fusing and tapering operations, while Table 3.1(b) shows the inter-relation of these parameters. Inevitably, some of the variables may be involved in more than one operation so that the control of the whole process may be complicated. It is important, therefore, to determine the most important parameters.

By generating a Polya-Fuller map (4,5), which is constructed in Figure 3.5 by joining common parameters listed in Table 3.1 together, the importance of the drawing force N is revealed.

The drawing force, N, is linked to all four simultaneous operations, so that the four operations need to be coordinated through this parameter.

A change in any parameter within the four operations will cause a disruption in the other three operations, because of the linkage through the drawing force. However, if the drawing force is maintained constant or under strict control, the four operations may be designed individually.

Clearly, special attention needs to be paid to the drawing force in the design of the fabrication apparatus.

3.2.1.1 Dynamic Analysis of Tapering Operation

Since the fibres have to be tapered longitudinally to form the coupler, the tapering operation requires a linear motion. The dynamics of two different types of linear motion control, variable-force control and constant-force control are investigated.

In the variable-force method, the drawing force generated must be sufficient to produce the necessary acceleration and velocity for the required motion. Conversely, in the constant-force method, the drawing force is intentionally maintained at the same level while the motion is taking place.

Because it controls the acceleration, the variable-force method can, at least in principle, produce any shape of taper. The constant-force method, on the other hand, requires a change in parameters outside of the tapering operation directly to produce a change in the taper shape, such as an alteration in the heater design.

The more detailed control analysis undertaken in Reference 6 indicates that the variable-force method is complicated in that its performance depends on having a feedback system which minimises the amount of sag in the fibre. In contrast, the constant-force method is found to be so simple that no dynamic control is required.

This comparison between the variable-force and the constant-force methods is summarised in Table 3.2.

3.3 Fabrication Process Development

The detailed design of a fabrication process for fused taper couplers based on the findings obtained in the previous sections will now be described. All essential operations are individually reviewed, with the condition that the four control operations are performed simultaneously.

3.3.1 Preparation

Generally, optical fibres for communication and sensor applications are coated to protect them from external abrasion. Most of the fibres used for the experiments were coated with a single urethane acrylate layer. This coated layer is easy to remove by a combination of mechanical and chemical means. It is necessary to remove the coating completely from that part of the fibre which is to be tapered and fused. The technique adopted was to immerse the fibre in a dichloromethane bath for approximately 30 seconds, Figure 3.6(a). The coating was then removed from approximately an 25 mm length with the fingers, Figure 3.6(b), and thoroughly cleaned with acetone.

3.3.2 Holding

The fibres must be kept as straight as possible during the entire thermal process. The simple method adopted was to hang the fibres vertically with a weight at the lower end

as shown in Figure 3.7. With the application of heat, the fibres are then tapered automatically. Alternatively, the fibres can be supported either vertically or horizontally at both ends, Figures 3.8 and 3.9. This arrangement required an initial tension to keep the fibres straight. This latter method was abandoned because it was difficult to prevent buckling of the fibres when they were heated.

3.3.3 Heating

The fundamental object of this operation is to heat the fibres to softening point so that fusing and tapering can take place. The softening temperature of silica (99.9%) glass is 1580°C, at which the viscosity is $10^{7.6}$ Poise (7). Three types of heat sources, namely electric arcs, electric furnaces and gas burners, were investigated.

3.3.3.1 Electric arc

Electric arc generators are widely used for fibre splicing. The arcs are instantaneous and localized, so that the timing of the application can be well controlled and the application region accurately defined. However, when an arc was used as the heat source for coupler fabrication, the tapers produced were very sharp. The resulting tapers and couplers suffered from high loss.

3.3.3.2 Electric furnace

Electric furnaces are widely used for fibre drawing and have gained an excellent reputation as clean and stable heat sources. For tapering applications, the fibre has to be

exposed to the heat source for a short time only, so that some form of timing control is essential. To switch the furnace on and off creates difficulties because of the thermal time lag caused by the large heat capacity of the furnace. An attempt was made to reduce the time-lag by using a strip of iridium so as to minimise the mass of the heat-generating element. However, the thermal energy obtained was not sufficient to soften the fibre without direct contact between the fibre and the element. A cylindrical element machined from graphite was found to give an adequate temperature. Nevertheless, the furnace required a purging arrangement to prevent oxidation of the heating element at the required temperature of around 1600°C. Water cooling on the outside of the furnace was also necessary. It was therefore concluded that the system was too bulky and impractical. In order to cope with this problem, the time-lag of the heat source would have to be taken into account in a rather complex way. An extensive study would be necessary to find the optimum parameters. In conclusion, the electric furnace was not adopted for the work described here, which required quick and simple fabrication with various types of fibre.

3.3.3.3 Gas burner

A gas burner provided a steady heat source when combined with a stable gas flow, and was found to be the most suitable heat source for this study because of its ease of handling and its stability.

A hydrogen-oxygen burner generated a sufficiently hot flame for fabrication to be performed rapidly. One disadvantage of this burner was that the flame tended to run back inside the burner due to the high combustion speed of hydrogen (approximately 3 m/sec) (7). This caused a small explosion in the burner and the extinguishing of the flame. Higher flows of the gases could alleviate this problem but then the high gas velocity would cause the fibre to break during the softening process. As a result, the hydrogen-oxygen gas burner was not used. However, it may be suitable for couplers made of large fibres, for many-fibre couplers, and where rapid fabrication is required.

A butane (combustion speed approximately 0.4 m/sec (7))- oxygen burner provided a small, stable flame of adequate temperature which did not necessitate a sophisticated device to control the timing of its application. In fact, the control was performed by removing the flame from the fibres manually.

3.3.4 Fusing

The fused taper coupler requires good fusion between the two fibres which, in turn, requires good fibre contact prior to fusion; therefore a force holding the fibres together is necessary during fabrication.

It was found that twisting the two fibres together in the preparation stage and pulling axially, as shown in Figure 3.10(a), was sufficient to provide an adequate

contracting force without causing any other difficulties.

The twist may be harmful for couplers made of polarization-maintaining fibres such as "Bow-Tie" fibres, since the twist disturbs the polarisation axis alignment between the two fibres. An attempt was made to produce fusion in untwisted fibres lying in the same plane. This method required a precise curvature of the fibres' arcs in air, Figure 3.10(b). The result showed promise but the success rate was low. The twisting method however was the simplest, and was therefore adopted for the purposes of this thesis.

It is clearly difficult to separate the degree of fusion from the extent of tapering, since the degree of fusion obtained depends not only on the initial size of the fibres but also on the intermediate sizes of the fibres as they are being tapered. Couplers with different degrees of fusion can, however, be obtained by varying the time the fibres are held in the heat with little or no drawing force applied.

3.3.5 Tapering

The fibres have to be tapered in such a way that the optical field is expanded and transferred laterally from one fibre to the other. Basically a force and a linear motion in the direction of the fibre axis are required for this drawing operation. As found in the Polya-Fuller map in Figure 3.5, many parameters are involved in this operation.

Obviously the control of the tapering operation can be simplified if as many of these parameters as possible can be kept constant.

The acceleration of the linear motion is zero before the motion starts, and takes positive and negative values while the operation is carried out. Similarly, neither the velocity of the motion nor the extent of the movement can be kept constant. Two parameters which can be constant are the drawing force and the duration of the tapering operation. Since the drawing force is involved in several other operations, as pointed out in Section 3.3.1, it is desirable to keep this drawing force as constant as possible.

In practice, the thermal energy supplied by the gas flame per unit time is constant, given that the gas flow is stable. Since the diameter of the fibre is decreasing, then the thermal energy received per unit volume per unit time is increasing, and softening therefore occurs more quickly. Using the motion control method the pulling speed must be increased in order to keep the tapered fibre straight in the flame.

Any sag during the process permanently deforms the taper and consequently causes high loss. If the fibres are fixed at two points as shown in Figures 3.8 and 3.9, then the tapering operation requires a precise speed and acceleration control. The speed must be modified instantaneously throughout the whole process by a closed-

loop feed-back apparatus monitoring the straightness of the taper.

3.3.5.1 Tapering Techniques

3.3.5.1.1 Motorised slide method

A motorised slide using either motion control stepping motors or analogue D.C. motors was studied. Acceleration of the motor speed was directly controlled, to generate a desired taper angle, by digital commands through a computer. Thus the drawing force was not controlled directly but depended on the movement required.

This open-loop system of fabricating couplers exhibited a very low success rate, for reasons discussed in Section 3.2.1.1. Most of the couplers made acquired a permanent curvature during the drawing operation, with an ensuing loss which makes this approach unsuitable for practical use.

Application of a slightly higher drawing speed, while yielding straight couplers, caused the fibres to break more frequently. Furthermore the fibres were inadequately fused, were easily separated, and gave insufficient power coupling.

It was found that the stepping-motor drive was unsuitable because it generated undesirable vibrations and intermittent linear motions.

While the analogue DC motor provided a smooth movement, the motor speed still needed to be closely controlled and

correlated with the other parameters of the system. Nevertheless, a feedback system capable of eliminating the sag could not be achieved, because a suitable sag detector was not available.

Consequently, the motorised slide scheme was abandoned because most attempts to fabricate couplers resulted in failure.

3.3.5.1.2 Gravity method - constant-force method

The fibres were held vertically at one point and pulled by a weight attached to the fibres as shown in Figure 3.7. This scheme did not need any sophisticated device to control the drawing force, and the fibres were drawn straight without the need for any speed-control apparatus. The speed was controlled by changing either the applied thermal energy or the size of the weight. When the coupler was pulled to the required length the gas flame was manually or electro-mechanically removed from the fibres, and the drawing process ceased. This method provided a perfect scheme for sag-free drawing with a virtual 100% success rate for very low-loss couplers.

There was an asymmetry between the taper angles at the upper and lower ends of the taper. However, the taper angles were independent of the taper length.

In addition, this constant-force method proved very flexible in its ready application to fibres of different

sizes and to couplers of various lengths, and so proved an ideal technique for coupler research.

3.4 Coupler Packaging

To package the fused taper coupler it is necessary to use materials and structures that will afford environmental isolation without imparting any significant stress on the coupling region.

For the low-expansion silica fibre coupler this means using materials with matched coefficients of thermal expansion - the most suitable being silica itself.

Starting with the fused taper coupler as in Figure 3.11(a), this is glued with an acrylic adhesive (Cemedine MC101) into a silica u-shaped rod with the coupler suspended in the centre of the u-shaped rod, as in Figure 3.11.(b). At this stage of packaging the coupler is kept under slight tension in order to keep the coupler straight.

The adhesive bond of the bare fibre to the silica substrate rod interface was obviously crucial in maintaining package integrity. Since the adhesive covered both bare and coated portions of fibre, a low temperature cure was necessary. The uncured adhesive must flow satisfactorily in the u-shaped rod and be rigid enough in the cured state to clamp the coupler securely. The chosen adhesive - Cemedine MC101 - proved equally strong and durable both before and after environmental tests.

To encapsulate the fused region itself there is the additional requirement that the material must have a sufficiently low refractive index to act as an optical cladding. It is possible to keep the coupler suspended in air but, as we shall see, this gives no mechanical protection against bump or vibration. The material chosen here was a silicone resin - Dow Corning 3-6527 - which has the required lower refractive index than silica (approximately 1.39 at 20°C). The resin provides excellent mechanical protection, is chemically inert and exhibits uniform properties over a wide temperature range. Its relatively high coefficient of thermal expansion is partly offset by its relatively low viscosity.

The coupler package, Figure 3.11(b), is then mounted in an aluminium or plastic box with the same adhesive - Cemedine MC101, as illustrated in Figure 3.11(c). This outer box provides mechanical strength for the coupler.

A photograph of the final coupler package is shown in Figure 3.12. It is this type of package which is subjected to the environmental tests discussed in the following section.

3.5 Environmental Stability and Reliability

It is only by subjecting the coupler to environmental tests that the stability and reliability of the package during development can be accessed. Tests undertaken on the coupler package were:-

(i) Temperature cycling

(ii) Vibration

(iii) Long term reliability

The results of which are now discussed.

3.5.1 Temperature Stability

Three different coupler types were examined in an environmental test chamber. The first coupler had the coupling region suspended in air while the other two were potted in a silicone rubber - Sylgard 184 - of nominal refractive index 1.42 at 20°C, and a silicone resin - Dow Corning 3-6527 - of nominal refractive index 1.39 at 20° C respectively.

The couplers were tested for the temperature range of -30°C to +80°C with increments of +10°C every 10 minutes. The sequence was repeated a number of times to ensure reliability of the measurements.

The results for the coupler with the coupling region suspended in air are shown in Figure 3.13. The coupler splitting ratio shows negligible variation with temperature, showing that there is no differential thermal expansion of the u-shaped rod, the adhesive and the coupler.

The results for the coupler potted in the silicone rubber are shown in Figure 3.14, with splitting ratio fluctuations of approximately ±1.0dB over the temperature cycling range. The silicone rubber seems to contribute two

effects to the change in splitting ratio. Firstly the refractive index reduces with increasing temperature, thereby causing a fluctuation in the waveguiding characteristics of the coupler, and secondly the rigidity of the rubber together with its large co-efficient of thermal expansion imparts a significant bending to the coupling region which varies with temperature.

In contrast with the coupler potted in silicone rubber the results for the coupler potted in silicone resin shown in Figure 3.15 are much more linearly related to temperature. The splitting ratio variation can be directly attributed to the decrease in refractive index of the resin with increase in temperature. Since the resin has no rigidity and will tend to flow around the coupler rather than bend the coupling region, there should be no fluctuation in splitting ratio due to bending effects.

3.5.2 Vibration Test

The coupler package is mounted on a mechanical vibrator whose frequency could be electrically varied from 300 Hz to 2200 Hz while maintaining a constant peak acceleration of 30 m/s^2.

Two couplers were tested. The first had its coupling region suspended in air and had a fundamental resonant frequency of 1000 Hz with a frequency band of approximately 20 Hz. The coupler optical outputs at resonance, as shown in Figure 3.16, oscillated at the resonant frequency. The

loss increase at resonance was estimated to be approximately 0.6dB.

The second coupler potted in silicone resin showed no disturbance whatsoever. The resin therefore provides a very effective damping medium for the suspended coupling region which seems to be the most susceptible to vibration effects.

3.5.3 Long Term Reliability

Many packaged couplers were tested after nearly two years and were found to have negligible change in characteristics.

For example, the spectral splitting ratio response of a coupler with 3dB power splitting at a wavelength of 820 nm was measured immediately after fabrication and is shown in Figure 3.17(a). The response after 22 months is shown in Figure 3.17(b). Clearly there has been no change in performance over this length of time.

3.6 Conclusion

A simple gravity pulling coupler rig has been designed which has almost 100% yield of low-loss single-mode fibre couplers. A coupler package has been developed which is stable with temperature and vibration and has a demonstrated long term reliability.

References to Chapter 3

1. Fowlkes, J.K.D., Ruggles, W.F. and Groothuis, J.D.:
"Advanced FAST diagramming",
Proc. of the SAVE conference 1972, pp. 45-52.

2. Cardos, G.:
"Devising a plan for problem solving",
Class note, Dept. of Mechanical and Aeronautical Engineering, Carlton University, 1980.

3. Mortimore D.B.:
"Wavelength-flattened fused couplers",
Electron. Lett., 1985, 21, pp.742-743.

4. Polya, G.:
"Mathematical discovery",
John Wiley & Sons, 1965.

5. Fuller, O.M.:
"Problem solving",
Class note, Dept. of Chemical Engineering,
McGill University, 1974.

6. Yataki, M.S.:
"Experimental Study of Optical Fibre Couplers",
Mini thesis, University of Southampton, Oct. 1986.

7. "Mechanical Engineering Handbook",
Ed., Japanese Association of Mechanical Engineers,
1976.

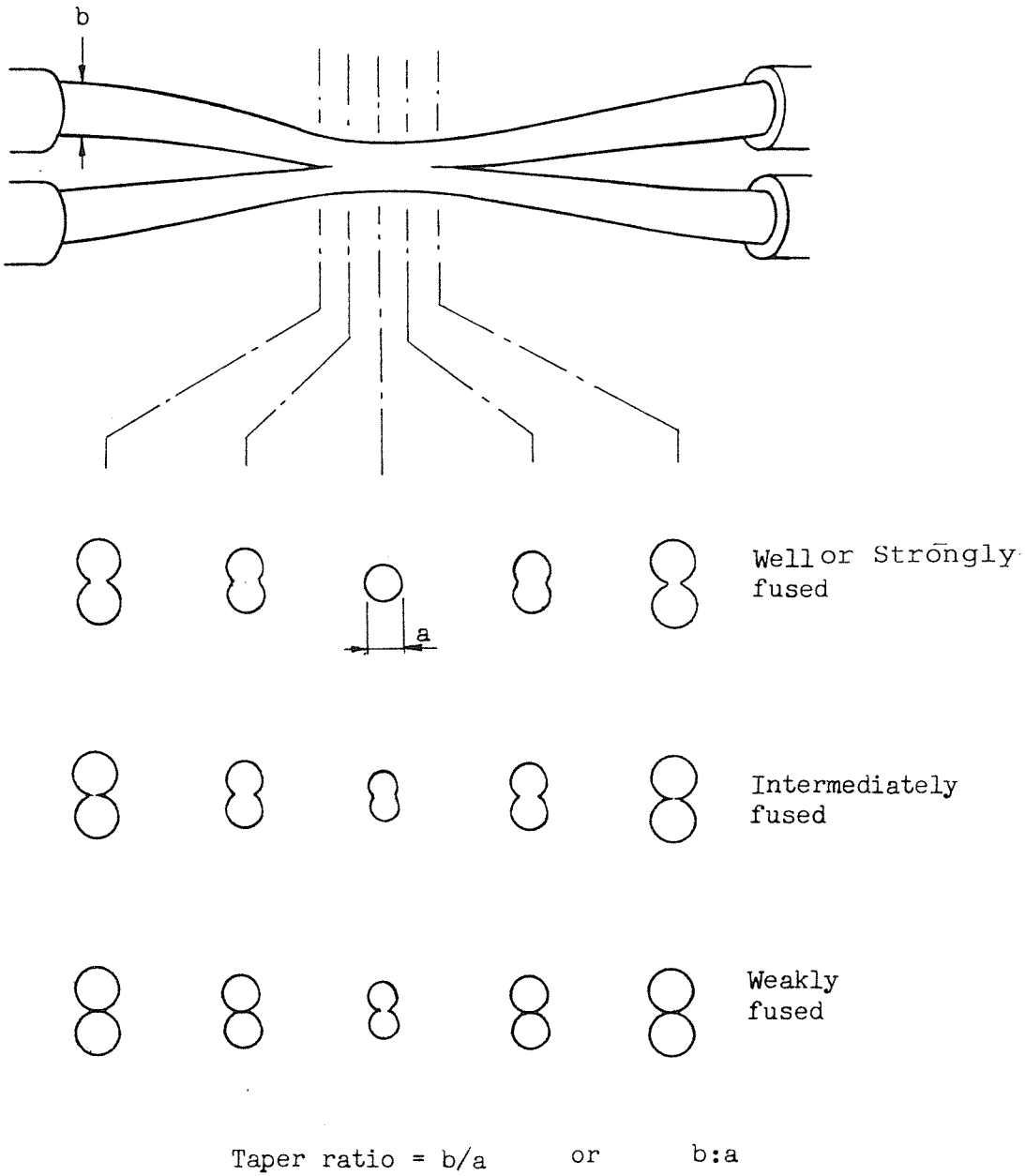

Figure 3.1.. Fused taper coupler showing the different possible cross sections of various stages along the coupler. The taper ratio is also defined.

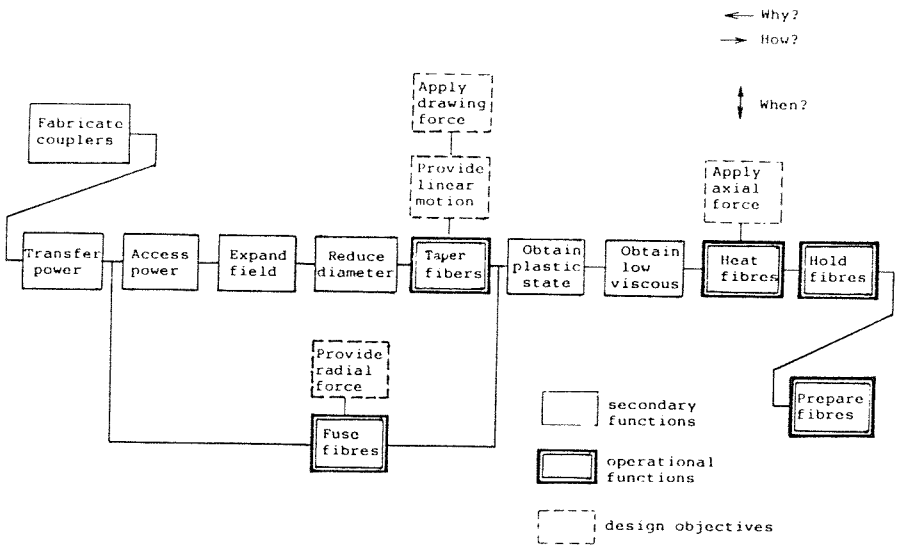

Figure 3.2. "FAST" diagram for coupler fabrication.

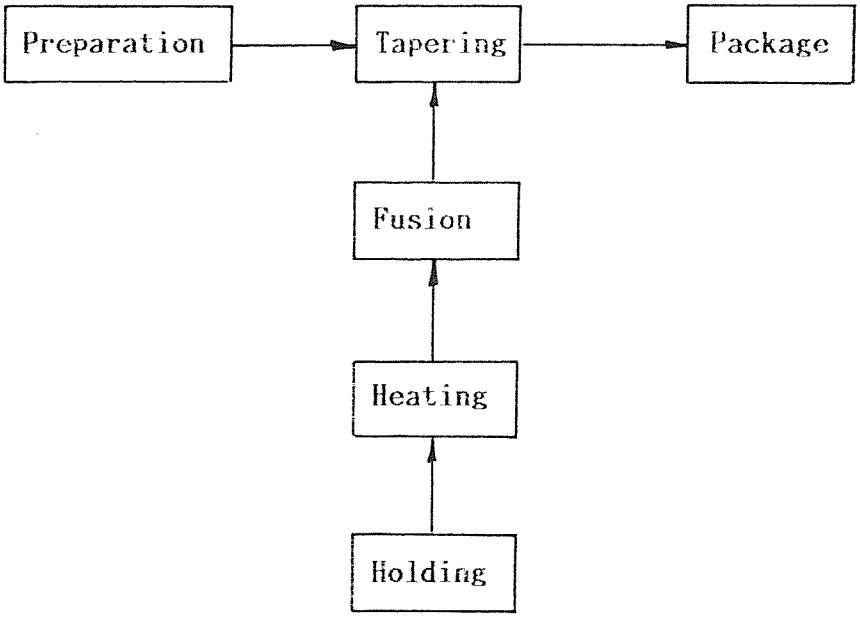

Figure 3.3. Coupler fabrication showing simplest case of four operations being performed simultaneously.

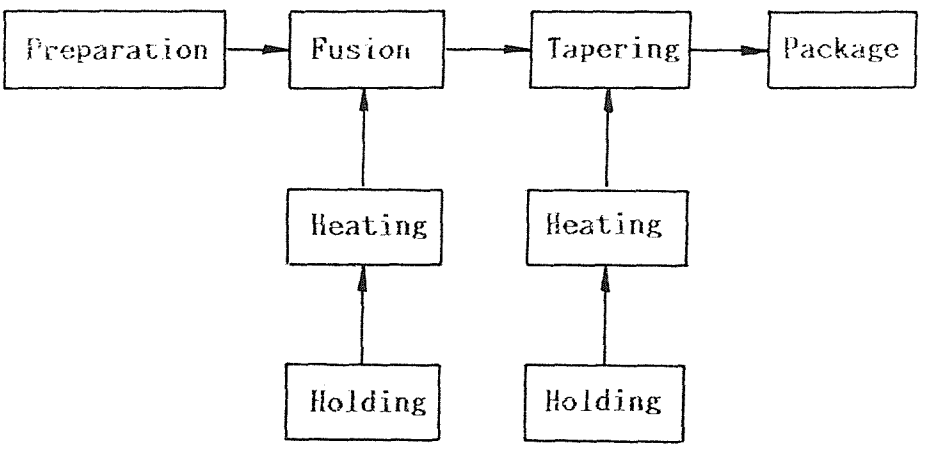

Figure 3.4. Coupler fabrication showing some operations being duplicated.

L	=	taper length
v	=	tapering velocity
α	=	tapering acceleration
t_m	=	tapering time
N	=	tapering force
m	=	mass of fibre
s	=	cross section of taper
γ	=	viscosity of fibre
T	=	temperature of heated fibre
E	=	thermal energy of flame
σ	=	energy transfer rate
F	=	taper angle
t_h	=	heating time
β	=	degree of fusion
R	=	contracting force
H	=	holding force
V	=	initial tension on fibre
θ	=	friction between fibre and holder
ι	=	overdrawn distance
z	=	position in z-axis

(a)

1	L	=	f	(v, t_m)
2	v	=	f	(α, t_m)
3	N	=	f	(m, α)
4	N	=	f	(s, γ)
5	γ	=	f	(T)
6	T	=	f	(E, σ)
7	F	=	f	(s, t_h, z)
8	β	=	f	(R, γ)
9	R	=	f	$(F_{(z)}, N)$
10	H	=	f	(V, θ, ι)
11	ι	=	f	(V, H, N)

(b)

Table 3.1. Parameters and correlation for Polya-Fuller map

(a) List of important parameters in coupler fabrication.

(b) Relationships between parameters.

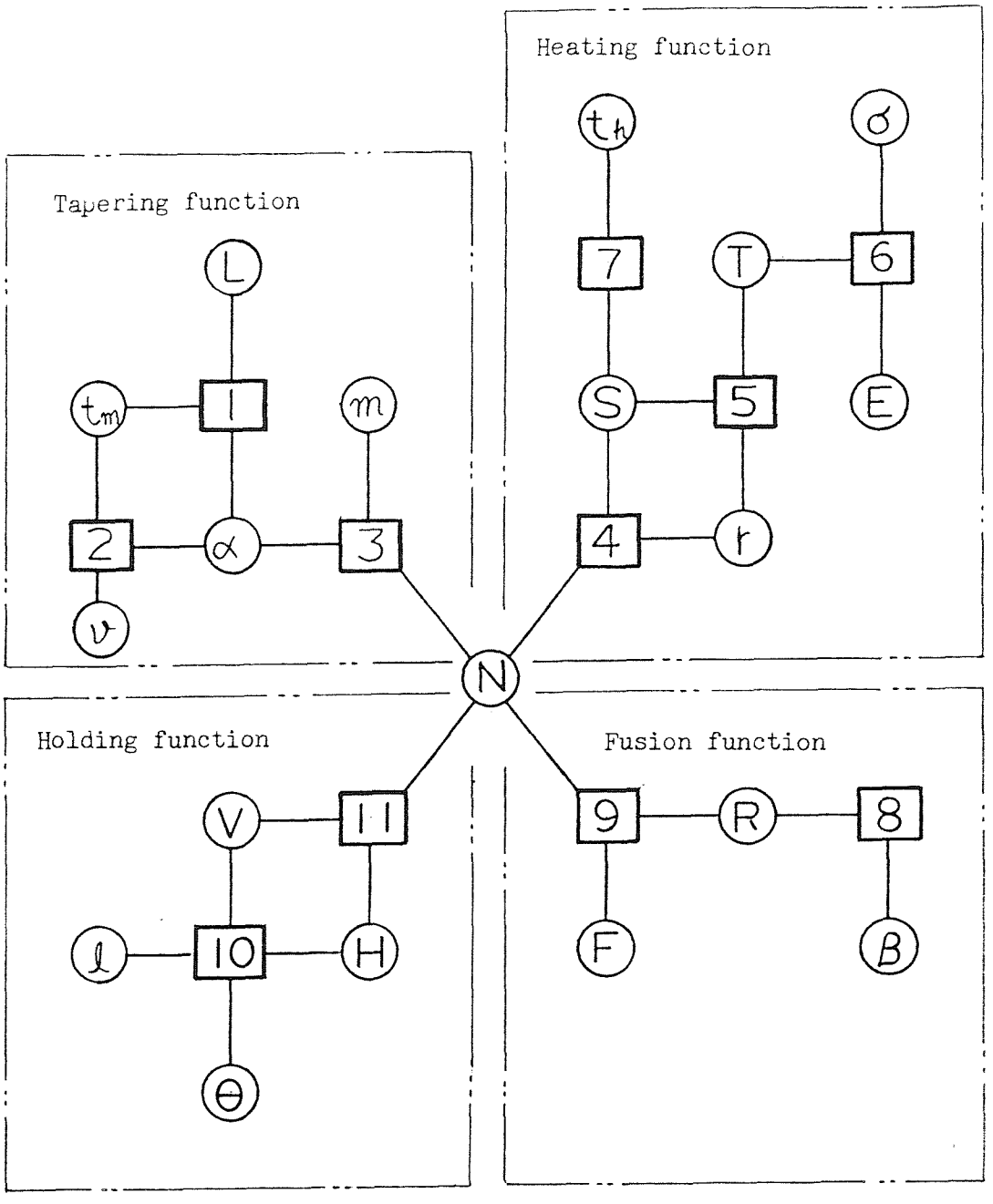

Figure 3.5. Polya-Fuller map of a fundamental fabrication system for fused taper couplers.

Type of control	Advantages	Disadvantages
Variable-force method	Feasible to tailor taper shape. Predetermined process time.	Expensive instrumentation. Control parameters depend on fibre. Complex control required.
Constant-force method	Simple process. Less expensive. Not necessary to change parameters for various fibres.	Taper shape depends on heat distribution Process time is not constant.

Table 3.2. Comparison of the two tapering methods.

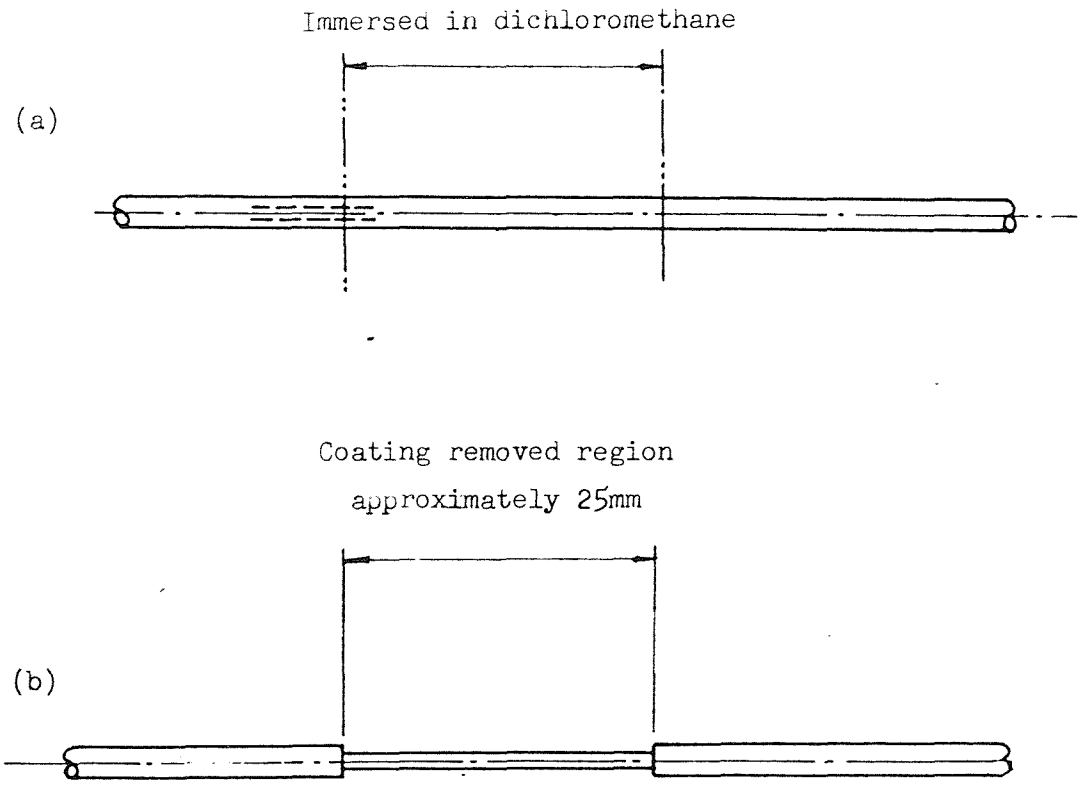

Figure 3.6. Fibre preparation before coupler fabrication.
(a) immersion in dichloromethane.
(b) removal of urethane acrylate coating.

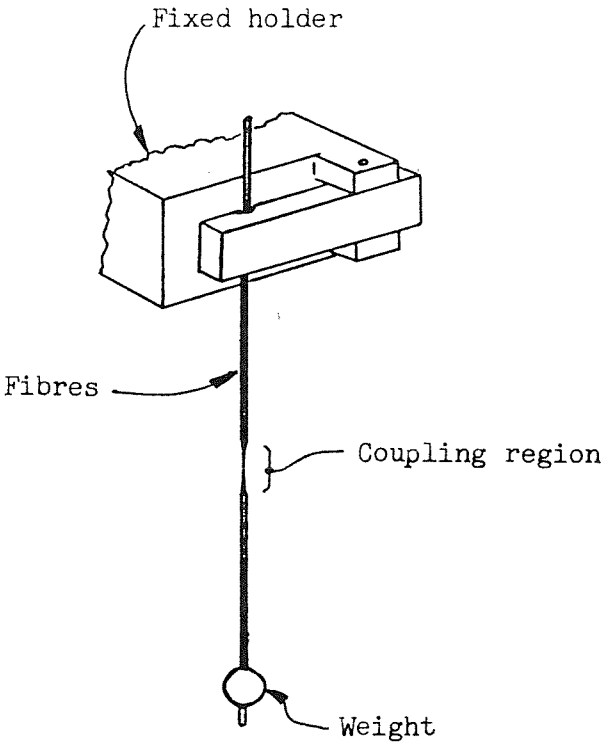

Figure 3.7. Vertical arrangement with one point holding.

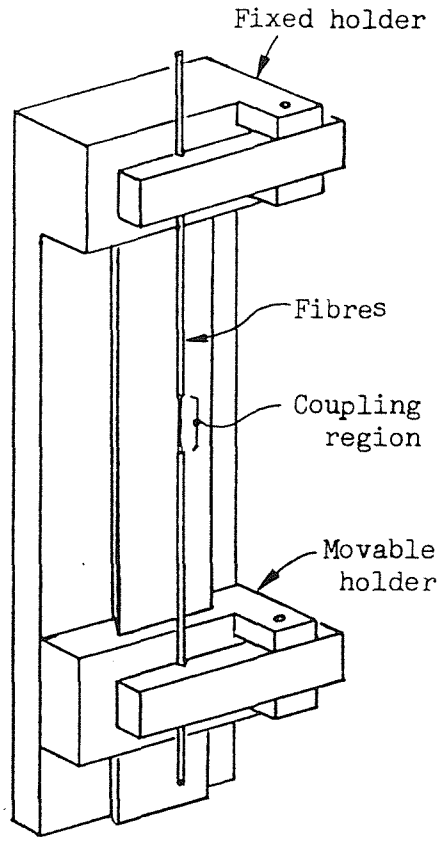

Figure 3.8. Vertical arrangement with two point holding.

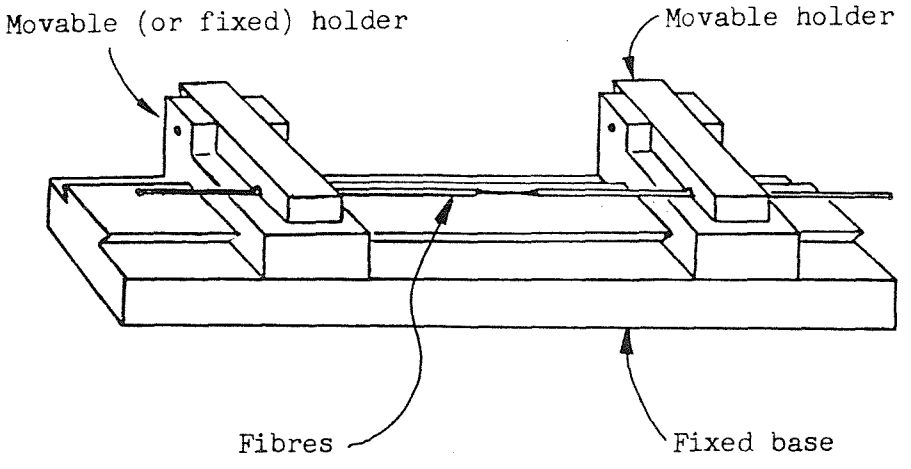

Figure 3.9. Horizontal tapering arrangement.

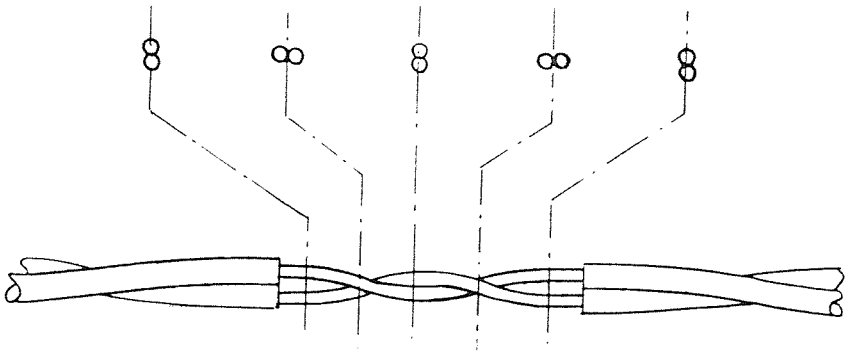

(a)

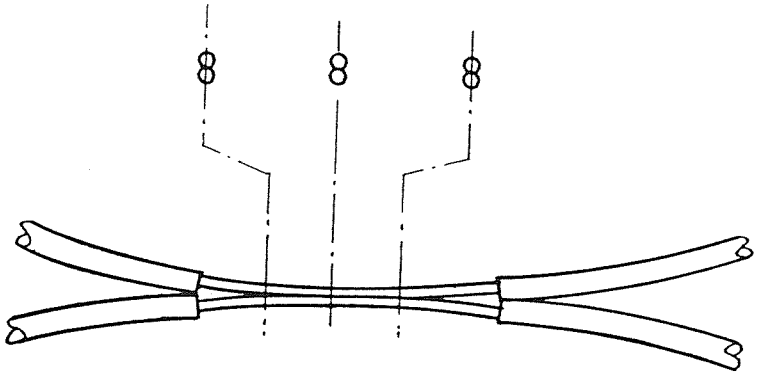

(b)

Figure 3.10. Fibre configuration prior to fusing and tapering.

(a) with twist.
(b) without twist.

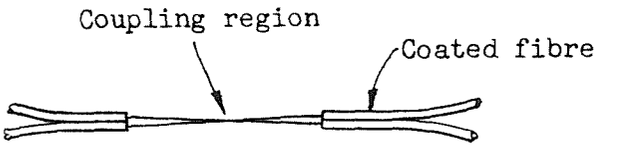

(a) Initial coupler

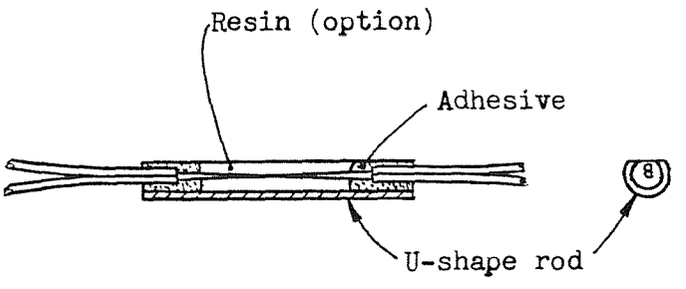

(b) Primary reinforcement

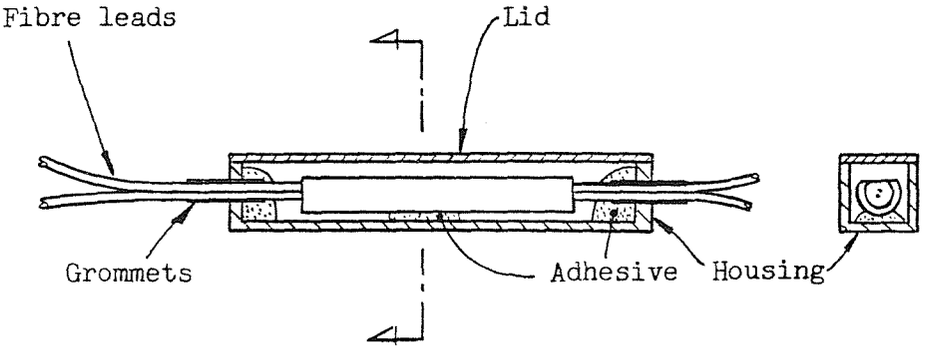

(c) Final package

Figure 3.11. Breakdown of the coupler packaging operation.

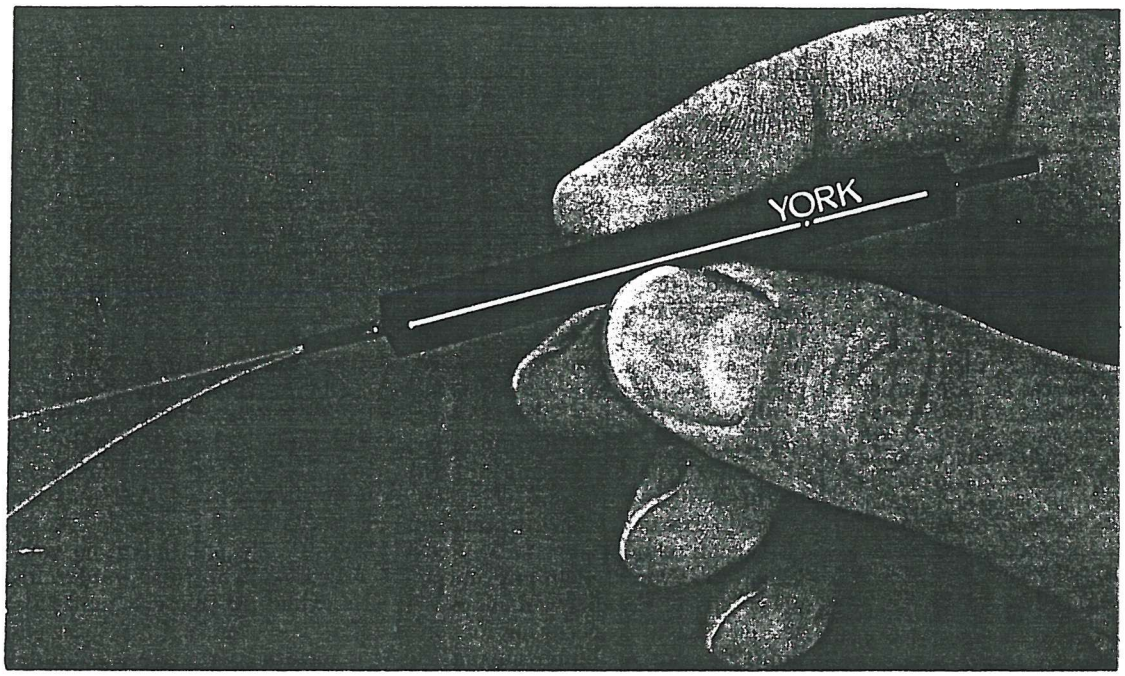

Figure 3.12 Photograph of final coupler package.

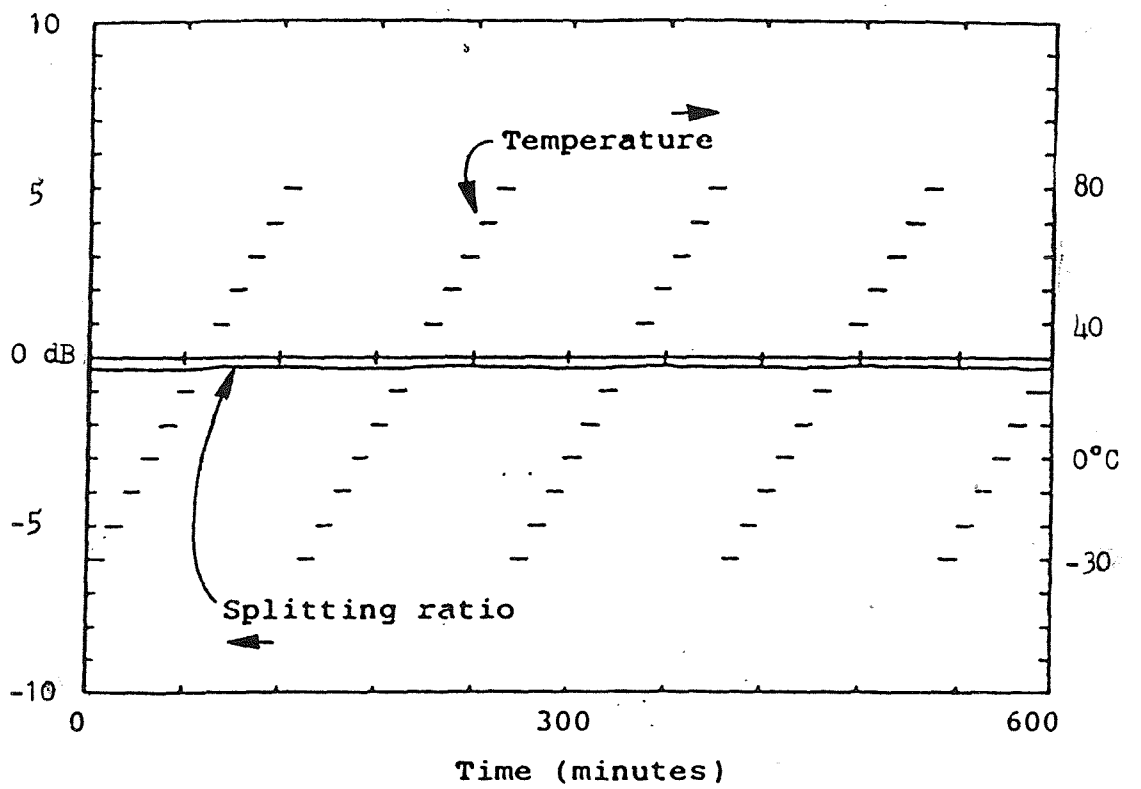

Figure 3.13. Temperature stability test on packaged coupler.

Temperature range -30 to 80°C.
Surrounding medium air

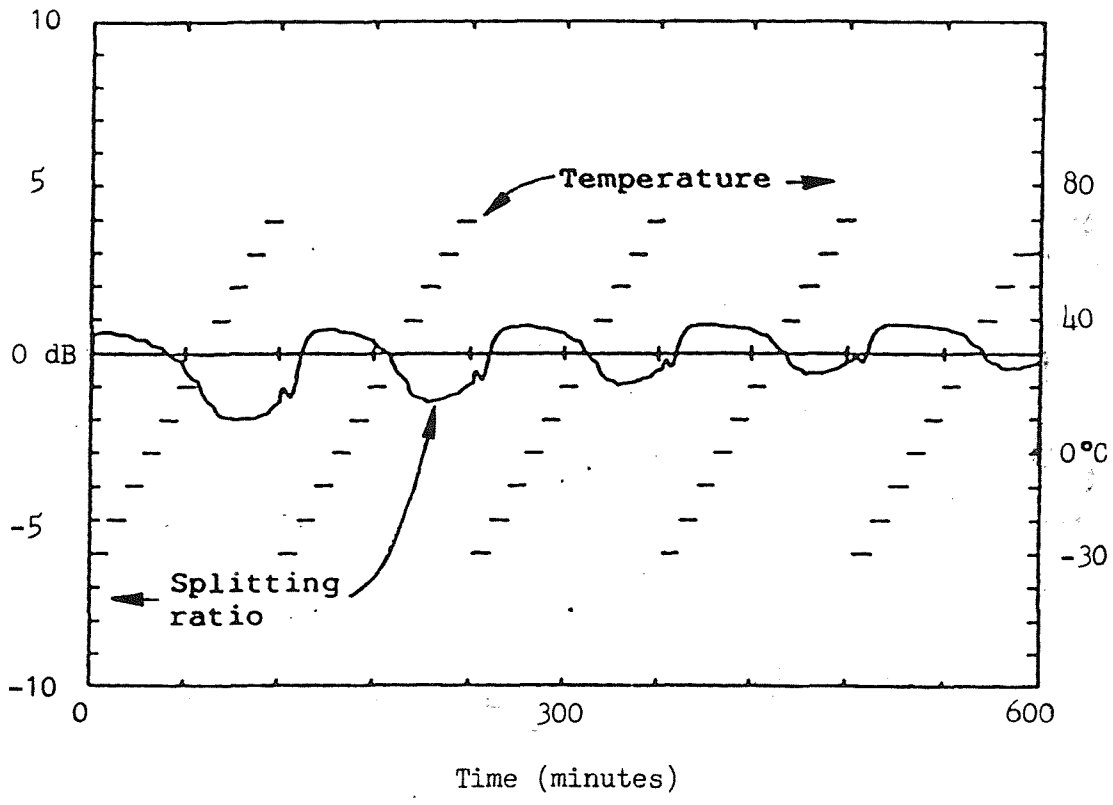

Figure 3.14. Temperature stability test on packaged coupler.

Temperature range -30 to 70°C.
Surrounding medium Sylguard 184.

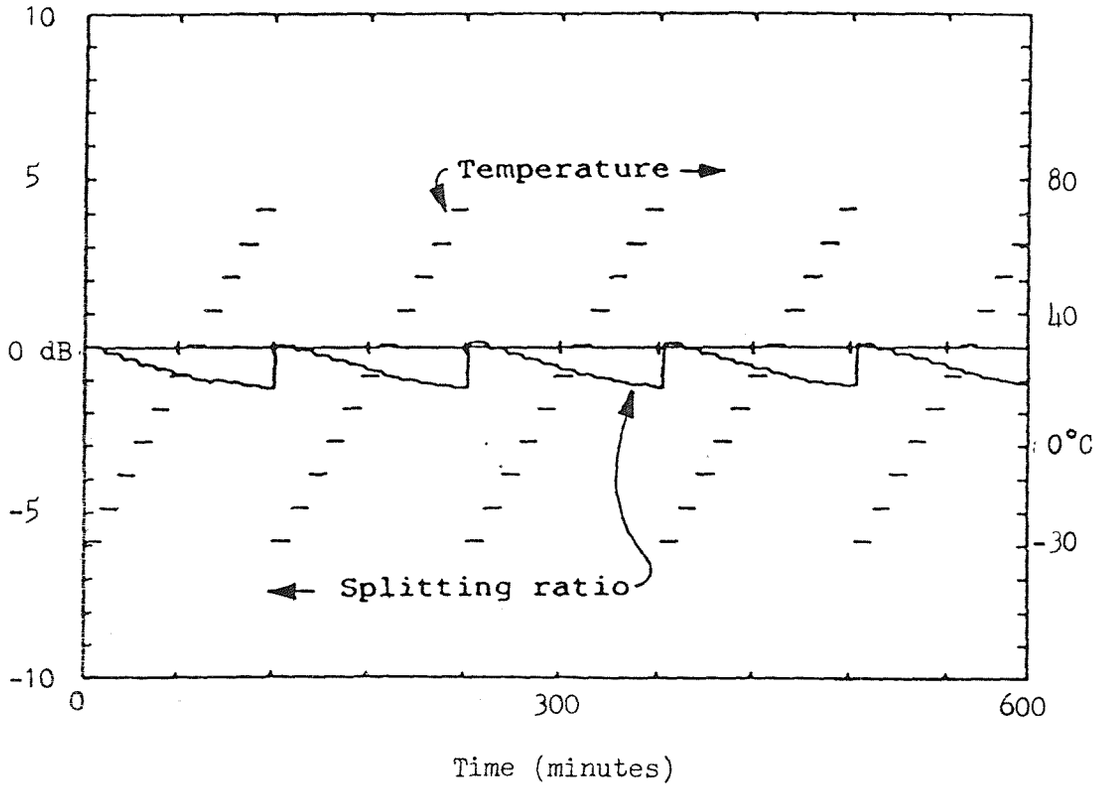

Figure 3.15. Temperature stability test on packaged coupler.

Temperature range -30 to 70°C.
Surrounding medium Dow Corning 3-6527.

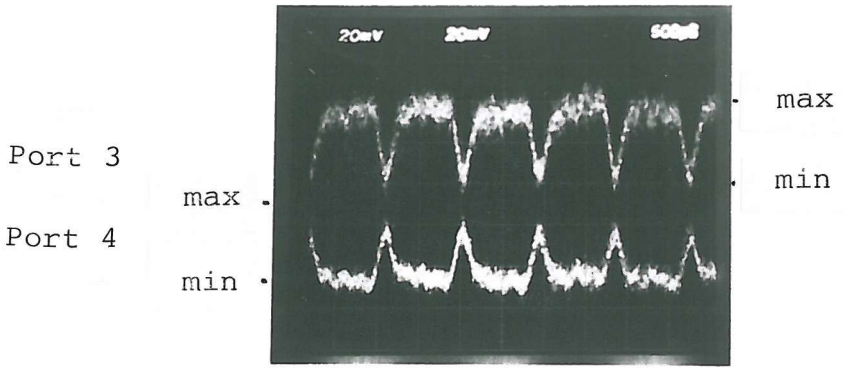

(a)

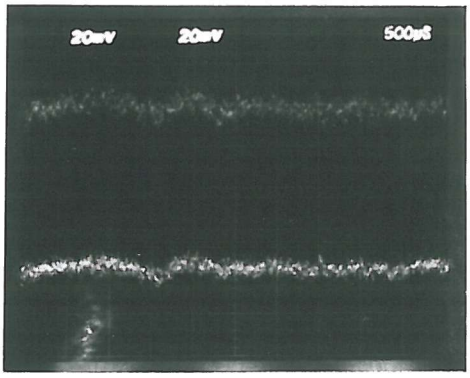

(b)

Figure 3.16. Vibration stability test.

(a) surrounding medium = air.

(b) surrounding medium = Dow Corning 3-6527.

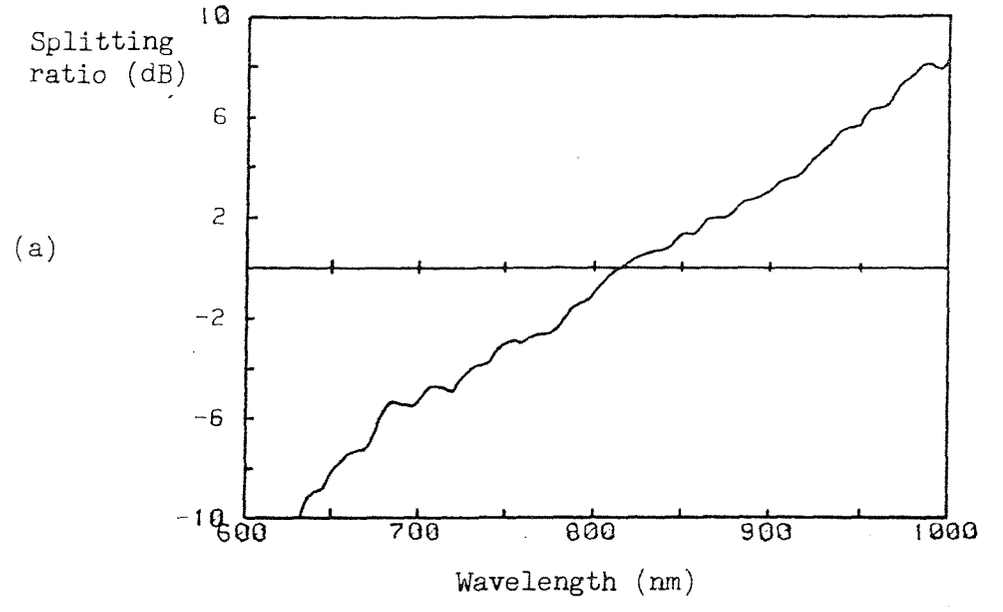

(a)

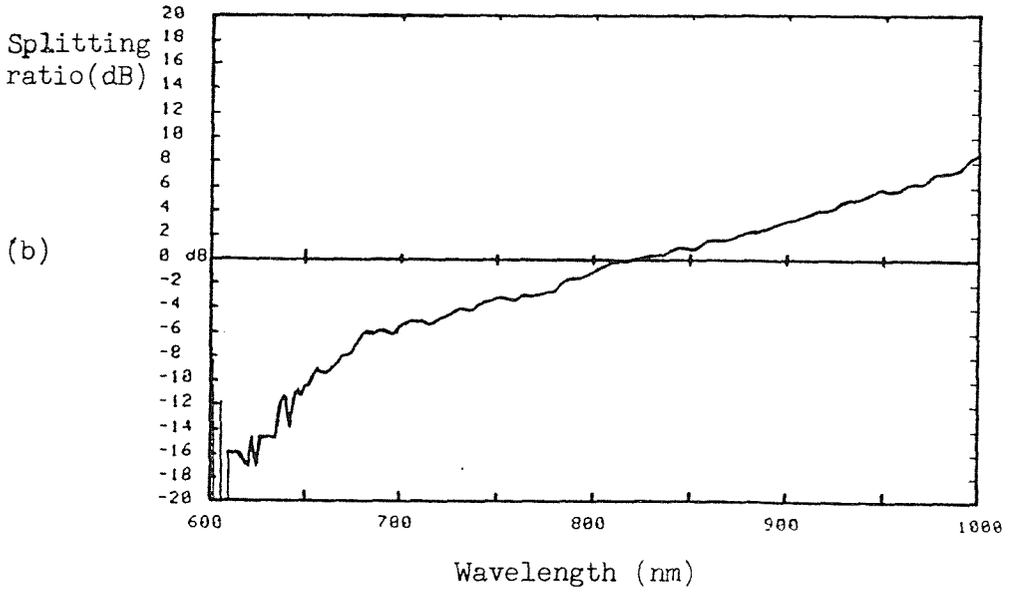

(b)

Figure 3.17. Long term reliability test.

(a) immediately after fabrication.
(b) 22 months after fabrication.

CHAPTER 4: TAPERS IN SINGLE MODE FIBRES

4.1 Introduction

In order to understand the behaviour of the fused taper coupler, and the steps required to optimise the fabrication and packaging processes to yield a viable mass-produced component, it is first essential to understand the operation of the simple taper in single-mode fibres.

At normal operating wavelengths the optical field of the fundamental mode is well guided by the core of the (single-mode) fibre, and while the evanescent field does tail into the cladding, the finite extent of the cladding has no influence on the propagation characteristics of the fundamental mode and we can generally assume a cladding of infinite extent (1).

Up until 1983 (2,3), the infinite cladding assumption was carried over into the tapered fibre. It was assumed that, irrespective of the extent of the taper and the resultant field-spreading due to the reduced fibre V-value, the propagating field was still guided by the core. One of the consequences of this thinking was the belief that the taper coupler operated through the overlap of the evanescent tails of the propagating modes of the two parallel fibre cores (2,3).

As the result of some very simple experiments on tapers and taper couplers it was soon realised that the above picture was completely wrong. For instance, certain tapers

and taper couplers when fabricated exhibited negligible loss and "normal" operation, yet when immersed in index matching fluid ($n_{fl} = n_{cl}$) these tapers and couplers lost all of their power. On removal of the index matching fluid all power was restored.

If the cores were dominating the modal guidance, the index matching fluid would simply provide a true infinite cladding and negligible change should occur. Clearly this was not the case. In fact the cladding was itself providing the guiding function, with the fibre cores playing no role in the guidance. The finite extent of the cladding was obviously an important feature for the successful operation of the taper and taper coupler. Yet if the cladding was providing the guidance in the taper, the cladding waveguide (which was the waveguide formed by the cladding to air boundary) was highly multimoded i.e. $V_{cl}>>2.4$. How was such a transition possible with negligible throughput loss?

What had been achieved was a transition in the fibre where the mode of the core waveguide evolved into a mode of the waveguide formed at the cladding to air boundary, and then re-emerged as the mode of the core waveguide of the output fibre, all with negligible loss and negligible wavelength variation! The mode was staying intact as a single mode throughout. Clearly the tapering transitions which were produced in the apparatus were satisfying some form of adiabatic condition.

Fortunately, therefore, it was possible to fabricate tapers and taper couplers to a satisfactory specification without a full understanding of their operation. However, in order to optimise these devices and perhaps to develop new devices, it was necessary to explore the taper in greater detail both experimentally and theoretically in order to exploit fully the new phenomenon.

In parallel with the work undertaken by the author, additional studies of the taper were progressing at Southampton (3,4) and elsewhere (5,6,7). While this chapter mainly reports on the author's work, it shall draw on such other peoples' results that have helped develop the present understanding of tapers and taper couplers.

4.2 Tapers in Single Mode Fibres

A single mode fibre supplied with a high index coating ($n_{coating} > n_{cladding}$) propagates only the fundamental core mode. Higher order cladding modes excited by the source at the fibre input will be extracted and attenuated rapidly by the coating. The effect of the coating on the fundamental mode is negligible since the mode is well confined to the core. Under normal operation the fibre can be assumed to have a cladding of infinite extent in the radial direction (1).

On removing the coating at some intermediate region for up to a few centimetres along the fibre (a process which is necessary to effect the tapering and fusion required in

tapers and couplers), the cladding to external medium boundary is again restored for optical guidance purposes, and the possibility then exists of propagating many thousands of modes in the bare fibre section. The fact that the fibre is bare over a short section has very little influence on the propagating core mode since this mode is dominated by the guidance of the core waveguide, and it therefore passes through the bare section with no loss.

The essential character of the mode in the bare section is however changed, as indicated in Figure 4.1. The mode now becomes the fundamental mode of the full fibre cross-section (8). Its effective index, β/k, lies somewhere in the range

$$n_{co} > \beta/k > n_{cl}$$

where $k = 2\pi/\lambda$, n_{co} is the maximum core refractive index and n_{cl} the uniform cladding refractive index.

Other possible modes of this full fibre cross section, at the operating wavelength, are by definition "cutoff" in the core waveguide and therefore have effective indices, β_i/k, in the range

$$n_{cl} > \beta_i/k > n_{ext}$$

where n_{ext} is the refractive index of the external medium which is, in this instance, air ($n_{ext} = 1$). These modes are referred to as "cladding modes", since they are guided and confined by the boundary between the cladding and the external medium (9). The situation is depicted in Figure

4.1(b).

On tapering this bare fibre section, a structure is obtained as shown in Figure 4.2. The fundamental mode, which was predominantly guided by and confined to the core waveguide, spreads out relative to the local core size because the guidance of the core is reduced. As a consequence, the mode's propagation constant decreases. Depending on the extent of fibre tapering, this fundamental mode can evolve through three stages.

(i) The mode remains mainly guided by the core - a core mode - its effective index, β/k, remains within the range

$$n_{co} > \beta/k > n_{cl}$$

(ii) The mode is significantly guided by both the core and the cladding waveguides. In this case the mode will be referred to as an intermediate mode where

$$\beta/k \approx n_{cl}$$

(iii) The mode is completely guided by the cladding to external medium boundary - a cladding mode - with

$$n_{cl} > \beta/k > n_{ext}$$

Strictly, the mode is either a core mode or a cladding mode, but it is found that the intermediate mode stage does have properties unique to itself and is therefore a convenient

extra category of mode.

4.2.1 Example

In order to quantify the foregoing discussion, it is necesssary to consider the evolution of the effective index and the mode shape of the fundamental mode as a step index fibre is tapered. The fibre parameters are n_{co} = 1.463, n_{cl} = 1.458, OD (outside diameter) = 80μm, core diameter = 4.8μm, λ_{co} = 633 nm. The calculated effective index as a function of the inverse of the taper ratio is shown in Figure 4.3.

In this example, core mode behaviour exists down to taper ratios of about 3:1 while full cladding mode behaviour tends to exist after taper ratios of about 6 or 7:1. These points correspond roughly to where the exact curve deviates from the "infinite cladding" and the "no-core" curves as indicated on the graph, Figure 4.3 (8).

In Figure 4.4 the modal field and refractive index distribution is shown for taper ratios of up to 20:1 for the above fibre parameters. The reader should realise that diagrams are all normalised to the same size to illustrate the relative mode size to waveguide size for each taper ratio. For taper ratios of up to 3:1 there is the anticipated field spread due to the reduction in V-values of the core waveguide. For taper ratios of between 3:1 and 7:1 the modal field exhibits intermediate behaviour where it looks like the superposition of a core field and a cladding field. For taper ratios of greater than 7:1 the gaussian

shape of the fundamental mode of the multimoded cladding waveguide becomes dominant, and the core waveguide introduces only a small perturbation on the field distribution.

4.3 Structure of the taper

In the vertical pulling arrangement, the top end of the stripped region is always fixed while the bottom end pulls out of the hot-zone of the oxy-butane burner. This leads to an asymmetry between the top and bottom transitions in the taper, with the bottom taper always tending to be slower than the top taper.

Figure 4.5 shows the variation of diameter with length for four different length tapers, drawn from the same fibre under identical drawing conditions. On the right hand side of the figure are the fixed top ends of the tapers, which are always sharper than the bottom tapers on the left hand side of the figure. It is important to note that after a certain elongation length both top and bottom tapers remain fixed while further elongation involves the lengthening and only slight reduction of a uniform neck region in the taper.

4.4 Transmission characteristics of the taper

This section reports on experiments which illustrate some of the salient features of tapers in single-mode fibres.

4.4.1 External Refractive Index Effects

As mentioned earlier, it was the behaviour of the taper when immersed in index matching fluid that brought into question the validity of the infinite cladding assumption. In this experiment, a step index fibre ND 53 (λ_{CO} = 633nm, NA = 0.09, OD = 80μm, core diam. = 3.4μm) was tapered to different lengths in the same burner and under the same conditions. Each taper was then immersed in index matching fluid and the throughput power was measured. The results are plotted in Figure 4.6.

For taper ratio of less than 3:1 the core still dominates the guidance and no power is lost, for taper ratios of greater than 5:1 total power is lost, while for taper ratios between 3:1 and 5:1 there is intermediate behaviour, with some power still guided by the core.

On examining the effective index curve in Figure 4.7 calculated for a fibre with the above parameters, it is indeed found that cladding mode behaviour begins at taper ratios of slightly greater than 4:1 while core mode behaviour stops at taper ratios of slightly greater than 2:1.

4.4.2 Length Dependent Effects

A taper was formed in fibre ND269 (λ_{CO} = 600 nm, NA = 0.19, OD = 80μm, core diam. = 2.4μm). The spectral response was measured using the measurement system described in Appendix A. The spectral response R(λ), which is defined as

$$R(\lambda) = 10 \text{ Log } \frac{P_L}{P_O}$$

where P_O is the throughput power with no elongation and P_L is the throughput power after an elongation L, was measured at each 1 mm incremental elongation up to a maximum of 50 mm. The general trends in the spectral response can be deduced from Figures 4.8.1-10, where the response for every 5mm elongation is presented. The feature to which attention is directed is the fairly regular periodic structure of the loss curves which is just barely discernable at the taper length of 15 mm, becomes more obvious at the length of 25 mm and then fades away for longer taper lengths. This wavelength dependent ripple is the result of mode coupling (10,11) and will be described in more detail in the following section.

The overall increase in loss which is observed here is the result of the necessary stop-start approach to the tapering required to undertake this specific experiment, together with the tendency for the taper to become contaminated in the period of the experiment. For reference, one other taper of 50 mm length was fabricated in the usual manner showing a typical maximum loss of 0.2 dB as shown in Figure 4.9, compared to the loss of 0.7dB as shown in Figure 4.8.

4.5 Adiabatic Condition

The taper is a longitudinal transition in the fibre, with the fibre diameter varying along the length of the

transition. As a consequence of this transition, mode coupling is induced between the local normal modes, since there are no true modes existing in the transition region (10,13). The local normal modes are the modes of an infinitely long circular cylindrical fibre with the same cross sectional dimensions as the local cross sections in the taper.

The fundamental mode in the input fibre acts as a source of excitation of higher order modes in the multimoded waveguide of the tapered section. Such excitation of higher order modes will generally be manifested as a wavelength dependent loss in the throughput power of the taper. At the output side of the taper, only that power remaining in or coupled back into the fundamental mode is recaptured into the core of the output fibre. The power in the higher order modes which are cut-off in the output core waveguide is lost, due to the high refractive index coating.

The extent of the excitation of the higher order modes can be kept to a minimum by keeping the rate of tapering "slow", the required slowness being determined by an adiabatic condition. The adiabatic condition is such that if the taper is less steep then this, negligible conversion to higher order modes will occur (10,12,13,14). The adiabatic condition for waveguide transitions is well known (8) and has been applied to the multimode fibre taper by Snyder (10), and to the tapered single mode fibre by Steward

and Love (12).

The adiabatic condition for a circular cylindrical fibre can be written as

$$\frac{d\rho}{dz} = \frac{\rho}{2\pi} (\beta_{11} - \beta_{12})$$

where ρ is a local fibre dimension, z is the distance along the fibre axis, and β_{11} is the propagation constant of the fundamental mode while β_{12} is that of the tubular HE_{12} mode which, from the symmetry of this case, is the next most likely mode to which coupling will occur (10,12).

In order to build up a feel for this adiabatic condition, the effective index curves for the HE_{11} and HE_{12} modes of a step index matched cladding fibre with n_{cl} = 1.458, n_{co} = 1.460, λ_{co} = 633nm and an OD of 80 μm, are drawn in Figure 4.10.

As can be seen from the curves, the adiabatic condition is strictest when the fundamental mode is in its intermediate mode stage, since β_{11} and β_{12} are very close in this region. Indeed, from the experimental curves in Figure 4.8, it is found that it is in the early stages of tapering that mode coupling occurs, while longer tapers actually eliminate mode coupling. This effect recurs throughout the work.

The more detailed study of the adiabatic condition by Stewart and Love (12) substantiates the above observations.

However, they also found that it should be virtually impossible to taper the W- or depressed cladding-fibre so that no loss or mode coupling occurs. This effect is due to the fundamental mode cut-off behaviour which these fibres exhibit even without tapering.

The W-fibre, which is becoming increasingly important for broad-band networks, is therefore excluded as a class of fibre from which tapers and taper-based components can be fabricated with satisfactory loss. The same applies to the polarisation maintaining fibres which have depressed claddings or depressed stress sectors.

Returning to consider the matched cladding fibres,it is found that even here the fibre design is quite strict. Fibres with eccentric cores (i.e. the core is not central in the fibre structure) and fibres with elliptical cores are found to be difficult to taper with low loss. The slight asymmetry in cross section creates the possibility of mode coupling to the asymmetric TE_{01} mode, whose propagation constant is closer to that of the fundamental mode than that of the HE_{12} mode, with the result that a very strict adiabatic condition ensues.

4.5.1 Example: Eccentric Core Fibres

A fibre with an eccentrically located core, with a cross section as shown in Figure 4.11(a) and with a refractive index profile showing the eccentricity as in Figure 4.11(b), was tapered, and the spectral responses for

different elongation lengths were measured as before. The fibre was elongated up to a total length of 30 mm and the response was measured at every 1 mm elongation. The responses for elongation length of 5, 7, 8, 10, 15, 20, 25, 30 mm are shown in Figures 4.12.1-8. The amplitude of the loss varied sinusoidally with wavelength, with amplitude variations as large as 2 dB obtained. In fact, higher losses of amplitude greater than 4dB were observed for elongation lengths of 7 mm and 8 mm; however, as found before, this loss decreased with increasing length. The higher amplitude sinusoidal oscillation remained even after the elongation length of 30 mm. This sinusoidal behaviour is due to interference between the fundamental mode and what is suspected to be the TE_{01} mode. If more than two modes were present the response would not resemble a sinusoid.

From this example it is clear that the concentricity of the core and the cladding is an important factor in the suitability of a fibre for producing low-loss tapers and couplers.

4.6 Other Loss Mechanisms

Almost all tapers and taper couplers fabricated at the laboratory exhibited low losses of less than 1 dB, and some as low as 0.1 dB. When high loss was encountered, obvious causes for the loss were found in most cases, as follows.

4.6.1 Defects in fibre

Fibre defects, such as air bubbles, caused

irregularities in the taper, as shown in Figure 4.13. This particular taper had infinite loss, i.e. no power transmission. The existence of smaller defects, undetectable by visual inspection, may cause an undesirably high loss. When a He/Ne laser was launched into the fibre, it was often noticed in cases where loss occurred,that scattering centres existed in the tapered region.

4.6.2 Air gaps

Air gaps in the cladding are another form of defect and are known to be caused by the imperfect collapse of a sleeved preform. Air gaps were found in a fibre which produced high-loss tapers. The photograph in Figure 4.14 was taken after cleaving such a fibre. The loss of the tapers fabricated from this fibre was over 6dB.

4.6.3 Foreign substances

The loss was also increased when foreign materials such as dirt, dust, moisture and soot from the burner were introduced into the tapered region. Figure 4.15 shows a particle attached to a high-loss taper. Light scattering from the particle was clearly seen when a strong light source, i.e. a He/Ne laser, was launched into the fibre.

4.6.4 Irregular tapers

Generally, the tapers produced in the laboratory were smooth. Some irregular deformations, as in the photograph of Figure 4.16, were found in high-loss tapers and couplers. It is believed that vibration due to perturbations in the

surrounding environment causes this type of deformation.

4.7 Discussion

This chapter has outlined the main characteristics of tapers in single-mode fibres. The main interest has been to set the scene for the further study of taper couplers. In particular the cladding mode nature of the operation of the taper leads to a particularly simple approach to the modelling of taper couplers - a topic that will be dealt with in great detail in Chapter 6.

The cladding mode nature of the taper and the modal field evolution in the simple taper is very important in its own right and has led, in recent years, to an expansion in the flexibility of single mode fibre technology. For instance, since the modal field in the neck region of a taper is determined mainly by the cladding to external medium boundary, such tapers can be joined together with negligible mismatch (and loss) for arbitrarily different fibres (15).

The modal field evolution in the taper can be exploited as a convenient in-line beam expander and should be useful in expanded-beam connectors and expanded-beam devices (4).

Non-adiabatic tapers have wavelength dependent mode coupling and wavelength dependent loss (11); such 'abrupt' tapers have been concatenated to yield narrow band filters (16, 17).

While the taper is a very versatile element, its use is restricted to matched cladding fibres with the core concentric to the fibre. In the following chapters it is only this class of fibre that is further considered.

References to Chapter 4

1. A.W. Snyder and J.D. Love,
"Optical Waveguide Theory", Chapman and Hall 1983.

2. F. de Fornel, C.M. Ragdale and R.J. Mears,
"Analysis of Single Mode Fused Tapered Fibre Couplers",
IEE Part H, Vol.131, No. 4, 1984, pp.221-228.

3. J.D. Love and A. Ankiewicz,
"Modal Cutoffs in Single-and Few-Mode Fiber Couplers",
IEEE J. Lightwave Tech., LT-3, No. 1, 1985, pp.100-110.

4. K.P. Jedrzejewski, F. Martinez, J.D. Minelly,
C.D. Hussey and F.P. Payne,
"Tapered-beam expander for single-mode optical-fibre gap devices",
Electron. Lett, 22, 1986, pp. 105-106.

5. R. Keil, F. Klemfut, K. Mathyssey, J. Wittmann,
"Experimental Investigation of the Beam Spot Size Radius in Single-Mode Fibre Tapers",
Electron. Lett., Vol. 2, No. 15, 1984, pp.621-622.

6. A.C. Boucouvalas, G. Georgiou,
"Tapering of Single Mode Optical Fibres",
ECOC. Venice 1985.

7. A.C. Boucouvalas, G.G. Georgiou,
"A Method of Beam Forming and Fabricating

Optical Fibre Gap Devices",
ECOC Barcelona 1986.

8. P.J.B. Clarricoats and K.B. Chan
"Propagation behaviour of cylindrical-dielectric-rod waveguides",
Proc. IEE, Vol. 120, 1973, pp. 1371-1378.

9. J. Bures, S. Lacroix, J. Laporre,
"Analyse d'un coupleur bidirectionnel a fibres optiques monomodes fusiones",
Appl. Opt. 1983, Vol, 22, pp. 1918-1922.

10. A.W. Snyder,
"Coupling of modes on a Tapered Dielectric Cylinder",
IEEE Trans. Microwave Theory Tech. MTT-18,
No. 7, 1970, pp. 383-392.

11. D.T. Cassidy, D.C. Johnson and K.O. Hill,
"Wavelength-dependent transmission of monomode optical fiber tapers",
Appl. Opt. 24, 1985, pp.945-950.

12. W.J. Stewart and J.D. Love,
"Design limitation on tapers and couplers in single mode fibres",
Tech. Digest (5th)IOOC/(11th) ECOC 1985,
Venice, pp. 559-562.

13. F. Sporleder and H.G. Unger,
"Waveguide Tapers Transitions and Couplers",
Peter Penigrinns, 1979.

14. J.D. Love and W.M. Henry,
"Quantifying loss minimisation in single-mode fibre tapers",
Electron. Lett., 22, 1986, pp. 912-914.

15. D.B. Mortimore and J.V. Wright,
"Low-loss joints between dissimilar fibres by tapering fusion splices",
Electron. Lett., 22, 1986, pp.318-319.

16. S. Lacroix, F. Gonthier, R. Bourbonnais,
R.J. Black, J. Bures, J. Lapierre,
"Abruptly Tapered Fibres",
ECOC, Barcelona 1986.

17. S. Lacroix, F. Gonthier and J. Bures,
"All-fiber wavelength filter from successive biconical tapers",
Optics. Lett. 11, 1986, pp. 671-673

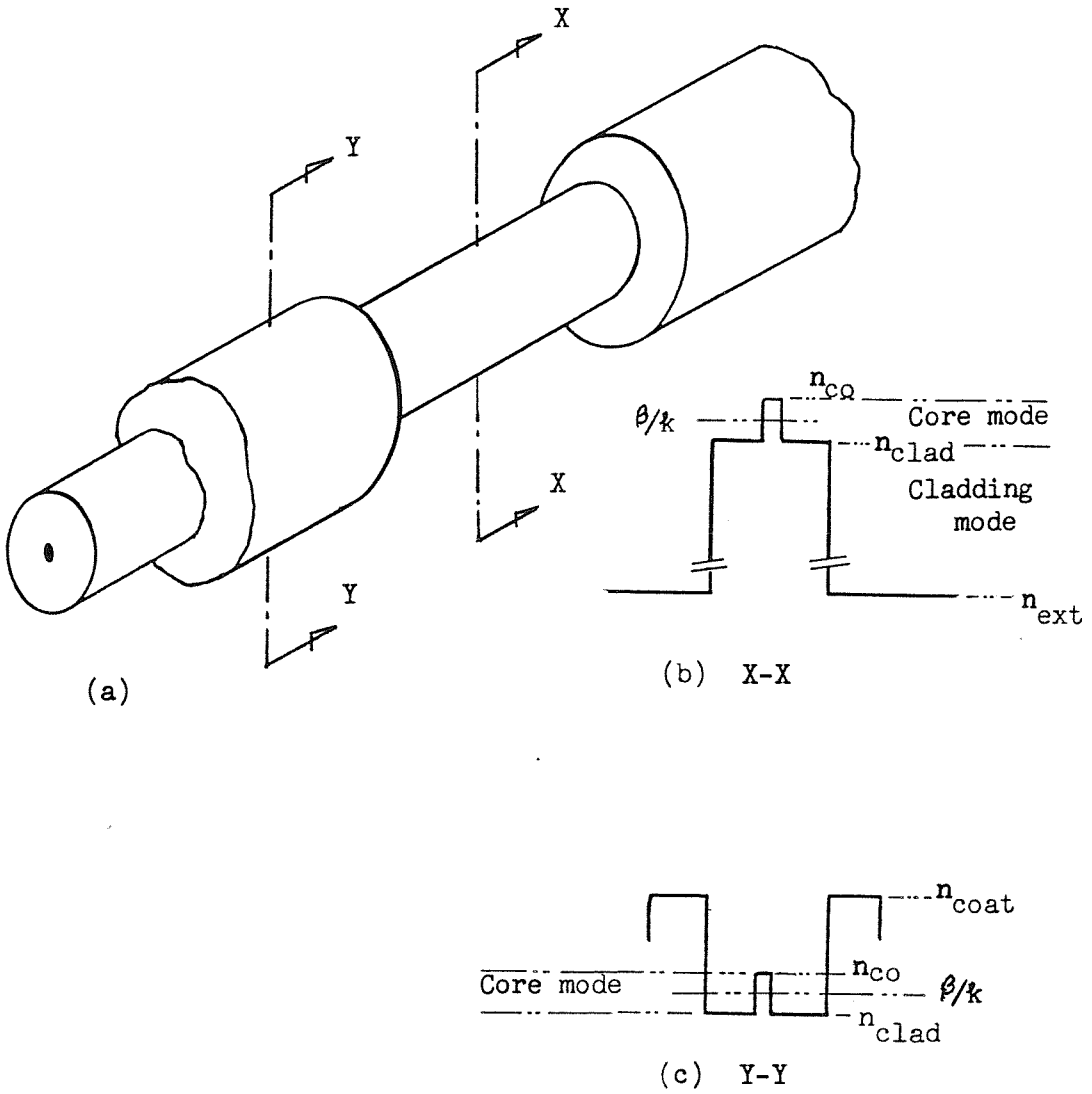

Figure 4.1. Effective index.

(a) Schematic of a coated fibre which has been stripped over a length of 20 - 30 mm.

(b) Refractive index profile of the bare fibre and the fundamental mode's effective index.

(c) Refractive index profile of the coated fibre and the fundamental mode's effective index.

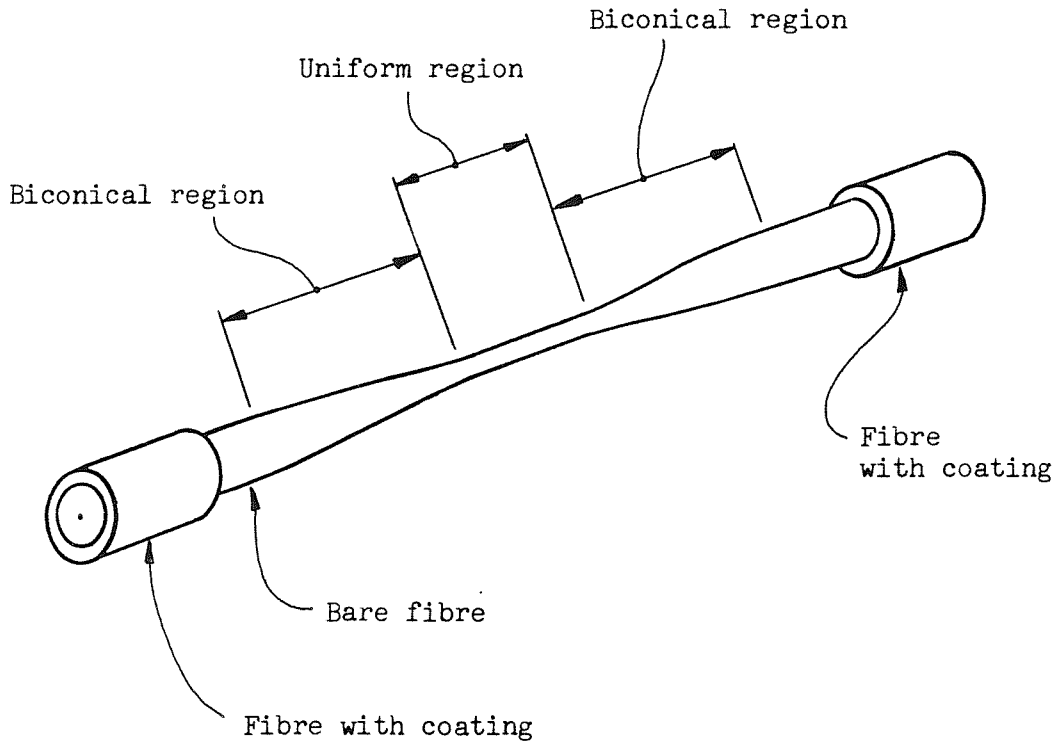

Figure 4.2. Schematic of a tapered section of fibre showing the main features.

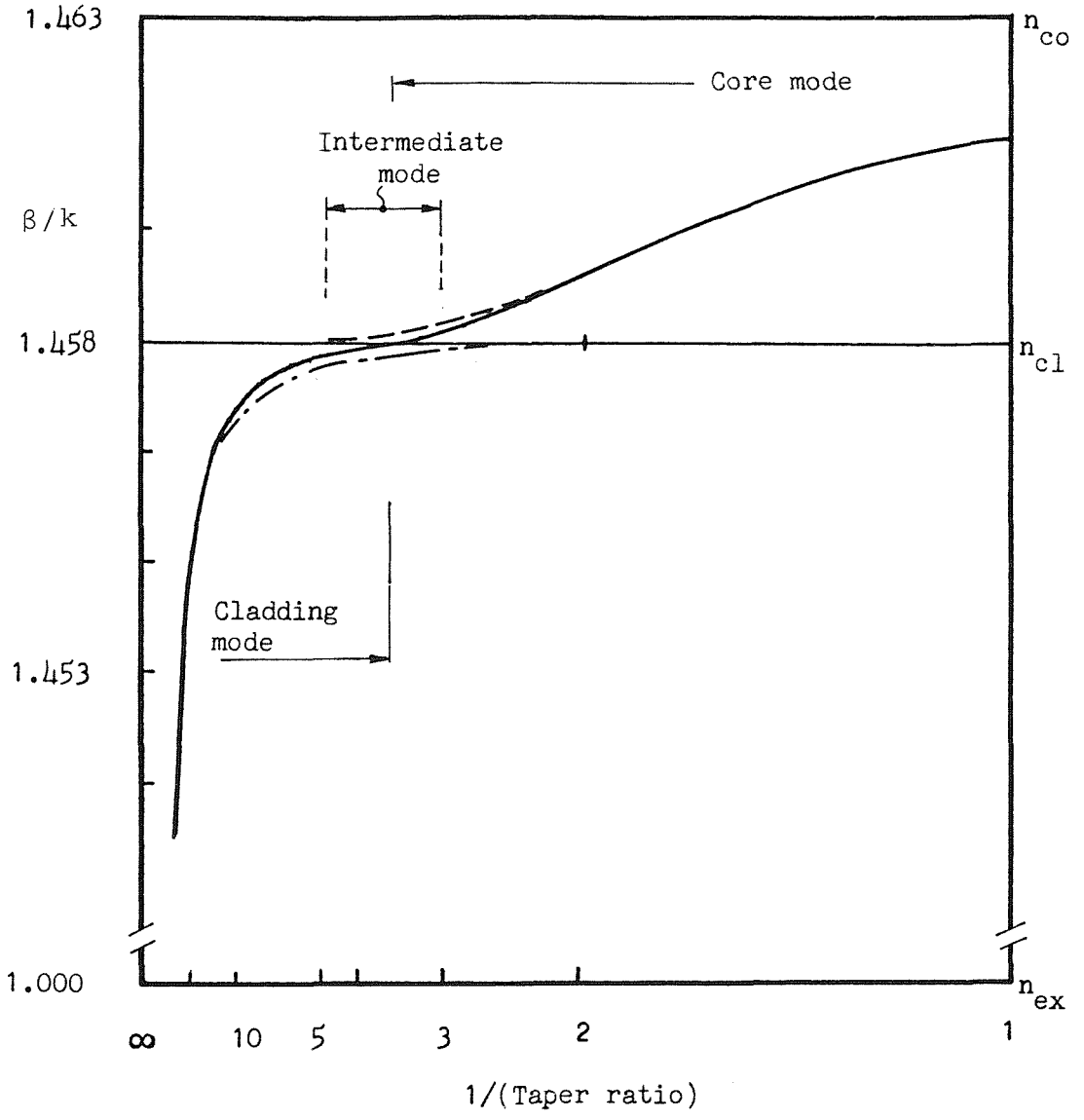

Figure 4.3. Effective refractive index of the fundamental mode in a single mode fibre taper showing the "core mode", "intermediate mode", and "cladding mode" categories as well as the "no core" and "infinite cladding" approximations.

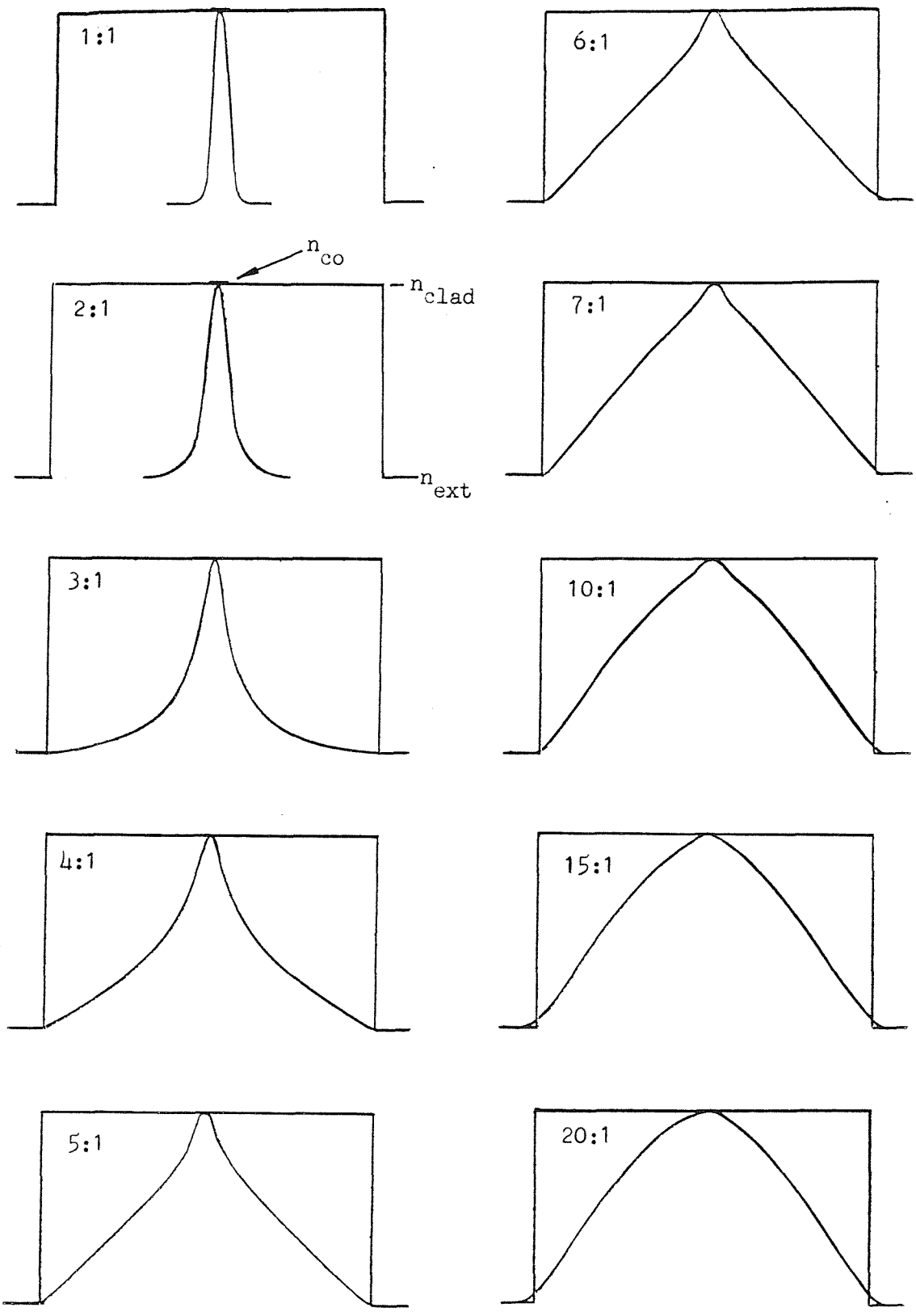

Figure 4.4. The modal fields and refractive index distributions for a single mode fibre taper at various stages of tapering for the fibre parameters outlined in the text.

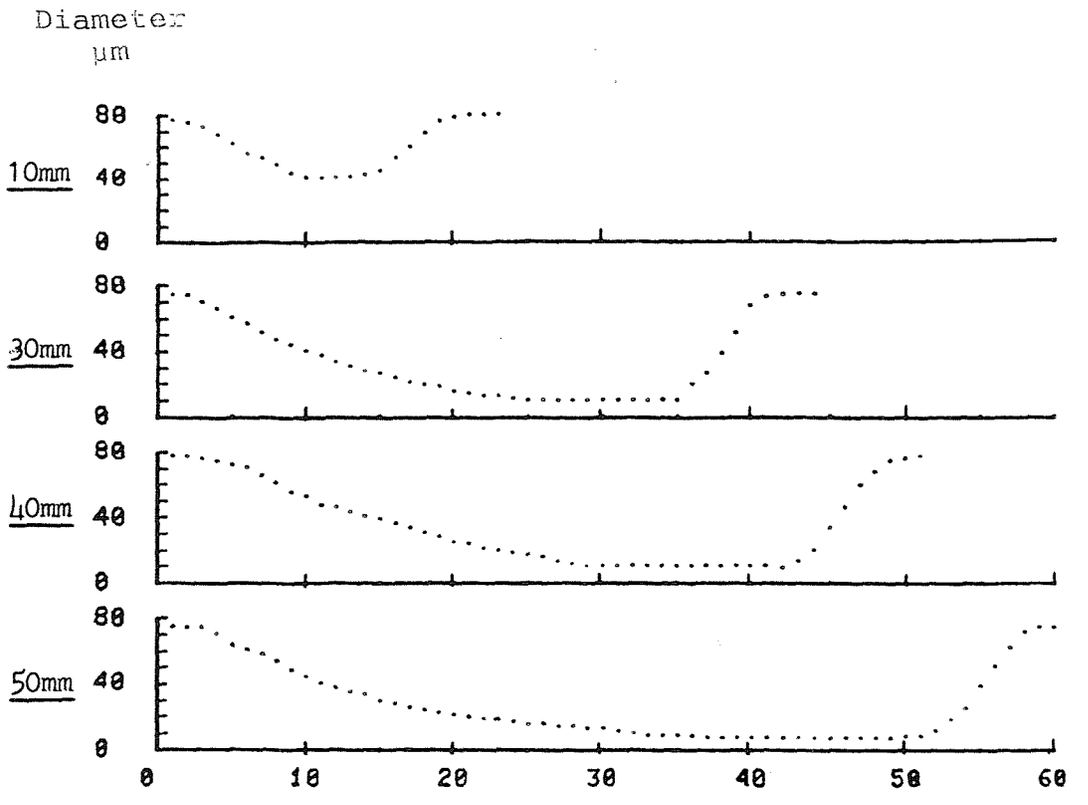

Figure 4.5. Taper shapes for different elongation lengths (10, 30, 40 and 50mm) for tapers drawn under identical conditions.

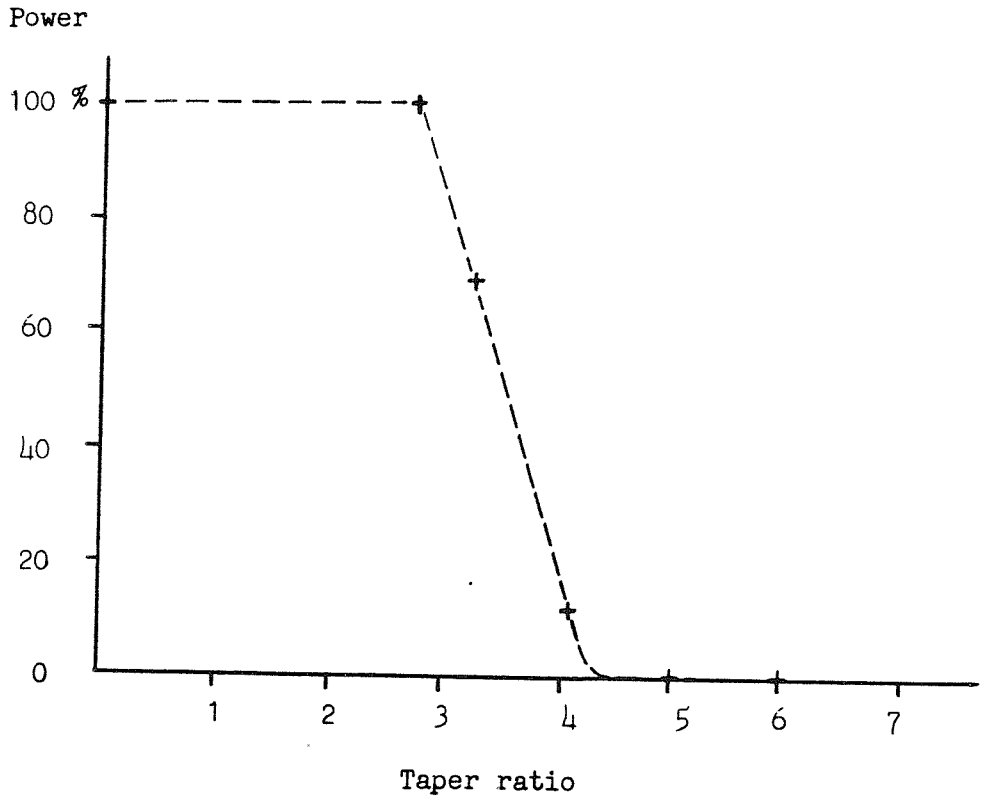

Figure 4.6. Percentage of power guided by the core when the refractive index of the external medium is matched to the cladding.

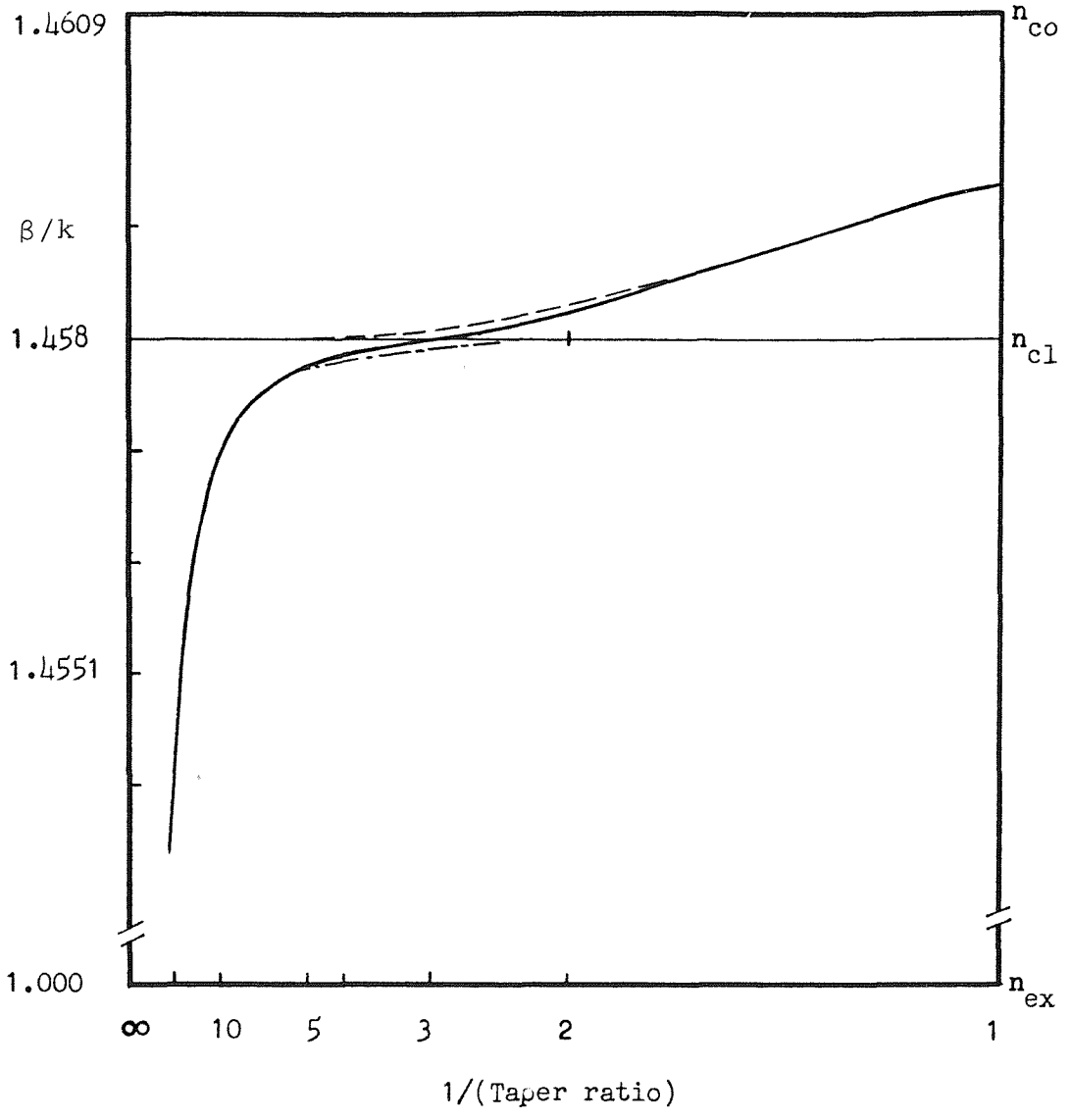

Figure 4.7. Effective refractive index of fundamental mode for the fibre with the same parameters as for the experimental results of Figure 4.6..

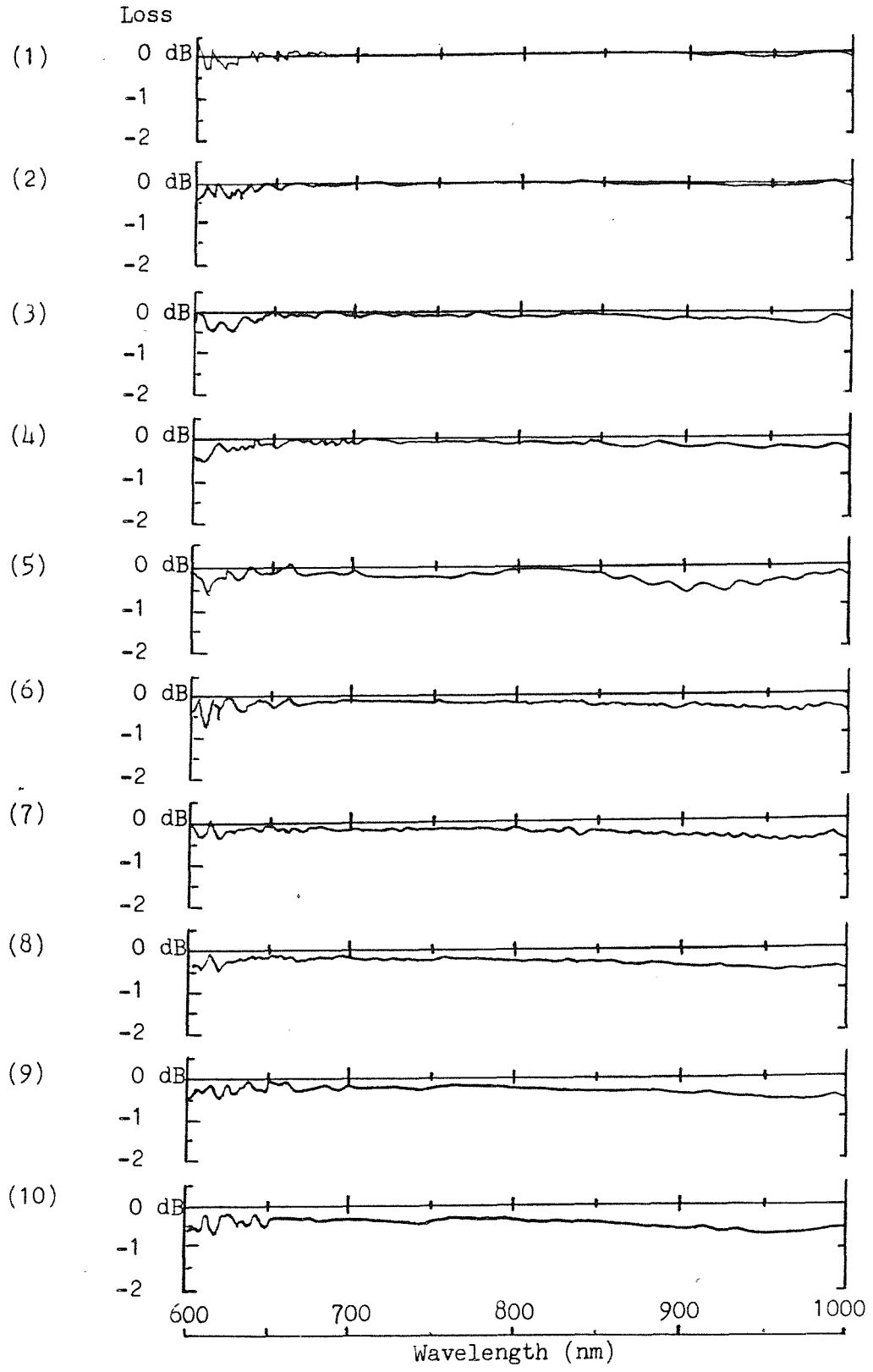

Figure 4.8. Spectral loss for the same fibre as it is elongated at every 5 mm from 5 mm (1) to 50 mm (10).

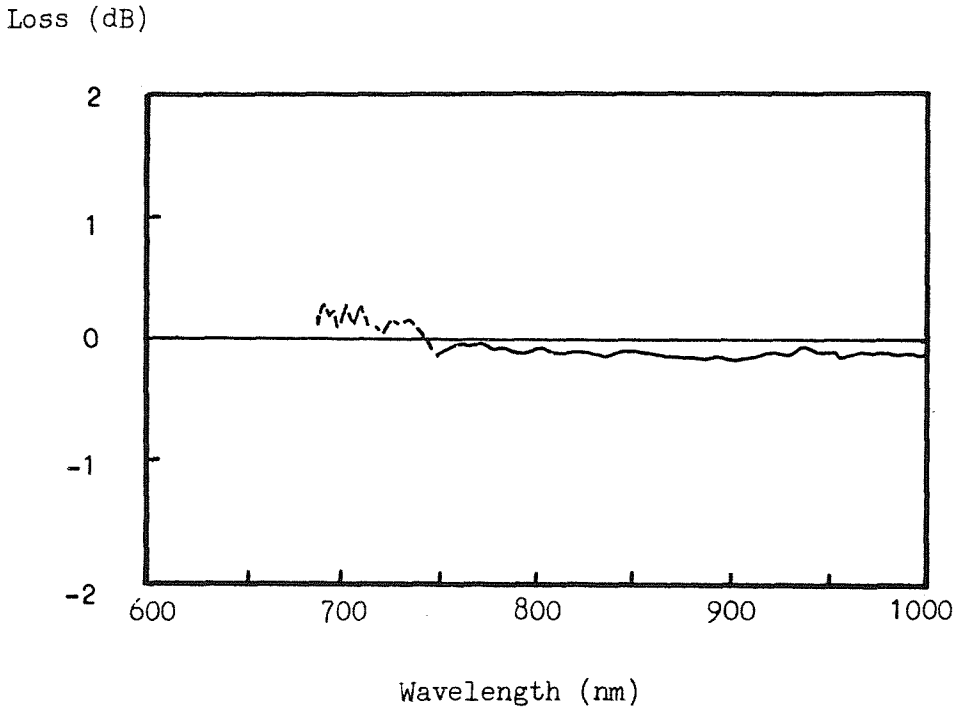

Figure 4.9. Spectral loss for a taper of 50mm elongated and fabricated in the normal manner to be used as a reference when examining Figures 4.8.1. - 10..

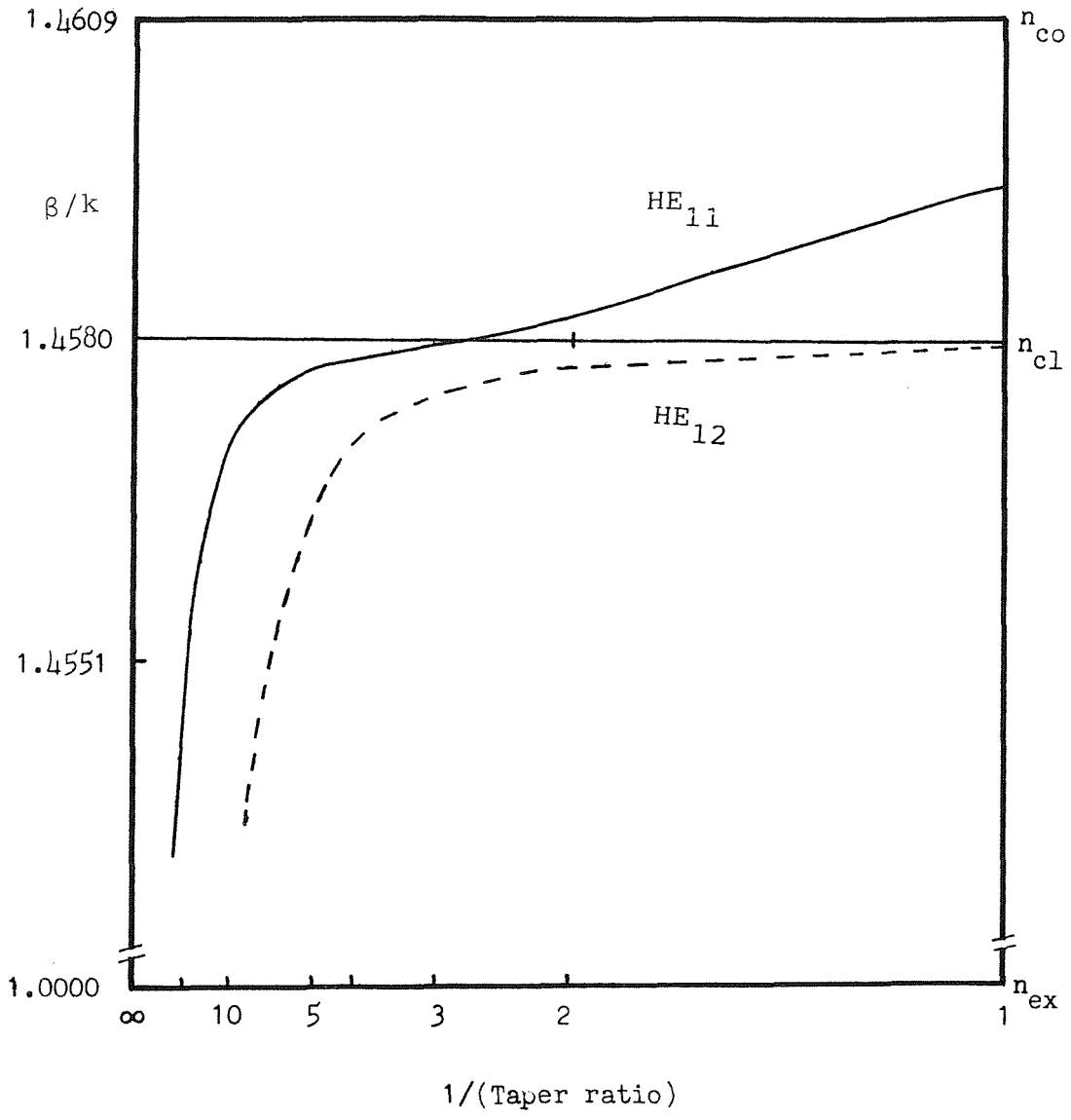

Figure 4.10. Effective refractive index for the HE_{11} and HE_{12} modes in a single mode fibre taper.

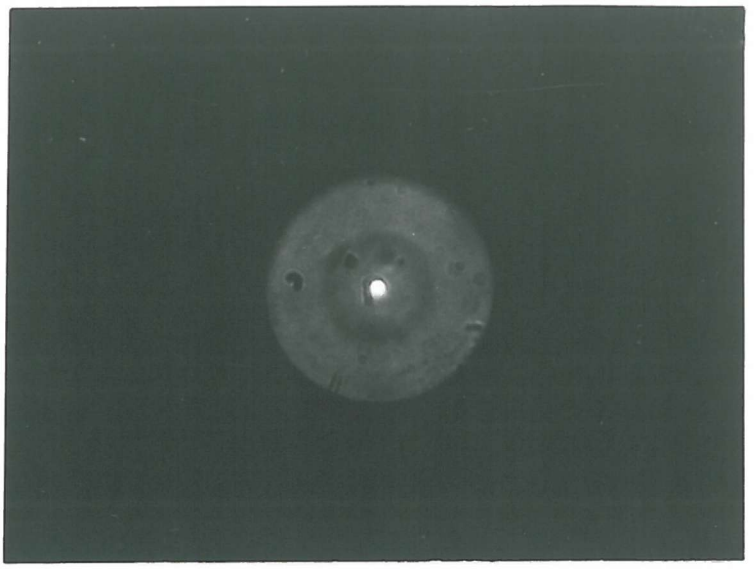

(a)

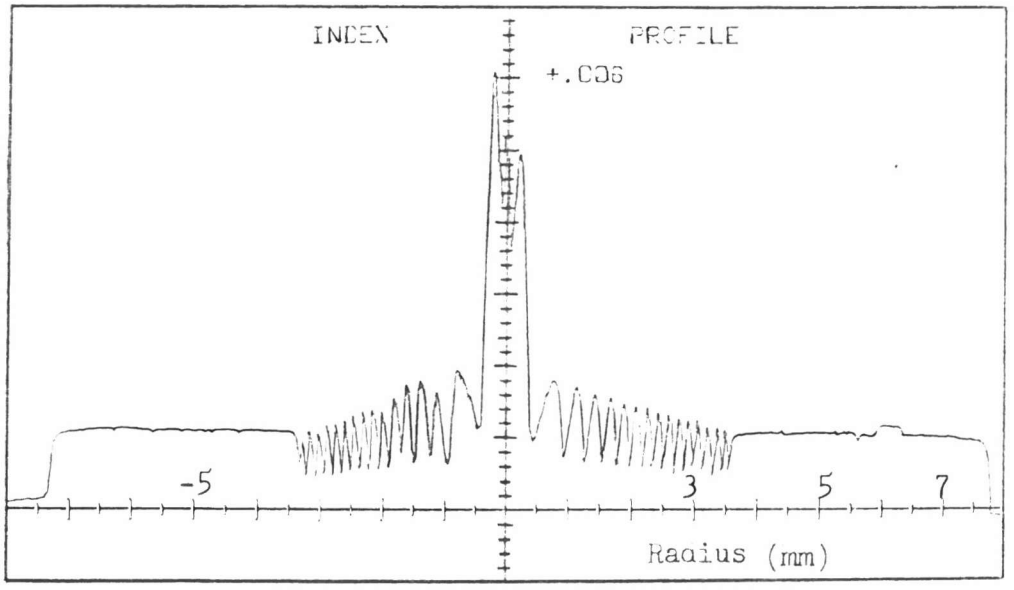

(b)

Figure 4.11. Eccentric core fibre (ND74).

(a) Photograph of cross-section.

(b) Refractive index profile.

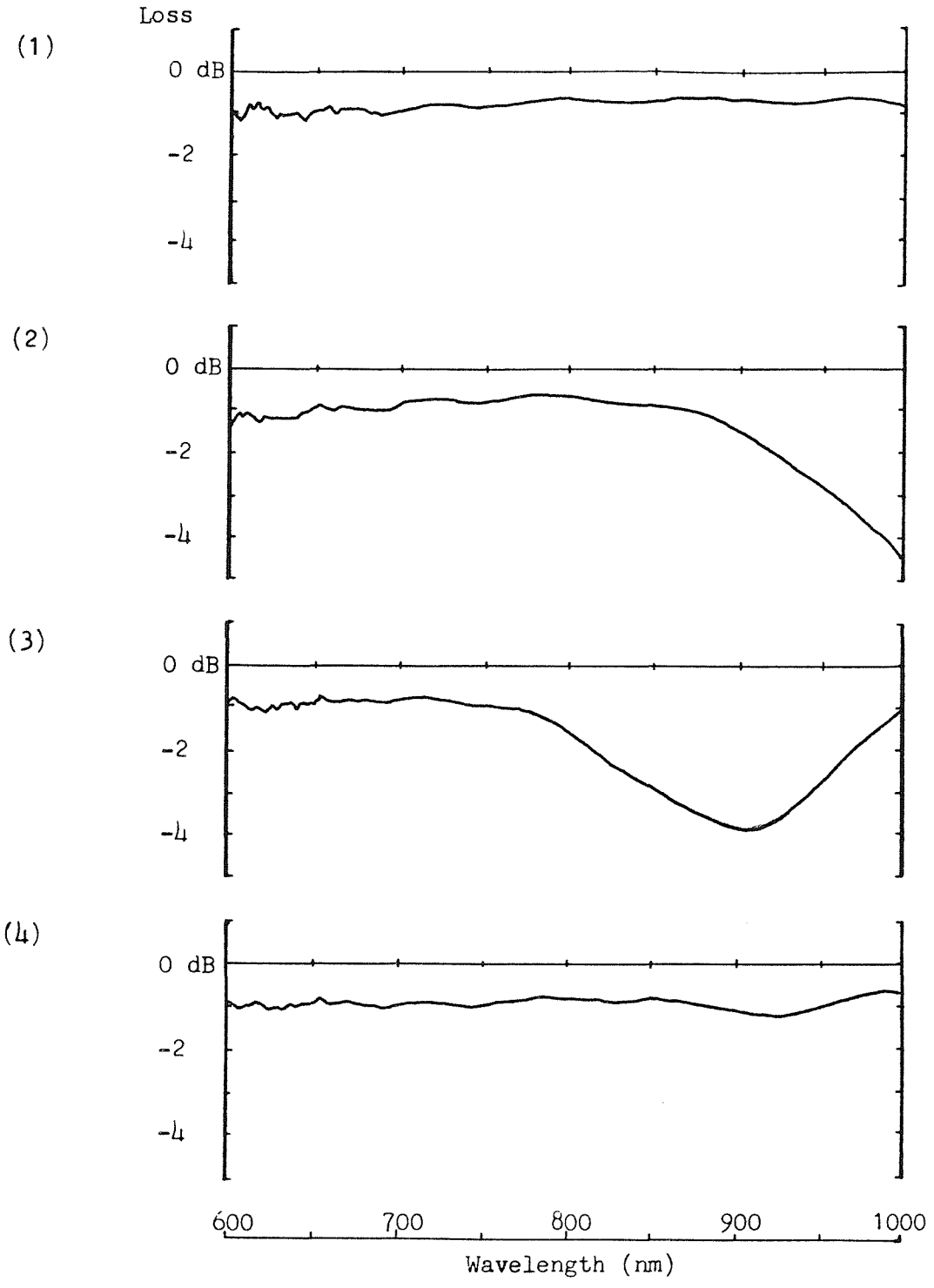

Figure 4.12. Spectral loss for an eccentric core fibre for various taper lengths.
(1) 5 mm, (2) 7 mm, (3) 8 mm and (4) 10 mm.

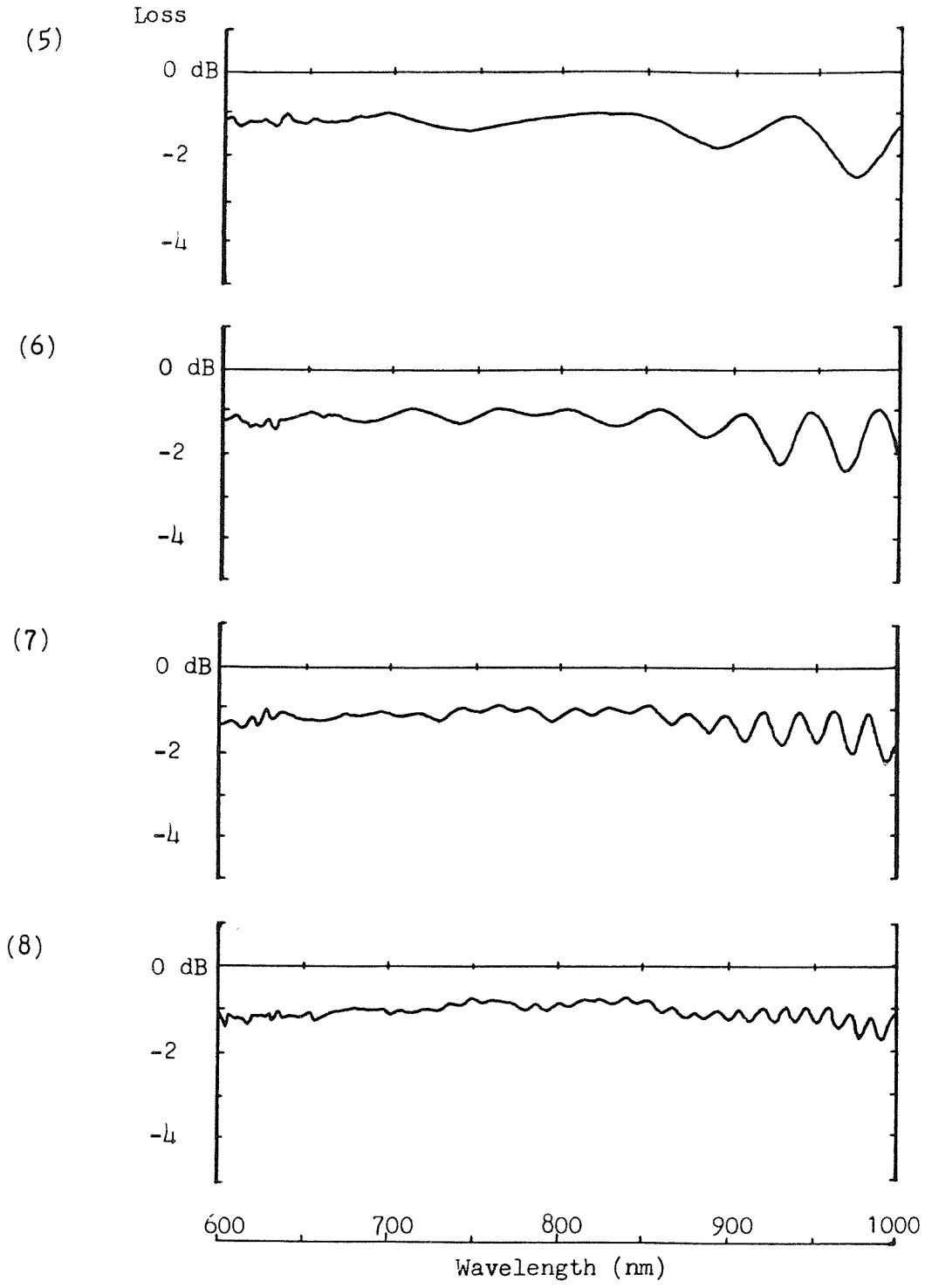

Figure 4.12. (contd.) Spectral loss for an eccentric core fibre for various taper lengths.
(5) 15 mm, (6) 20 mm, (7) 25 mm and (8) 30 mm.

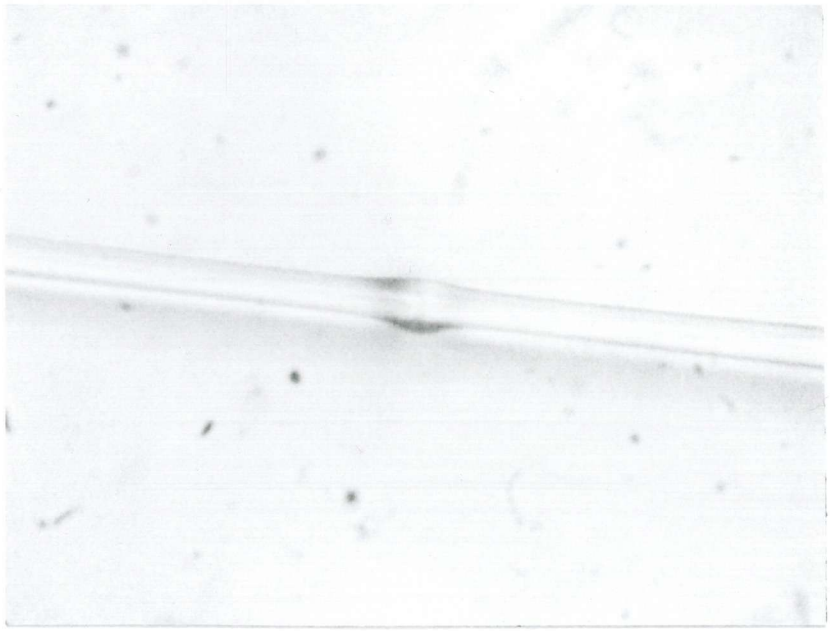

Figure 4.13. Defects in the fibre ; e.g. air bubble.

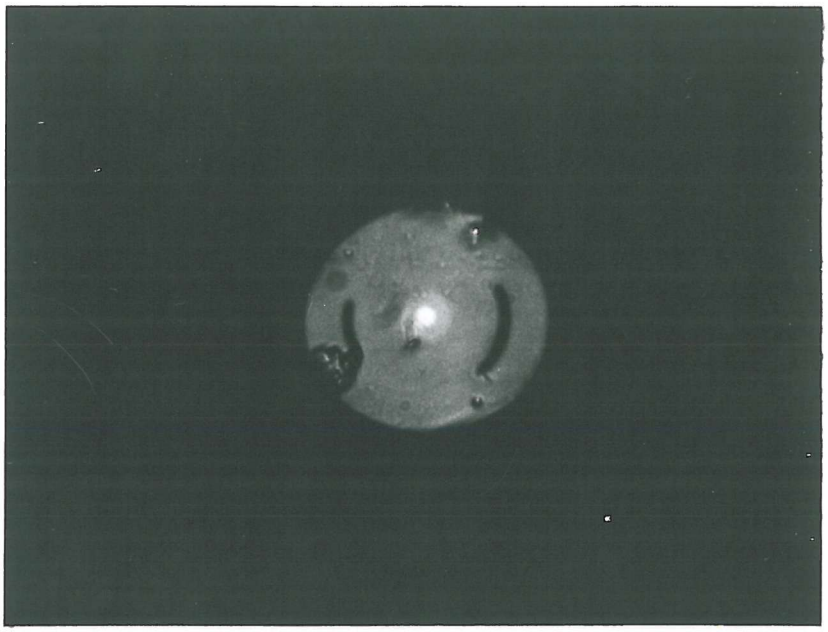

Figure 4.14. Defects in the fibre ; e.g. air gaps.

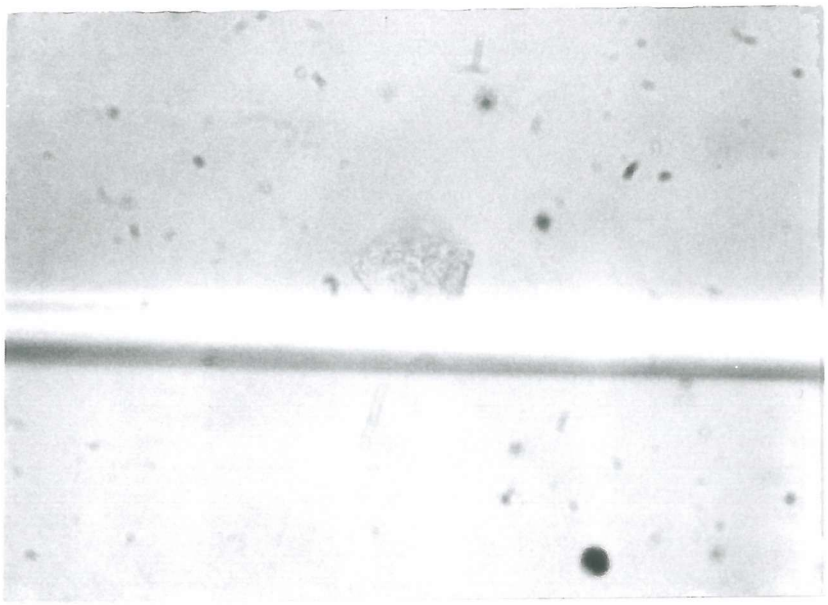

Figure 4.15. Foreign substances; e.g. particle on coupler.

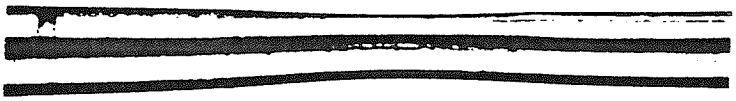

Figure 4.16. Irregular taper.

CHAPTER 5: CHARACTERISTICS OF TAPER COUPLERS

5.1 Introduction

Chapter 2 described the general features of single mode fibre directional couplers, while Chapter 4 showed that taper based devices relied of necessity, on cladding mode behaviour. This chapter examines the experimental responses of a range of taper couplers, from short to medium to long lengths, with respect to coupler dimensions, wavelength, external refractive index and polarisation. More complete data is presented elsewhere (1) for some of the examples presented in this chapter.

5.2 Structure and Features of Taper Couplers

Figure 5.1(a) gives a schematic of the fused taper coupler structure showing the asymmetrical input and output taper transitions, the region in the waist of the coupler having a fairly constant dimension irrespective of coupler length. The cross sectional shape may or may not vary along the coupler length depending on the extent of fusion of the fibres. In any case, the cross section of the waist region tends to be uniform for a particular coupler. Different cases are illustrated in Figure 5.1(b).

5.2.1 Spectral response with length

In the first experiment, the loss and the power splitting ratio with respect to wavelength and pulling length for a coupler fabricated from fibre YD2 (λ_{CO} = 633 nm, OD = 80μm, NA = 0.1) is investigated.

The fibres were prepared for coupler fabrication and the loss and power splitting ratio were measured for the wavelength range 600-1000nm. The fibres were then elongated in steps of 1 mm up to a total of 70 mm, with the loss and power splitting ratio measured at each step. The loss and splitting ratio for each 7 mm increment from 7-70 mm are shown in Figures 5.2.1-10. The following observations are made from this data:-

(i) High loss was encountered at the beginning of the process before coupling was initiated. A maximum loss of 2dB occurring at an elongation length of 6 mm. The loss then decreased and stabilised with length and follows the same pattern as the initial loss occurring in simple tapers, as discussed in the previous chapter.

(ii) Coupling initially occurs at longer wavelength.

(iii) The spectral splitting ratio is periodic with wavelength. The oscillation period decreases with increase in coupler length.

(iv) The overall loss increased slightly with elongation owing to the increase in susceptibility to contamination, since the whole experiment took approximately five hours to complete. In addition, heat was applied intermittently seventy times over this period.

5.2.2. Length Response with Wavelength

The data generated in the previous experiment were

reprocessed in order to generate the loss and splitting ratio responses as functions of length at different wavelengths. Figure 5.3.1-5 shows the loss and splitting ratio variation with length for the wavelengths 600 nm, 700 nm, 800 nm, 900 nm and 1000 nm. The data was compiled with a 50 nm spectral interval so that the responses are smoothed out to a certain extent. The following observations are made:-

(i) At each wavelength the initial coupling takes place slowly, but after the first coupling oscillation the period of oscillation remains virtually constant.

(ii) Coupling occurs sooner (i.e. at shorter elongation lengths) and the coupling oscillations are more rapid for longer wavelengths.

5.2.3 Summary Graphs

The general behaviour of the splitting ratio with wavelength and coupler length are summarised in Figures 5.4 and 5.5. In Figure 5.4 the oscillation period, $\Delta\lambda$, is plotted as a function of the elongation length.

The oscillation period is clearly inversely related to the coupler length. Indeed, by allowing a lag in the length of approximately 25 mm before the regular wavelength oscillations occur then the relationship is a direct inverse

$$\Delta\lambda \quad \alpha \quad \frac{1}{L} \qquad (5.1)$$

where L is the elongation length minus 25 mm.

In Figure 5.5 the oscillation length, Δz, is plotted as a function of wavelength. Since this oscillation length remains fairly constant for elongation lengths greater than 40 mm, in this graph the oscillation length, Δz, as measured at the 60 mm elongation length is plotted. In this case the relationship between Δz and λ is again approximately a direct inverse, viz.

$$\Delta z \propto \frac{1}{\lambda} \qquad (5.2)$$

5.3 Effect of Fibre Diameter and Very Long Lengths

For this experiment an optical fibre preform was fabricated to produce a fibre with an outside diameter (OD) of 40 μm and a second mode cutoff wavelength of 600 nm. A portion of this preform was then sleeved in order to yield an 80 μm OD fibre with the same cutoff wavelength. The process is shown schematically in Figure 5.6, the purpose being to keep all parameters except the fibre OD fixed in order to isolate the effects of the OD.

5.3.1 Taper Geometries

In the first stage of this experiment, tapers of different lengths were formed from each of the two fibres using identical burners. The taper shapes were measured as shown in Figure 5.7 for similar elongation lengths. The shapes tend to be the same with only their diameters scaled with the fibres' ODs.

5.3.2 Spectral Response with Length

Couplers using these two different fibres were elongated up to 60mm, and the spectral splitting ratio responses were measured at each 10mm elongation. The responses are shown in Figures 5.8.1-6. For both couplers the oscillation period, $\Delta\lambda$, decreases with elongation length as shown in Figure 5.9, a trend which was found previously. The coupler made from the 40μm fibre has a much smaller oscillation period for a given length - indicating much stronger coupling than for the 80μm fibre coupler.

In both couplers an additional modulation appears in the spectral splitting ratio responses after a certain elongation length, with the modulation appearing sooner in the smaller diameter fibre coupler.

The period of this new modulation, $\delta\lambda$, tends to decrease with increasing wavelength. This additional modulation is due to the polarisation behaviour of the coupler as is described in Chapter 2 and which is examined in detail in the following section.

5.4 Polarisation Effects

A coupler was fabricated from a fibre (ND 53) with a diameter of 80μm an NA of 0.13 and a cutoff wavelength of 580nm. The elongation length of the coupler was 200mm. The spectral splitting ratio response is shown in Figure 5.10 for the usual unpolarised input and the polarisation modulation is found to be present.

In order to verify that the modulation was indeed due to polarisation effects as outlined in Chapter 2 the following procedure was undertaken. The linearly polarised eigenstates of the coupler were individually identified by inserting a polariser at the input port and tuning the wavelength to 880 nm, where the coupling responses for the two orthogonal polarisations are completely dephased.

The spectral responses of the splitting ratio were then individually measured for both orthogonal polarisations and are shown in Figure 5.11. Each polarisation has a constant oscillation with wavelength (i.e. with no modulation) but the oscillation periods are slightly different. In this case the responses are in phase at approximately 750 nm and out of phase at approximately 880 nm, which correspond to the maximum and minimum, respectively, of the modulation in the spectral response to unpolarised light as in Figure 5.10. Indeed, on adding the two responses in Figure 5.11 using the data as stored in the computer Figure 5.12 was obtained, which is virtually identical to Figure 5.10.

5.4.1 Variation of Modulation Period with Wavelength

In order to investigate the variation of the modulation period with wavelength, an extremely long coupler with a lot of modulation periods within the wavelength range of the measurements was required. A coupler was fabricated with the fibre ND 53 to an elongation length of 300mm. There were eleven modulation periods in the wavelength range 500-1000

nm as shown in Figure 5.13. Figure 5.14 plots the ratio of the modulation period $\delta\lambda$ with the wavelength oscillation period $\Delta\lambda$ as a function of λ^{-1}, and a straight line dependence is found.

5.5 Effects of the Surrounding Medium

In packaging the coupler it is generally required to surround the tapered region with a low index resin in order to provide a very robust device as described in Chapter 3. Since the operation of the coupler depends on the waveguide formed at the cladding to external medium interface, any coupler characteristics which have been measured during fabrication (i.e. in air) will be changed, with the extent of the change depending on the characteristics of that surrounding medium.

To explore the effects in detail, the variation in the spectral splitting ratio response was investigated by placing fluids of different refractive indices around the coupling region.

Immediately after fabrication the coupler is fixed in a housing with adhesive as shown in Figure 5.15(a). The spectral splitting ratio response is first measured in air and again measured when different fluids are applied as indicated in Figure 5.15(b). Couplers of three different lengths were examined.

5.5.1 Short Coupler

A short coupler with a 4:1 splitting ratio at a

wavelength of 850 nm on the first coupling oscillation was fabricated. The splitting ratio in air and in two different oils of refractive indices 1.426 and 1.446 respectively were measured and plotted in Figure 5.16. Care was taken to completely remove the first oil before the second was applied. From Figure 5.16 it is found that the coupling increases with increase in the refractive index of the surrounding medium. Transmission ceased altogether when an oil of refractive index 1.458 was applied to the coupler.

5.5.2 Medium Length Coupler

For this experiment the coupler which was elongated up to 70 mm as described in section 5.2 was employed. The spectral splitting ratio for the unpackaged coupler at room temperature ($24^{o}C$) is shown in Figure 5.2.10. The coupler was then packaged as in Figure 5.15. The spectral splitting ratio of the secured coupler was again measured at room temperature as shown in Figure 5.17. Comparing Figure 5.17 with Figure 5.2.10 it is found that the splitting ratio response was slightly modified with significant power remaining in the coupling port over the entire wavelength range: an effect which may be due to the adhesive causing an asymmetric stress in the coupler thereby restricting the extent of power transfer. However, the oscillation period $\Delta\lambda$ remained the same in each case, and it is this parameter that is of interest here.

The coupler was then placed in an environmental

chamber, the temperature was raised to 70°C and the spectral splitting ratio was measured and found to be identical to that of Figure 5.18, confirming the temperature stability of the packaged coupler.

Fluid whose refractive index was known to be 1.4602 - 0.00038/°C at 25°C at a wavelength of 656.3nm was poured into the coupler container as in Figure 5.15(b). The spectral splitting ratio responses for this coupler were then measured at the temperature of 90°C, and then for -10°C steps in temperature down to 30°C; the responses are shown in Figures. 5.18.1-7. Figure 5.19 plots the variation in oscillation period $\Delta\lambda$ with refractive index change as derived from Figures. 5.18.1-7. It is found that the oscillation period decreases with increasing refractive index.

5.5.3 Long Coupler

A coupler was drawn to an elongation length of over 100 mm until the polarisation characteristics appeared. The coupler was then packaged as before. The spectral splitting ratio responses for this coupler in air and in water (n = 1.33) were measured and shown in Figures. 5.20 (a) and (b) respectively.

It is found that the oscillation period $\Delta\lambda$ decreases with increasing refractive index, while the polarisation modulation period $\delta\lambda$ increases with increasing refractive index.

5.6 Reciprocity

In the 4-port directional coupler there are two input and two output ports. From reciprocity, the transfer characteristic of the coupler (i.e. spectral splitting ratio) should remain the same irrespective of propagation direction through the coupler, that is, if the ouput ports are used as input ports and vice-versa.

A number of couplers were tested and reciprocity was confirmed in each case. For example, in the inset of Figure 5.21 a schematic coupler is drawn showing the input ports 1 and 2 and the output ports 3 and 4. Also shown are the spectral splitting ratio responses between ports 3 and 4 for input in port 1, and between ports 1 and 2 for input in port 3. The responses are identical but for a slight offset introduced for illustrative purposes.

5.7 Conclusion

This chapter has presented a lot of experimental results on the behaviour of the fused taper coupler with very little attempt at interpreting or explaining that behaviour. Such detailed discussion is left to the following chapter in the context of explaining the behaviour of the taper coupler in terms of a very simple coupler model.

References to Chapter 5

1. M.S. Yataki,

"Experimental Study of Optical Fibre Couplers",

Mini thesis, Southampton University, October 1986.

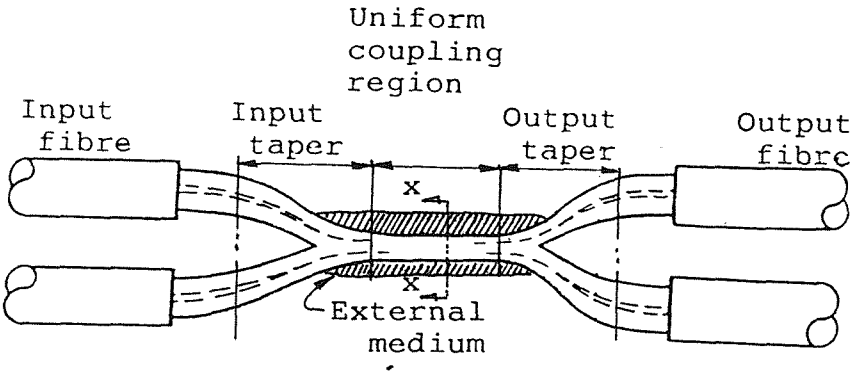

(a)

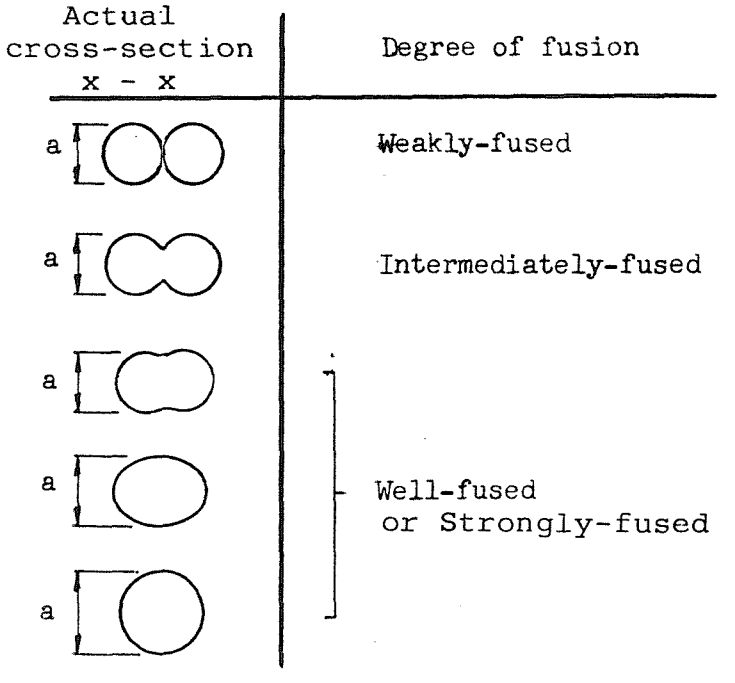

(b)

Figure 5.1.(a) Schematic of the fused taper coupler showing input and output tapers, the uniform coupling region and the external medium.

(b) Possible cross-sections of the uniform coupling region.

Figure 5.2. Excess loss and spectral power splitting ratio for the same coupler as it is being elongated at every 7 mm elongation length.

Figure 5.2.1. 7 mm

5.2.2. 14 mm

5.2.3. 21 mm

5.2.4. 28 mm

5.2.5. 35 mm

5.2.6. 42 mm

5.2.7. 49 mm

5.2.8. 56 mm

5.2.9. 63 mm

5.2.10. 70 mm

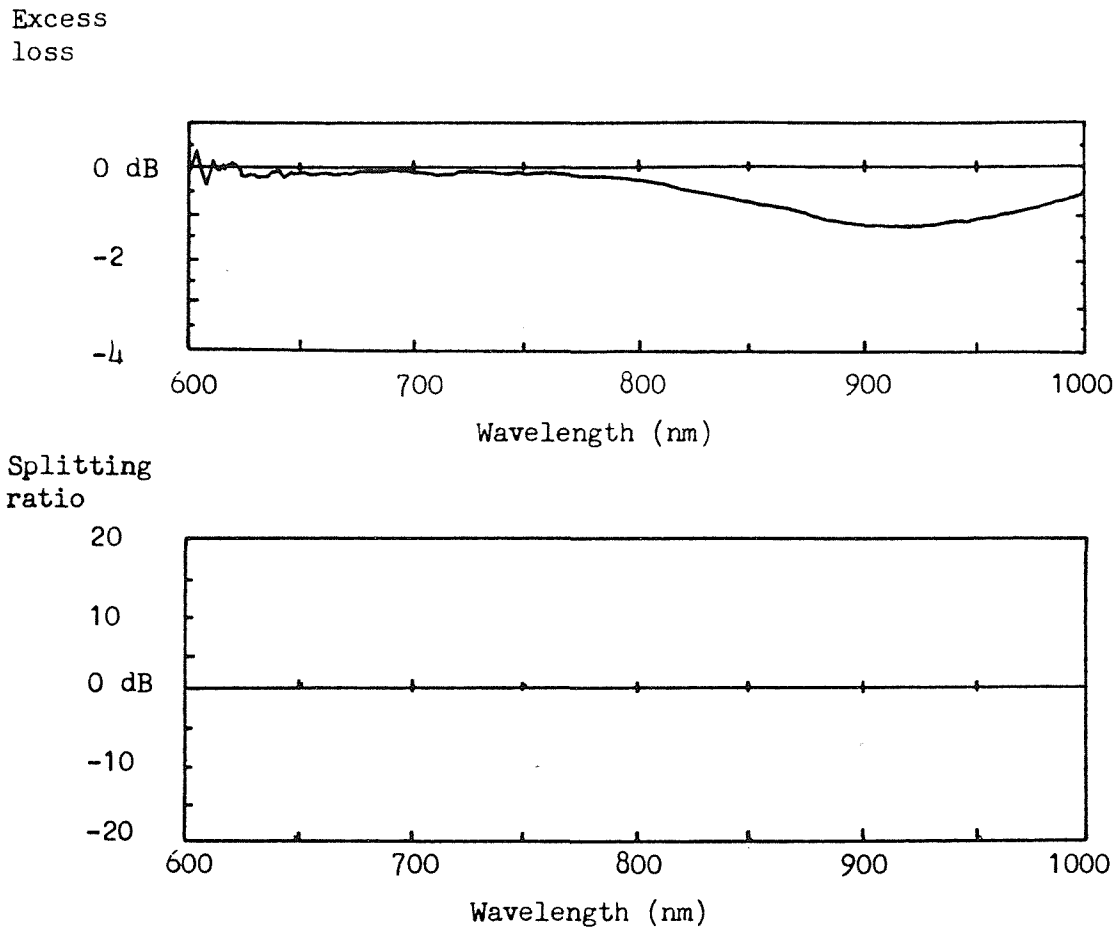

Figure 5.2.1. Elongation length 7 mm.

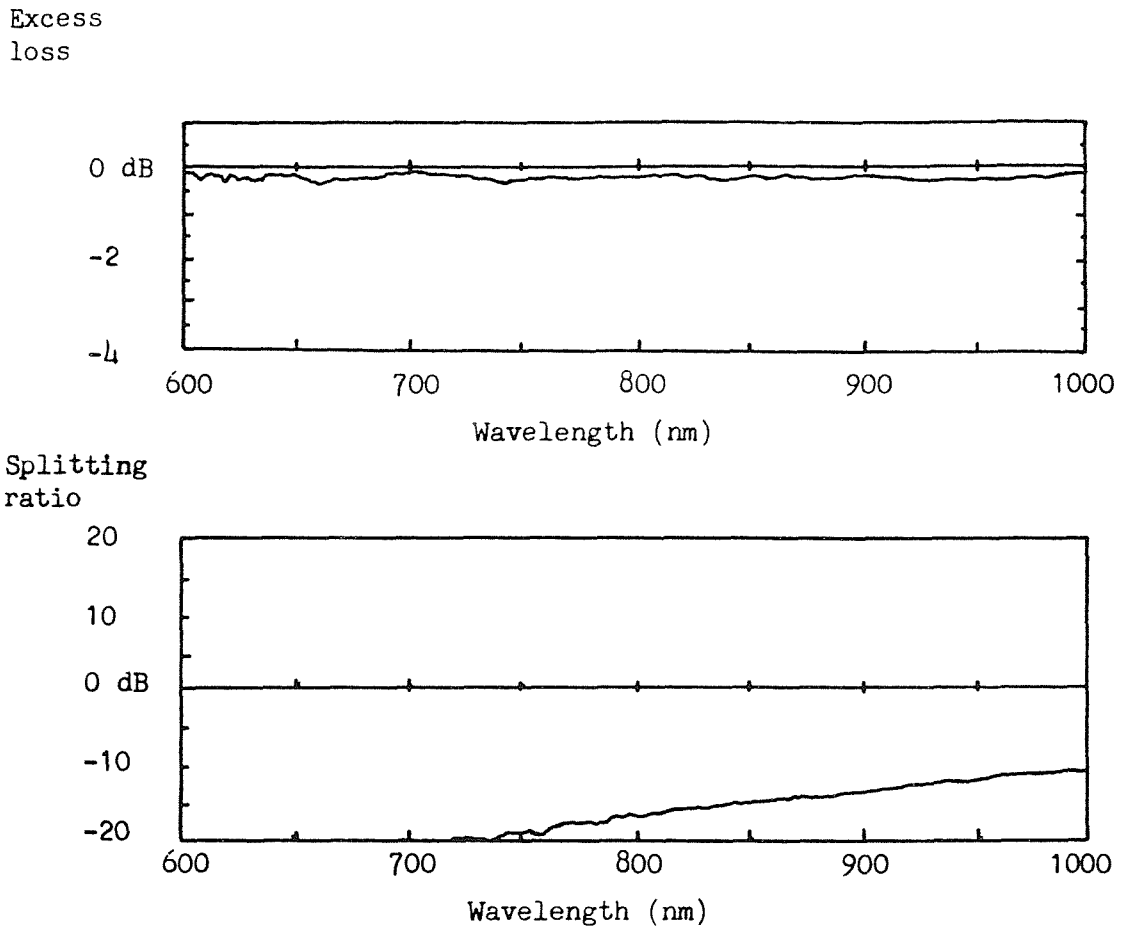

Figure 5.2.2. Elongation length 14 mm.

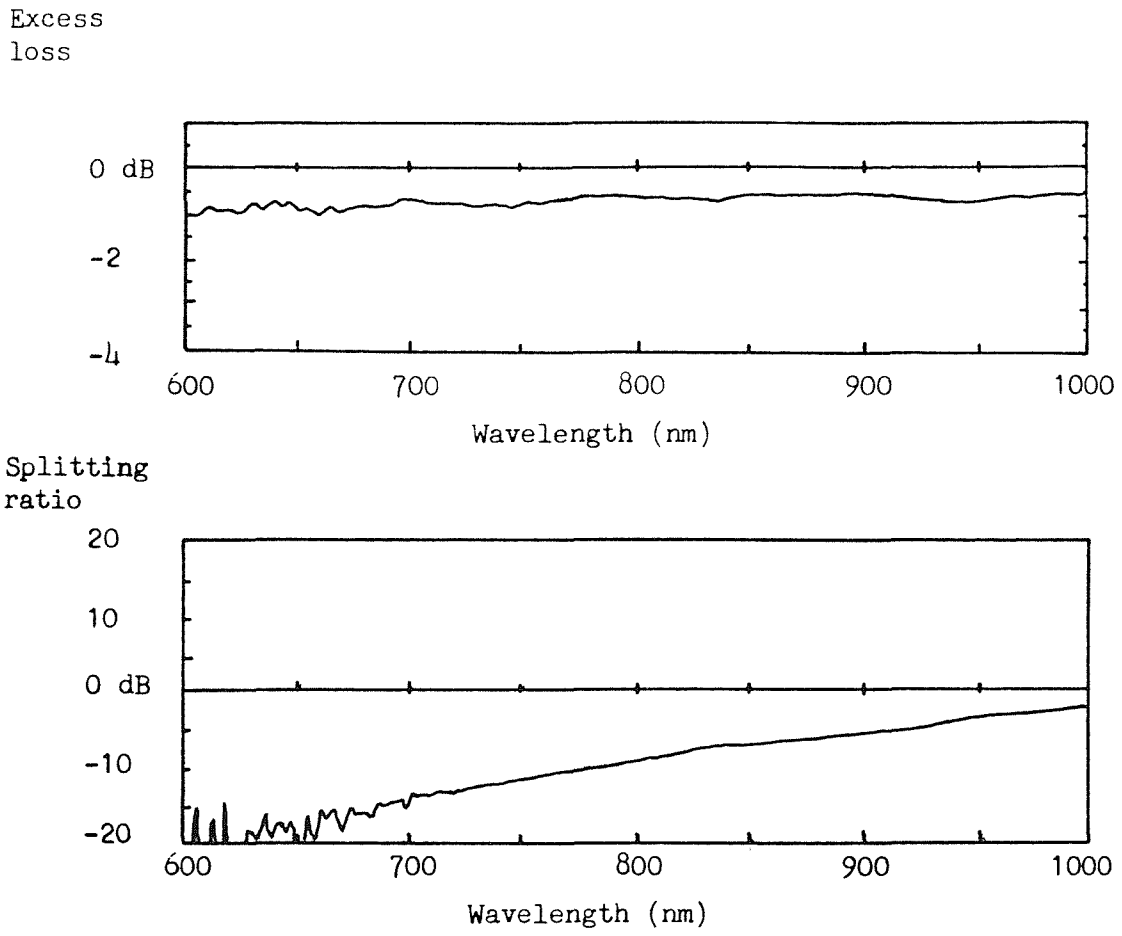

Figure 5.2.3. Elongation length 21 mm.

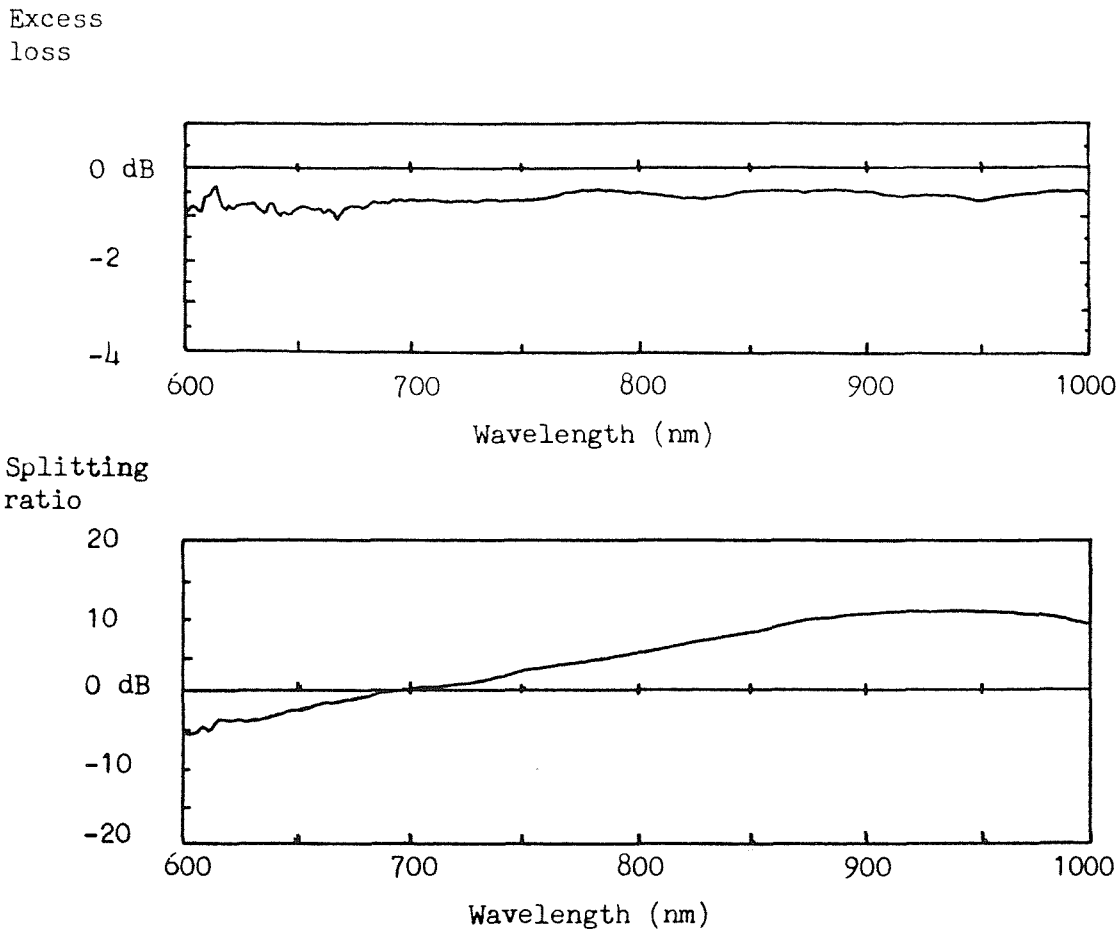

Figure 5.2.4. Elongation length 28 mm.

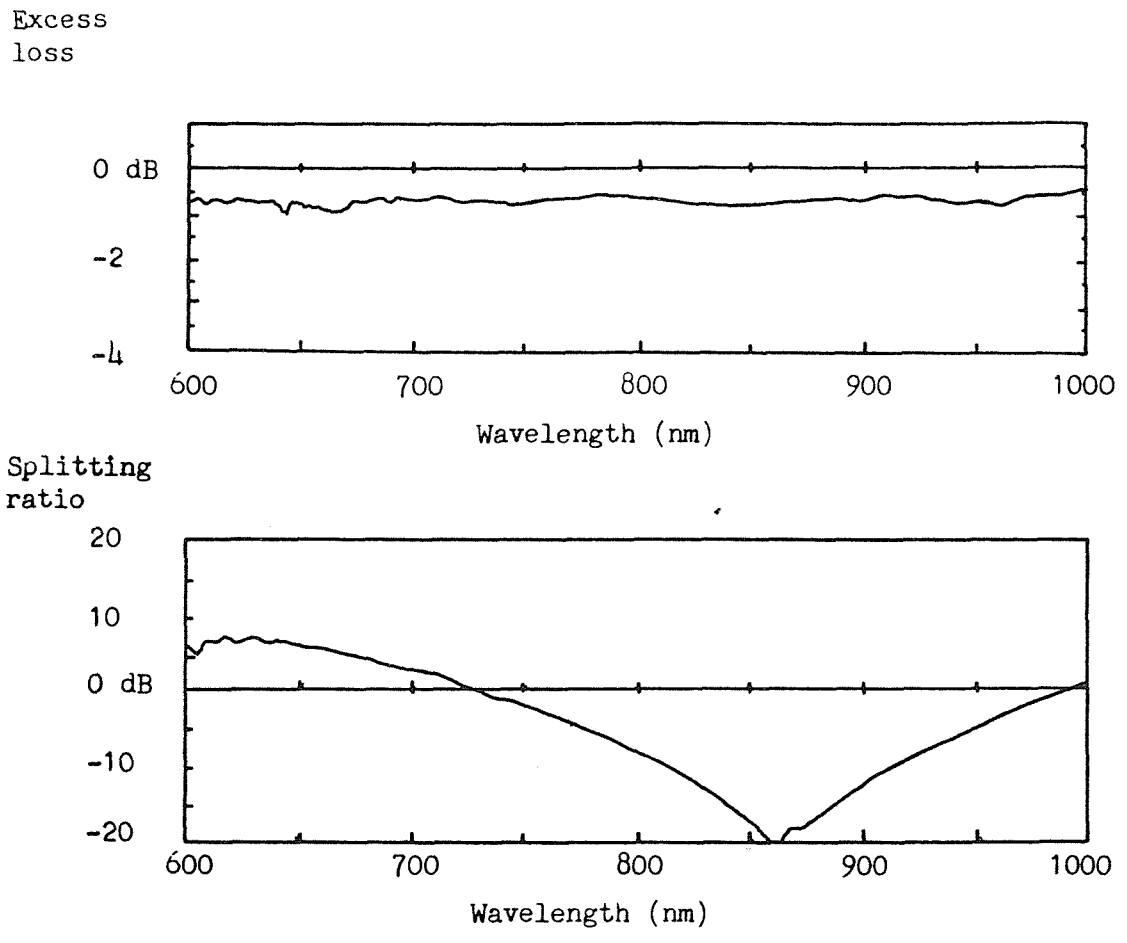

Figure 5.2.5. Elongation length 35 mm.

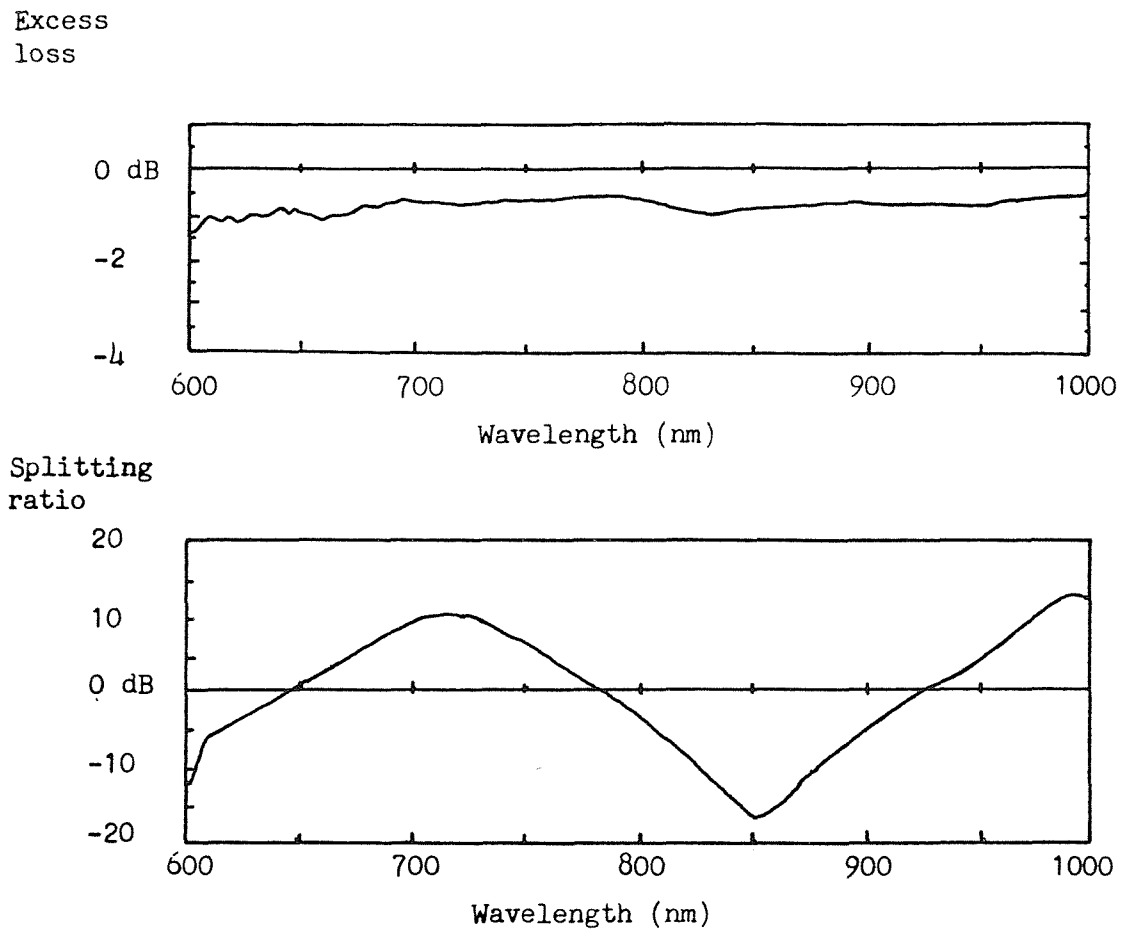

Figure 5.2.6. Elongation length 42 mm.

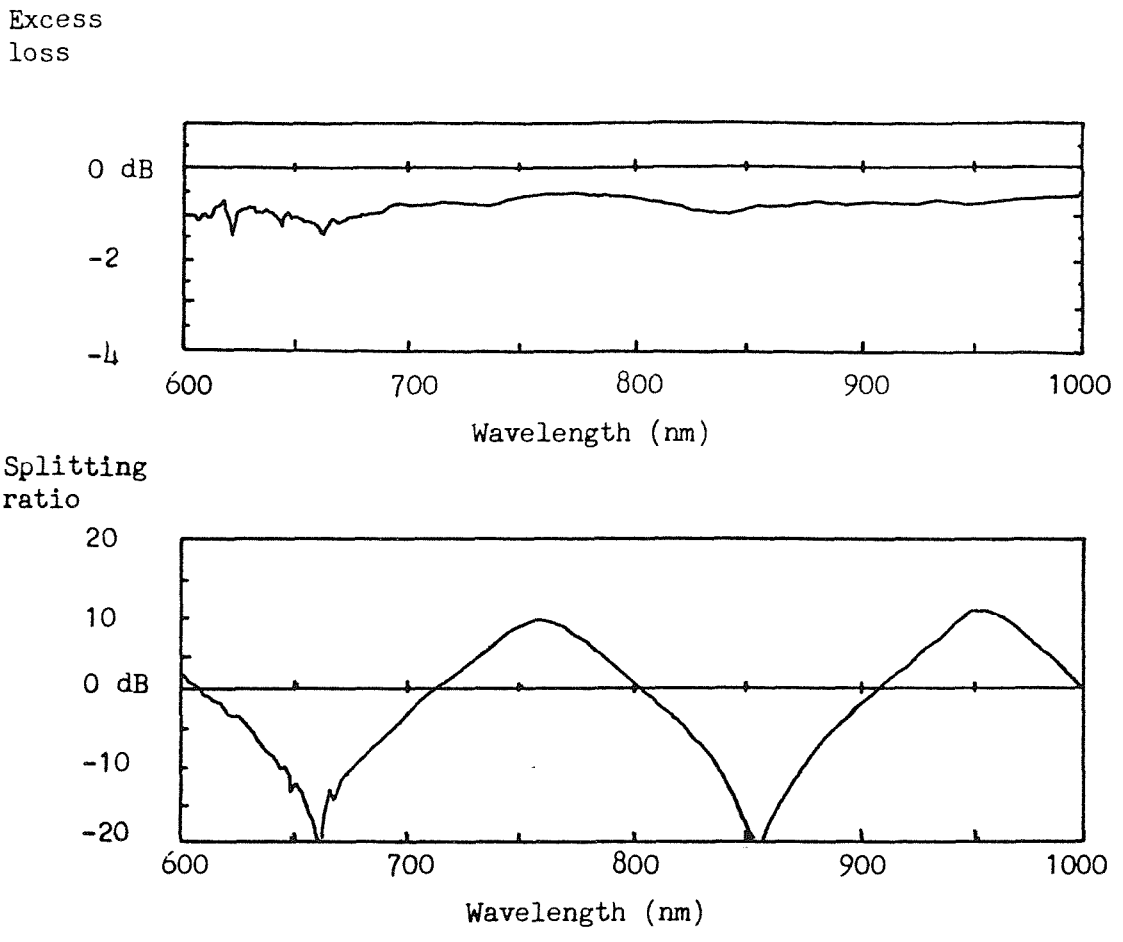

Figure 5.2.7. Elongation length 49 mm.

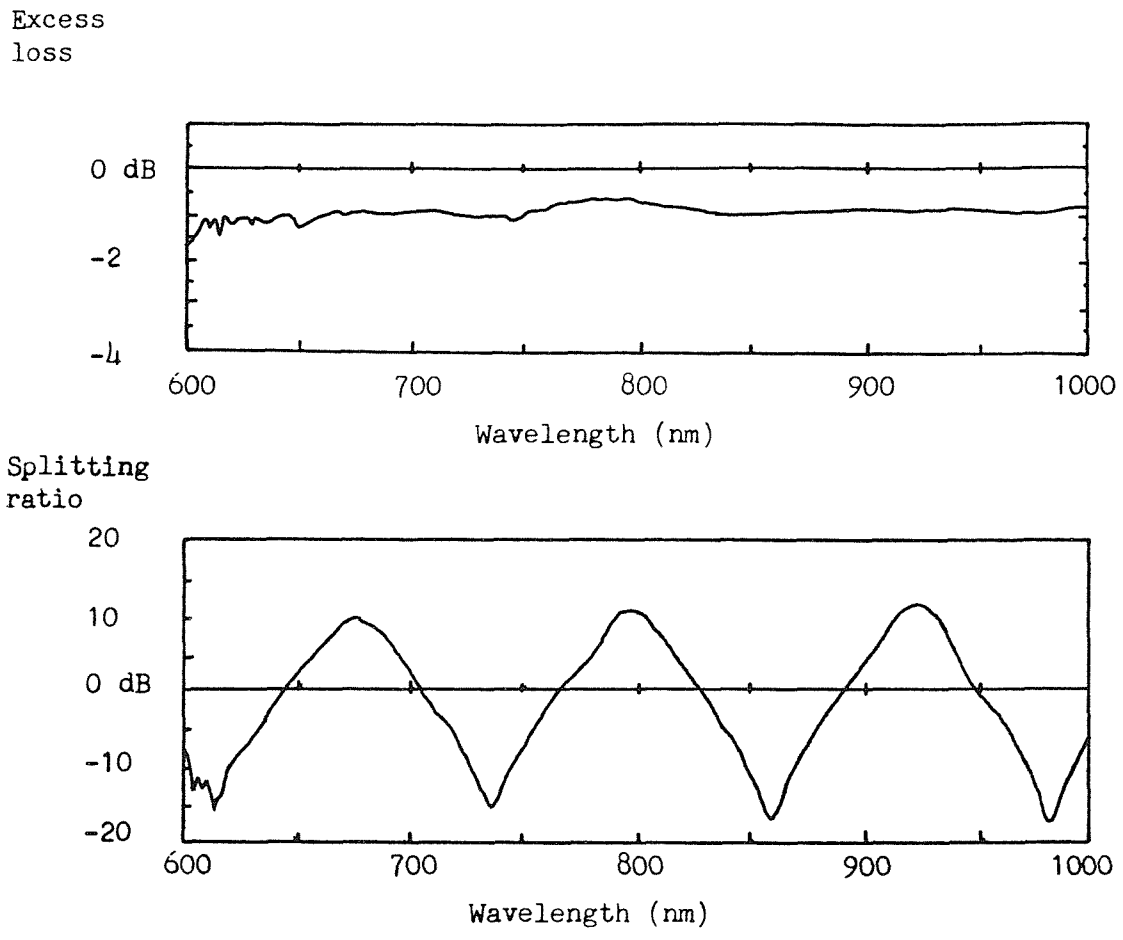

Figure 5.2.8. Elongation length 56 mm.

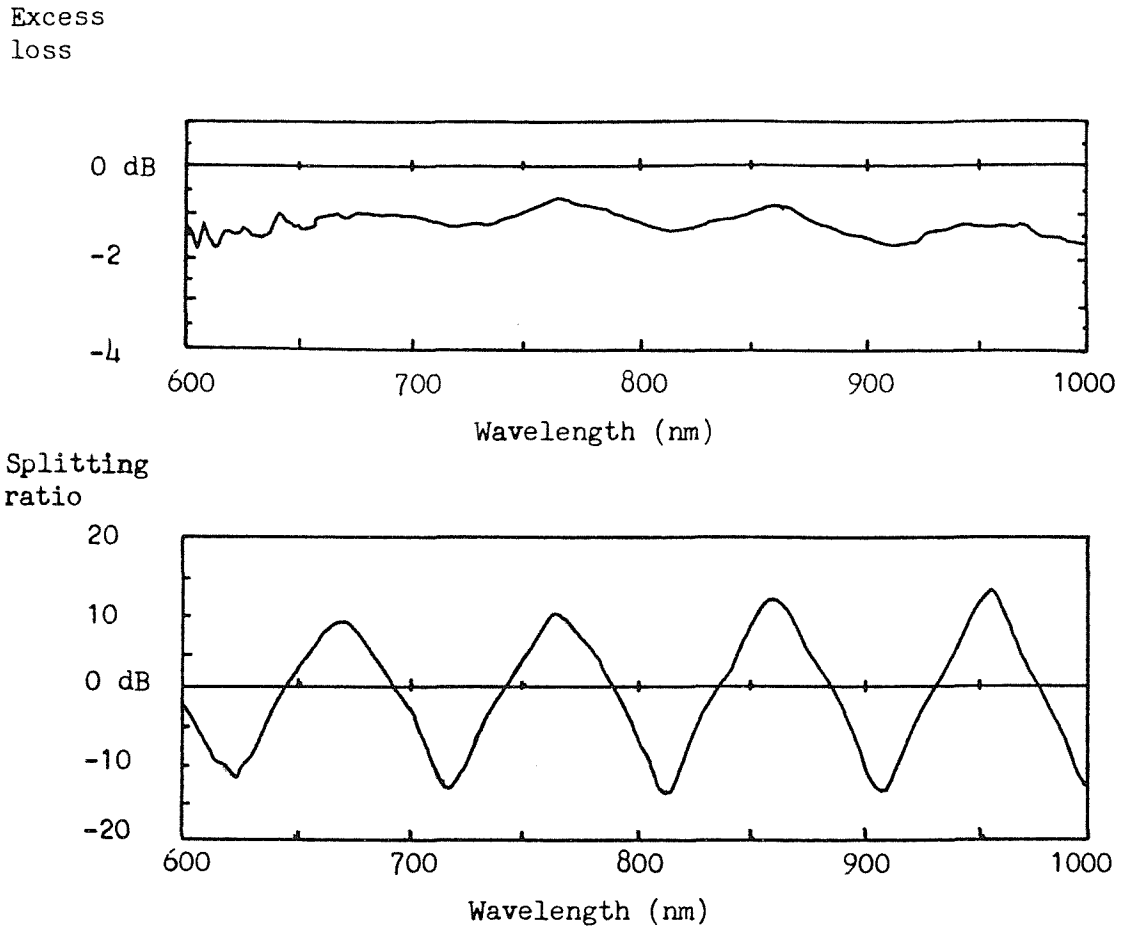

Figure 5.2.9. Elongation length 63 mm.

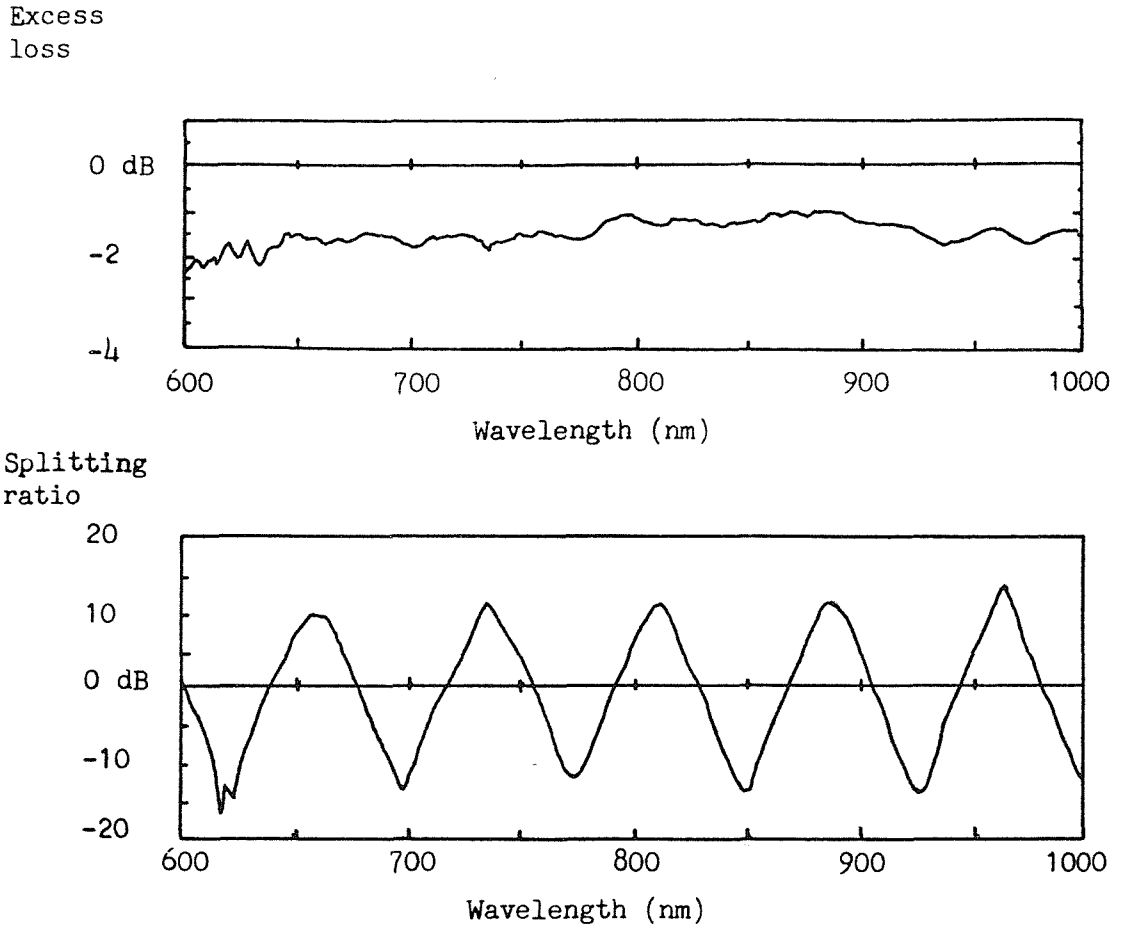

Figure 5.2.10. Elongation length 70 mm.

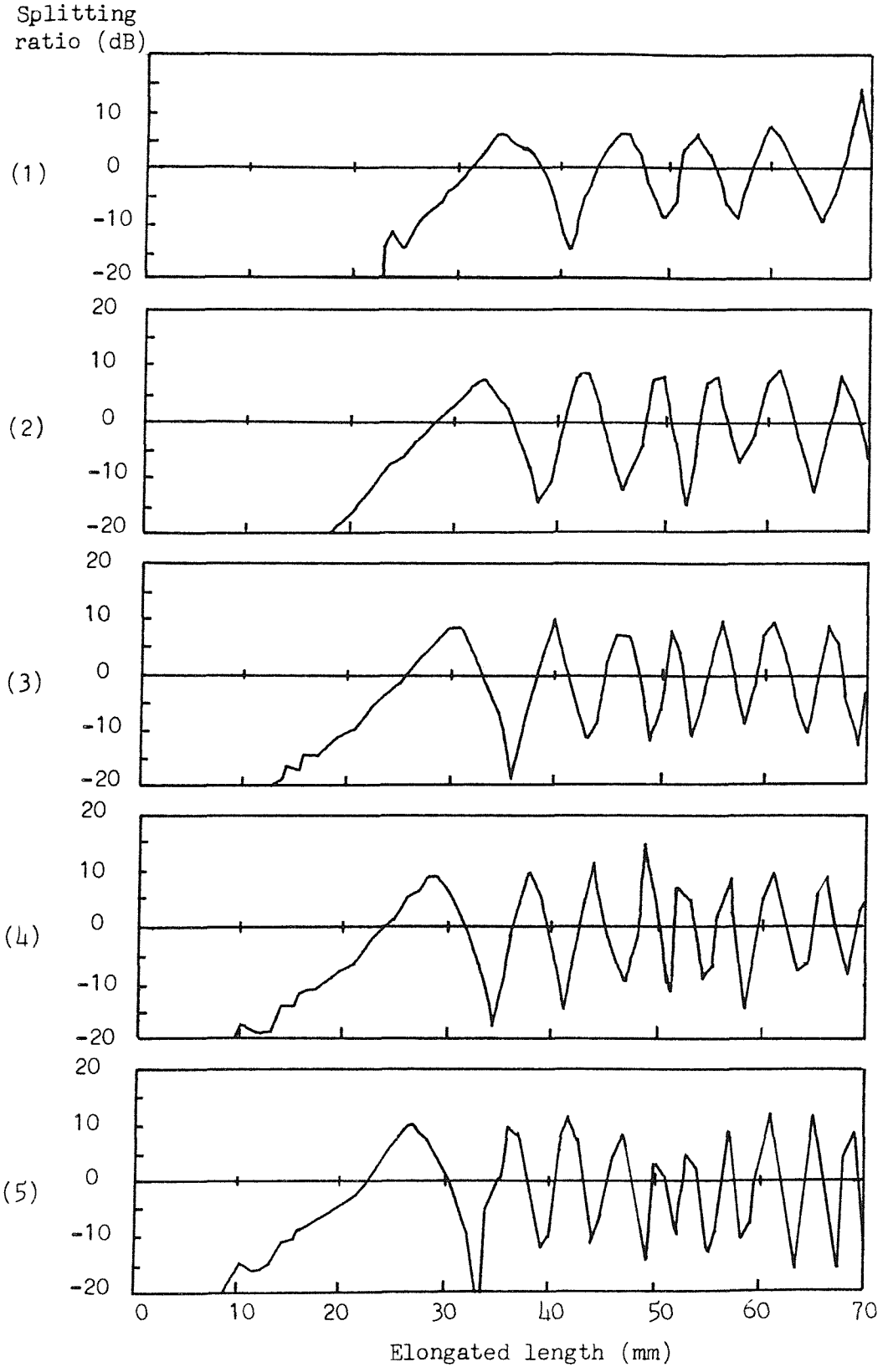

Figure 5.3. Power splitting ratio variation with elongated length as deduced from the spectral measurements for wavelengths of (1) 600 nm, (2) 700 nm, (3) 800 nm, (4) 900 nm and (5) 1000 nm.

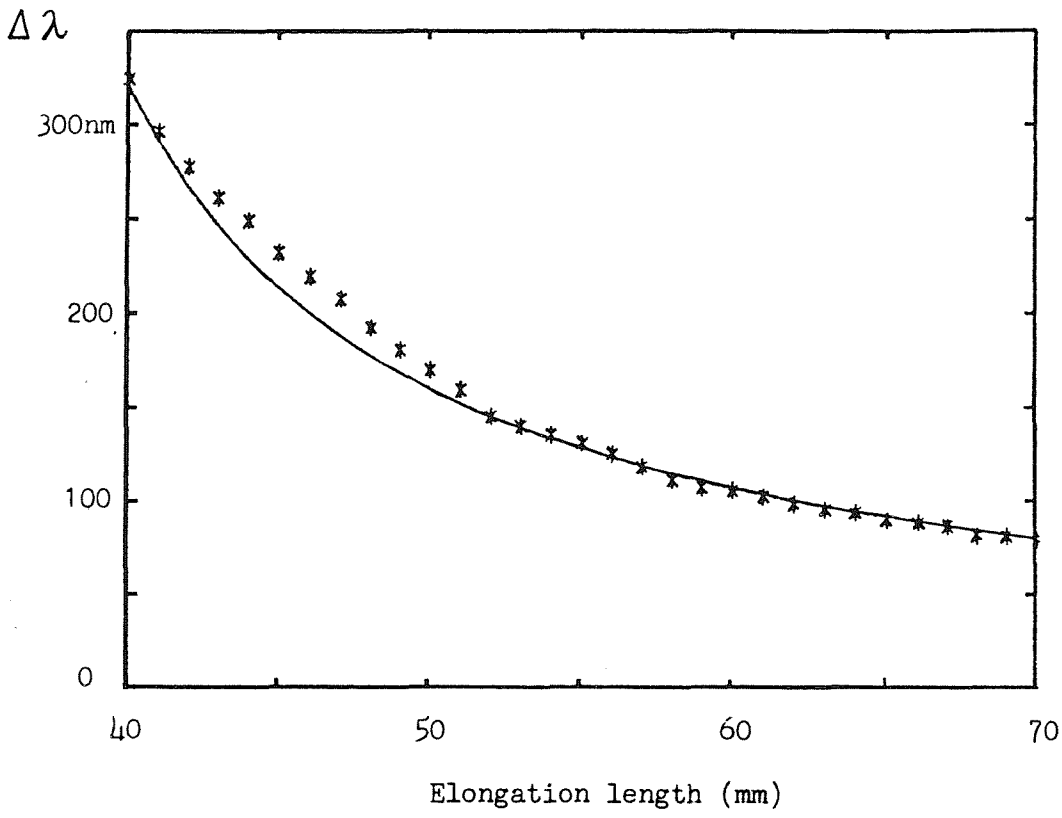

Figure 5.4. Oscillation period, $\Delta\lambda$, as a function of the taper elongation length.

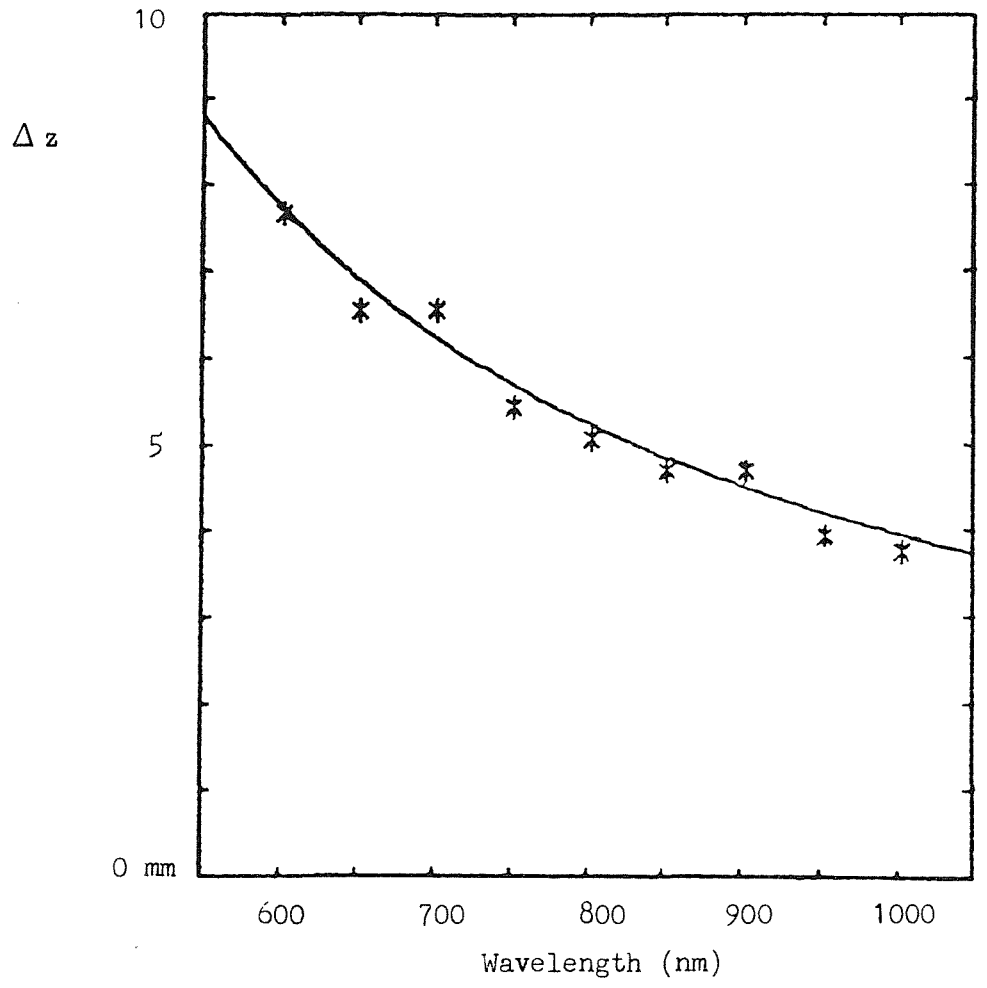

Figure 5.5. Oscillation length, Δz, as a function of wavelength for an elongation length of approximately 60 mm.

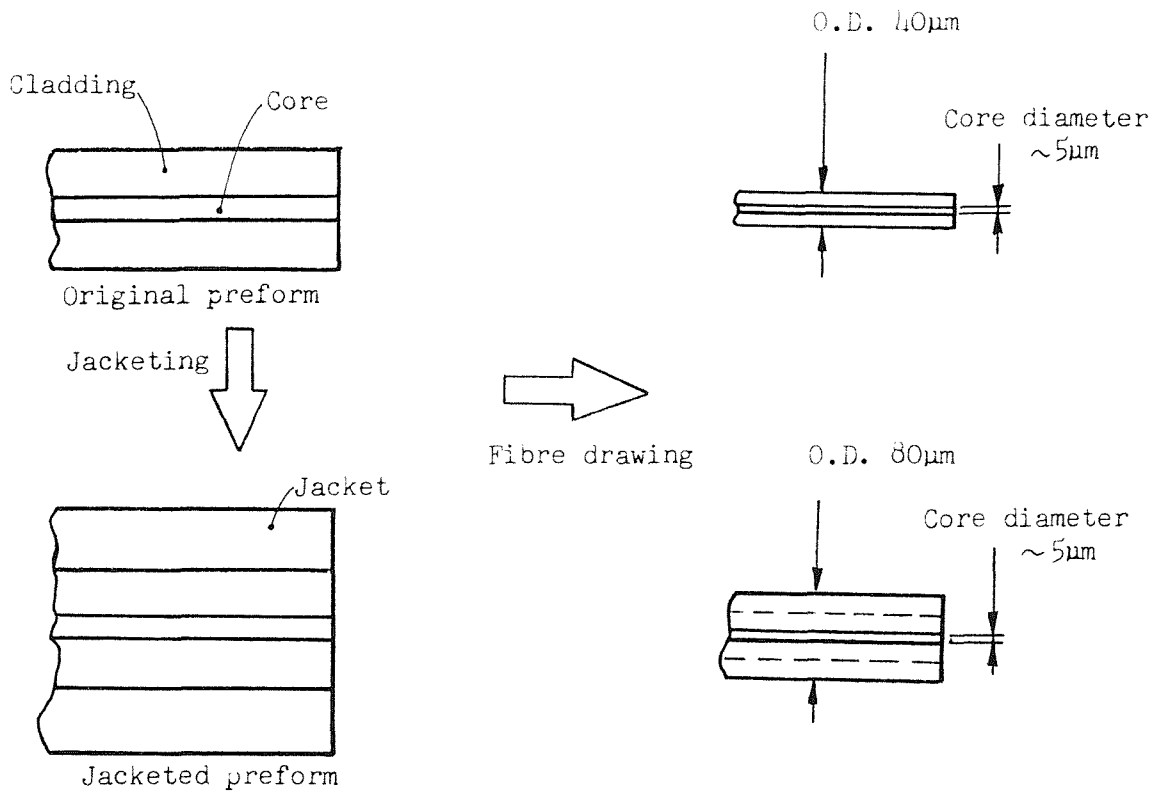

Figure 5.6. Schematic of the process whereby two fibres were fabricated which had different outside diameter but which were identical in every other respects.

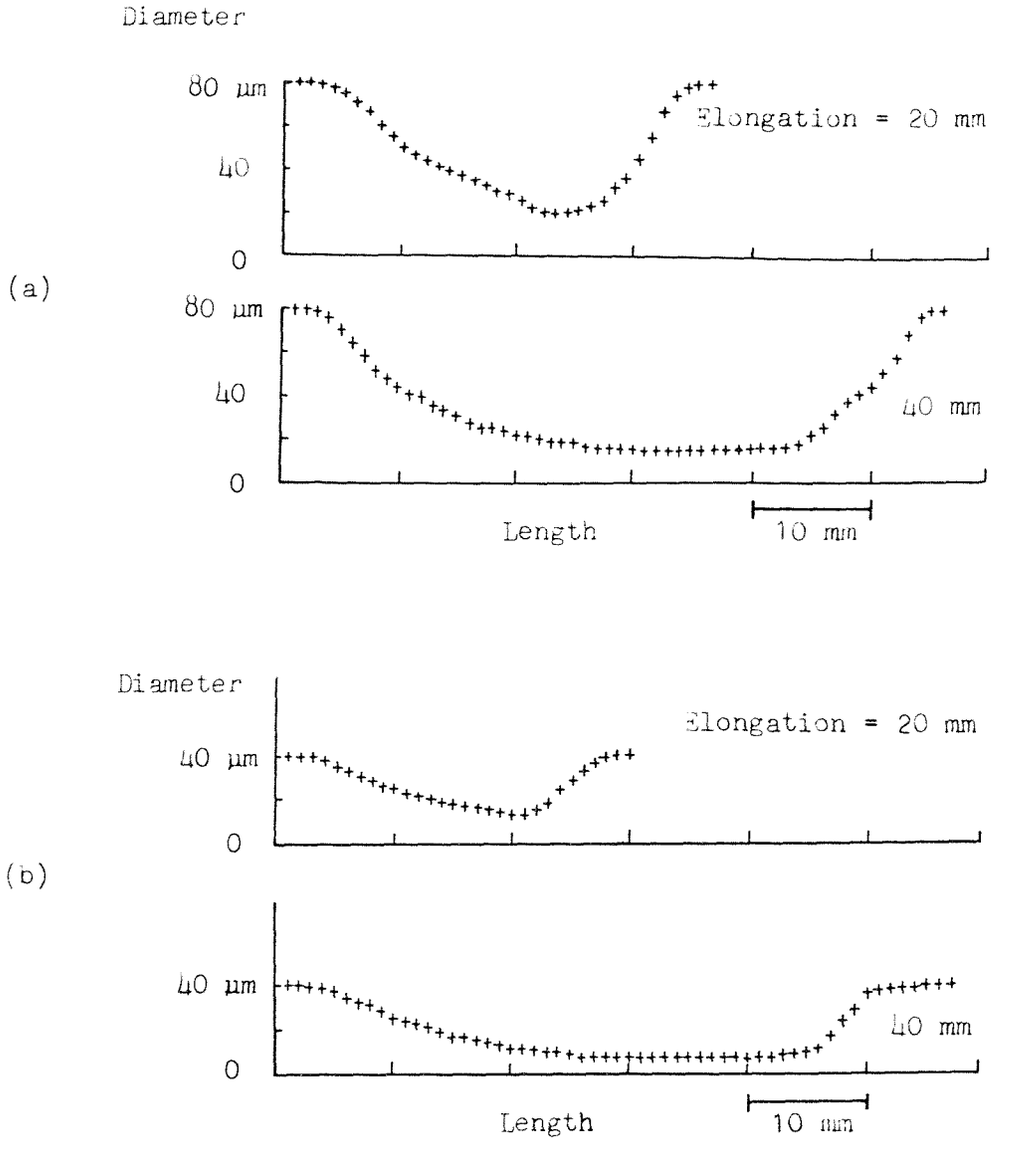

Figure 5.7. Taper geometries for two different elongation lengths for:

(a) 80 μm O.D. fibre,

(b) 40 μm O.D. fibre.

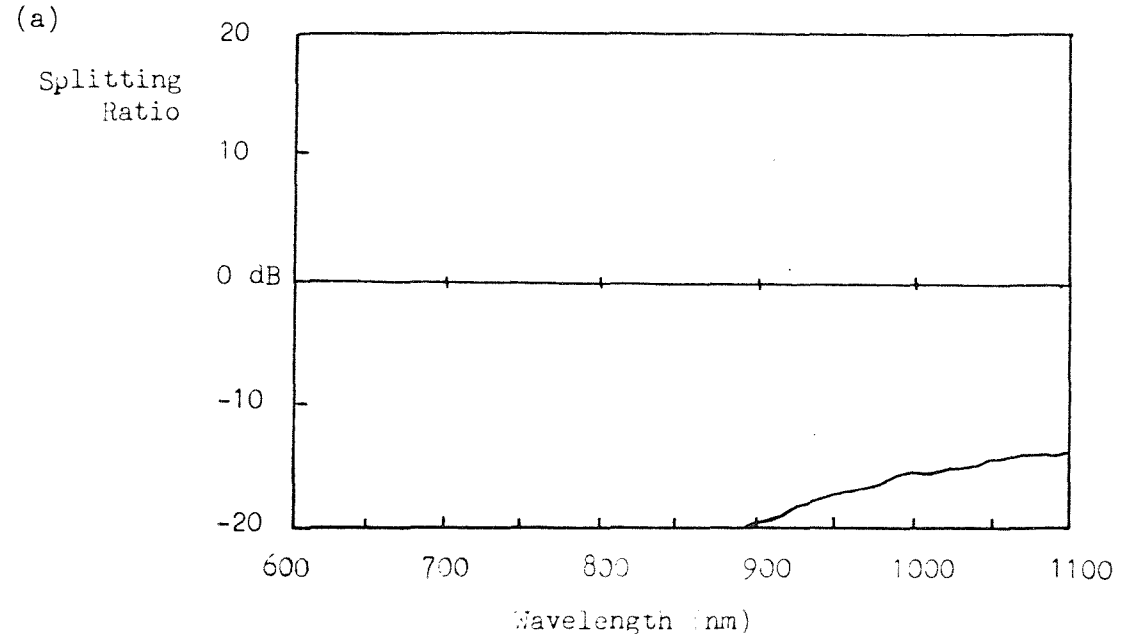

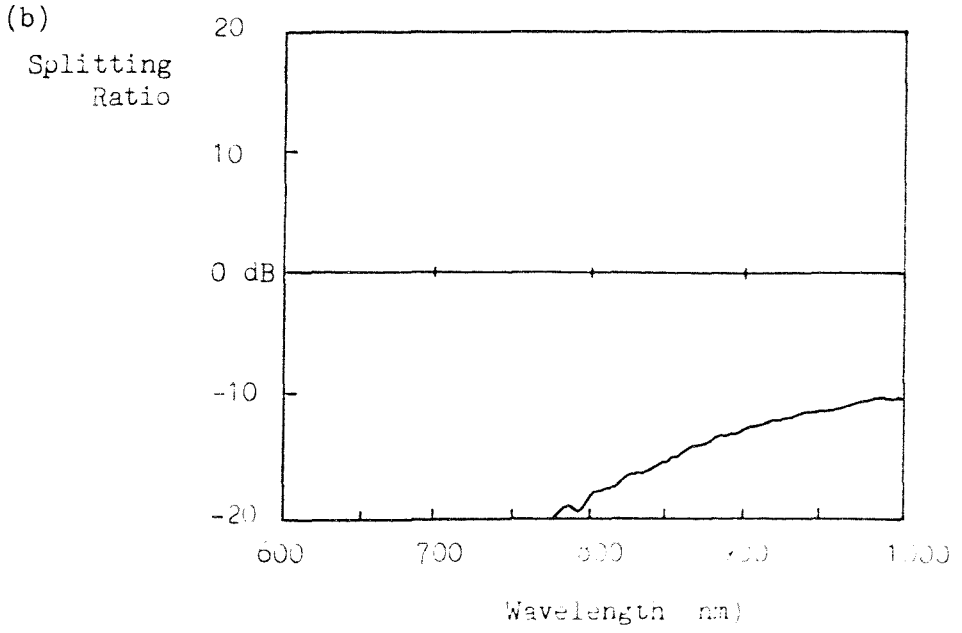

Figure 5.8.1. Spectral splitting ratio responses for the two different diameter fibres (a) O.D. 80 μm and (b) O.D. 40 μm for an elongation length of 10 mm.

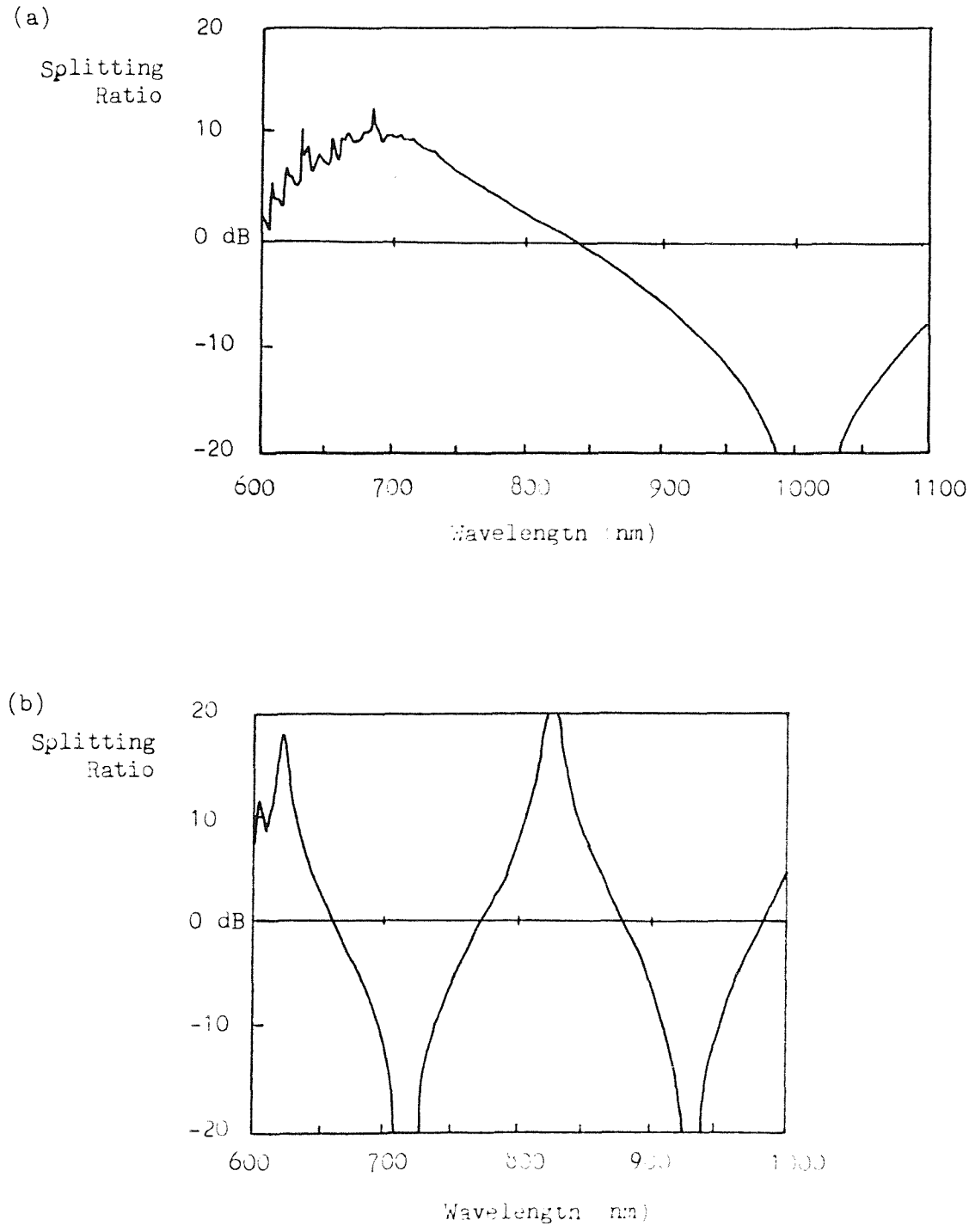

Figure 5.8.2. Spectral splitting ratio responses for the two different diameter fibres (a) O.D. 80 μm and (b) O.D. 40 μm for an elongation length of 20 mm.

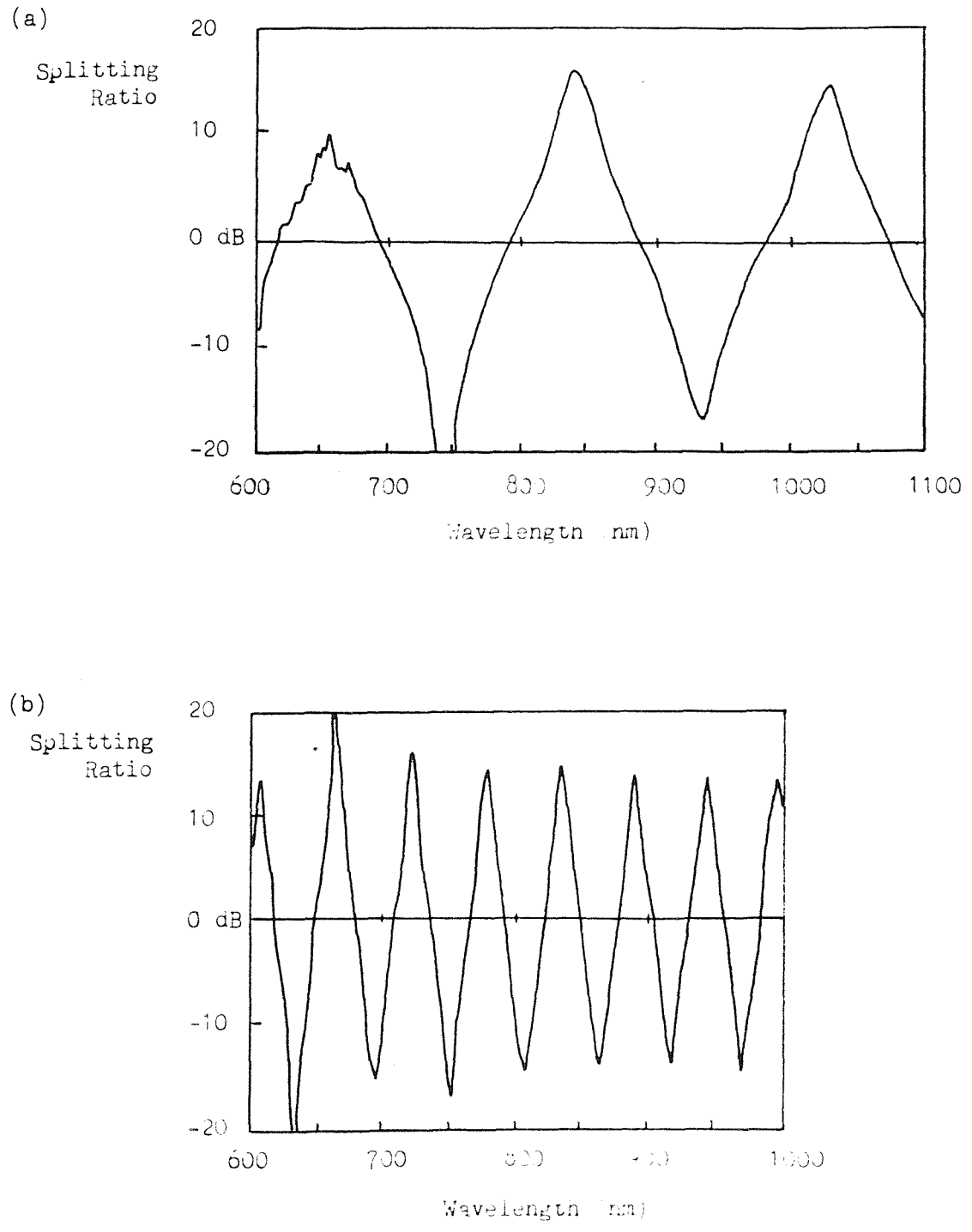

Figure 5.8.3. Spectral splitting ratio responses for the two different diameter fibres (a) O.D. 80 μm and (b) O.D. 40 μm for an elongation length of 30 mm.

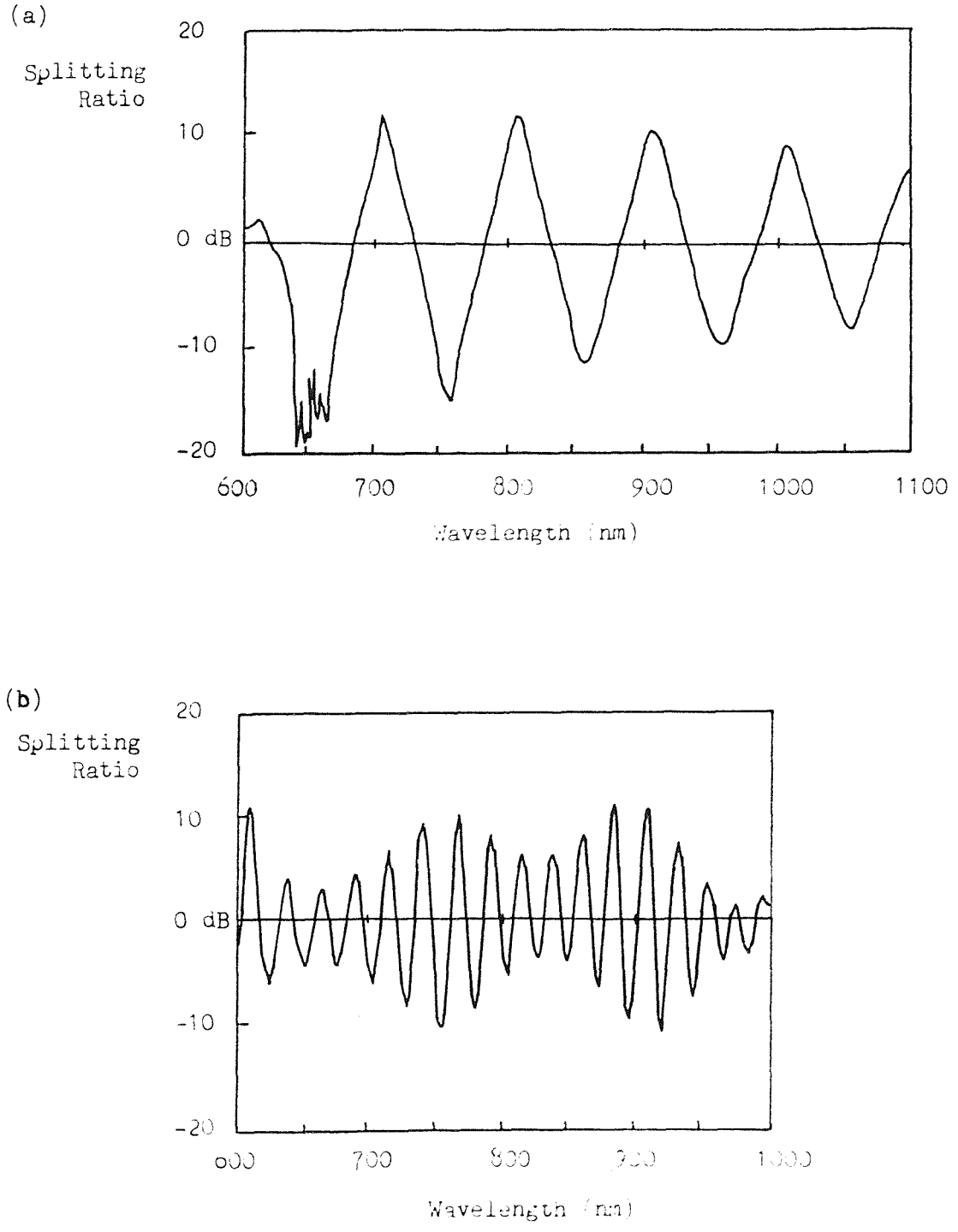

Figure 5.8.4. Spectral splitting ratio responses for the two different diameter fibres (a) O.D. 80 μm and (b) O.D. 40 μm for an elongation length of 40 mm.

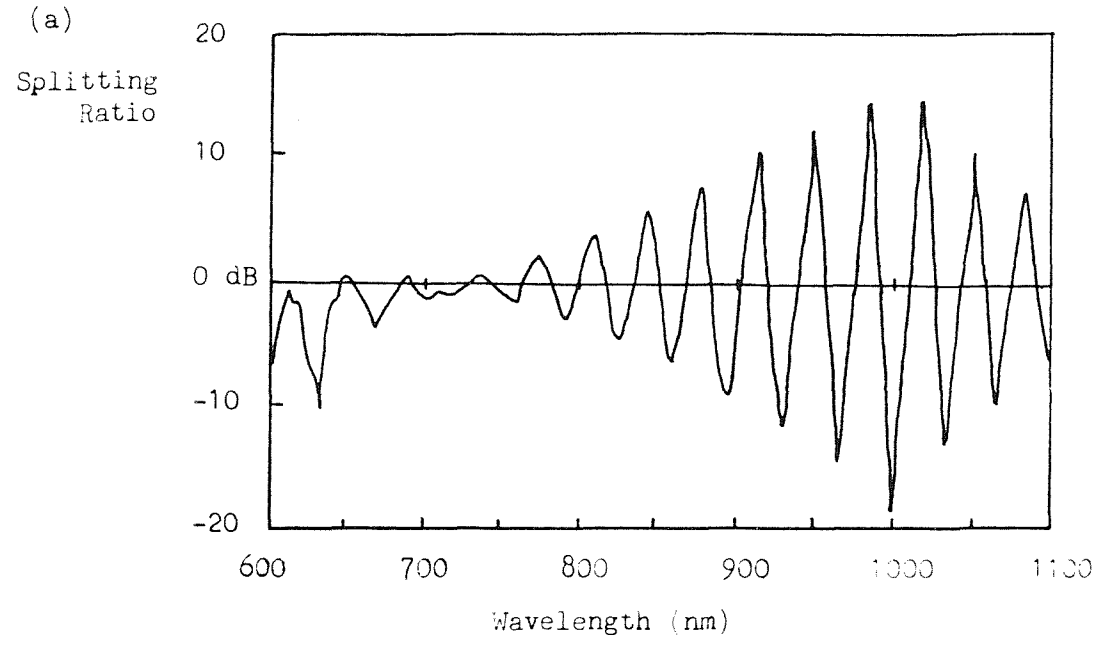

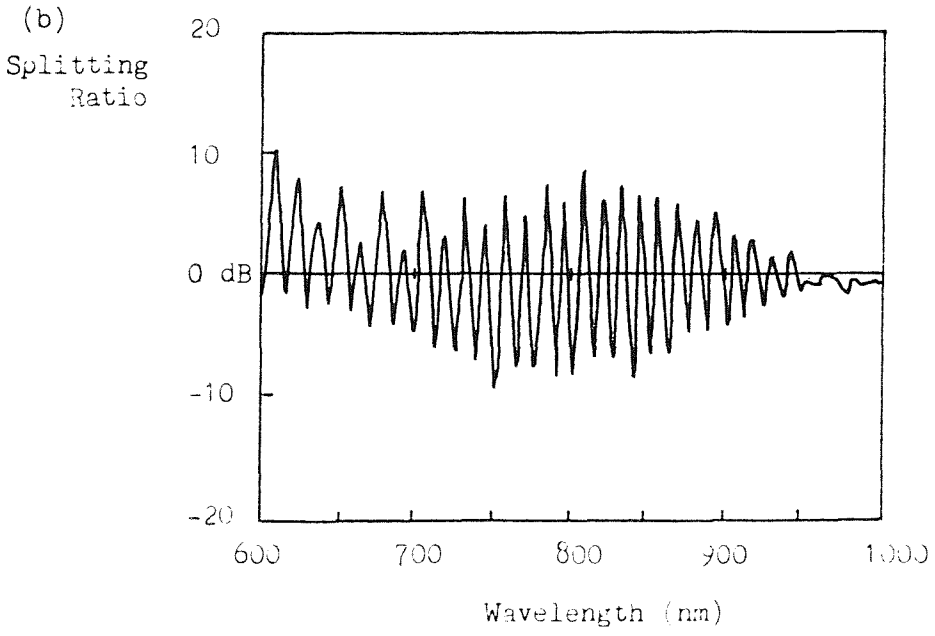

Figure 5.8.5. Spectral splitting ratio responses for the two different diameter fibres (a) O.D. 80 μm and (b) O.D. 40 μm for an elongation length of 50 mm.

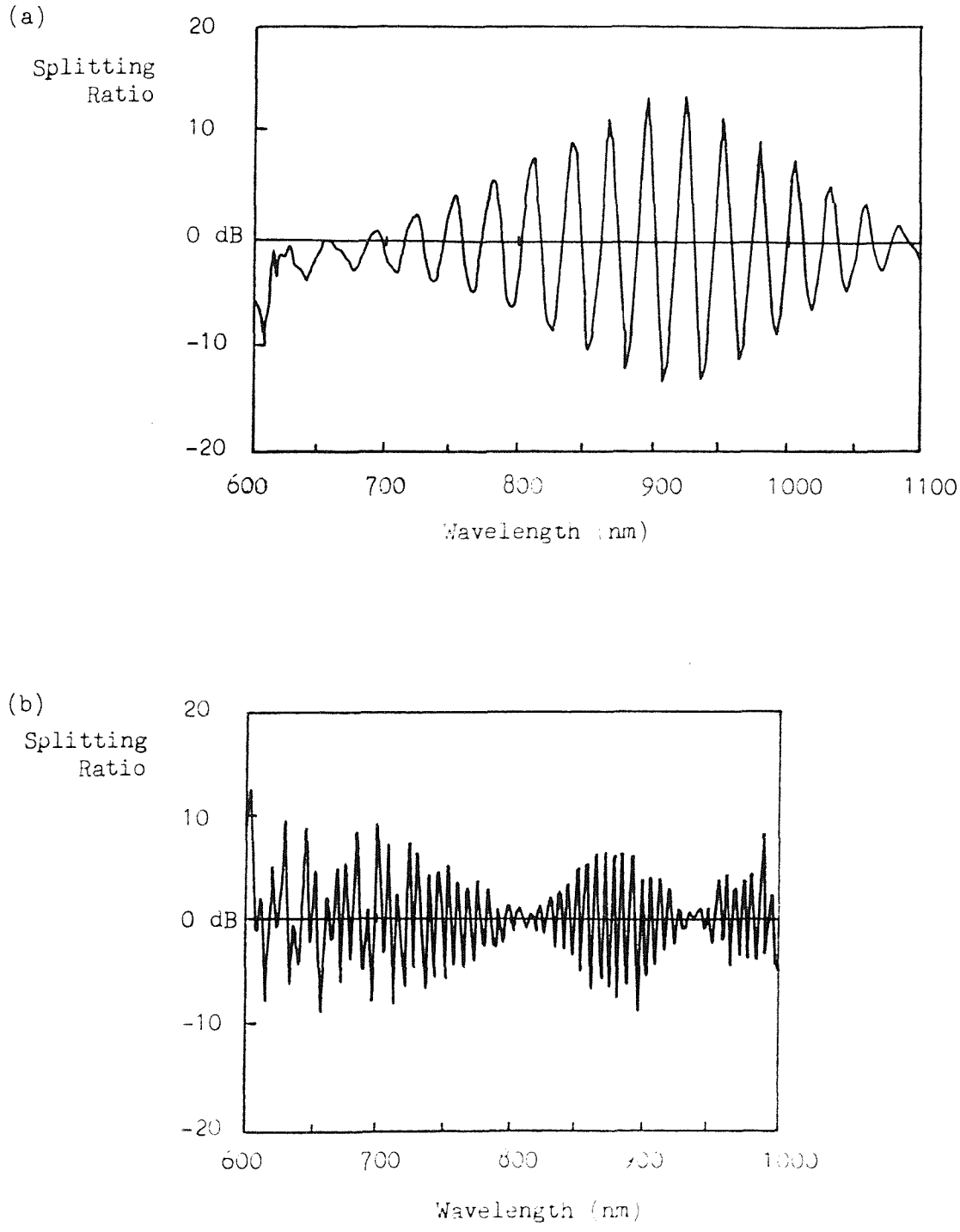

Figure 5.8.6. Spectral splitting ratio responses for the two different diameter fibres (a) O.D. 80 μm and (b) O.D. 40 μm for elongation lengths of 56 mm and 60 mm, respectively.

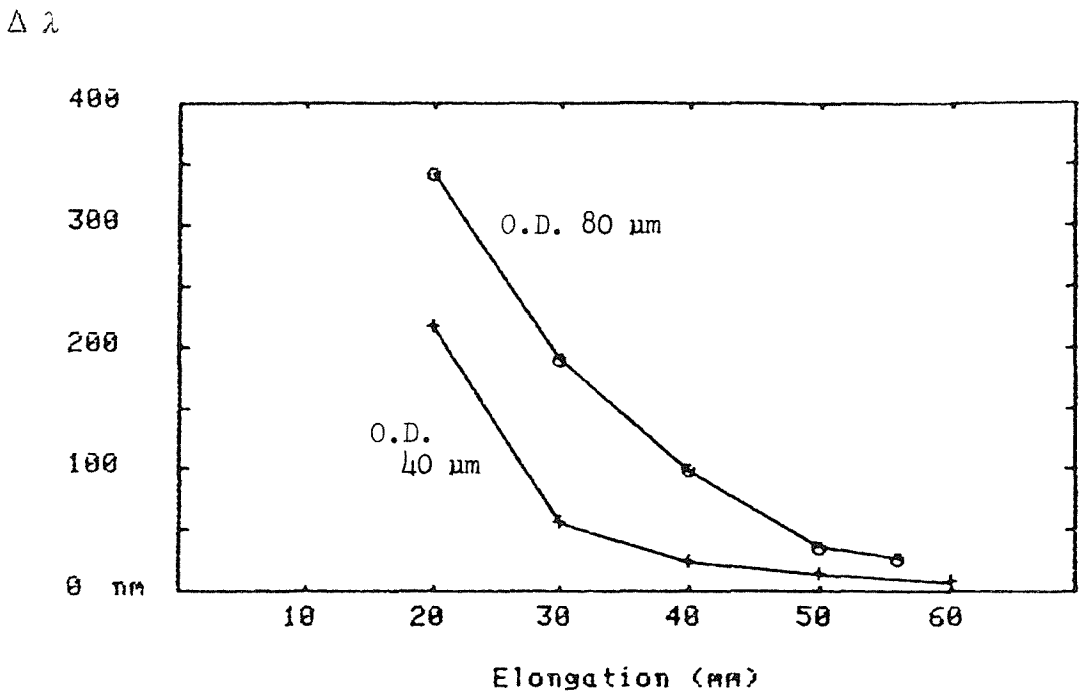

Figure 5.9. Oscillation period, $\Delta\lambda$, as a function of the taper elongation length for the two different diameter fibres.

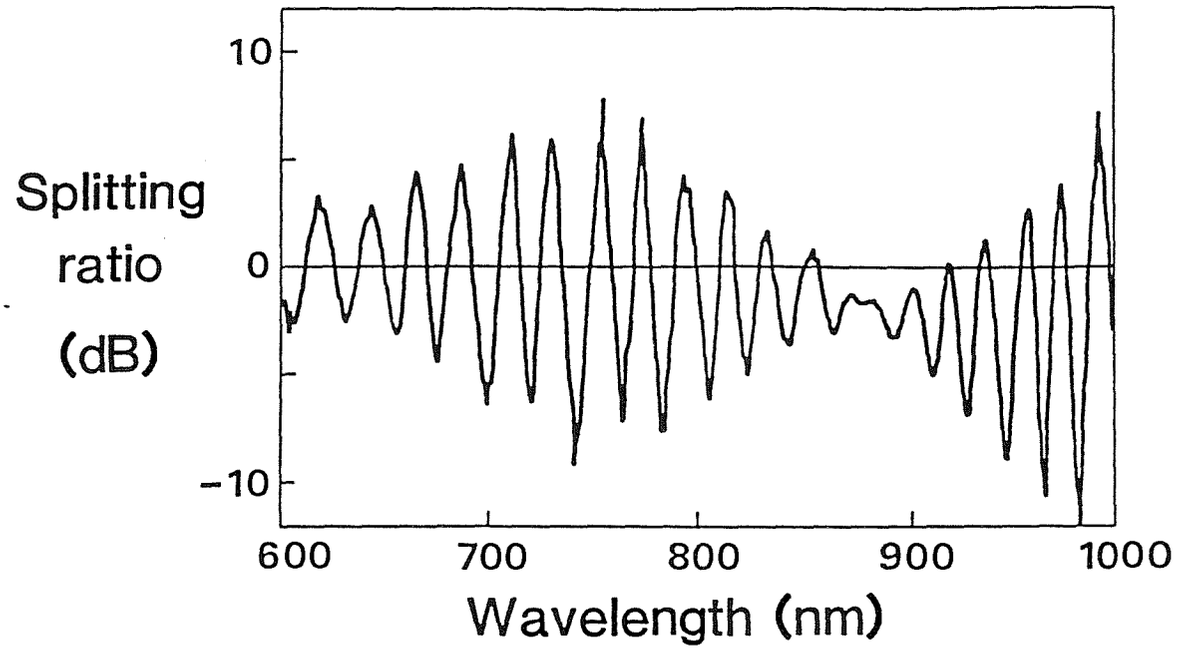

Figure 5.10. Spectral response of the coupler to unpolarised input light.

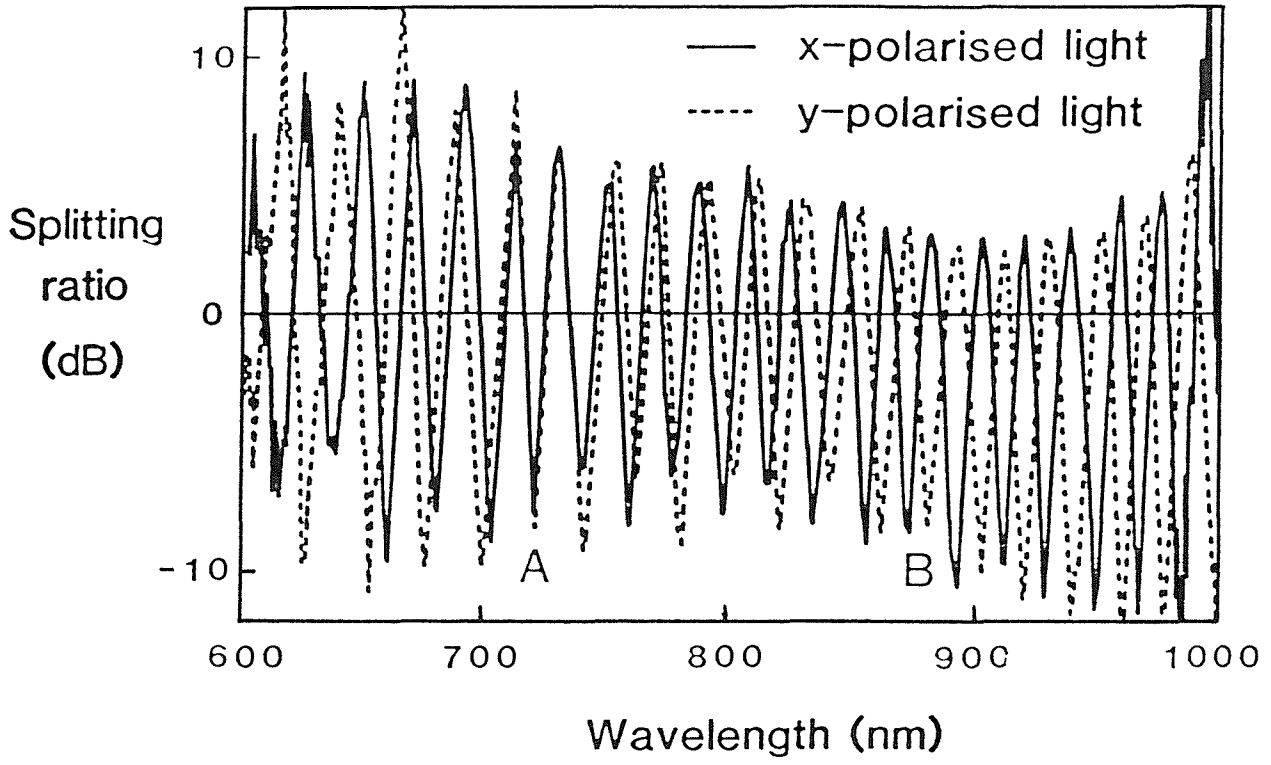

Figure 5.11. Spectral responses for two polarisation states of the input light when each input polarisation corresponds to a polarisation eigenstate of the coupler

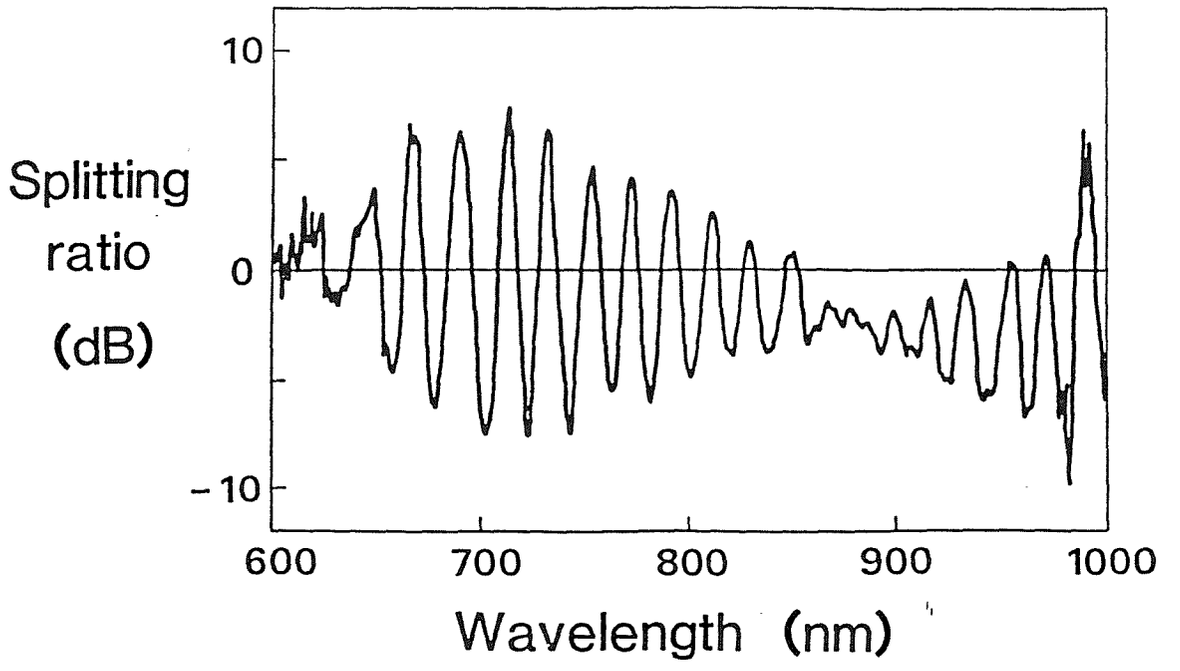

Figure 5.12. The superposition of the two responses in Figure 5.11..

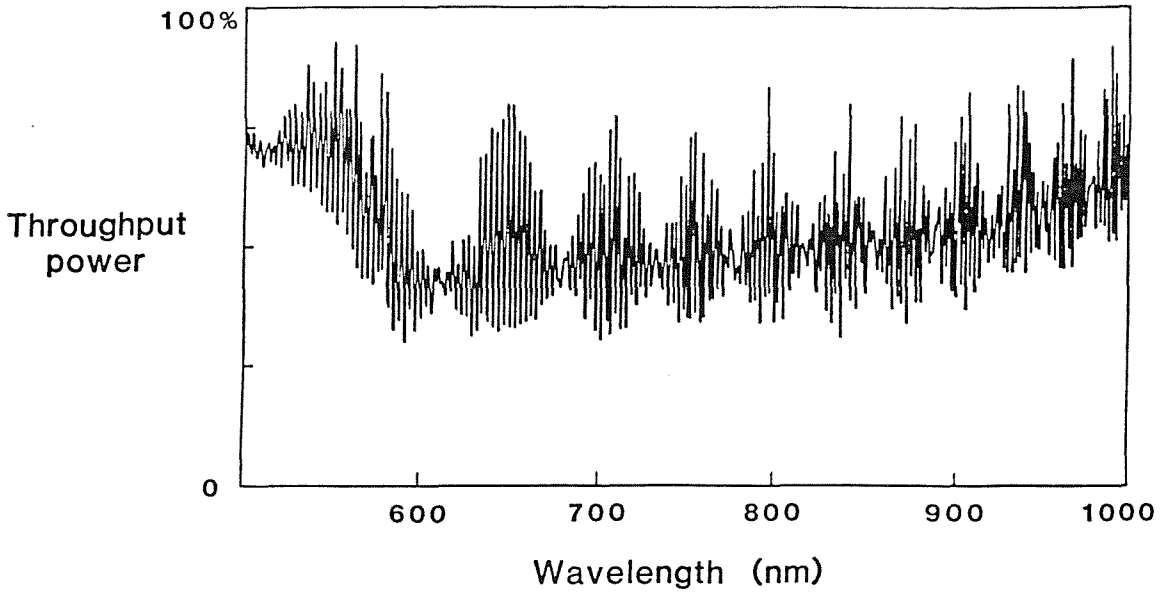

Figure 5.13. The spectral response of a coupler with an elongation length of 300 mm.

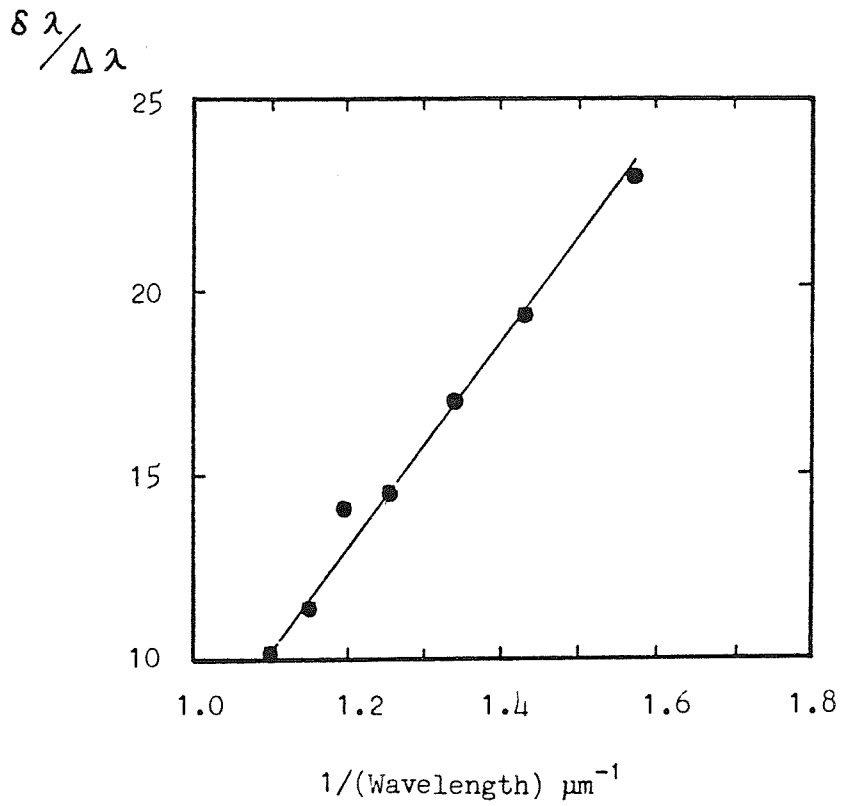

Figure 5.14. A plot of the ratio $\delta\lambda / \Delta\lambda$ as a function of λ^{-1} corresponding to the spectral response in Figure 5.13.

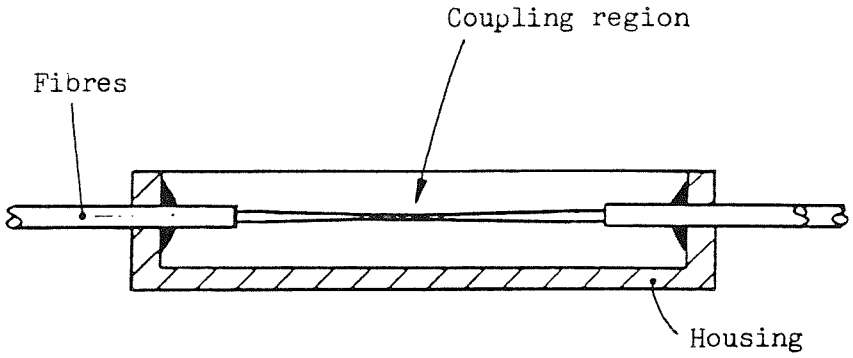

(a)

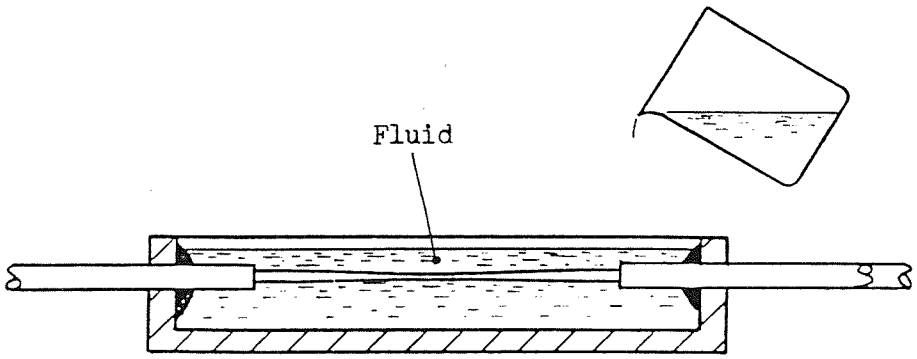

(b)

Figure 5.15. Effects of the surrounding medium.

(a) Coupler package.
(b) Fluid application.

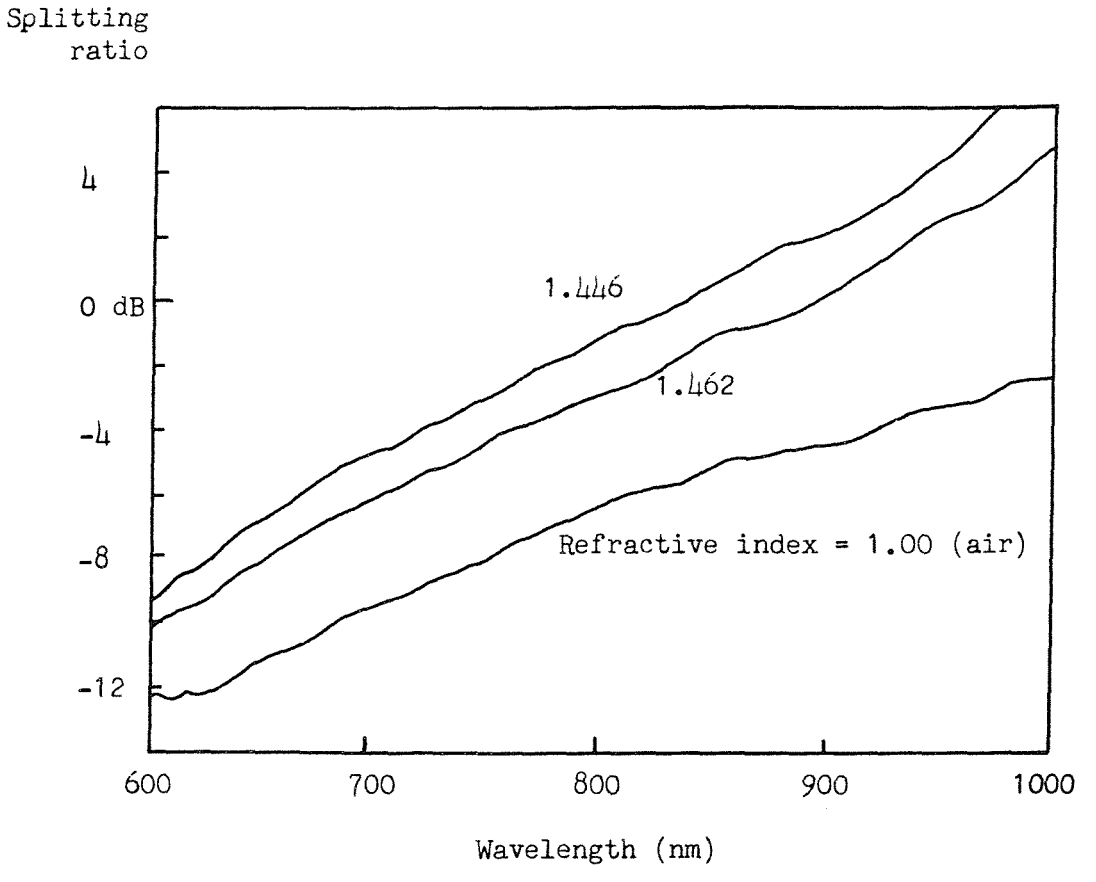

Figure 5.16. Effects of surrounding medium on the splitting ratio response of a short coupler.

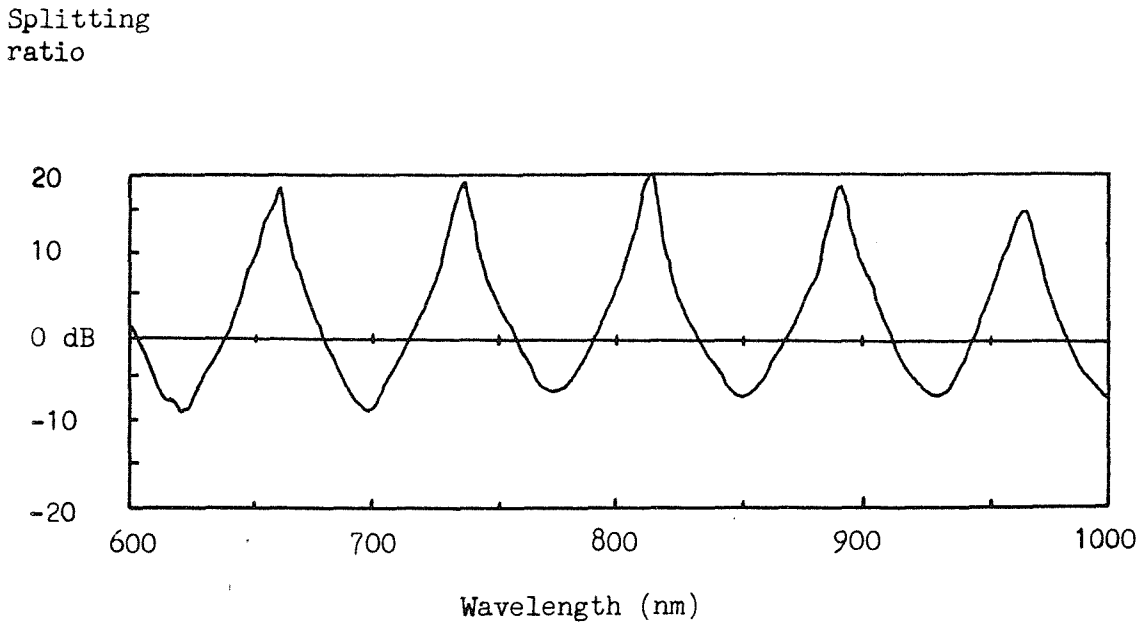

Figure 5.17. Spectral splitting ratio response of the coupler after it is packaged as in Figure 5.15.(a). The coupler's pre-packaged response is in Figure 5.2.10.

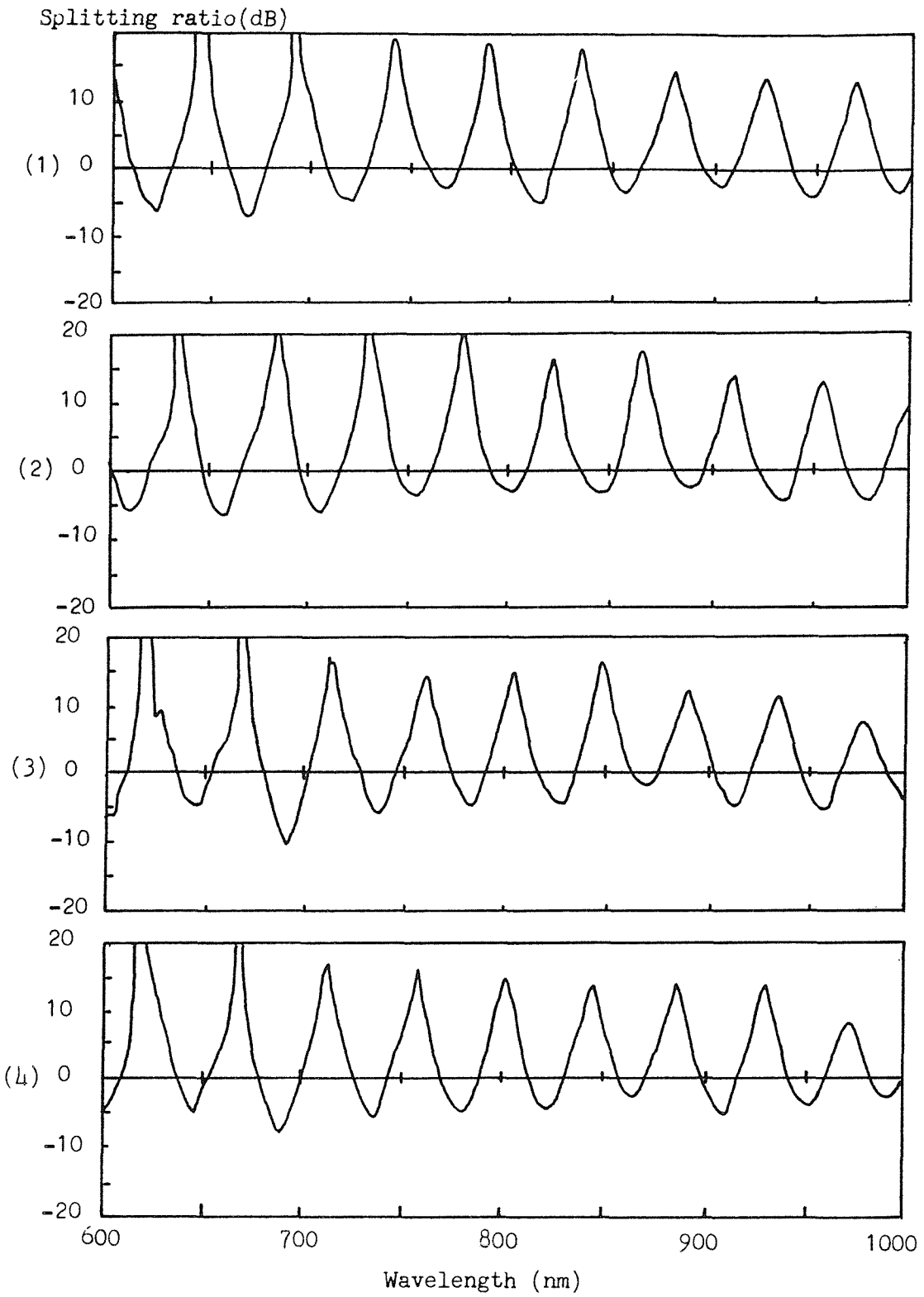

Figure 5.18. The spectral splitting ratio responses for different external media refractive indices. The refractive index was 1.4602 - 0.00038/ ℃ at 25℃ and the temperature was (1) 90℃ , (2) 80 ℃, (3) 70℃, (4) 60℃, (5) 50℃, (6) 40 ℃ and (7) 30℃

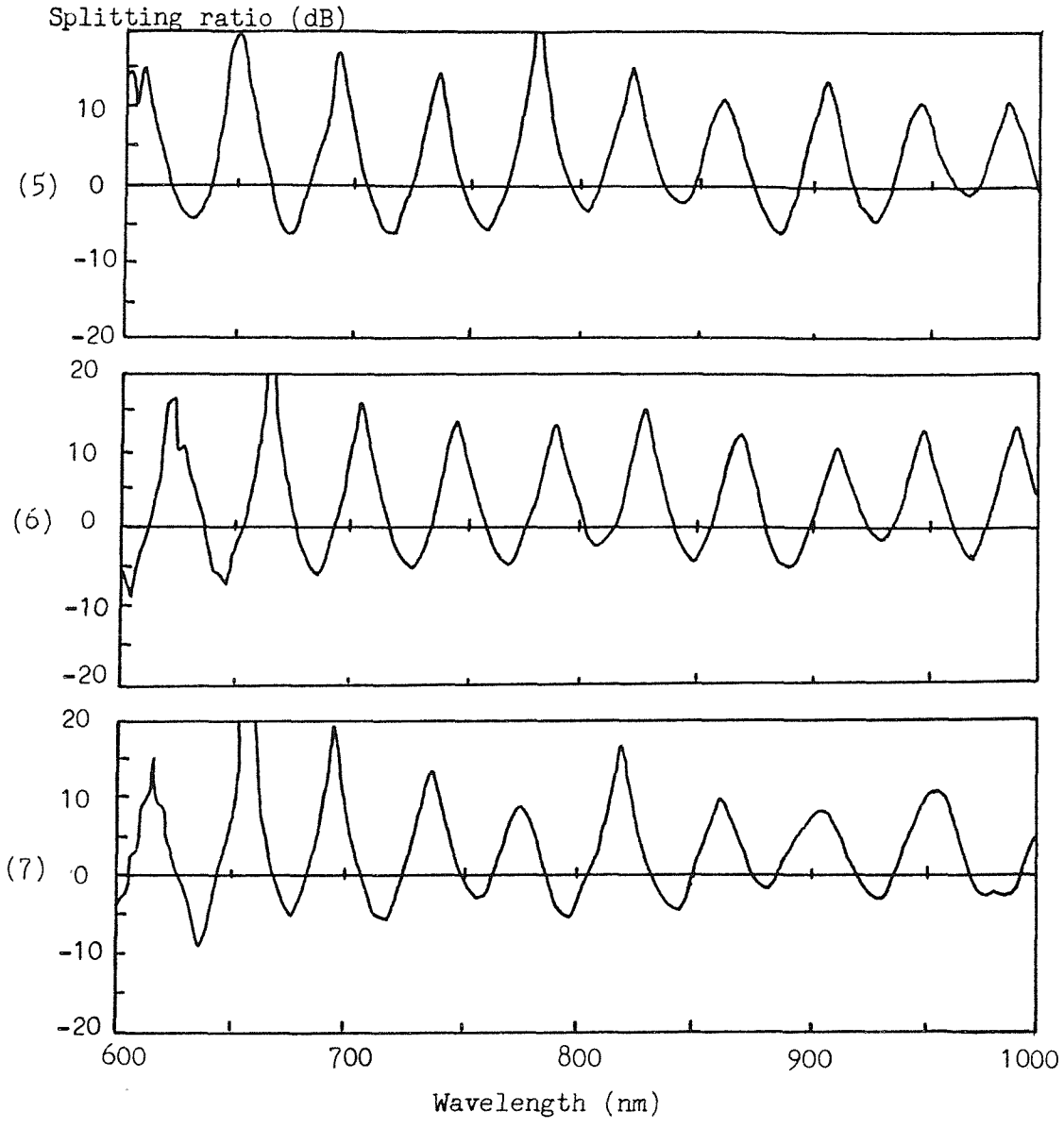

Figure 5.18. (contd.) The spectral splitting ratio responses for different external media refractive indices. The refractive index was 1.4602 - 0.00038/ ℃ at 25℃ and the temperature was (1) 90℃ , (2) 80 ℃, (3) 70℃, (4) 60℃, (5) 50℃, (6) 40 ℃ and (7) 30℃

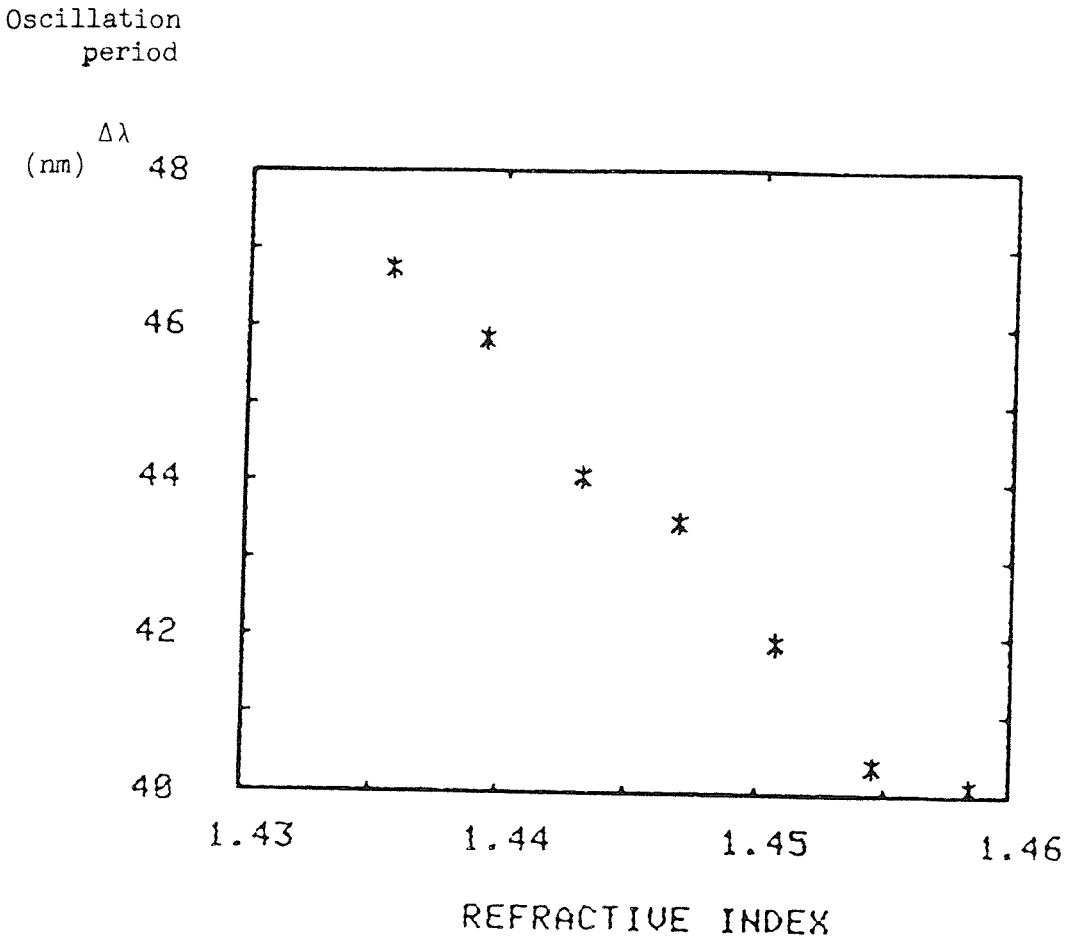

Figure 5.19. Variation of spectral oscillation period with external refractive index deduced from Figure 5.18.

(a)

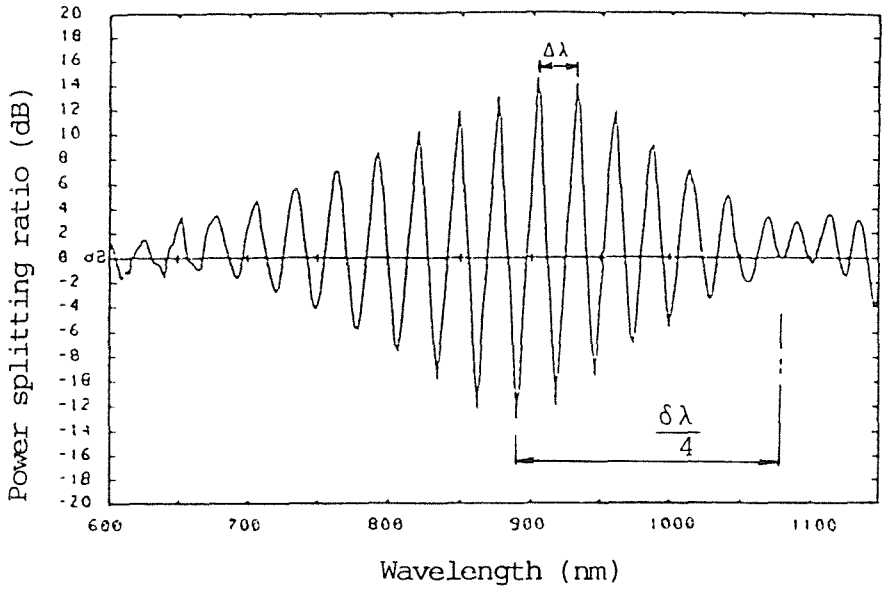

(b)

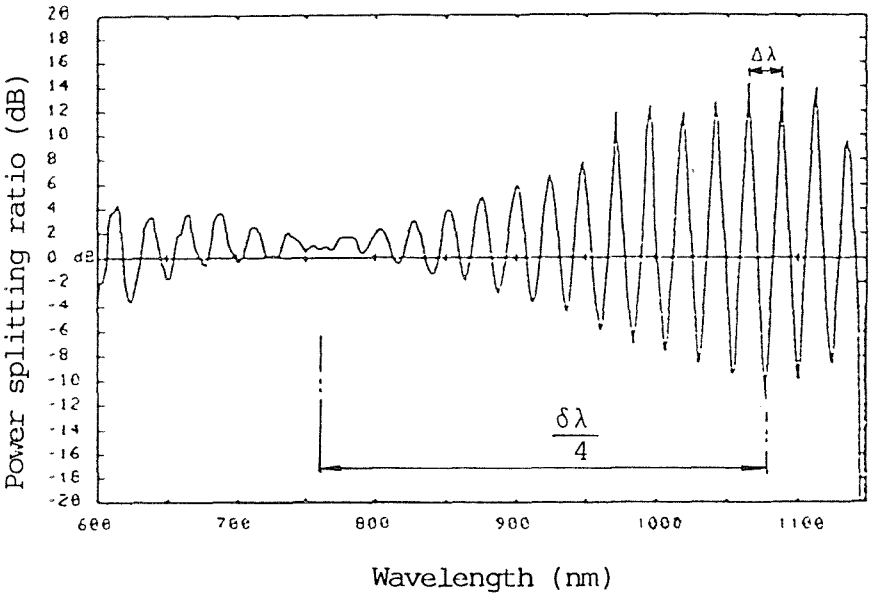

Figure 5.20. Spectral response of the power splitting ratio for a coupler,

(a) in air showing the parameters $\Delta\lambda$ and $\delta\lambda$.

(b) in a medium of refractive index 1.33.

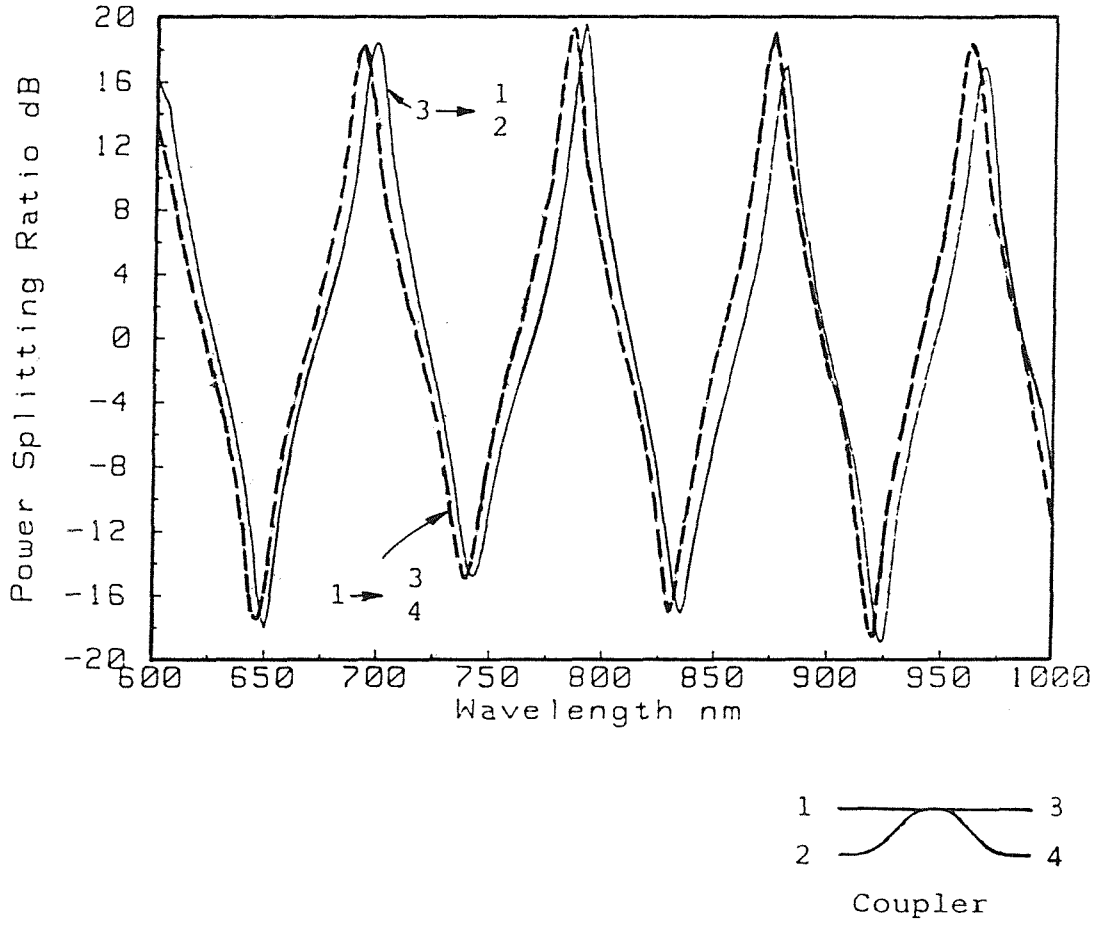

Figure 5.21. Reciprocity in taper couplers.
The offset is for illustration only.

CHAPTER 6: CLADDING MODE DESCRIPTION OF TAPER COUPLERS

6.1 Introduction

The performance of the fused taper coupler has been found in the previous Chapter to be a complicated function of the extent of tapering, the rate of tapering, the cross-sectional geometry and length of the uniform waist region, the refractive index of the external medium and the wavelength and polarisation state of the incoming light.

In this Chapter it is shown that all of the above dependences can be explained in terms of a cladding mode picture of the coupler (1-6).

By reducing the cross-section of the coupler waist to a tractable geometry, explicit analytic expressions can be obtained for the coupling coefficients (including polarisation effects) as functions of the wavelength, the coupler waist dimensions and the external refractive index, for couplers whose cross-sections are classed as either strongly-fused or weakly-fused. Couplers with intermediate cross-sections (as applies to most couplers) tend to require numerical methods (7,8) which lie well beyond the scope of the present work. However, one can at least qualitatively examine the effects of cross-sectional shape by reducing the coupler to a pair of parallel slab waveguides with the distance between the slabs representing the degree of fusion in the coupler. This model does also require numerical methods but at a very elementary level.

While most models are used to determine the coupling coefficients only, the slab model allows the qualitative examination of the dependence of extinction ratio (i.e. maximum extent of coupling) and coupler loss on the cross-sectional shape - topics which have not before been addressed for taper couplers.

6.2 Basic Considerations

The fused taper coupler has a structure similar to that shown in Figure 6.1(a). The taper waist region (CD) is approximately cylindrical (i.e. translationally invariant) and typically has a length of 10-20 mm, although much longer fused lengths are possible. A cross-section through the taper waist can have any shape varying from a circle to a figure of eight, as shown in Figure 6.1(b), depending on the degree of fusion of the fibres. The dimension a can typically lie anywhere in the range 2 μm to 30 μm depending on the taper ratio.

An optical field propagating along the input fibre (AB) will be in the LP_{01} mode of the fibre, or equivalently in the degenerate LP_{01} and LP_{11} modes of the composite parallel waveguide system. On propagating along the taper transition (BC) the core diameter will gradually decrease. The power in the modes will spread out and eventually the modes will become cladding modes. As discussed in Chapter 4 it is important that the field spreading occurs adiabatically, thereby avoiding coupling to higher order modes and resultant power loss in the coupler (9,10).

The taper waist (CD), is now an effective cladding waveguide consisting of the full coupler cross-section in which the cores are so small that they have no significant effect on the modal guidance (1,2). On leaving the taper waist the optical field adiabatically evolves into the core modes along the upward taper transitions (DE).

This coupler clearly satisfies all of the general conditions assumed for couplers in Chapter 2. The full coupling coefficient C_L is given by the total phase shift between the lowest order even and odd modes propagating through the full coupler length (BCDE); this is given by

$$C_L = \frac{1}{2} \int |\beta_e - \beta_o| dz \qquad (6.1)$$

where β_e and β_o are the propagation constants of the coupler's even (LP_{01}) and odd (LP_{11}) modes. As it stands, equation (6.1) is an exact expression for the full coupling coefficient. However, for any practical device it is virtually impossible to evaluate equation (6.1) exactly without making some approximations. To proceed further three approximations are made.

(1) The integral in equation (6.1) is dominated by the taper waist region (CD).

(2) All coupling is assumed to take place in the taper waist region which is assumed to have a constant cross-section, a length L, and a constant refractive index n_2.

(3) The cross-section of the coupler is represented by a rectangle with sides 2a and a for strongly-fused couplers (see Figure 6.2(a)), and by a figure-of-eight cross-section with dimensions 2a and a for weakly-fused couplers (see Figure 6.2(b)). These cross-sections are chosen since waveguides with these two cross-sections are analytically tractable. The full coupling coefficient can now be expressed as

$$C_L = \frac{1}{2} |\beta_e - \beta_o| L \qquad (6.2a)$$

where β_e and β_o are the propagation constants of the lowest order even and odd modes of the tractable waveguide, and L is the effective length of the taper waist. If the full coupling coefficient is divided by L, what will in future be called the coupling coefficient results;

$$C = \frac{C_L}{L} \qquad (6.2b)$$

Since the couplers are generally suspended either in air or in a potting material of refractive index much less than that of the silica cladding, the V-value of the waveguide in the taper waist is always much greater than 2.4. Asymptotic methods are then appropriate in analysing the waveguides (11) yielding explicit formulae for the coupling coefficients as now presented.

6.3 Coupling Coefficients

6.3.1 Short Couplers

If the length of the coupling region is such that polarisation effects can be ignored, then the power in one of the output ports, for a power P_o in one of the input ports, is given by

$$P = P_o \sin^2 CL \qquad (6.3)$$

For the rectangular waveguide it can be shown that (2)

$$C = \frac{3\pi\lambda}{32\, n_2 a} \quad \frac{1}{\left(1+\frac{1}{V}\right)^2} \qquad (6.4)$$

and for the figure-of-eight waveguide (3)

$$C = \frac{2^{7/2}\, U_\infty\, (n_2^2 - n_3^2)^{1/2}}{\sqrt{\pi}\, n_2\, a\, V^{5/2}} \qquad (6.5)$$

where $U_\infty = 2.405$, $V = \frac{2\pi a}{\lambda} (n_2^2 - n_3^2)^{1/2}$

and n_2, n_3 are the refractive indices of the fibre cladding and the external medium respectively.

6.3.2 Long Couplers

For long couplers the modal polarisations need to be taken into account. Power in one of the output ports is then given by

$$P = \frac{P_o}{2} \{1 + \cos (C_x+C_y)L \cos (C_x-C_y)L\} \qquad (6.6)$$

as outlined in Chapter 2.

For the rectangular guide it is found that (3,5)

$$C_x+C_y = \frac{3\pi\lambda}{32n_2a} \left[\frac{1}{\left(1+\frac{1}{V}\right)^2} + \frac{1}{\left(1+\left(\frac{n_3}{n_2}\right)^2\frac{1}{V}\right)^2}\right] \quad (6.7)$$

and

$$C_x-C_y = \frac{3\pi\lambda}{16n_2a} \frac{1}{V}\left(1 - \frac{n_3^2}{n_2^2}\right) \quad (6.8)$$

while for the figure-of-eight waveguide (3)

$$C_x+C_y = \frac{2^{7/2}\, U\infty\, (n_2^2 - n_3^2)^{1/2}}{\sqrt{\pi}\, n_2\, a\, V^{5/2}} \quad (6.9)$$

and

$$C_x-C_y = \frac{2^{5/2}\, U\infty^2\, (n_2^2 - n_3^2)^{1/2}}{\sqrt{\pi}\, n_2^3\, a\, V^{7/2}} \quad (6.10)$$

These equations (6.4) to (6.10) display explicitly the dependence of the performance of a coupler on wavelength, refractive index, coupler size and polarisation, for two extremes in cross-sectional shape.

6.4 Correspondence with Experimental Results

6.4.1 Effect of the Tapering Transition

In the above models it is assumed that the coupling coefficient is constant in the waist region of the coupler and that it is zero elsewhere. In practice the coupling coefficient increases slowly, from zero to its uniform constant value, in the input taper transition. It is this initial variation in coupling coefficient that gives the

initial slow coupling with length that was evident in the results shown in Figure 5.3.1-10.

6.4.2 Effect of the Coupler Length

After a certain elongation length the period of oscillation Δz remains constant for each value of the wavelength as in Figure 5.5, thereby confirming that the total coupling coefficient is linear with length L and is described by

$$C_L = C \times L \qquad (6.11)$$

a relationship which has been assumed in the models by equation (6.2a).

6.4.3 Wavelength Dependence

All of the couplers examined in Chapter 5 exhibit a wavelength dependence of the output power-splitting ratio which is periodic, with a period that is virtually constant or decreases slightly with wavelength. A constant period would imply, from equation (2.13), that the coupling coefficient is proportional to the wavelength;

$$C = \alpha\lambda \qquad (6.12)$$

Indeed, on examining the coupling coefficient as derived for strongly-fused couplers in equation (6.4), it is found that the coupling coefficient is mainly described by equation (6.12), with a small additional wavelength dependence contained in the 1/V term in the denominator of equation (6.4). For weakly-fused couplers the coupling coefficient

from equation (6.5) has a wavelength dependence of

$$C = \alpha\lambda^{5/2} \qquad (6.13)$$

which appears "locally linear" in the wavelength range of the measurements, since the wavelength period seems constant even for this type of coupler.

The result that the coupling coefficient is proportional either to the wavelength or to the wavelength raised to some positive power is important, as a naive argument would suggest that the modal propagation constants would be proportional to the wavenumber and hence imply a coupling coefficient proportional to $1/\lambda$. This is clearly not the case.

6.4.4 Example: Strongly-Fused Coupler

Figure 6.3(a) gives the measured spectral power-splitting ratio (12) for a strongly-fused coupler with the following parameters; a = 2.63 μm, L = 15 mm, n_2 = 1.458 (silica), n_3 = 1.42. Figure 6.3(b) gives the calculated variation of output power with wavelength for these parameters using equation (6.4) for strongly-fused couplers.

The wavelength oscillation period $\Delta\lambda$ is given by

$$\Delta\lambda = \frac{32n_2\, a^2}{3L} \quad \frac{(1+\frac{1}{V})^3}{(1-\frac{1}{V})} \qquad (6.14)$$

At two different wavelengths, the predicted and

measured oscillation periods $\Delta\lambda$ are given in Table 6.1. The error of 10% in the nanometer range is very good given the nature of our approximation, and even the observed small increase in $\Delta\lambda$ with wavelength is accounted for.

6.4.5 Polarisation Effects

As has been seen in the previous Chapter, polarisation effects in the coupler give rise to an additional periodic modulation with period $\delta\lambda$, in addition to the oscillation period $\Delta\lambda$. From equations (6.7) to (6.10) it can be shown that the ratio of these two quantities has a particularly simple form and is given by

$$\frac{\delta\lambda}{\Delta\lambda} = G \frac{V}{1+\frac{n_3^2}{n_2^2}} \qquad (6.15)$$

where G = 5/7 for the weakly-fused case and 1/4 for the strongly-fused case. This equation predicts that the ratio should be proportional to λ^{-1}. Figure 6.4 plots $\delta\lambda/\Delta\lambda$ against $1/\lambda$ for the coupler with a 300 mm interaction length whose response is shown in Figure 5.13. The points lie close to a straight line as predicted by equation (6.15). The fact that this graph does not pass through the origin is a consequence of neglecting higher order 1/V terms which result in a constant being added to the right hand side of equation (6.15). The cross section of this coupler shows that it was weakly-fused. The gradient of the best straight line fit to Figure 6.4 allows the coupler's cross-sectional dimension to be determined using equation (6.15) with G

appropriate to the weakly-fused case. It is found that a = 3 μm, in excellent agreement with the measured cross-section of the coupler.

6.4.6 Dependence on External Refractive Index

The experimental variation of the output characteristics with external refractive index for two strongly-fused couplers with taper ratios of 10 and 20 is shown in Figure 6.5(a).

The tapered lengths of these couplers is about 10 mm. Several interesting features are revealed in Figure 6.5(a). The taper ratio has a profound effect on the dependence with external refractive index. The curves in Figure 6.5(a) show that as the external index approaches that of silica (1.458) one of the couplers shows rapid oscillations in output power, while for both couplers all of the power is lost as index matching is reached.

This is additional confirmation that in the tapered section of the coupler, the light must be guided by the waveguide formed by the fibre cladding and the external medium. In other words the coupler is a cladding mode device. The sensitivity to the external medium is such that very small changes in refractive index can cause complete switching of the power between the two output ports.

The sensitivity to external medium comes from the V-dependence in equation (6.4). This sensitivity increases

with the taper ratio through the $1/a^2$ dependence in this equation and also as n_3 approaches n_2. Both these conclusions are in general agreement with the measurements given in Figure 6.5(a). For both of these couplers the initial fibre diameter was 105_{μ}m and the taper waist length was approximately 10 mm. The measurement wavelength was 633 nm. After substituting these parameters in equation (6.4), the predicted variation in output power with refractive index is given in Figure 6.5(b). By comparing this with Figure 6.5(a) and bearing in mind the simplicity of the model, the theory is shown to provide a very good description of the measured results. In particular, the positions of the maxima and minima are very well reproduced.

6.5 Effects of Cross-Sectional Shape

6.5.1 A Slab Waveguide Model

The approach is illustrated schematically in Figure 6.6. The coupler is represented by a pair of parallel slab waveguides with an overall thickness equal to that of the widest coupler cross-section. There is a gap between the two slabs representing the degree of fusion of the coupler. The gap width for the weakly-fused coupler is approximately 0.5% of the total waveguide thickness, with the gap width reducing to zero for the strongly-fused coupler.

The justification for this model is that the effective index profile (13,14) of the weakly fused coupler cross section taken on its widest side does resemble such a

parallel slab structure, with refractive indices approximately those of the actual waveguide and a gap where the refractive index reduces to that of the external medium (13,14). A greater degree of fusion would lead to an effective index profile, with a smaller gap of a higher refractive index than the external medium. However, this model simply allows the gap to vary and keeps the refractive index fixed at n_2 - thereby reducing the complexity of the numerical analysis.

There is no direct comparison between a specific cross-sectional shape and a gap size; however, varying the gap width allows a scan between the extremes of strong and weak fusion and hence allows the build up of a good qualitative picture of the changes in coupler performance with variation in cross-sectional shape.

As with previous models it is assumed that only the lowest order modes are excited, i.e. TE_o, TM_o, TE_1, TM_1, corresponding to the coupler modes LP^x_{01}, LP^y_{01}, LP^x_{11}, LP^y_{11} respectively. Numerically, the propagation constants of these modes for the parallel slab waveguide system are solved, yielding the coupling coefficients C_x and C_y as required.

6.5.2 Variation of Coupling Coefficient with Wavelength

The graphs in Figures 6.7.1-3 give the variation in the coupling coefficients C_x and C_y with wavelength, for couplers with three different degrees of fusion (strong,

medium and weak) as calculated from this slab waveguide model. In all cases the gross coupler parameters are kept constant at the values shown in the Figure caption.

For the strongly-fused coupler, (Figure 6.7.1), the coupling coefficients C_x and C_y are seen to vary linearly with wavelength as predicted previously by equation (6.12).

For the medium-fused coupler, (Figure 6.7.2), the coupling coefficients vary as the wavelength raised to some positive power greater than one. For the weakly-fused coupler, (Figure 6.7.3), the coupling coefficients have the clear $\lambda^{5/2}$ dependence.

The coupling coefficients are greatest for the strongly-fused coupler, and decrease with decreasing degrees of fusion when all other parameters are kept fixed.

The above trends confirm that the slab model exhibits the correct wavelength dependence both for the strongly-fused (gap=0) and for the weakly-fused (gap=0.5% of total waveguide width) cross-sections. It is therefore possible to proceed with confidence in using this model to explore other coupler properties.

Polarisation effects are given by the difference in coupling coefficients, i.e.C_x-C_y. Figures 6.8.1-3 are graphs of C_x-C_y for the same conditions as for Figures 6.7.1-3. The magnitude of C_x-C_y for each cross-section tends to incrase with increasing wavelength.

The difference C_x-C_y changes sign between strongly-fused and weakly-fused cross-sections, suggesting that there is a cross-section for which the coupler could be polarisation transparent at a certain wavelength.

It is worth noting here that the strength of polarisation effects, i.e. $(C_x-C_y)/(C_x+C_y)$, is much larger for weakly-fused couplers than for strongly-fused couplers. However, since C_x-C_y changes sign between the extremes in cross-sectional shape, a local maximum in the strength of polarisation effects occurs for very strongly-fused couplers, as Snyder found for couplers with circular or square cross-sections (7).

6.5.3 Variation of Coupling Coefficient with External Refractive Index

Figure 6.9 shows the coupling coefficients C_x and C_y as functions of the external refractive index for couplers with weakly-, medium-, and strongly-fused cross-sections.

In the strongly-fused case, the coupling coefficients tend to decrease with increasing external refractive index. This implies that the field spread into the external medium causes the field at the centre of the parallel two-waveguide structure to reduce. This reduces the coupling between the two parallel waveguides.

In contrast, the coupling coefficients for weakly fused couplers tend to increase with increasing external

refractive index. The additional field spread in the gap (or cusp regions of the real coupler cross-section) due to the rise in external index causes the increase in coupling strength.

The change in behaviour between the strongly and weakly fused couplers suggests that there may be some cross section for which the coupling coefficient is entirely insensitive to the external medium.

The variation in polarisation properties, as measured by the difference in the coupling coefficients C_x-C_y, is shown in Figure 6.10, where the magnitude of C_x-C_y reduces with increasing external refractive index.

In Figure 6.11 the coupling coefficients C_x and C_y and their difference C_x-C_y are plotted for a coupler with a very small gap size (gap=.0005% of the total waveguide width). The polarisation term C_x-C_y is approximately zero for all values of external index, implying that this coupler should be transparent to polarisation for all values of external refractive index.

The coupling coefficients are practically constant with external index although a coupler with a larger gap would be needed to achieve true insensitivity to external index for these coupler parameters.

6.5.4 Variation in Coupling Coefficients with Cladding Thickness

The coupling coefficients were calculated for two different couplers with individual waveguide dimensions of 6 μm and 8 μm respectively. The gap was kept at zero in each case so that the comparison between the two couplers would be meaningful and unambiguous.

The results are plotted in Figure 6.12 for the coupling coefficients and in Figure 6.13 for the coupling coefficient difference C_x-C_y. The coupling coefficients are much larger for the coupler with the smaller cross-section, and similarly the polarisation effects are also stronger in the case of the smaller cross-section. This trend agrees completely with the experimental results for couplers with different dimensions presented in Section 5.3.2.

6.5.5 Comparison between Slab Waveguide Model and Other Models for Cross Sectional Shape Dependence

It is suggested that the slab waveguide model is ideal for indicating the trends in coupler behaviour under various conditions and can guide the fabricator towards an optimum design of coupler for any specific application. In coupler fabrication there is not generally a very fine control over all of the couplers parameters, so that in practice the optimisation of the coupler tends to be by trial and error.

There have been attempts to find the exact cross-sectional shape for which the coupler would be insensitive

to external index, (13,15) i.e. to find the coupler cross-section corresponding approximately to the slab waveguide whose results are shown in Figure 6.11. Similarly, Snyder examined waveguides of various cross-sections (7,8) and found that the coupling coefficient difference C_x-C_y changed sign as couplers became more well fused, and thus he found that an elliptical waveguide with a certain aspect ratio would be transparent to polarisation (7).

While such studies on exact coupler cross-sections are necessary and valuable, they do not tell the fabricator how to proceed to obtain, say, a polarisation transparent coupler, any better than does the slab model.

The treatment so far, whether it be for exact cross-sections or in terms of the slab waveguide model, have only dealt with finding expressions and trends for the coupling coefficients and had little consideration for the excitation mechanisms of the even and odd modes. In fact it has always been tacitly assumed that only the lowest order even and odd modes are excited in the coupler's waist region. While the experimental results tend to confirm this assumption in terms of the gross features of the couplers' responses, one subtle feature has not previously been addressed. While in theory there ought to be total power transfer between the coupling waveguides, in practice it is found that there is always a limit to the extent of power transfer. This problem is examined in the following Section and it is seen

how the slab model allows some kind of measure of this phenomenon, for different cross-sectional shapes, to be obtained.

6.6 Cross Talk in Fused Taper Couplers

There is always found to be a limit to the amount of power that is transferred in the fused taper coupler, with the result that undesirable cross talk always exists. This has been attributed to measurement resolution (5) but it is shown here that the extent of cross talk is fundamentally related to the cross-sectional shape of the coupler and to the tapering transition regions of the coupler. While this fact has been recognised in integrated optical couplers it has never been considered before in fibre optic couplers (16).

Let ψ_1 and ψ_2 be the modes of the two decoupled (or optically isolated) identical waveguides, and ψ_e and ψ_o the two lowest order exact even and odd normal modes in the coupling region, where all modes are normalised to unit power. Under the extreme case of weak coupling these even and odd modes approach, but are never equal to, $\frac{1}{2}(\psi_1 + \psi_2)$ and $\frac{1}{2}(\psi_1 - \psi_2)$ respectively as given by equations (2.1) and (2.2). The input field ψ_1 excites, nearly equally, the two modes ψ_e and ψ_o and the cross-talk is small or zero i.e. nearly all power is transferred. In the other extreme case where the two coupling waveguides are so small and so close together that ψ_o is cut off (17), the outputs always have equal power, giving 100% cross-talk. Therefore the

excitation of the ψ_e and ψ_o normal modes by the decoupled waveguide modes ψ_1 and ψ_2 is crucial in determining the cross-talk level.

In general since no waveguide transition can ever be truly adiabatic it cannot be assumed that the lowest order even and odd normal modes will be excited equally. Indeed, it is the unequal excitation of these normal modes that gives rise to unwanted cross-talk. In the input port 1, the excitation of ψ_e and ψ_o at the beginning of the coupling region will depend on the geometry of the transition region and has the following form:

$$\psi_1 = \{a_e \psi_e + a_o \psi_o\} + \Sigma a_n \psi_n \qquad (6.16)$$

where a_e, a_o are the excitation coefficients of the even and odd normal modes, and the a_n are the excitation coefficients of both the higher order and the radiation modes denoted by ψ_n which for simplicity are considered as loss. At the output transition the even ψ_e (odd ψ_o) modes excite the decoupled modes ψ_1, ψ_2 with excitation coefficients a_e', a_e' (and a_o', $-a_o'$) respectively. It can be readily shown that the power in the output ports, for unit input power, will be

$$P_3 = (a_e a_e')^2 + (a_o a_o')^2 + 2a_e a_e a_o' a_o' \cos\Delta\beta L \qquad (6.17)$$

$$P_4 = (a_e a_e')^2 + (a_o a_o')^2 - 2a_e a_e a_o' a_o' \cos\Delta\beta L \qquad (6.18)$$

where $\Delta\beta = |\beta e - \beta o|$

The power loss through the coupler is given by

$$\text{Loss} = 1 - (p_3+p_4) = 1 - 2\{(a_e\ a'_e)^2 + (a_o\ a'_o)^2\} \tag{6.19}$$

The cross-talk level is given by the ratio of the two output powers when one is a maximum and the other is a minimum, which is known as the extinction ratio,

$$\text{extinction ratio} = \frac{p_3 max}{p_4 min} = \left[\frac{a_e a'_e + a_o a'_o}{a_e a'_e - a_o a'_o}\right]^2 \tag{6.20}$$

In general couplers will exhibit a finite extinction ratio and a non-zero loss although the two properties are not mutually inclusive.

If the input and output transitions are equal, then by reciprocity between ψ_1, ψ_2 and ψ_e, ψ_o the excitation coefficients a_e and a_o will equal a'_e and a'_o respectively, and equations (6.19) and (6.20) will reduce to

$$\text{Loss} = 1 - 2\,[a_e^4 + a_o^4] \tag{6.21}$$

$$\text{extinction ratio} = \left[\frac{a_e^2 + a_o^2}{a_e^2 - a_o^2}\right]^2 \tag{6.22}$$

respectively.

If $a_e = a_o = 2^{-\frac{1}{2}}$ then equations (6.21) and (6.22) reduce to the ideal case of zero loss and infinite extinction ratio. Likewise if $a_e = a_o \neq 2^{-\frac{1}{2}}$ the loss will be non-zero but the extinction ratio will be infinite.

6.6.1 Estimation of Trends in Extinction Ratio and Loss with Coupler Cross-Section

Since a_e, a_o, a'_e and a'_o depend on the taper transitions and coupler cross-section they are not easy to calculate. For simplicity the coupler is modelled by the two parallel multimode slab waveguide system as described above. The excitation coefficients are estimated from butt jointed input and output transitions as shown in the inset in Figure 6.14. Though this is a rather severe model for the gradual taper transitions in the coupler, the abrupt transition provides a useful first-order approximation for non-adiabatic effects.

Three different coupler cross-sections are modelled in Figure 6.15 showing the input field ψ_1 and the even ψ_e, and odd ψ_o, modes, together with the refractive index distribution.

From Figure 6.14 it is clear that the extinction ratio is greatest and the loss least for weakly-fused couplers. This is not surprising, since the less is the extent of fusion the more weakly coupled are the waveguides and the more close to ideal is the performance.

In the measurements shown in Chapter 5, in this Chapter and in Reference 18, the weakly-fused coupler is found to have extinction ratios of typically -15dB with negligible loss, while strongly-fused couplers have extinction ratios of approximately -5dB with losses consistently above 1dB.

The optimum for maximum extinction ratio and minimum loss is found to be the weakly-fused coupler.

6.7 Effects of the fibre core

In all of the models so far described in this Chapter, there has been no consideration of the residual effects of the fibre cores in the coupling behaviour of fused taper couplers. The reduction of the coupler cross-section to a waveguide with a homogeneous refractive index has greatly simplified the task of modelling the coupler, and it is found that such models correctly describe the overall behaviour of fused taper couplers.

The study of the effects of the fibre core on the performance of the taper coupler lies well outside the aims of the present Thesis. However, a number of other authors (10,19,20,21) have addressed this problem. The conclusions are that the effect of the cores can cause the coupling strength to be weaker than predicted by the exclusive cladding mode model, but that the influence of the cores is only significant if the fibres are not tapered very much. In this case the modes tend to be intermediate modes as described in Chapter 4, and of course the cladding mode picture is not completely adequate in these circumstances although it still predicts general trends in the behaviour of fused taper couplers.

6.8 Summary

This Chapter has shown that the cladding mode picture of fused taper couplers leads to some useful models for predicting coupler behaviour. For certain specific cross-sectional shapes some very simple, explicit, analytic formulae can be derived for the coupling coefficients in terms of coupler dimensions, wavelength, external refractive index and polarisation.

REFERENCES FOR CHAPTER 6

1. J. Bures, S. Lacroix and J. Lapierre,
"Analyse d'un coupleur bidirectional a fibres optiques monomodes fusionees",
Appl. Opt., 1983, 22, pp. 1918-1922.

2. F.P. Payne, C.D. Hussey and M.S. Yataki,
"Modelling fused single-mode fibre couplers",
Electron. Lett., 1985, 21, pp. 461-462.

3. F.P. Payne, C.D. Hussey and M.S. Yataki,
"Polarisation analysis of strongly fused and weakly fused tapered couplers",
Electron. Lett., 1985, 21, pp. 561-563.

4. F.P. Payne, C.D. Hussey and M.S. Yataki,
"Polarisation in fused single-mode fibre couplers",
Tech. Digest IOOC-ECOC, Venice, 1985,
pp. 571-573.

5. J.D. Love and M. Hall,
"Polarisation modulation in long couplers",
Electron. Lett., 1985, 21, pp. 519-521.

6. A.W. Snyder,
"Polarising beam splitter from fused taper couplers",
Electron. Lett., 1985, 21, pp. 623-625.

7. A.W. Snyder and X.H. Zheng,
"Optical fibres of arbitrary cross-section",
Electron. Lett., 1985, 21, pp. 1079-1080.

8. A.W. Snyder and X.H. Zheng,
"Optical fibres of arbitrary cross-sections",
J. Opt. Soc. Amer., 1986, A3, pp. 600-609.

9. W.J. Stewart and J.D. Love,
"Design limitation on tapers and couplers in single mode fibres",
Tech. Digest IOOC/ECOC, Venice, 1985,
pp. 559-562.

10. K.S. Chiang,
"Design Criterion for low-loss optical coupler tapers",
Electron. Lett., 1987, 23, pp. 112-113.

11. A.W. Snyder, J.D. Love,
"Optical Waveguide Theory",
Chapman and Hall Ltd., (New York, London) 1983.

12. F. de Fornel, C.M. Ragdale, R.J. Mears,
"Analysis of single mode fused tapered fibre couplers",
IEE Proc., Vol. 131, part II, 1984, pp.221-228.

13. F.P. Payne, T. Finnegan, M.S. Yataki, R.J. Mears and C.D. Hussey,
"Dependence of fused taper couplers on external

refractive index",
Electron. Lett., 1986, 22, pp.1207-1209.

14. K.S. Chiang,
"Analysis of Fused Couplers by the effective index method",
Electron. Lett., 1986, pp.1221-1222.

15. X.H. Zheng,
"Fused Couplers: Condition for insensitivity to external refractive index",
Electron. Lett., 1987, 23, pp.182-184.

16. K.L. Chen and S. Wang,
"Cross-talk problems in optical directional couplers",
Appl. Phys. Letter., 1984, 44, pp. 166-168.

17. J.D. Love and A. Ankiewicz,
"Cut off in single-mode optical couplers",
Electron. Lett., 1984, 20, pp. 362-363.

18. J.M.P. Rodrigues, T.S.M. Maclean, B.K. Gazey, J.F. Miller,
"Completely fused tapered couplers: comparison of theoretical and experimental results",
Electron. Lett., 1986, 22, pp. 402-404.

19. J.V. Wright,
"Variational analysis of fused tapered couplers",

Electron. Lett., 1985, 21, pp. 1064-1065.

20. K.S. Chiang,
"Perturbation Analysis of fused tapered single mode fibre couplers",
Electron. Lett., 1987, 23, pp. 717-718.

21. M.N. Mclandrich,
"Core dopant profiles in weakly fused single mode fibres",
Electron. Lett., 1988, 24, pp.8-10.

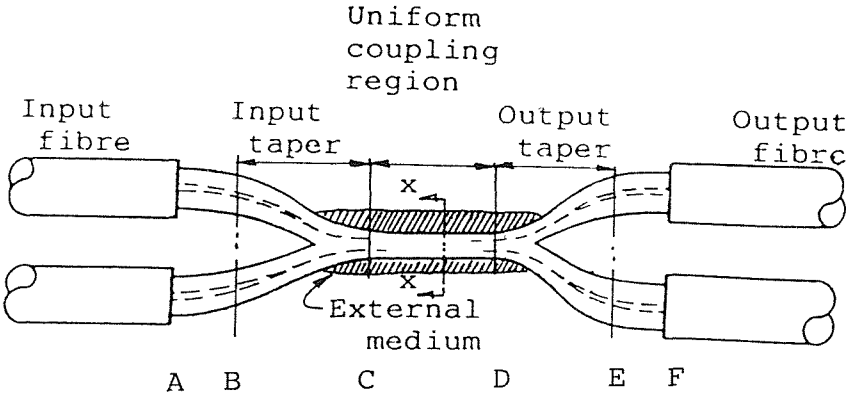

(a)

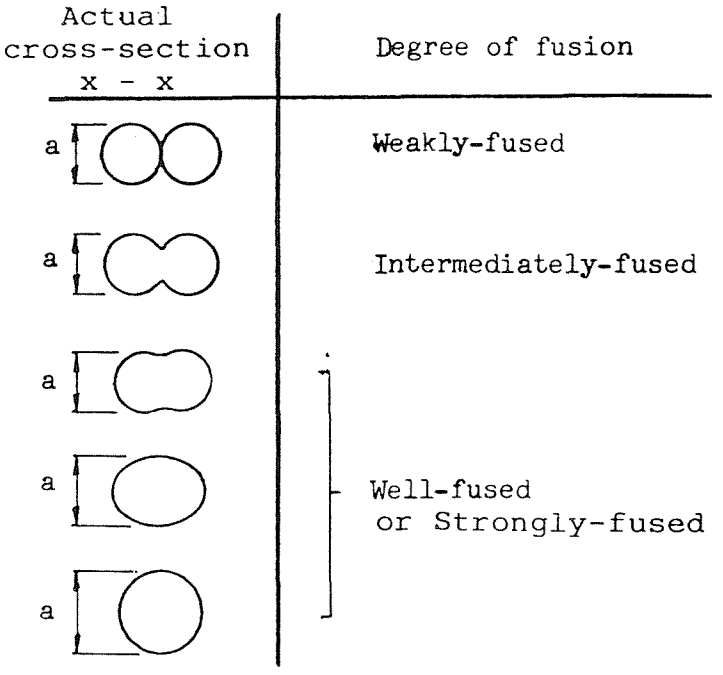

(b)

Figure 6.1. (a) Schematic of the fused taper coupler showing input and output tapers, the uniform coupling region and the external medium.

(b) Possible cross-sections of the uniform coupling region.

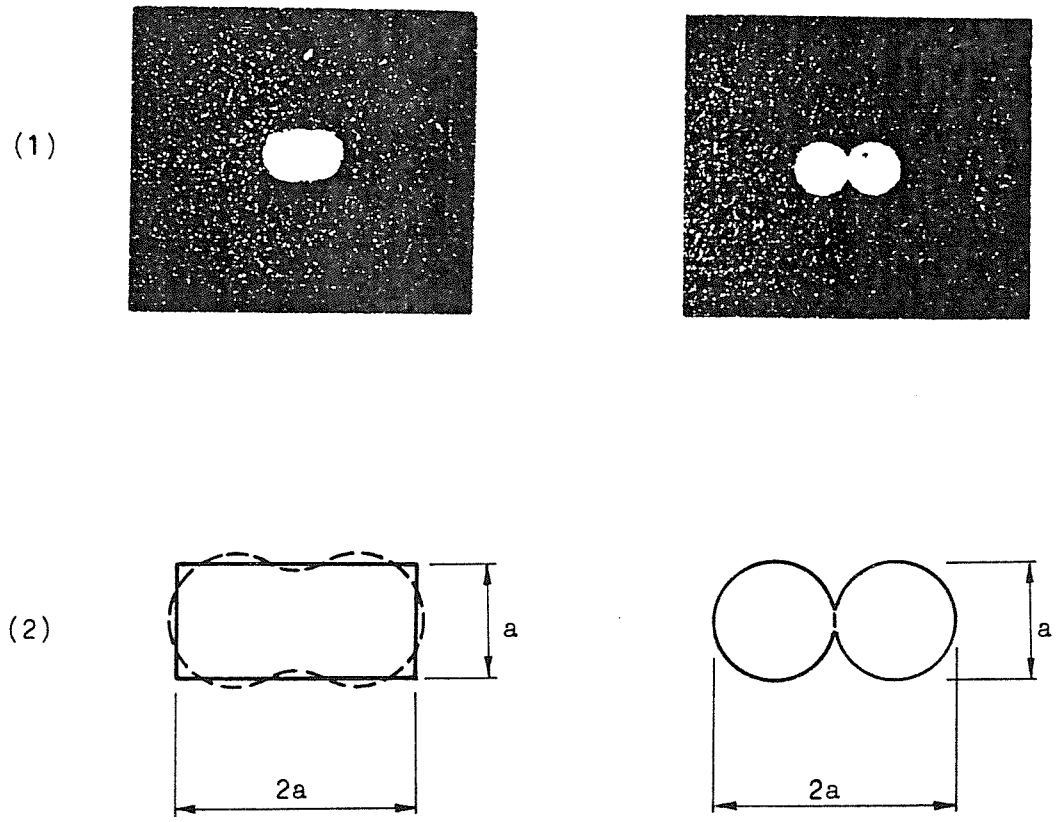

Figure 6.2. Coupler cross-sections (1) and their tractable approximations (2).

(a) Well-fused (rectangle),
(b) Weakly-fused (figure-of-eight).

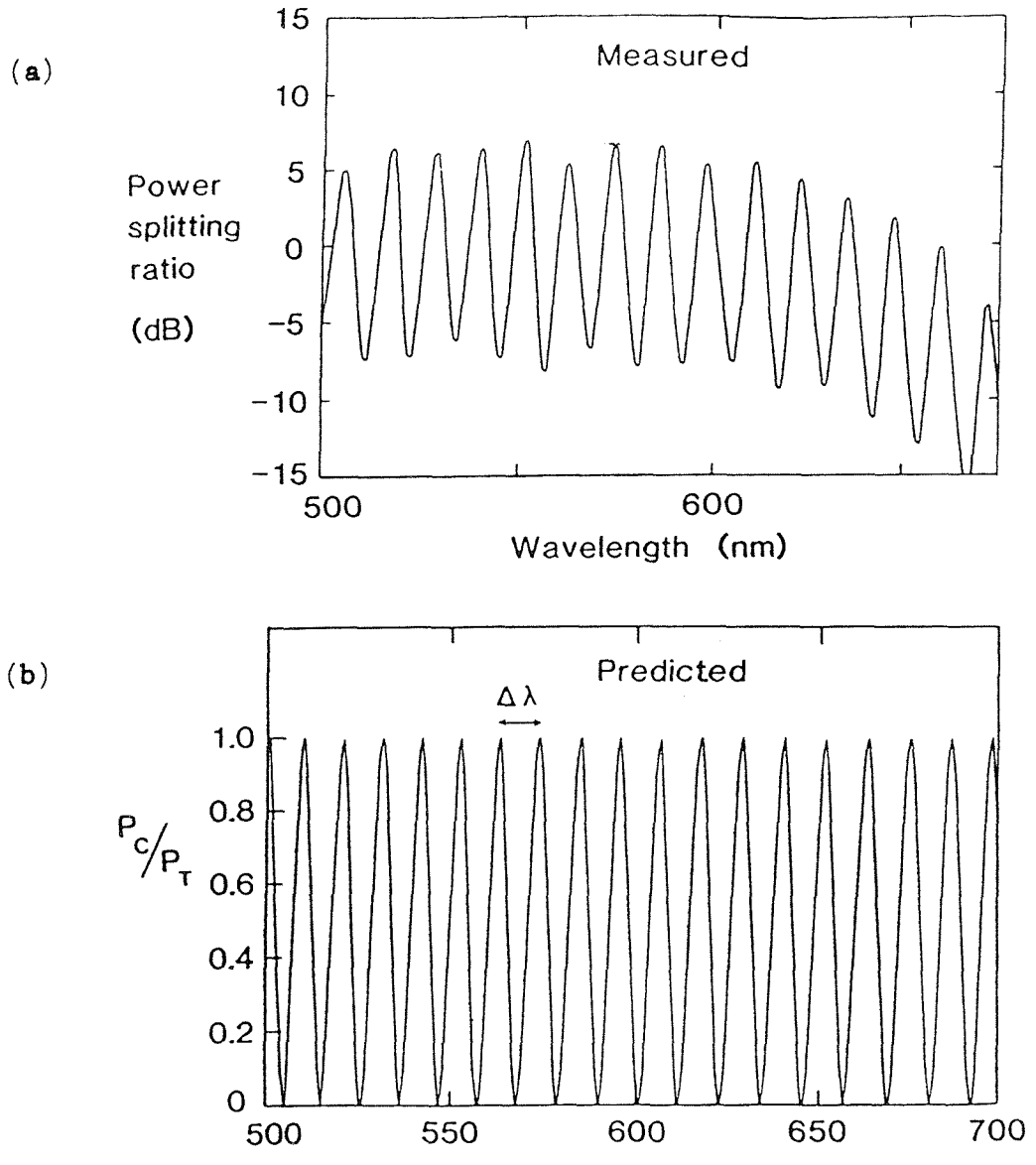

Figure 6.3. Variation of output power with wavelength for a well-fused coupler.

(a) Measured spectral splitting ratio.

(b) Calculated spectral variation of output power for ideal couplers.

Wavelength λ (nm)	500	700
$\Delta\lambda$ measured (nm)	11.3	13.2
$\Delta\lambda$ predicted (nm) equ. (6.14)	10.2	11.8

Table 6.1. Measured and predicted values for the wavelength oscillation period $\Delta\lambda$ corresponding to Figures 6.3(a) and (b) respectively at two different wavelengths.

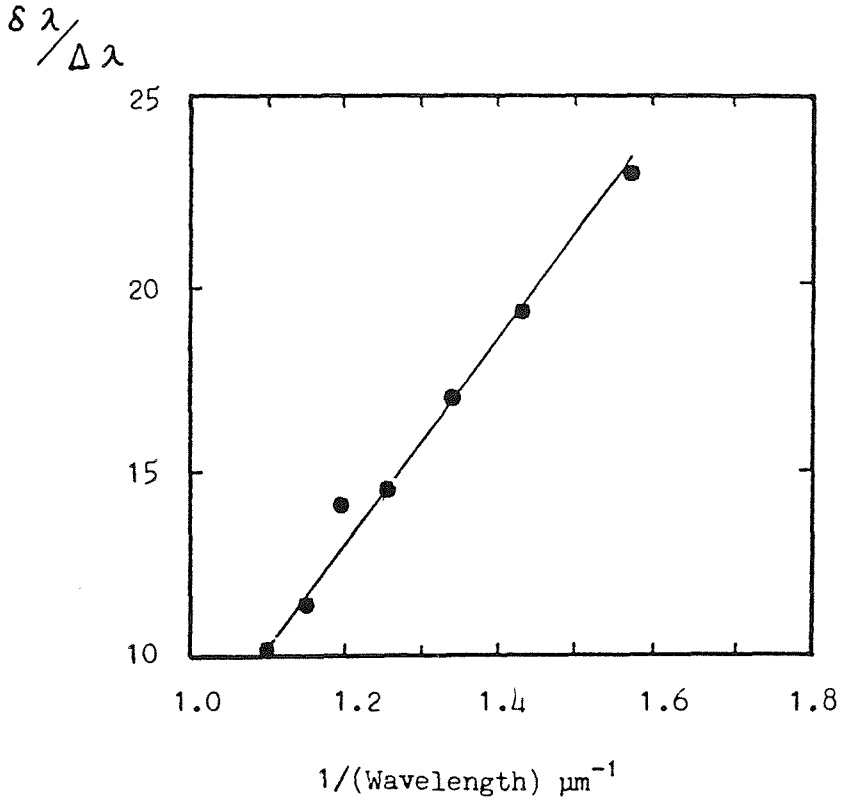

Figure 6.4. A plot of the ratio $\delta\lambda / \Delta\lambda$ as a function of λ^{-1} corresponding to the spectral response in Figure 5.13.

(a)

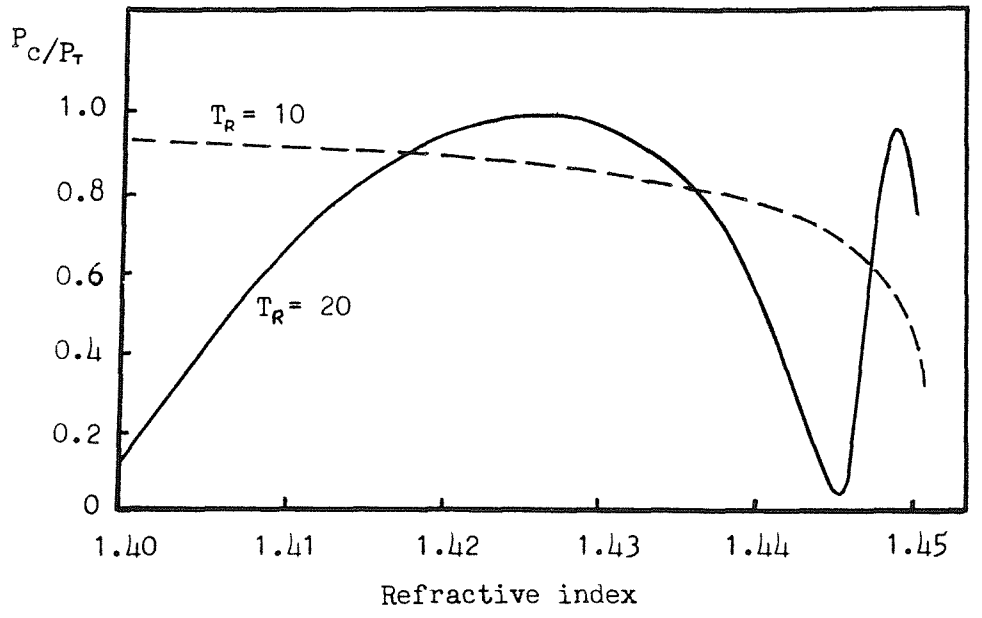

(b)

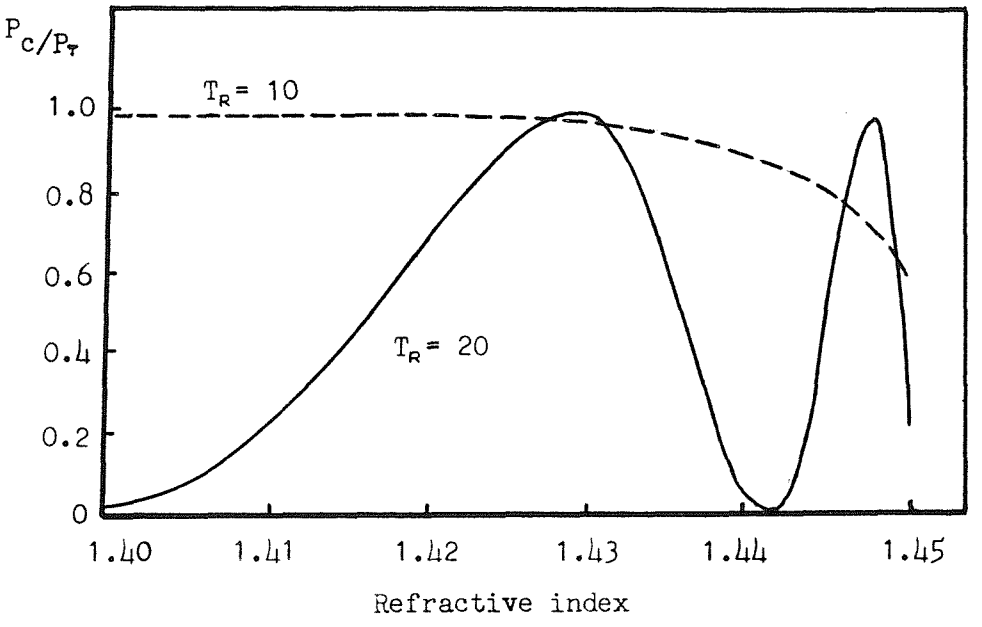

Figure 6.5. Measured (a) and predicted (b) variation of output power with external refractive index for two couplers with different taper ratios T_R .

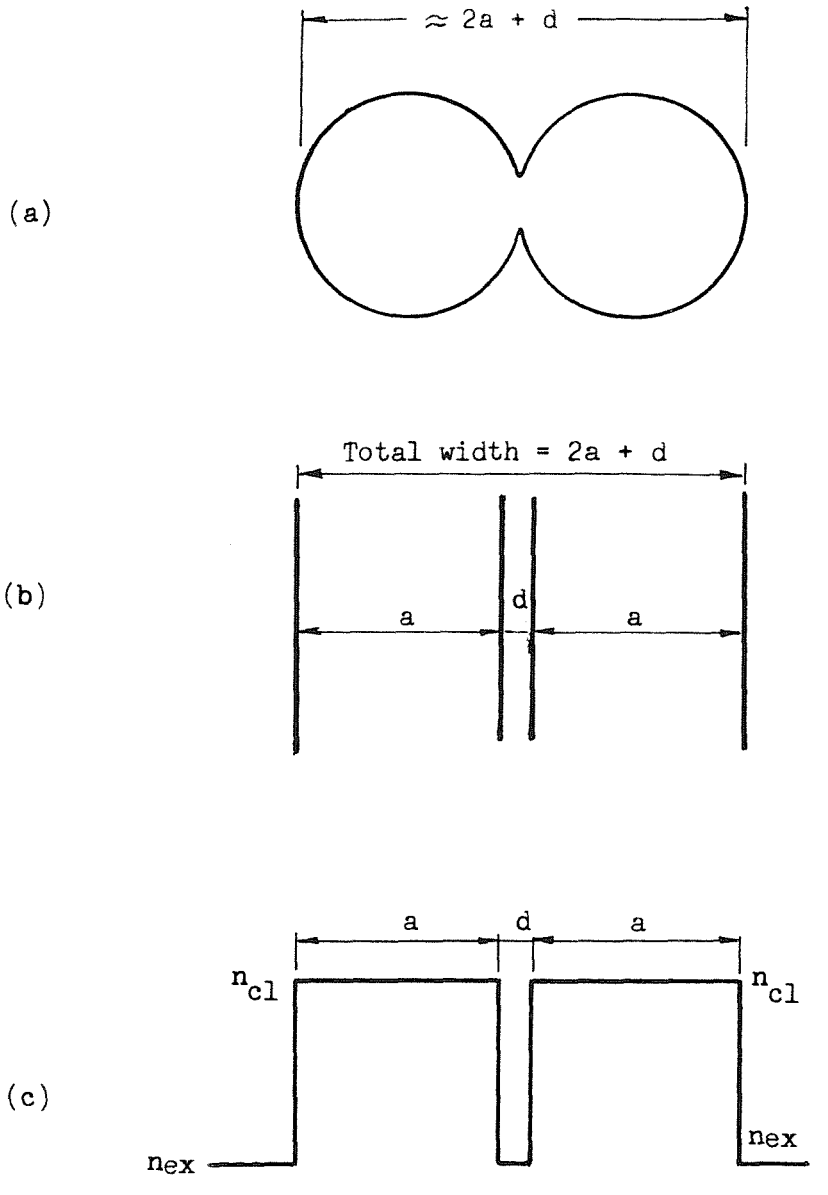

Figure 6.6. Slab waveguide model for a fused taper coupler.

(a) Schematic of coupler cross-section.
(b) Parallel slab geometry.
(c) Parallel slab refractive index.

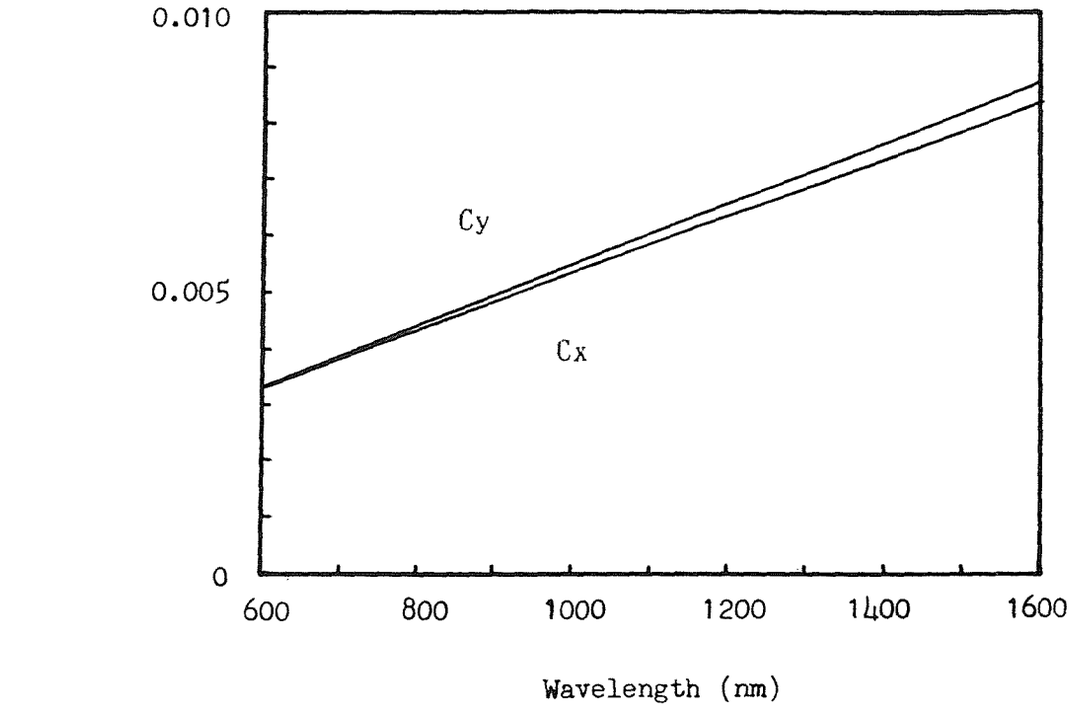

Figure 6.7.1. Coupling coefficients for the two polarisation states for $n_{ex} = 1.00$, $a = 6\ \mu m$ and $d = 0\ \mu m$, i.e. strongly-fused.

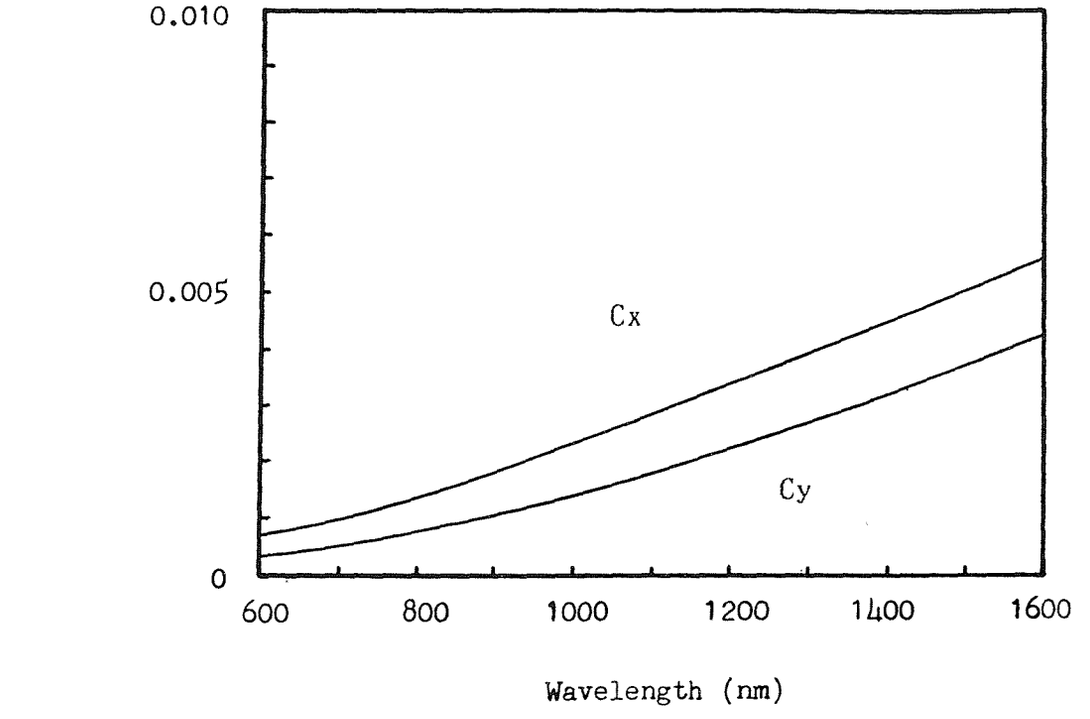

Figure 6.7.2. Coupling coefficients for the two polarisation states for $n_{ex} = 1.00$, $a = 6\,\mu m$ and $d = 0.03\,\mu m$, i.e. medium-fused.

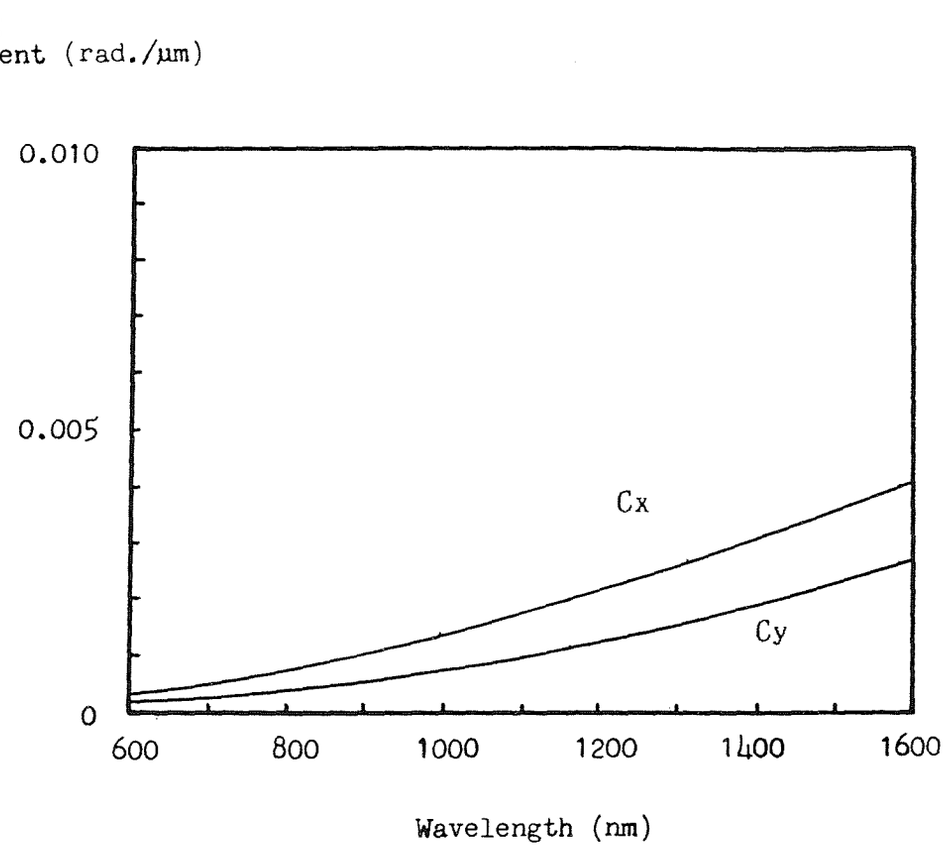

Figure 6.7.3. Coupling coefficients for the two polarisation states for n_{ex} = 1.00, a = 6 μm and d = 0.06 μm , i.e. weakly-fused.

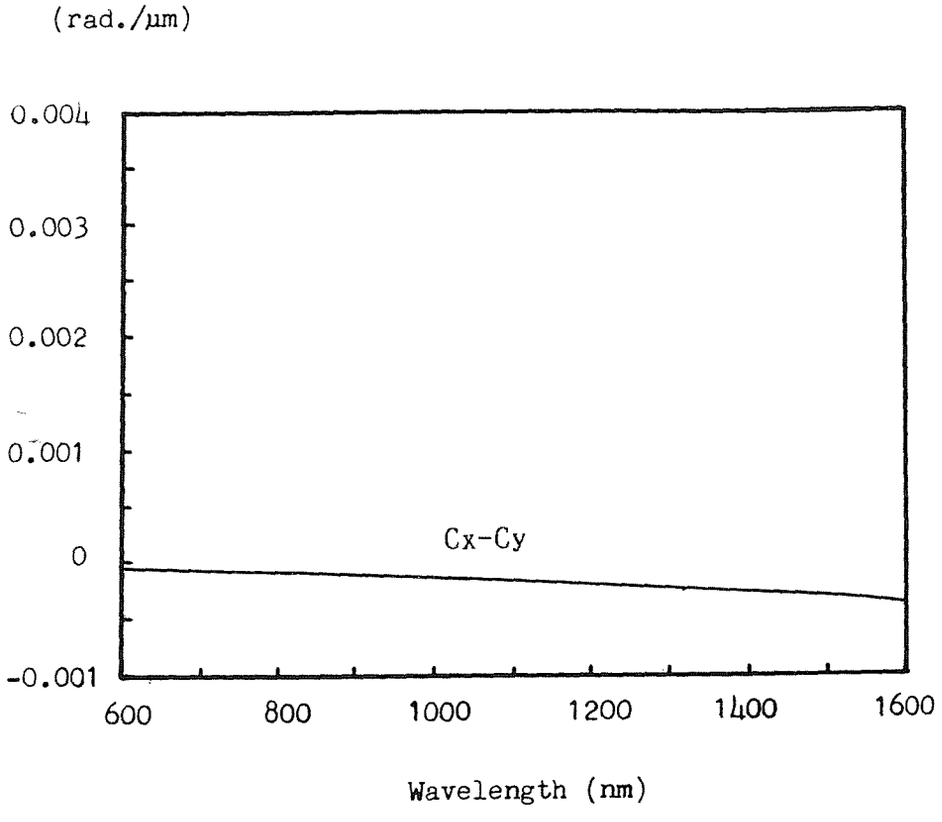

Figure 6.8.1. Coupling coefficient difference between the two polarisation states for $n_{ex} = 1.00$, $a = 6\ \mu m$ and $d = 0\ \mu m$, i.e. strongly-fused.

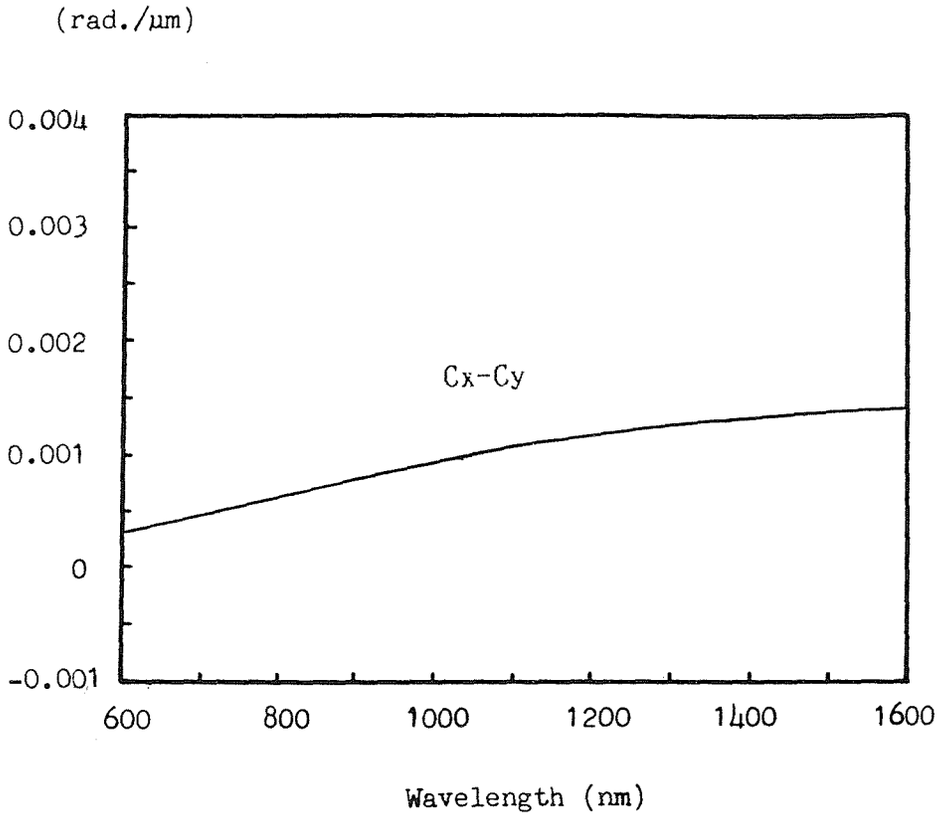

Figure 6.8.2. Coupling coefficient difference between the two polarisation states for $n_{ex} = 1.00$, $a = 6\ \mu m$ and $d = 0.03\ \mu m$, i.e. medium-fused.

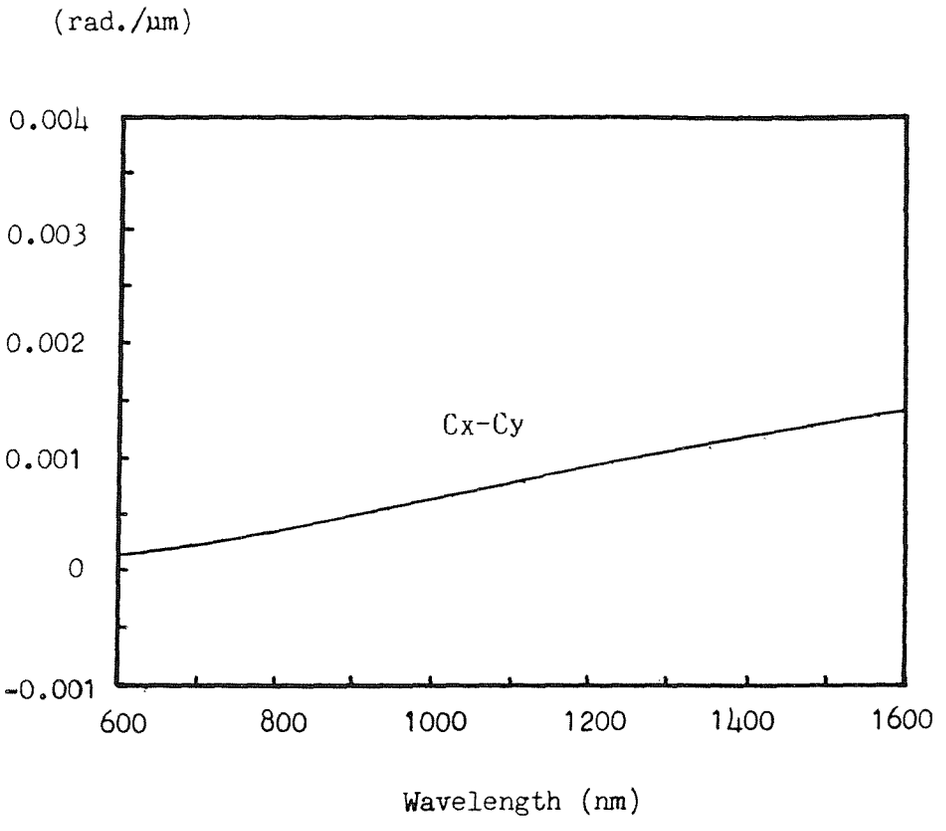

Figure 6.8.3. Coupling coefficient difference between the two polarisation states for $n_{ex} = 1.00$, $a = 6\ \mu m$ and $d = 0.06\ \mu m$, i.e. weakly-fused.

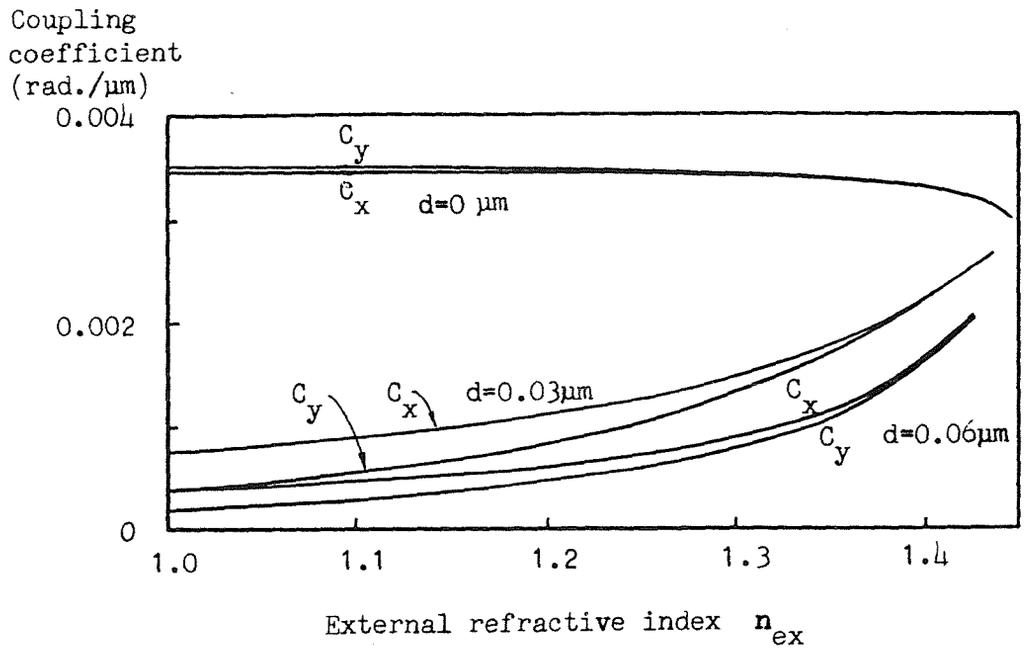

Figure 6.9. Dependence of the coupling coefficients Cx and Cy on the external refractive index n_{ex} for a = 6 μm and three different gap thicknesses d = 0 μm (strongly-fused), 0.03 μm (medium-fused) and 0.06 μm (weakly-fused).

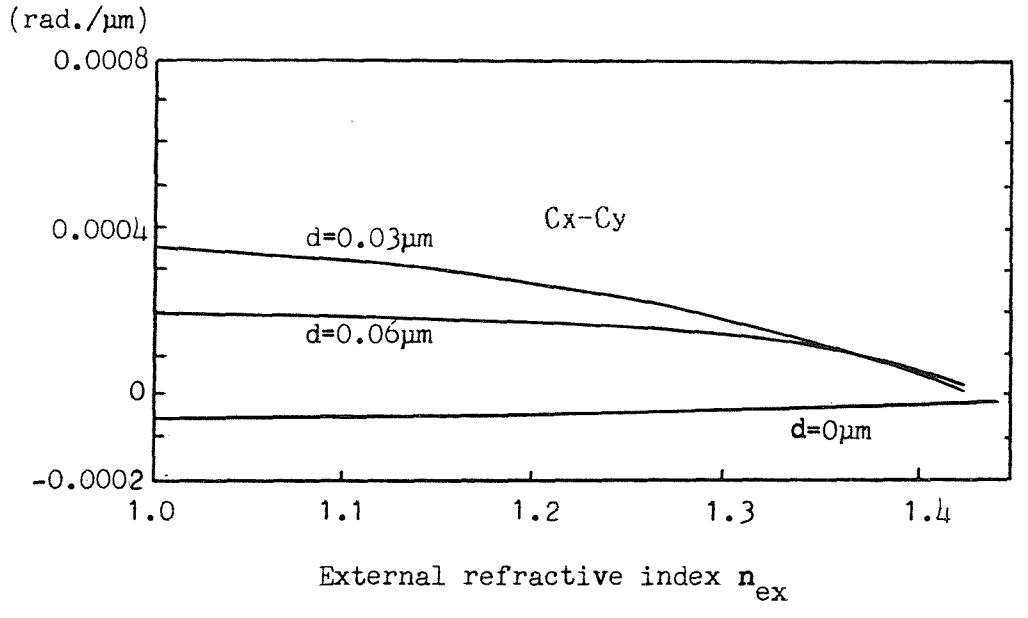

Figure 6.10. Dependence of the coupling coefficient difference (Cx-Cy) on the external refractive index n_{ex}. Parameters are as same as in Figure 6.9..

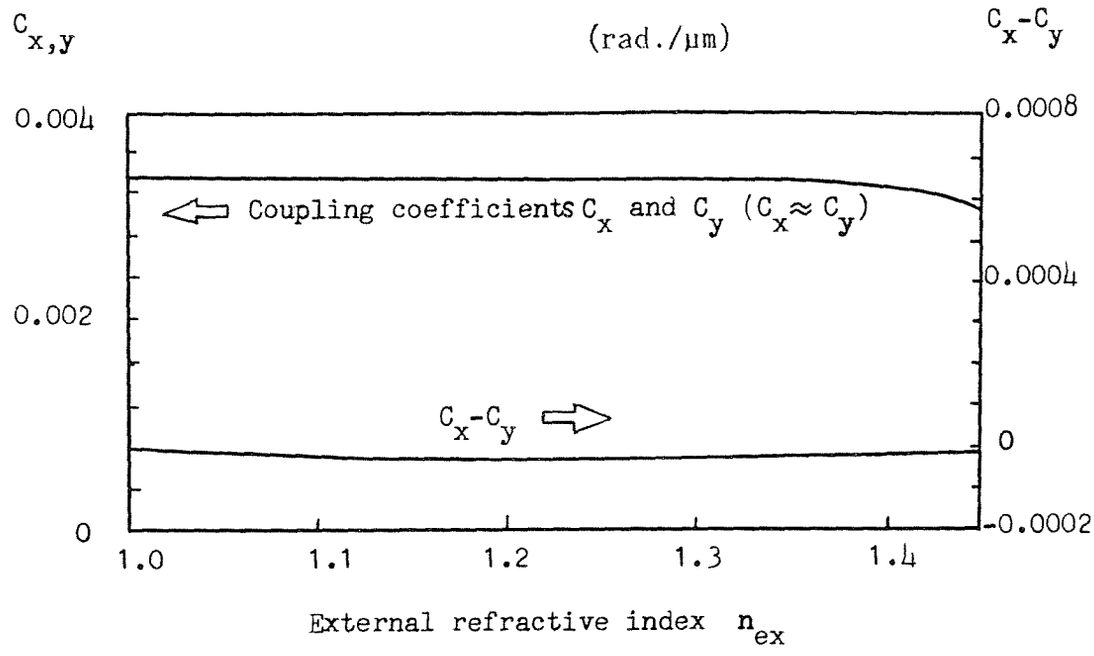

Figure 6.11. Dependence of the external refractive index n_{ex} on the coupling coefficients Cx and Cy and the polarisation effect Cx-Cy for a = 6 μm, d = 0.00012 μm, , refractive index of waveguide n = 1.458 and wavelength λ = 0.63 μm,

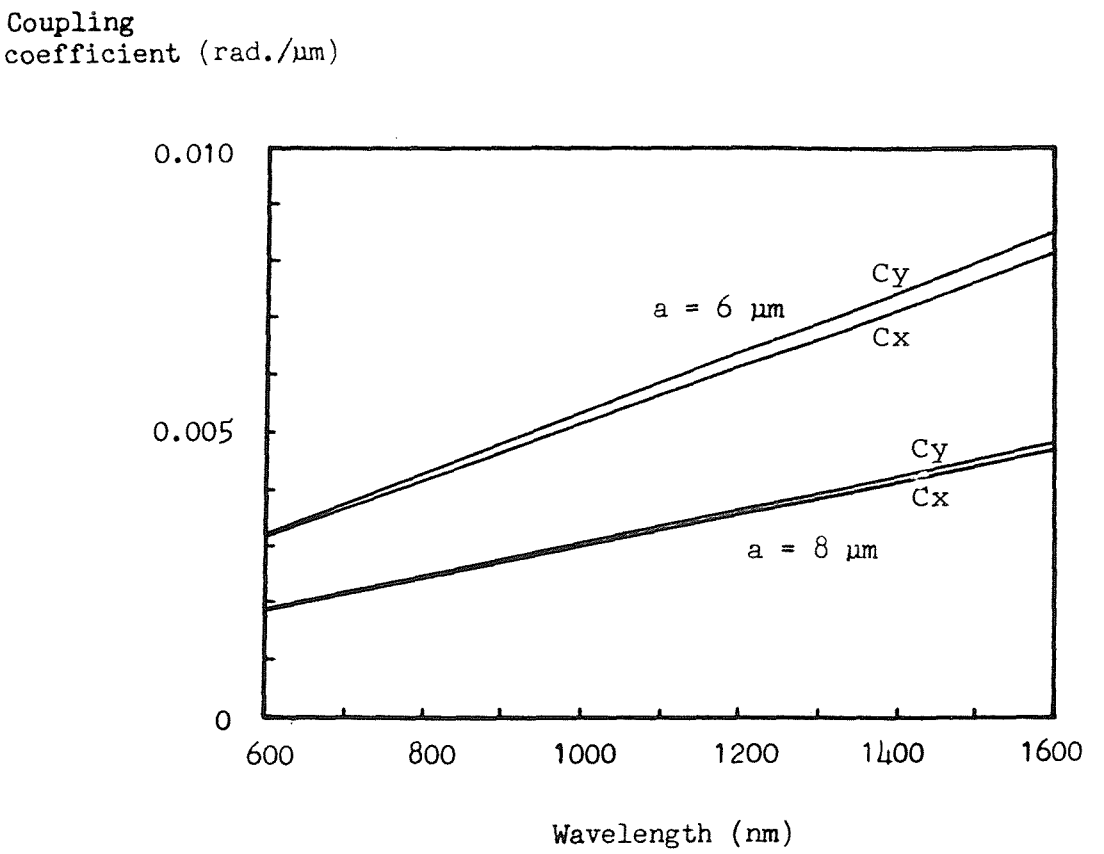

Figure 6.12. Coupling coefficients for the two polarisation states for strongly-fused waveguides of sizes $a = 6\ \mu m$ and $a = 8\ \mu m$ with respect to wavelength.

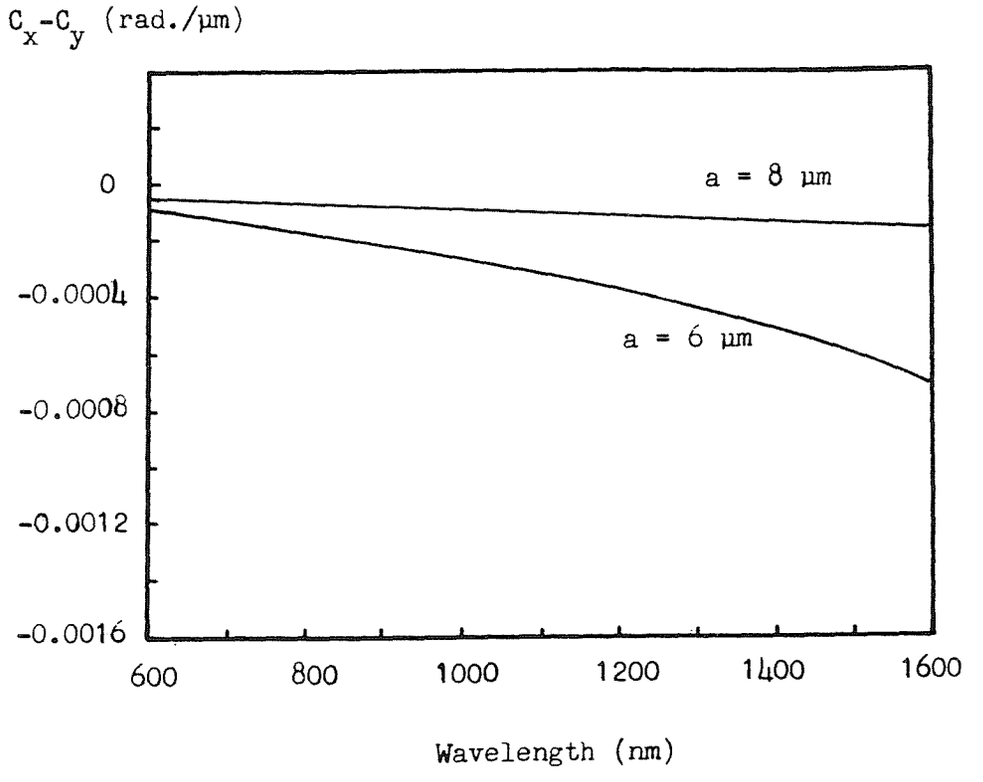

Figure 6.13. Difference in coupling coefficients between the two polarisation states for strongly-fused waveguides of sizes a = 6 μm and a = 8 μm with respect to wavelength.

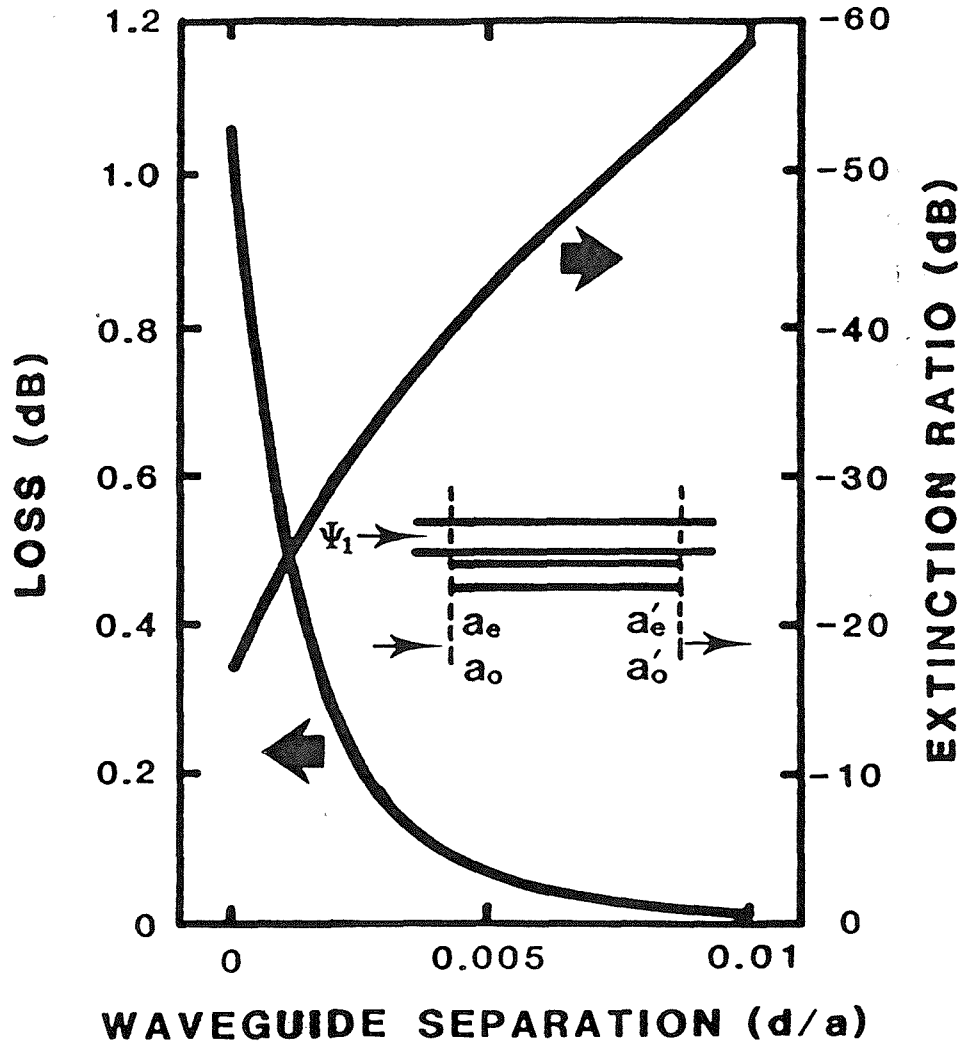

Figure 6.14. The extinction ratio and loss for the parallel slab waveguide model (inset) as a function of the distance between two waveguides.

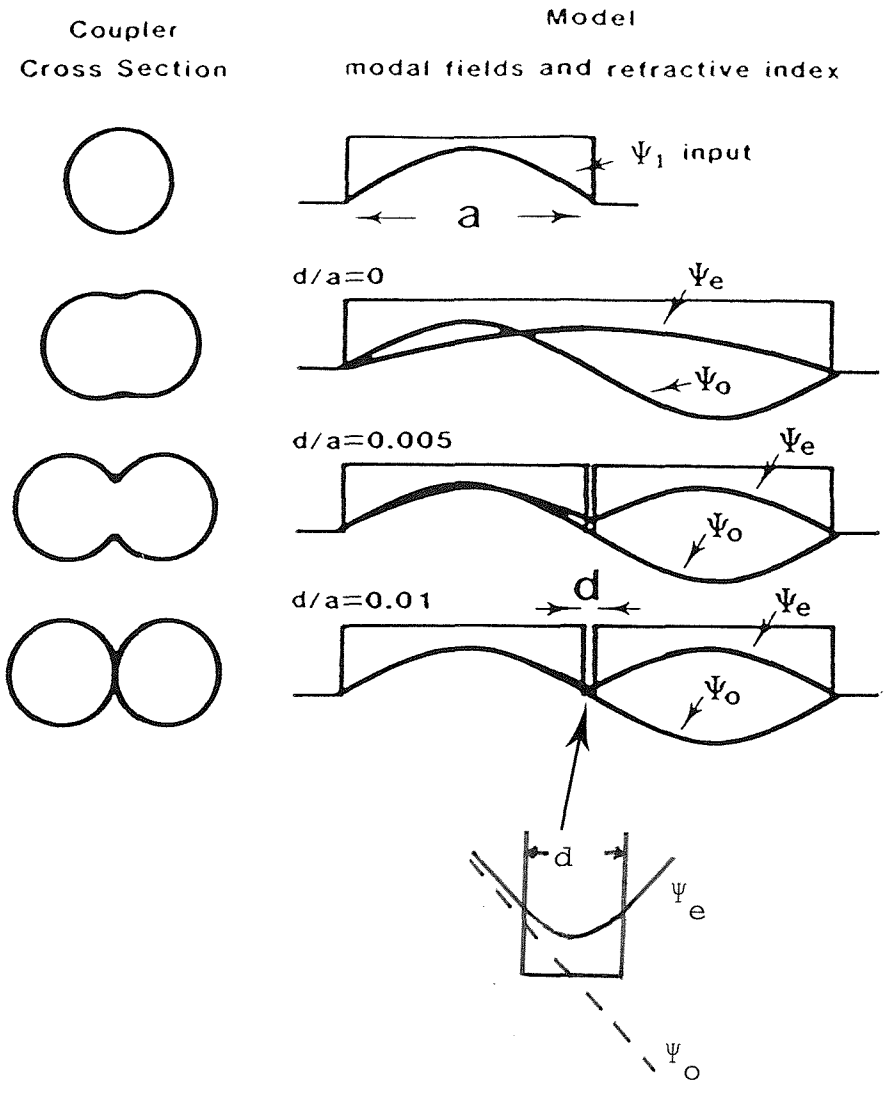

Figure 6.15. Actual coupler cross-sections and their models showing the refractive index distribution, the input field Ψ_1 and the even (Ψe) and the odd (Ψo) normal modes.

CHAPTER 7: APPLICATIONS AND NEW DEVELOPMENTS IN TAPER BASED COMPONENTS

7.1 Introduction

The cladding mode picture of single-mode fibre tapers and taper couplers has been proposed and exhaustively developed in this Thesis. It has been found that the cladding mode theory successfully accounts for the main characteristics of these components in both quantitative and qualitative terms. However, the true test of a new theory is not in explaining existing results but in suggesting new applications and devices which require the understanding that this new theory gives.

The main function of a coupler is to divide power between two or more fibres. During the course of this study other useful properties of the fused taper coupler have been discovered, and it is found that taper couplers can have quite diverse applications. This Chapter examines two different applications areas for fused taper couplers: fibre circuits - a spectral band-pass filter, and fibre sensors - a thermal sensor.

Other more recent developments in taper components which rely explicitly on the cladding mode understanding of taper-couplers will also be outlined, although they were undertaken later than the time frame of the present Thesis.

7.2 Spectral Band-Pass Filter

Single-mode optical fibre couplers are being actively

developed for wavelength multiplexing applications (1,2). Several fabrication approaches to provide the coupling action have been reported, the two most common being the polished coupler and the fused biconical-taper coupler. The main advantage of the polished coupler is that it is readily wavelength tunable by adjusting the coupling length, while the advantage of the fused taper coupler is that it is more thermally stable and is quicker and more convenient to make.

The ability of a taper coupler to wavelength filter light results from the rapid variation of coupled power with wavelength which occurs in an overcoupled coupler, i.e. one in which the power transfers to and fro between the fibres several times along the length. The length for which complete power transfer takes place is approximately proportional to wavelength, so changing the wavelength varies the number of times the light oscillates between the two fibres. A periodic coupled-power response with wavelength is found, as has been described in Chapter 5 where the properties of very long fused-taper couplers have been described (3). These couplers have low loss and very small, controllable channel separations. This suggests the possibility of concatenating several couplers together to tailor a given wavelength response such as a narrowband optical-filter, in spike or comb form.

The present Section describes the realisation of a narrow-band optical-filter. The design of the concatenated

filters is first given, followed by the practical implementation of a simple two-coupler narrow-band filter. The possibility of multicoupler designs and their potential spectral passband is discussed.

7.2.1 Principles of Operation

The spectral response $R(\lambda)$ of a highly-overcoupled 4-port coupler is approximately sinusoidal with wavelength oscillation period $\Delta\lambda$, where $\Delta\lambda$ depends on the coupling strength. If two or more couplers are concatenated (insets Figure 7.1), the throughput will be given by

$$P(\lambda) = \frac{1}{4}\left[1+\text{Sin}\left(\frac{2\pi\lambda}{\Delta\lambda_1} + \Theta_1\right)\right]\left[1+\text{Sin}\left(\frac{2\pi\lambda}{\Delta\lambda_2} + \Theta_2\right)\right] \quad (7.1)$$

where $P(\lambda)$ is the power in the output port, $\Delta\lambda_1$, and $\Delta\lambda_2$ are the channel spacings of the 1st and 2nd couplers, and Θ_1 and Θ_2 are the phase parameters of the couplers. From equation (7.1), the spectral throughput of two concatenated couplers was calculated for $\Delta\lambda_1 = 2(\Delta\lambda_2) = 100$ nm and $\Theta_1 = \Theta_2 = 0$. The result, Figure 7.1(a), shows a spike filter characteristic. As in a Lyott filter, the response can be improved by concatenating several couplers together as shown in Figure 7.1(b), where the theoretical response of four concatenated couplers is shown. Here the parameters $\Delta\lambda_1 = 2(\Delta\lambda_2) = 3(\Delta\lambda_3) = 4(\Delta\lambda_4) = 100$ nm were used. It is clear from these figures that if the channel spacing of the couplers can be narrowed sufficiently, an excellent spike

filter characteristic can be obtained. Such a filter could be used, for example, as a wavelength drop-off filter in a wavelength-division multiplexed communication link, or to separate a single line from a multi-longitudinal mode laser.

7.2.2 Experimental Results

An optical bandpass filter was fabricated from two concatenated overcoupled single mode fibre couplers which had 20mm and 150mm interaction lengths respectively. To avoid the necessity of splicing the couplers together, they were made in succession on the same fibre. The spectral throughput of this dual-coupler bandpass filter is shown in Figure 7.2. At the centre wavelength, 650nm, the filter has a throughput of 95% (a loss of only 0.2dB) and a 3dB spectral width of 20nm. The two side lobes at 620nm and 675nm are present at 25%.

Although the response betwen 600nm to 700nm clearly resembles the theory given above, the repeat response between 700nm and 800nm was found to be somewhat distorted. This is due to the phase parameter terms in equation (7.1), and also to the fact that the channel spacings $\Delta\lambda_1$ and $\Delta\lambda_2$ are not uniform with wavelength.

Measurements of the thermal stability of overcoupled couplers in the temperature range $20^{o}C$-$70^{o}C$ has shown that their wavelength characteristics can be surprisingly stable.

7.2.3 Discussion

The above experiment clearly demonstrates that low-loss optical bandpass filters can be fabricated by concatenating fused-taper couplers.

Couplers have been successfully fabricated with interaction lengths as large as 600mm, all with losses less than 1dB. However, the wavelength oscillation period in these couplers was too small for the measurement system to resolve, and therefore the potential bandwidth of a spike filter is as yet unknown, but is certainly much less than 2.5nm.

7.3 Taper Coupler Based Temperature Sensor

The ground-work for the temperature sensor has already been prepared in the experimental study in Section 5.5.2 of the effects of the refractive index of the medium surrounding the coupler, and the use there of temperature to vary that external refractive index. In the present Section, that study is turned around and the changes in coupler characteristics now directly monitor temperature changes. For instance, if the graph for the variation in oscillation period with external refractive index (Figure 5.19) for the coupler studied in Section 5.5.2 is now plotted against temperature, the equivalent graph in Figure 7.3 is obtained, with the result that the oscillation period $\Delta\lambda$ can be considered as being proportional to the incremental changes in temperature within the limits in the example of $40^{o}C < T < 90^{o}C$, i.e.

$$\Delta\lambda \quad \alpha \quad \Delta T \qquad (7.2)$$

A more practical sensor, however, is one based on the power-splitting ratio variation with temperature, once the coupler is embedded in a suitable medium. Figure 7.4 is a graph of the variation of power-splitting ratio with temperature for a specific coupler at the wavelength of 633 nm. The coupler was immersed in oil which had a known refractive index of 1.406 - .00042/^{o}C (at 25^{o}C and at a wavelength of 589 nm). In this example the power-splitting ratio was zero (i.e. equal power in the two output ports) close to zero degrees centigrade, so that the characteristic appears linear from 0^{o}C to approximately 40^{o}C. If the zero splitting ratio point of the coupler was made to occur at a higher temperature, then the overall dynamic range of the sensor could be expanded beyond the 8-9dBs as found in Figure 7.4. The operation of the sensor at temperatures lower than zero would depend on the characteristics of the oil surrounding the coupler.

To examine the repeatibility of the temperature sensor response, a temperature cycling test was performed while monitoring the output power-splitting ratio.

Figure 7.5 gives the power-splitting ratio as it varied with the temperature during four cycles of the temperature test, where in each cycle the temperature went from 2^{o}C to 52^{o}C in 10^{o}C steps, with 20 mins. allowed for the

temperature to settle down after each step. The repeatibility of the sensor characteristics is thus confirmed.

7.4 New Developments: Equalisation Effects of the Taper

One of the most exciting result from the study of tapers in single mode fibres is that once a fibre is tapered, the properties of the modes in the taper waist are governed, for all intents and purposes, only by the local diameter of the fibre cladding, the refractive index of the cladding, and the external medium surrounding the coupler - the residual cores having no significant influence over the modes. This result implies that arbitrarily different fibres can be "equalised" simply by tapering them to a given diameter. Already it has been noted in Chapter 4 how this property of the taper allows for the construction of low-loss joints between dissimilar fibres (4).

Much broader implications of this equalisation effect have been realised recently in the construction of the single mode fibre Y- junction (5), and asymmetric couplers between dissimilar fibres (6-8).

7.4.1 The Y-Junction Beamsplitter

The basic structure of the beamsplitter is shown in Figure 7.6(a). The device has three ports, one input and two output ports, arranged as a letter Y.

A single-mode fibre taper, which forms the stem of the

Y, is spliced to a matched half of a circularly fused tapered coupler which forms the fork. As analysed in Chapters 2 and 5, the conventional 4-port coupler requires the equal excitation of the two lowest order (LP_{01} and LP_{11}) modes of the cladding/air waveguide formed in the coupler waist. Coupling results from the interference between these two modes. The output power-splitting ratio thus depends on the length, the cross-sectional size and shape of the coupling region, the external refractive index, and the polarisation state and wavelength of the input light.

The Y-junction approach eliminates all these dependences by exciting only one cladding mode at the waist of the device. Its operation is similar to that of the mode transformer of Mortimore and Wright (4) used in the production of low loss splices between dissimilar fibres.

The light propagates across the splice point with little loss, since the geometrical matching of the taper and circularly fused half-coupler causes the modal fields on either side of this point to be reasonably well matched. The excitation symmetry in a perfect Y-junction ensures that there is no wavelength dependence in the device. The adiabatically increasing cores at the fork side of the junction now guide power equally into the two output ports for all wavelengths, irrespective of external index and polarisation. The LP_{01} field evolution in the tapered Y-junction is shown schematically in Fig. 7.6(b).

7.4.2 Asymmetric Couplers

Fused-taper single-mode fibre couplers are available which have a flattened wavelength response. Such couplers are fabricated by inducing an asymmetry in the constituent fibres, for example by pre-tapering one fibre prior to coupler fabrication (6), by similarly pre-etching (7), or indeed by using two unlike fibres (7,8). In essence, all of these methods produce an equivalent coupling structure; the single-mode fibre taper is a cladding-mode device, and the main differentiating factor between tapered fibres is therefore their overall diameter.

It is worth noting here that the simple slab waveguide model which was presented in Chapter 6 has been successfully extended in Reference 8 to provide design guidelines for asymmetric couplers and is perhaps to only convenient model for the analysis of such couplers.

7.5 New Developments: External Index Effects

Two applications have recently been reported where the coupler is encapsulated in a silicone resin whose refractive index is changed through thermal effects; the result being a tunable WDM coupler (9) or a simple thermo-optic switch (10). In both devices the couplers were weakly-fused in order to exploit the maximum sensitivity to external index change.

The fundamental operation of these devices is exactly analogous to that of the temperature sensor described in

Section 7.3 so further detail is not provided here.

7.6 Conclusions

In this Chapter a very brief overview of some applications and some new devices based on the taper coupler has been presented. The purpose has been to indicate directions in which further progress can be made in the exploitation of the taper and taper-coupler in the provision of all-fibre devices and components. Progress which can only be made with a thorough understanding of the single-mode-fibre taper.

REFERENCES FOR CHAPTER 7

1. M. Dignonnet, H.J. Shaw,
"Analysis of tunable single-mode optical fibre couplers",
IEEE J. Quant. Electron., 1982, QE-18, 746-754.

2. C.M. Ragdale, D.N. Payne, F. De Fornel, R.J. Mears,
"Single-mode fused biconical couplers",
Proc. 1st Int. Conf. on Optical Fibre Sensors,
London, 1983.

3. M.S. Yataki, M.P. Varnham, D.N. Payne,
"Fabrication and properties of very-long fused taper couplers",
Proc. 8th Optical Fibre Conference, San Diego, 1985.

4. D.B. Mortimore, J.V. Wright,
"Low Loss joints between dissimilar fibres by tapering fusion splices",
Electron. Lett. 1986, 22, pp. 318-319.

5. J.D. Minelly, C.D. Hussey,
"Single Mode Fibre Y-Junction Beamsplitter",
Electron. Lett. 1987, 23, pp.1087-1088.

6. D.B. Mortimore,
"Wavelength-Flattened Fused Couplers",
Electron. Lett., 1985, 21, pp. 742-743.

7. R.G. Lamont, K.O. Hill, D.C. Johnson,

"Tuned-Port Twin Biconical-Taper Fiber Splitters: fabrication from dissimilar low mode - number fibres",
Opt. Lett., 1985, 10, pp. 46-48.

8. T.A. Birks, C.D. Hussey,
"Behaviour of Asymmetric Fused-Tapered Single-Mode Fibre Couplers",
IEE Colloquium "All Fibre Devices", June 1988.

9. S.P. Shipley, A El Fatatry,
"All single-mode optical fibre wavelength-tunable WDM with very narrow pass/stopband separations",
Electron. Lett., 1987, 23, pp. 523-524.

10. M.B.J. Dumeer, W.J. De Vries,
"Fused coupler switch using a thermo-optic cladding",
Electron. Lett., 1988, 24, pp. 457-458.

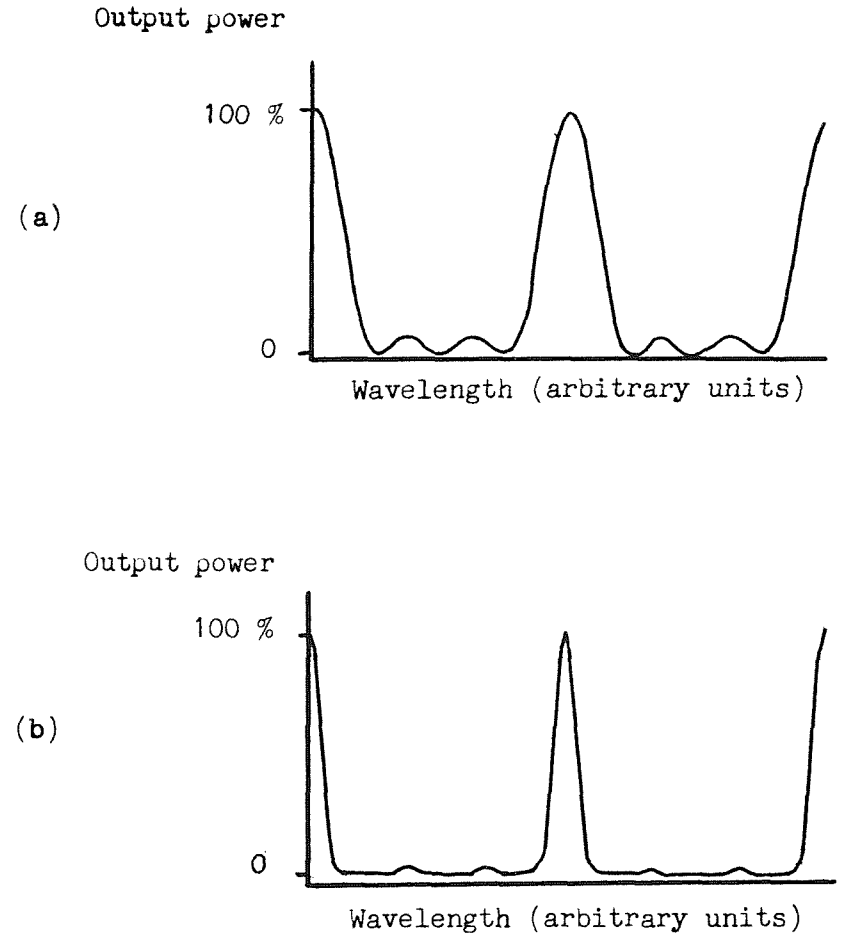

Figure 7.1. Calculated spectral response of concatenated overcoupled 4-port couplers.

(a) Two series-couplers.
(b) Four series-couplers.

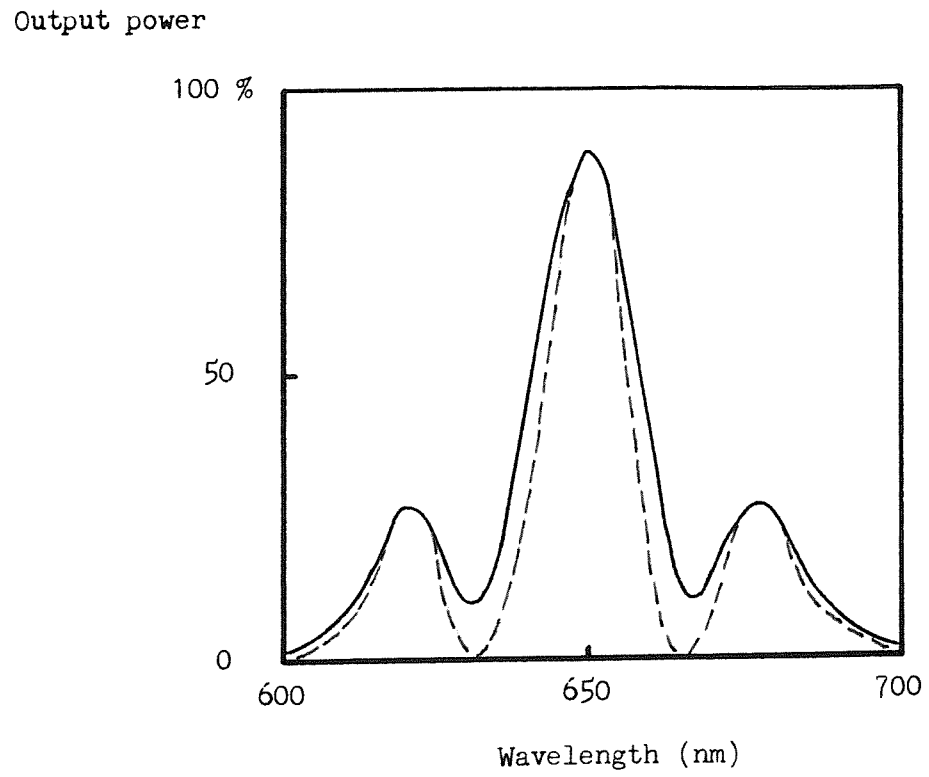

Figure 7.2. Experimental spectral response of two series 4-port couplers. Also shown is the theoretical response with loss taken into consideration(---)

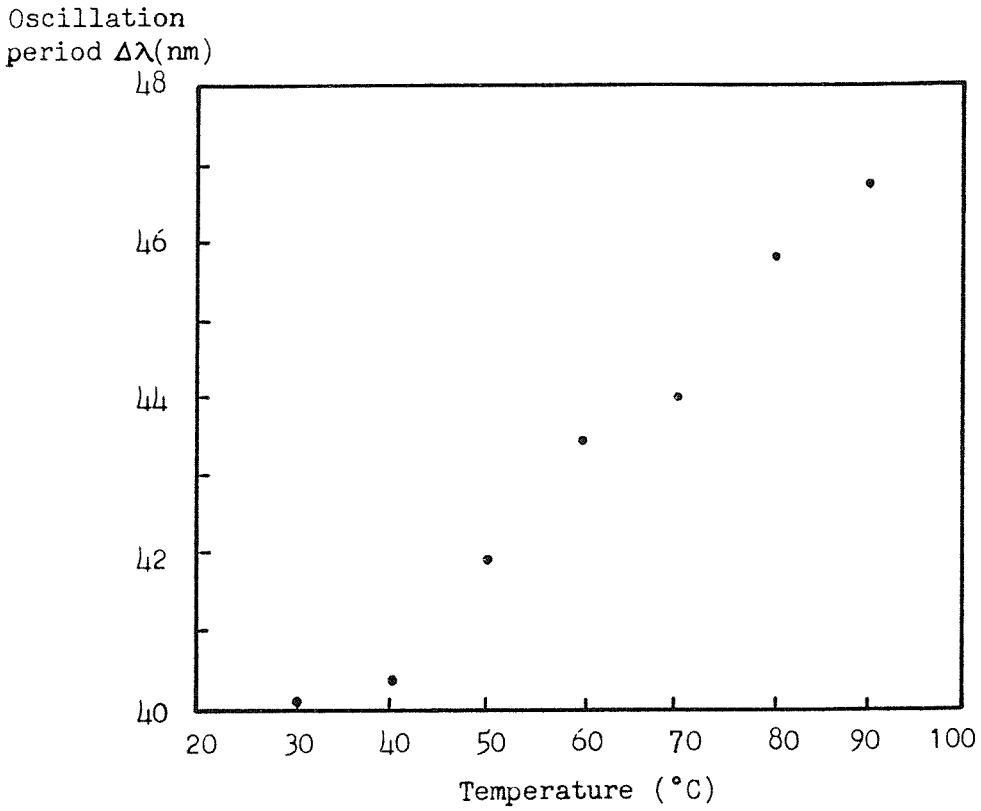

Figure 7.3. Oscillation period plotted against temperature.

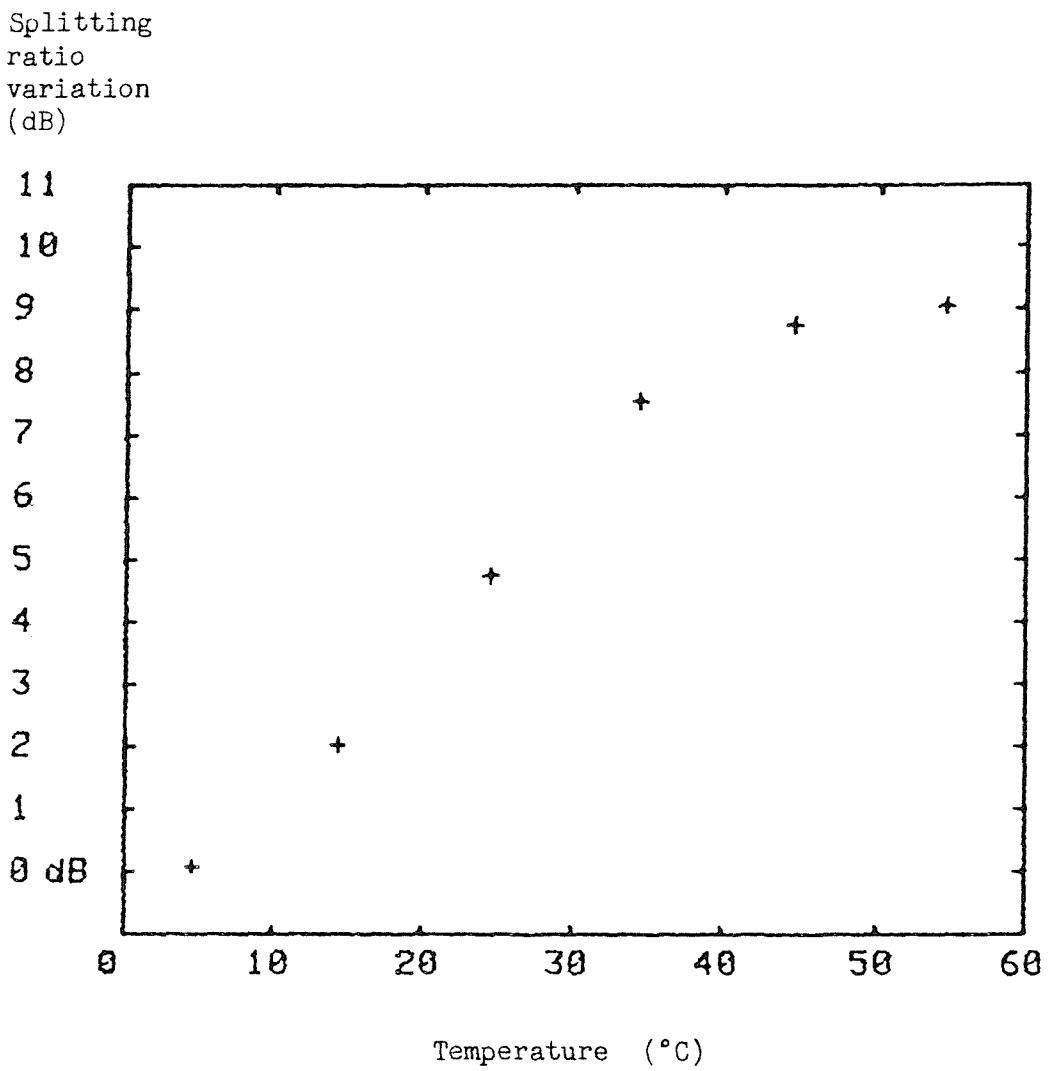

Figure 7.4. Splitting ratio variation versus temperature.

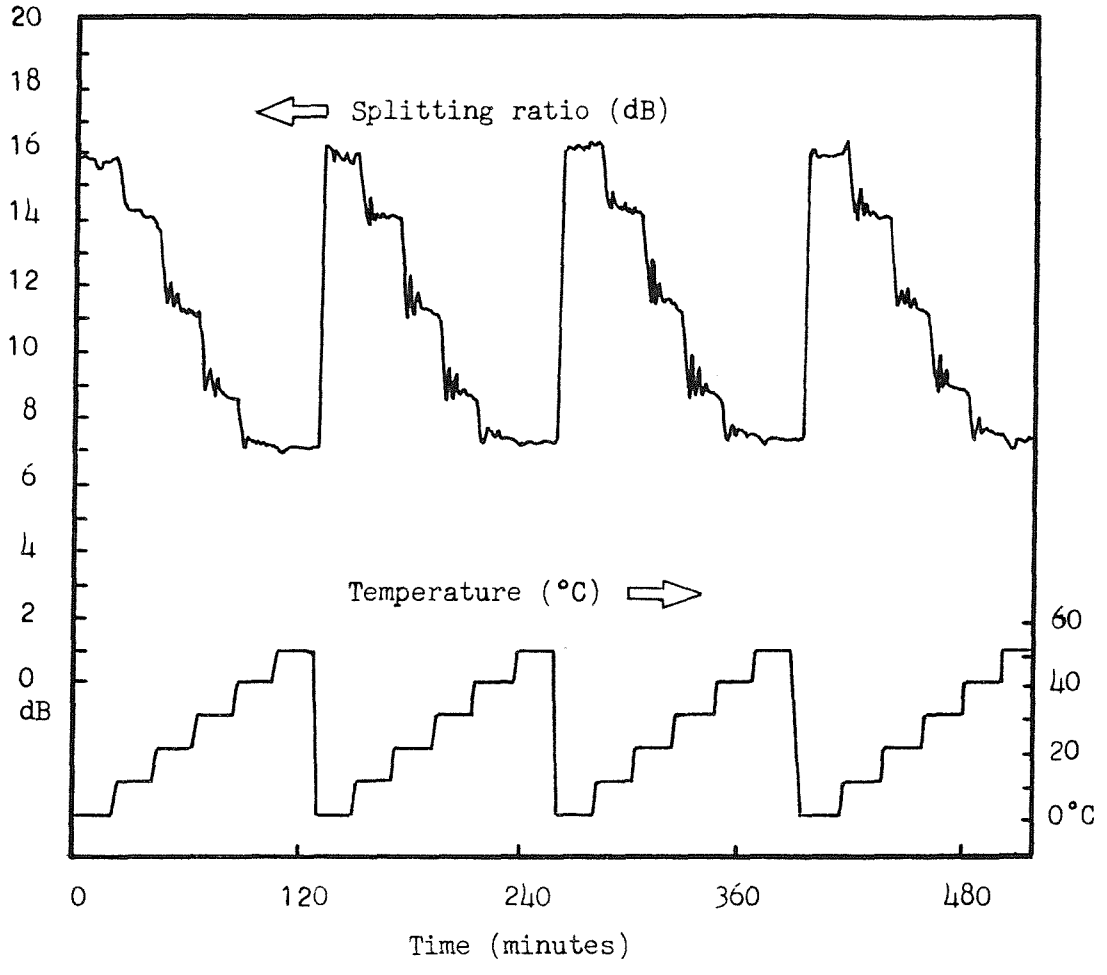

Figure 7.5. Splitting ratio variation under temperature cycling test.

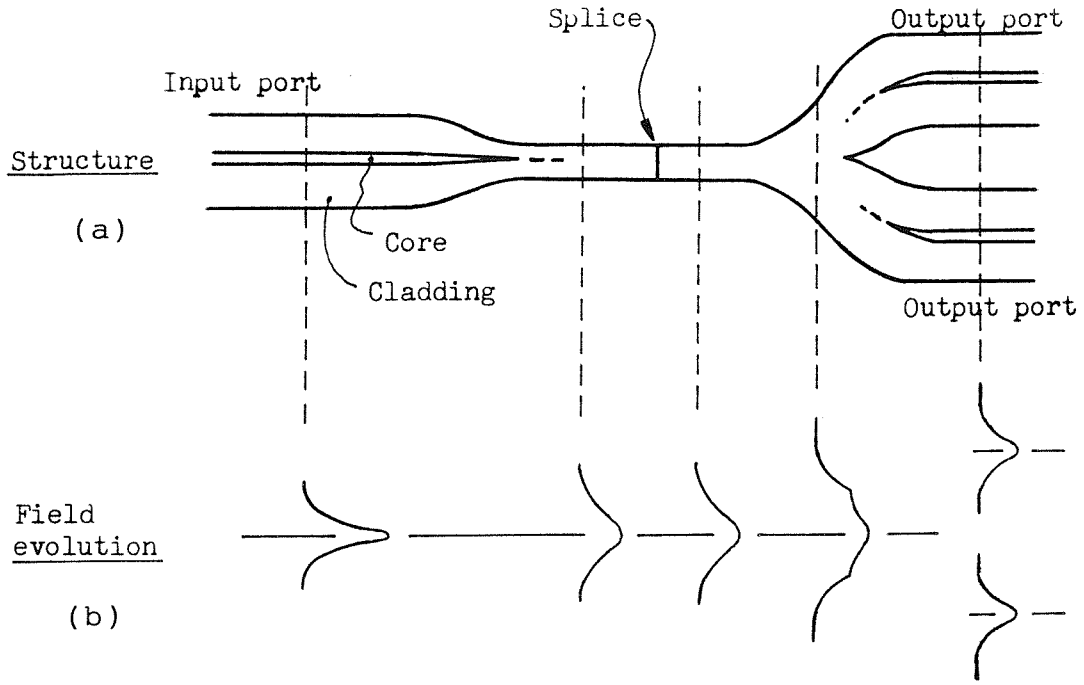

Figure 7.6. Structure and field evolution in the single mode fibre Y-junction beam splitter.

APPENDIX A

Measurement System

A1 Introduction

In this Appendix the basic measurement system is described, including the instrumentation, some measurement considerations and the environmental test (temperature and vibration) equipment.

A2 Measuring System

The system used for the spectral loss and spectral splitting ratio measurements consisted of the items listed in Table A1 arranged as shown in Figure A1. The main instruments and their roles are described in the following sections.

A2.1 The dual detectors

The powers from the two output ports of the coupler were measured simultaneously using two identical detecting systems in preference to a single detecting system. The necessity of changing the geometrical relationship between each fibre and the detector during the measurement is thereby eliminated. Similarly, the measuring time required was significantly reduced, and the possibility of error due to the fibre handling, i.e. cleaving and alignment etc., was minimized.

A2.2 Phase-sensitive detection

When a gas flame was applied to the fibres during coupler fabrication, the light due to the flame was

transmitted through the fibres to the detectors. Consequently the detected power was not a measure of the coupler characteristics. However, a phase-sensitive detector in combination with a chopper in the input beam largely eliminates the effect of the flame radiation and other stray light.

A2.3 Computer-aided measurement

The computer performs several functions, its main tasks being:

(i) to gather and record data,
(ii) to command the monochrometer for spectral scanning,
(iii) to apply a suitable filter when necessary,
(iv) to perform calculations using the data obtained,
(v) to plot the result in visual format
(vi) to control the environmental test chamber.

The computer significantly reduces the measuring time and improves repeatability by eliminating human involvement in the measurement operation.

A2.4 Problems of incompatibility between the Input Spectrum and the Coupler's Wavelength Response

The accurate measurement of the spectral characteristics of the coupler requires that the input spectrum from the monochrometer into the fibre be narrow relative to the spectral features of the coupler's response.

The normalized detectable power, P, can be expressed as

$$P = \int_0^{+\infty} I(\lambda)\ R(\lambda)\ d\lambda \qquad (A.1)$$

where, λ is the wavelength, $I(\lambda)$ is the normalized input response and $R(\lambda)$ is the normalized coupler response.

If the spectral width of the input is small compared with the oscillation period of the spectral response, then the coupler can be accurately measured as illustrated schematically in Figure A2. Conversely, if the spectral width of the input is large compared with the oscillation period of the spectral response, the coupler response cannot be accurately measured, as shown schematically in Figure A3.

An example of the effects of a wide input spectrum on the measured power characteristics at the output of the coupler as the coupler is being elongated is given in Figure A4.

The input to the coupler was white light passed through an interference filter with a peak wavelength of 835 nm and a full-width-half-maximum of approximately 20 nm. The oscillation of the coupled power as measured under these circumstances decayed as the coupler was elongated, and the power became equally split after a certain elongation length. The wide input spectrum is clearly averaging the many power oscillations that occur in the longer couplers.

A2.5 Problems of incompatibility between the data acquisition time and the coupler response time during fabrication

Examples of fluctuations in loss measured during coupler fabrication are given in Figure A5. The fluctuations were caused by the fact that the sampling speed of the data acquisition system could not adjust to the rapidity of the power exchanges occurring in the coupler. When the power exchanges occur quickly the powers from the throughput and coupling ports are not measured simultaneously but alternatively on both ports with a corresponding time delay. Consequently, the power variation within the time delay becomes significant if the power exchange occurs rapidly. The data obtained in the measurement system thus gives an inaccurate value for the loss and the power splitting ratio.

In the investigation of long couplers described in Chapter 5, an alternative approach was adopted in order to overcome the limitations imposed by the dynamic characteristics outlined above. The couplers were elongated by small incremented lengths, and at every increment the full spectral response was measured. After the final elongation, all of the data was processed to provide loss and power splitting ratio graphs as functions of the elongation length, for fixed wavelengths.

A3. Measurement procedures

Power measurements at the output ports of the coupler were made before, during and after fabrication, packaging, and environmental testing. The sequence of the measurements is described in flow-chart form in Figure A6 and is described in detail below:

[Measurement I - Input spectral response]

Prior to coupler fabrication, the power from the throughput port was measured over the required wavelength range by scanning the monochrometer. The data were stored in the computer memory to be used for reference.

[Measurement II - Output variation during fabrication]

After the fibres had been prepared for fabrication the monochrometer was set at the monitoring wavelength, the oxy-butane burner was applied to the fibres and the powers from both through and coupled ports were measured. During the entire process, the data obtained were recorded by the computer. After completing the fabrication, the excess loss variation and the splitting ratio at the monitored wavelength were displayed.

[Measurement III - Spectral response]

After the fabrication, the powers from both output ports were measured again over the required wavelength range. The wavelength variation of the splitting ratio was obtained from these measurements. The spectral loss was also calculated by comparing these results with those

obtained in measurement I. Measurements II and III were also carried out after packaging the coupler to see whether its performance had been affected, and to study the effect of temperature variation (Measurement IV) and other environmental changes (Measurement V).

[Measurement VI - Cutback for input response]

The input power launched into the coupler was measured by cutting the input fibre and measuring the power emerging from the remaining piece.

A4. Presentation and definitions of experimental data

The coupler characteristics were obtained easily from the variation of output power with

(a) fabrication time,
(b) tapering length,
(c) wavelength,
(d) temperature, and
(e) polarisation state.

The splitting ratio, coupling ratio and loss in dB were calculated as follows

[Splitting Ratio]

The splitting ratio R is defined as

$$R = 10 \log(P_4/P_3)[dB] \qquad (A.2)$$

where P_3, and P_4 are the powers from the throughput and coupled ports respectively. Thus $R<0$ indicates $P_3>P_4$, and

R<0 always at the beginning of the fabrication. R = 0 dB means that the power is equally distributed between the throughput and coupled ports.

[Coupling Ratio/Coupling Strength]

Alternatively the coupling ratio/strength Q is defined as

$$Q = 10 \log [P_4/(P_3+P_4)] \text{ [dB]} \qquad (A.3)$$

Q specifies the degree of coupling and is rarely used in this Thesis because it is the relationship between P_3 and P_4 that is the main interest rather than that between P_4 and $(P_3 + P_4)$.

It should be noted that some people may refer to the equal power splitting coupler, i.e. R = 0dB, as a "3dB coupler" since Q=3dB.

[Loss]

Loss α is defined as

$$\alpha = 10 \log [(P_3+P_4)/P_1] \text{[dB]} \qquad (A.4)$$

where P_1 = input power.

The back-reflected power P_b was observed to be less than 3% of the input power. When the throughput and coupled ports were immersed in index matching oil, P_b was too small to be measured. Therefore the back-reflected power is always neglected in this Thesis.

A5. Environmental Testing

A5.1 Temperature test apparatus and method

An environment test chamber, Astell BM50/60RC was employed; Figure A7 shows the experimental arrangement. The coupler under test was placed in the chamber while the optical performance was monitored, and the temperature in the chamber was set to the lowest test temperature. Maintaining the temperature for a certain period, to ensure that the temperature in the coupler was uniform, the optical performance was measured ten times at intervals of one minute. Then the temperature was raised by $10^{o}C$ and the optical performance was measured again in the same manner. The measurement sequence was repeated several times to ensure that performance of the coupler was stable and repeatable under fluctuating environmental conditions.

A5.2 Vibration Test Rig

A schematic diagram of the experimental set-up is given in Figure A8. The coupler is mounted alternately on its base and on its side on a mechanical shaker which is powered by an electronic oscillator in order to simulate environmental vibration conditions, and the optical output of the coupler was monitored.

The shaker could scan the frequency range of 300 Hz to 2200 Hz while maintaining a peak acceleration of 30 MS^{-2}.

Apparatus	Supplier / Type
Lamp	Atlas: Tungsten/halogen A1/216 240V 150W
Monochrometer	Bentham: M300 with 600 lp/mm grating (Some data were obtained with Oriel 7240)
Filters	Bentham: For 750 nm and 1000 nm
Chopper	Bentham: 218F (Adjusted 100-150 Hz)
Objective lens	Nikon: Magnification 10X
Fibre manipulator	25 mm stroke XYZ Table
Silicon detector	Centronic: OSD-100-2
Amplifier	Southampton University: Dual channels. Capable of 22 dB amplification.
Phase-sensitive detectors	Brookdale Electronics: Type 411
A-D converter	CIL Electronics: PL1 1000
D-A converter	CIL Electronics: PL1 3000
Computer	Tektronix: Model 4052
Alternative light source	Spectra Physics: He/Ne laser 155 and 105-2

Table A.1. Coupler fabrication rig equipment.

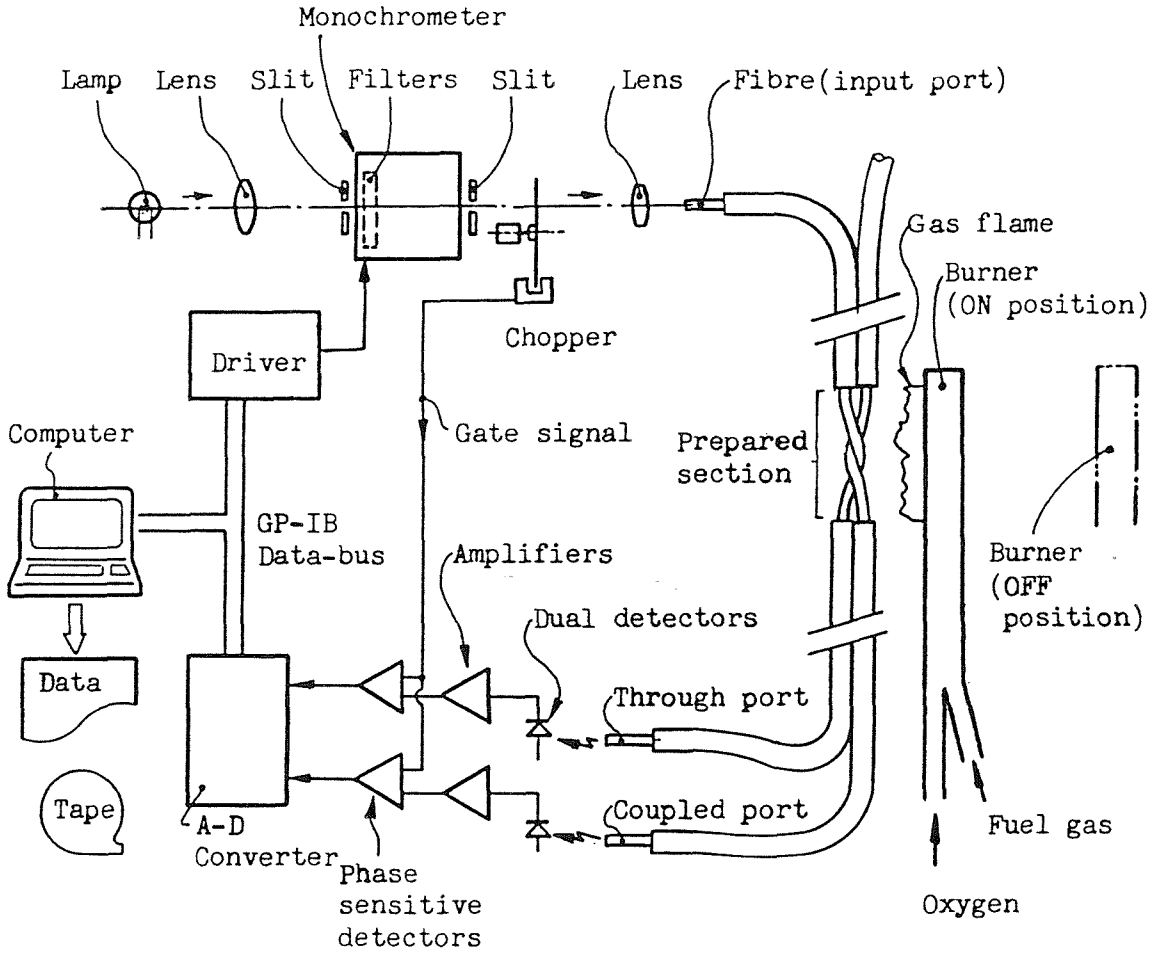

Figure A.1. Measurement system for taper/coupler fabrication.

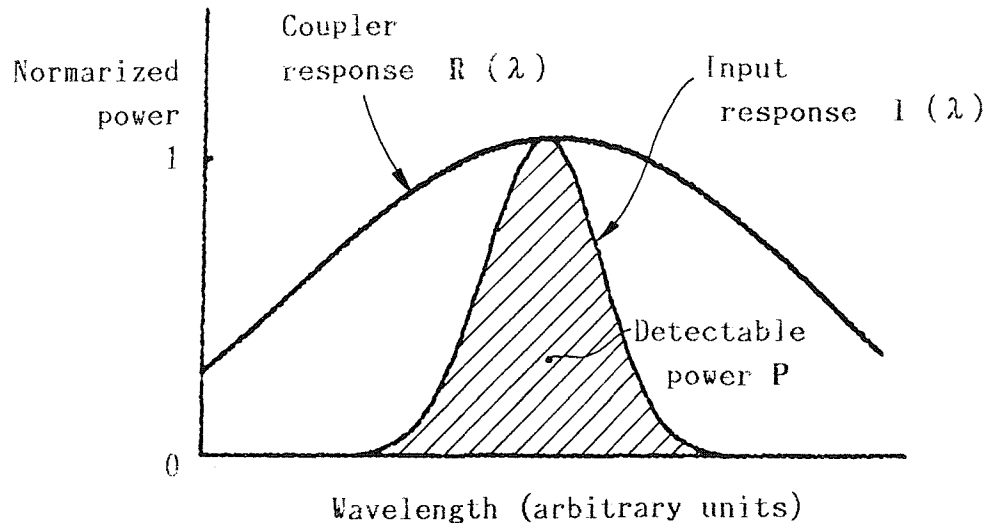

(a) Tapering time t_1

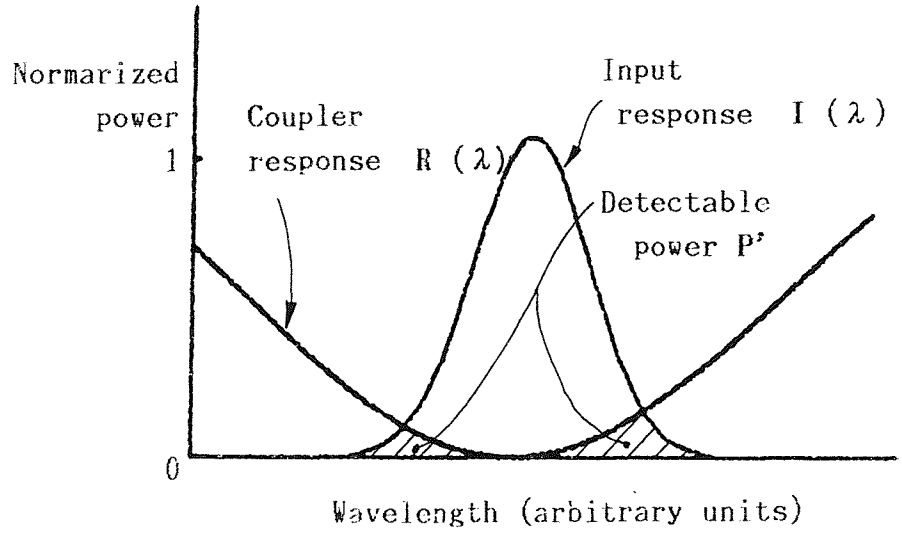

(b) Tapering time $t_1 + \Delta t$

Figure A.2. Power measurement with a narrow input spectrum as compared with the spectral oscillation period of the coupler. $P >> P'$.

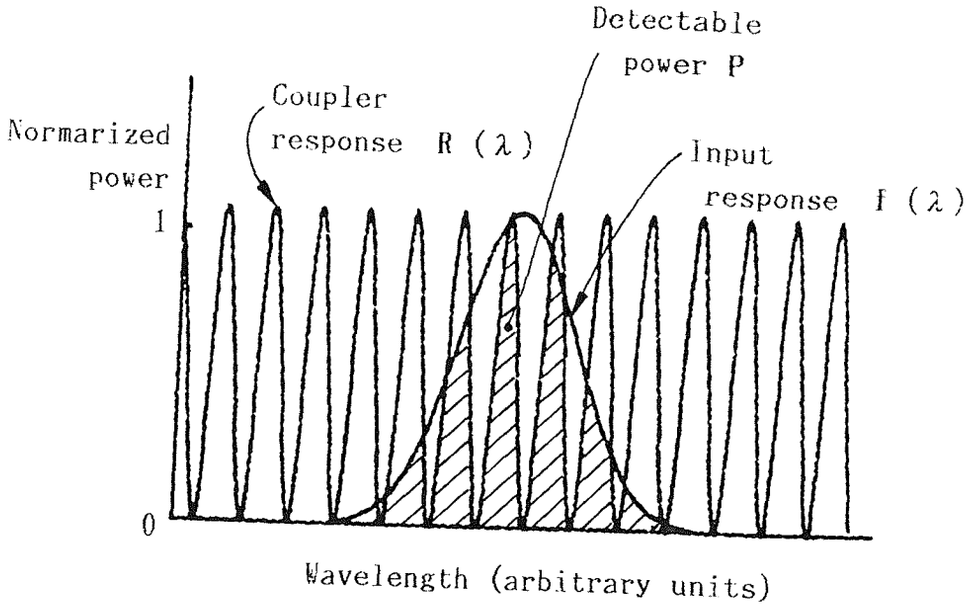

(a) Tapering time t_2

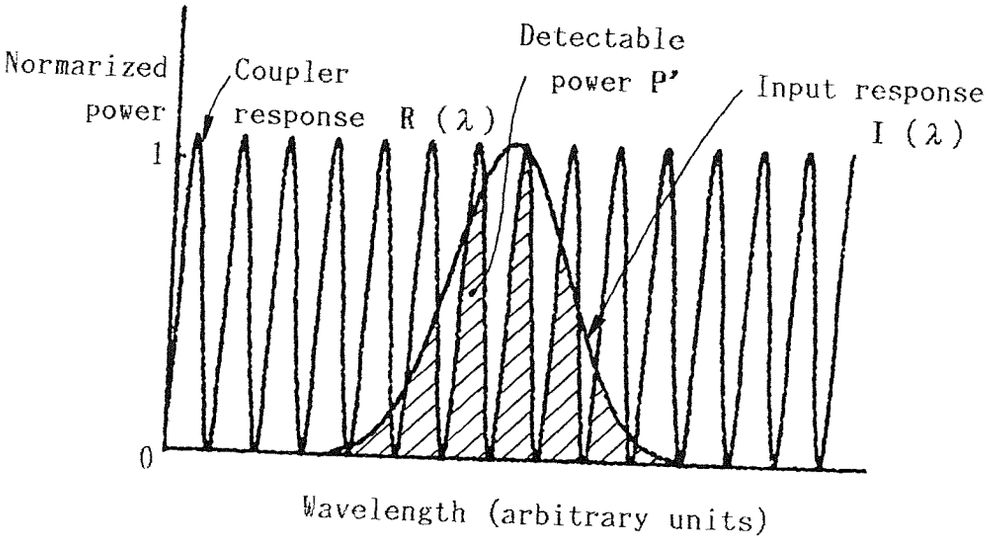

(b) Tapering time $t_2 + \Delta t$

Figure A.3. Power measurement with a wide input spectrum as compared with the spectral oscillation period of the coupler. $P \approx P'$.

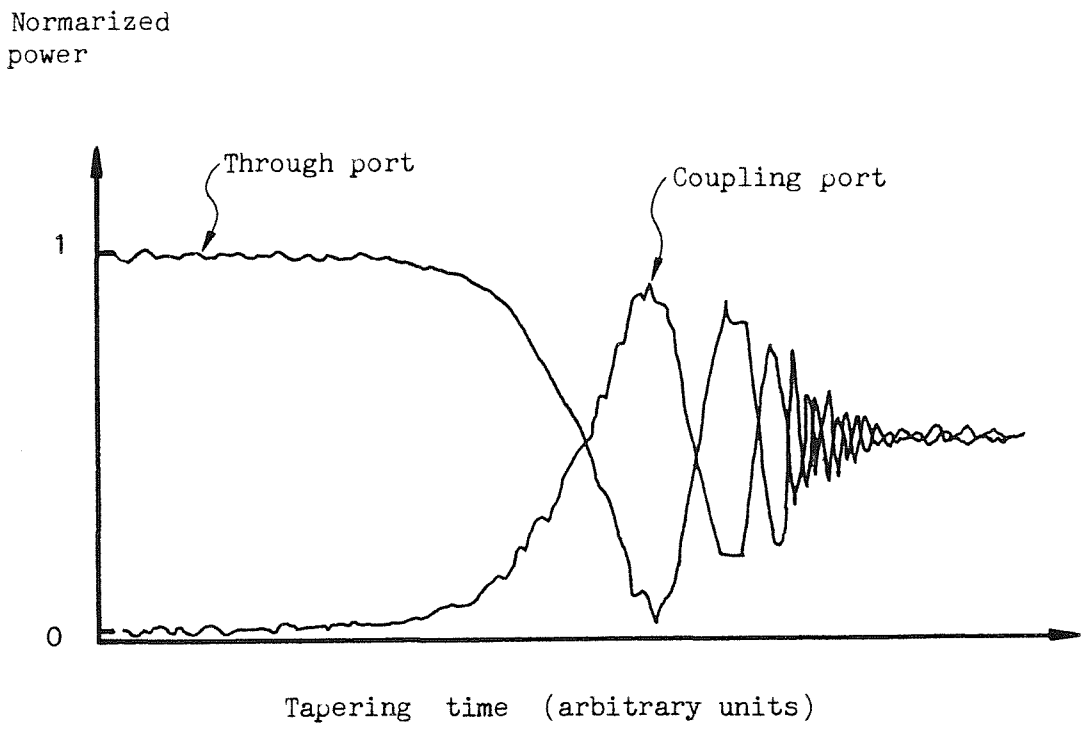

Figure A.4. Coupling characteristics as measured during fabrication using a Tektronix P7001 storage oscilloscope and an input source with a spectral width of 20 nm.

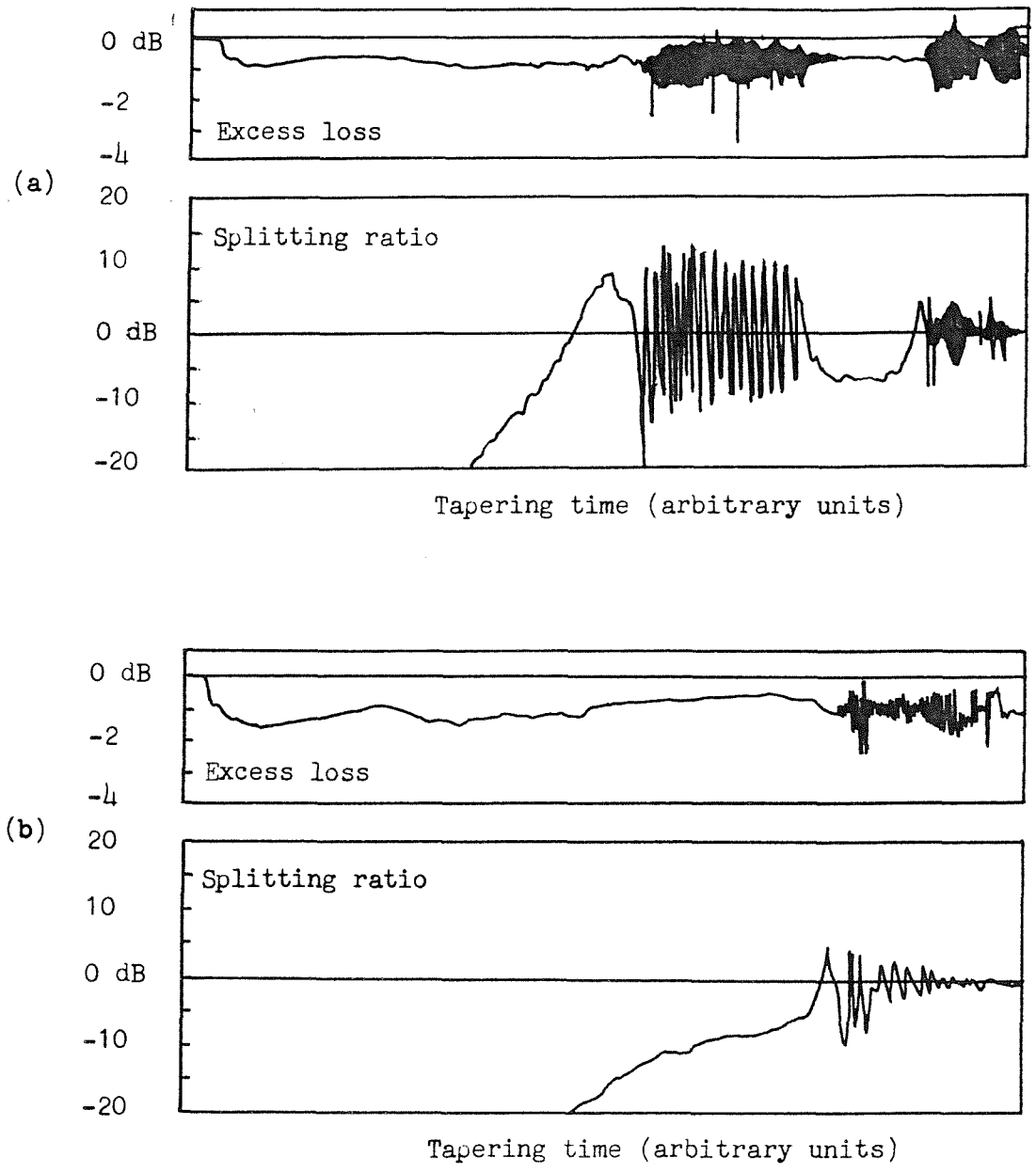

Figure A.5. Coupling characteristics obtained during fabrication as measured with

(a) a He-Ne laser λ = 633 nm , and
(b) monochrometer/lamp
FWMH = 20 nm approximately.

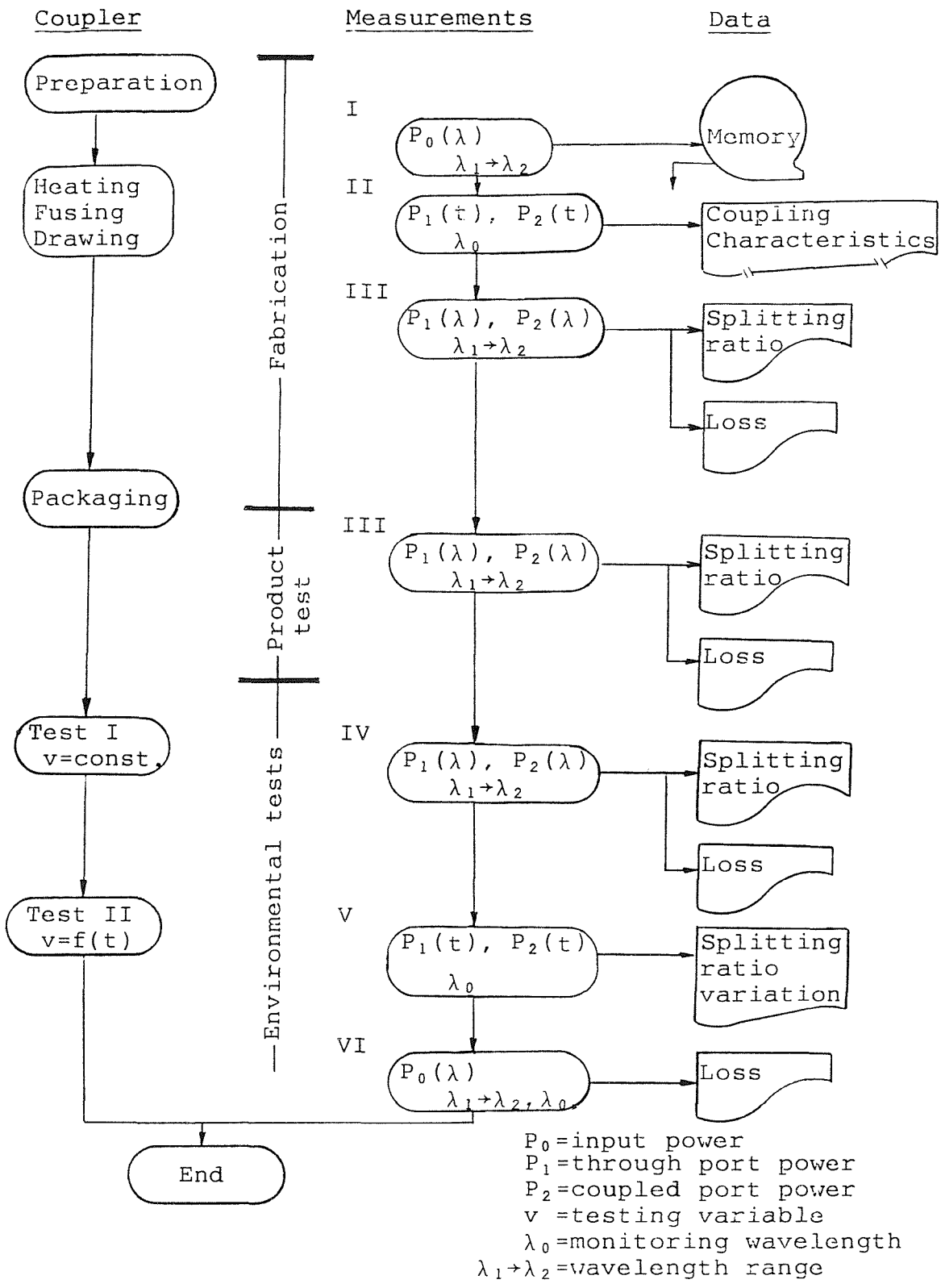

Figure A.6. Flow-chart for coupler measurements referring to fabrication processes and test conditions.

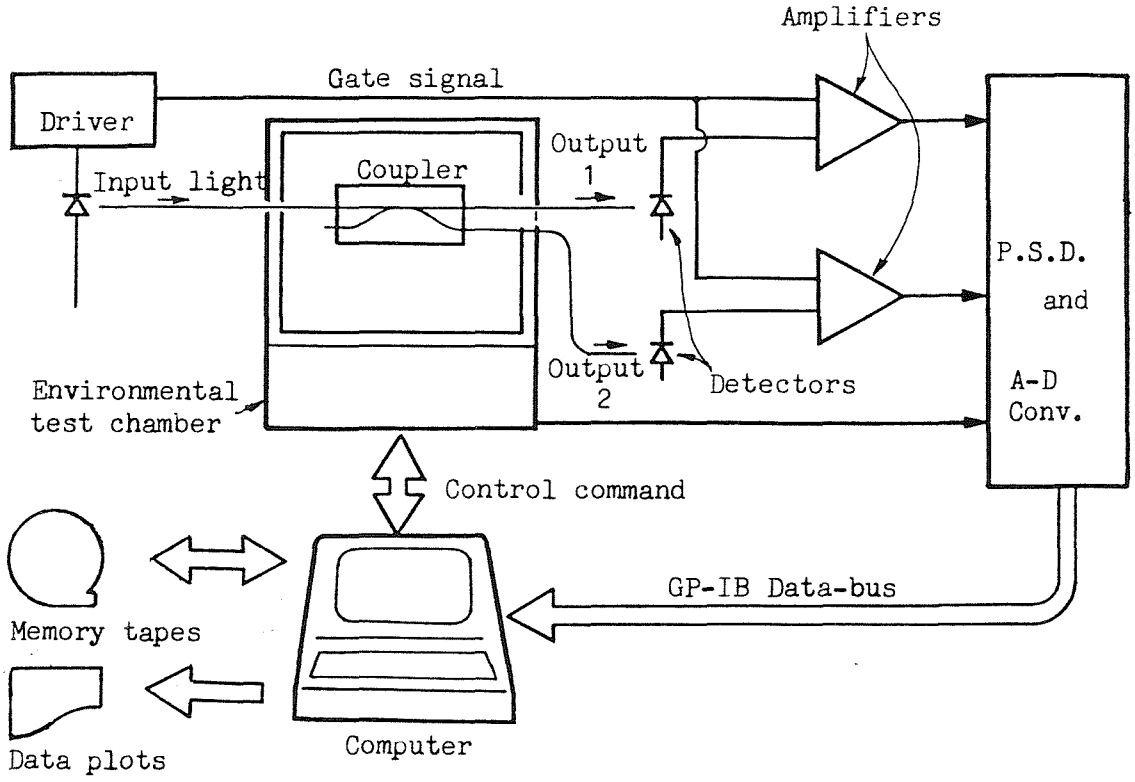

Figure A.7. Experimental arrangement for temperature cycling test.

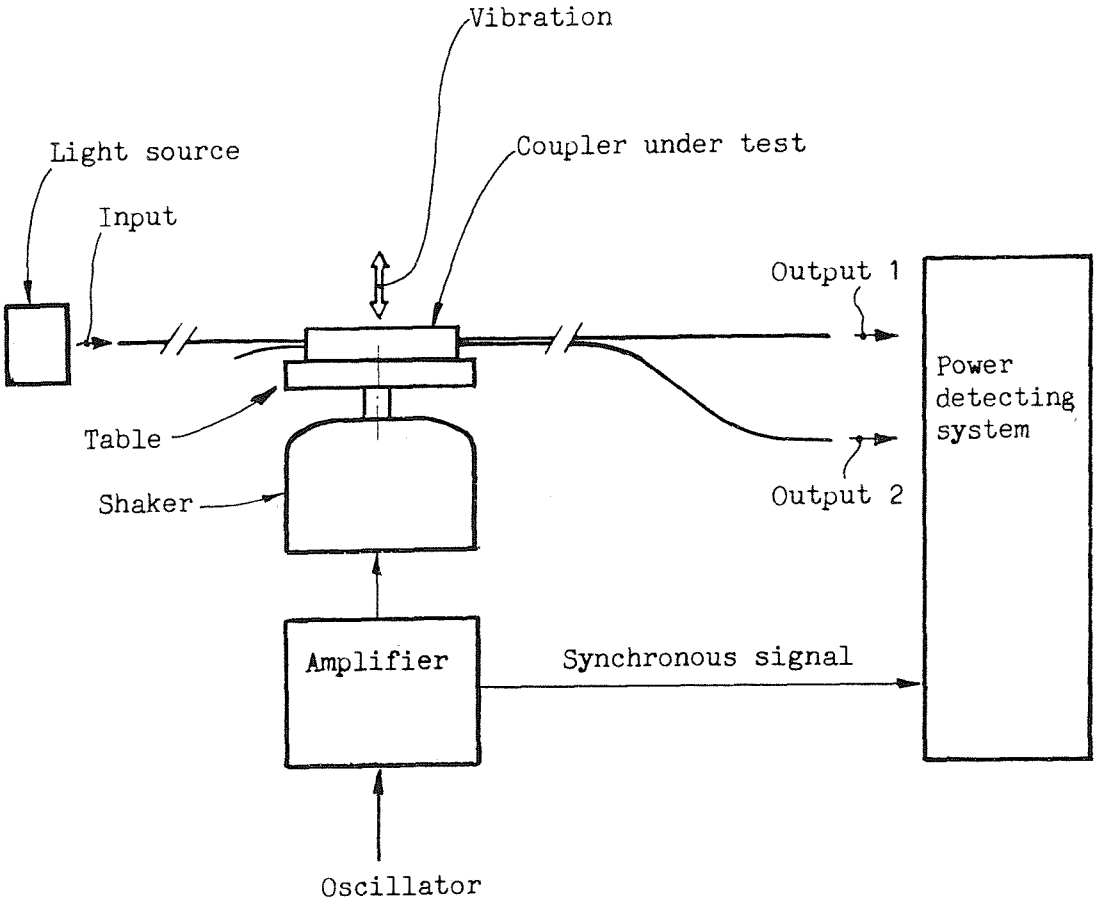

Figure A.8. Experimental arrangement for vibration test.